

City Research Online

City St George's, University of London

Citation: Ashaju, D. I. (1988). Experimental and theoretical analysis of coefficient of friction and redundant deformation in tube sinking process. (Unpublished Doctoral thesis, The City University)

This is the accepted version of the paper.

This version of the publication may differ from the final published version. To cite this item please consult the publisher's version.

Permanent repository link: https://openaccess.city.ac.uk/id/eprint/34296/

Copyright and Reuse: Copyright and Moral Rights remain with the author(s) and/or copyright holders. Copies of full items can be used for personal research or study, educational, or not-for-profit purposes without prior permission or charge, unless otherwise indicated, provided that the authors, title and full bibliographic details are credited, a hyperlink and/or URL is given for the original metadata page and the content is not changed in any way. For full details of reuse please refer to City Research Online policy.

City Research Online: http://openaccess.city.ac.uk/ publications@citystgeorges.ac.uk

THE CITY UNIVERSITY

DEPARTMENT OF MECHANICAL ENGINEERING

EXPERIMENTAL AND THEORETICAL ANALYSIS OF COEFFICIENT OF FRICTION AND REDUNDANT DEFORMATION IN TUBE SINKING PROCESS

by

DANIEL IDOWU ASHAJU

H.N.D. (Eng.), B.Sc.(Hons.), M.Sc.(Eng.)

A Thesis submitted in fulfilment of
the requirements for the award
of the Degree of
Doctor of Philosophy

LONDON 1988

SUMMARY

There are aspects of wire and tube drawing processes which have not received sufficient attention by the past workers. The equation relating drawing force and wall thickness in the tube sinking process includes terms involving the coefficient of friction at the die-workpiece interface and redundant deformation. The use of this equation necessitates estimation of the values of these parameters and often leads to significant errors. The two basic equations of drawing force and wall thickness in the tube sinking process are:

$$(1)\quad F_D = \left[\frac{\pi D_1 t}{\cos\alpha}\right].\bar{m\gamma}\left[\frac{(1+\mu\cot\alpha)}{\mu\cot\alpha}\right]\left[1-\left[\frac{D_2}{D_1}\right]^{\mu\cot\alpha}\right] + \frac{2\pi D_1 t\bar{\gamma}\alpha}{3} \quad \text{and}$$

$$(2)\quad \ell n\left[\frac{t}{t_1}\right] = \left[\frac{3}{(\mu\cot\alpha-1)}\right].\ell n\left[\frac{2\left[\frac{D_2}{D_1}\right]^{\mu\cot\alpha}}{2-\left\{\frac{1+\mu\cot\alpha}{\mu\cot\alpha}\right\}\left\{1-\left[\frac{D_2}{D_1}\right]^{\mu\cot\alpha}\right\}}\right] - 2\ell n\left[\frac{D_2}{D_1}\right]$$

Various workers have carried out experiments and theoretical analysis to develop and verify these equations. Unfortunately, the fundamental weakness has been determining values of the coefficient of friction, μ, for various materials, die configurations and tribological conditions. It has been assumed that the frictional stress, τ, at die-tube interface cannot be greater than yield shear stress at the interface, i.e. $\tau = \mu p \leqslant k$ where p is the absolute radial pressure and k is the yield stress is shear. There has been doubt on the validity of the upper bound values of μ attained from the upper bound hypothesis based on plain strain theory which is far from an ideal tube sinking process. The work carried out under the research presented in this thesis includes:

1) Devising an elemental die theory to facilitate the analysis of elemental force across a conical die pass

2) The use of the elemental die theory to provide a method for theoretical and experimental accurate analysis of the coefficient of friction across a die-pass

3) Employment of the elemental die theory to prove and to assess theoretically and experimentally the redundant deformation force at the entry and exit of conical die.

From the results attained, the existence of redundant deformation was connoted and correction factors to eliminate the under-estimation by Penny's proposed redundant deformation theory were deduced and presented. Both the elemental and the significant values of μ attained were employed in conjunction with results of radial pressure experiment to check the validity of the upper bound assumption as applied to tube sinking process. It is concluded that the proposed elemental die theory can be employed to determine accurately the profile of μ across a die pass and most importantly to estimate accurately the significant μ value needed for accurate calculation of the total drawing force due to redundant deformation.

LIST OF CONTENTS

		Page
SUMMARY		1
LIST OF CONTENTS		2
NOMENCLATURE		5
LIST OF FIGURES		9
LIST OF TABLES		12
ACKNOWLEDGEMENTS		21
CHAPTER 1:	INTRODUCTION	22
1.11.	Friction	22
1.12.	Historical Background of Friction	23
1.13.	Lubricant	24
1.14.	History of Tubular Products	25
1.15.	Wooden Tubes	25
1.16.	Iron Tubes	26
1.17.	Stone Tubes	27
1.18.	Modern Manufacture of Tubular Products	27
1.19.	Seamed Tubes	28
1.20.	Seamless Tubes	28
CHAPTER 2:	OBJECTIVES OF THE STUDY	31
2.11.	Objectives of the study	31
2.12.	Review of Previous Work	33
2.13.	Theories	33
2.14.	Differential equations of equilibrium	34
2.15.	Epsey and Sachs - Drawing with Moving Mandrel	34
2.16.	Upper Bound Estimates	35
2.17.	Blazyinski and Cole	36
2.18.	Wall Thickness	37
2.19.	Flinn	38
2.20.	Others	39
2.21.	Folding Phenomenon	40
2.22.	Redundant Deformation	41
CHAPTER 3:	THEORY OF TUBE SINKING THROUGH A CONICAL DIE	43
3.11.	Method of making allowance for Drawing Stress due to Redundant Deformation in Tube Sinking Process	48
3.12.	A proposed Elemental Die Theory for Analysis of Coefficient of Friction across Working Face and Analysis of Redundant Deformation at the Entry and Exit of a Typical Conical Die.	50
3.13.	Design of Dies for the Analysis of Coefficient of Friction and Redundant Deformation	55
3.14.	Elemental Fractional Reduction	56

Page

CHAPTER 4: DESIGN OF THE EXPERIMENT 57

4.11. Previous Work 57
4.12. The Draw Bench 57
4.13. Materials for Specimen Workpiece 58
4.14. Die Design 59
4.15. Preparation of Specimen Workpiece 63
4.16. Method used in Industry 63
4.17. Method used for the Project 64

CHAPTER 5: QUASI-STATIC AXISYMMETRIC COMPRESSION TEST 66

5.11. Objective of the Experiment 66
5.12. Theory 67
5.13. Strain Rate in Uniaxial Compression 69
5.14. Fractional Reduction, R 70
5.15. Apparatus and Equipment 70
5.16. Test Procedure 72
5.17. Results from the Experiment 73
5.18. Summary of Elemental Yield Stress 75
5.19. Estimation of Errors 76
5.20. Discussion 78
5.21. Conclusions 81

CHAPTER 6: EXPERIMENTAL ANALYSIS OF COEFFICIENT OF FRICTION IN TUBE SINKING PROCESS 82

6.11. Objective of the Experiment 82
6.12. Theory 83
6.13. Equipment 84
6.14. Procedure 85
6.15. Analysis of Results 88
6.16. Results from the Experiment 99
6.17. Correlating Upper Bound Theorem with Experimental Results 103
6.18. Discussion 104
6.19. Conclusions 111

CHAPTER 7: RADIAL PRESSURE EXPERIMENT 113

7.11. Objective of the Experiment 113
7.12. Theory 114
7.13. Apparatus and Equipment 117
7.14. Procedure 118
7.15. Part I 118
7.16. Part II Calibration 120
7.17. Results from the Experiment 122
7.18. Discussion 123
7.19. Conclusions 124

Page

CHAPTER 8: EXPERIMENT TO VERIFY AND TO ASSESS REDUNDANT DEFORMATION DUE TO PLASTIC AND ELASTIC WORK AND ELASTIC RECOVERY AT ENTRY AND EXIT RESPECTIVELY DURING DRAWING OF A THIN WALLED TUBE SLOWLY THROUGH A CONICAL DIE 126

8.11. Objective of the Experiment 126
8.12. Theory 126
8.13. Equipment 128
8.14. Test Procedure 132
8.15. Stage IA 133
8.16. Stage IB 135
8.17. Stage II 136
8.18. Stage IIIA 139
8.19. Stage IIIB 140
8.20. Results Analysis 142
8.21. Results Summary 146
8.22. Checking Validity of the Proposed Elemental Die Theory 150
8.23. Results from the Experiment 156
8.24. Discussion 159
8.25. Conclusions 165

CHAPTER 9: CONCLUSION 167

9.11. Summary Conclusions 167
9.12. Suggestions for Further Work 171

REFERENCES 172

APPENDIX 175

NOMENCLATURE

SYMBOL	UNITS	DESCRIPTION
F_{DT}	(N)	total drawing force
D_1	(mm)	mean external diameter at die entrance
D_2	(mm)	mean external diameter at die exit
t	(mm)	mean tube wall thickness
α	(rad/degree)	die half-angle
μ		coefficient of friction
$\bar{y}$	(MPa)	mean yield stress
q	(MPa)	longitudinal stress in wall parallel to die face
σ_θ	(MPa)	circumferential stress
p	(MPa)	normal die pressure
F_{red}	(N)	drawing force due to redundant deformation
σ_{red}	(MPa)	drawing stress due to redundant deformation
D_{e1}	(mm)	diameter at elemental die entrance
D_{e2}	(mm)	diameter at elemental die exit
L_w	(mm)	pass length of typical die
ℓ_e	(mm)	pass length of an elemental die
F_{Deu}	(N)	elemental drawing force due to redundant deformation
F_{De}	(N)	corrected elemental drawing force
R_{De}	(N)	theoretical redundant force
μ_e, μ_{eL}		elemental coefficient of friction
μ_s, μ_{sL}		significant coefficient of friction
y_e		elemental yield stress

R_{De*}	(N)	experimental redundant force
R_e		elemental fractional reduction
R_T		total fractional reduction
P_e	(MPa)	elemental radial pressure
F_e	(N)	elemental frictional force
τ	(N/m^2)	frictional shear stress
k	(MPa)	yield stress in shear
ϵ_{DT}	(micro)	total drawing strain
ϵ_{Deu}	(micro)	elemental drawing strain due to elemental redundant strain
ϵ_{re*}	(micro)	experimental elemental redundant strain
ϵ_{re}	(micro)	theoretical elemental redundant strain
ϵ_{rem*}	(micro)	mean experimental elemental redundant strain
ϵ_{rem}	(micro)	mean theoretical elemental redundant strain
s		number of specimens
$\Delta\epsilon_r$	(micro)	difference betweeen theoretical and experimental elemental redundant strain
ΔR_D	(N)	difference between theoretical and experimental elemental redundant force
n_s		number of strain readings per pass
ϵ_e	(micro)	uncorrected strain reading
ϵ_{ea}	(micro)	average modulus of uncorrected strain reading
En		die entry
Ex		die exit
Δ	(%)	percentage difference
ee	(N)	error between sum of corrected elemental drawing forces and the measured total drawing force
ΣF_{De}	(N)	sum of corrected elemental drawing forces
F_{dT}	(N)	measured total drawing force

C_n		correction factor at die entry
C_x		correction factor at die exit
C_{nx}		sum of correction factor
C_f		actual correction factor
F_c	(N)	compression force
ΔH	(mm)	compression
Ho	(mm)	initial height of specimen
H	(mm)	current height of specimen
A_o	(mm^2)	initial cross-sectional area
A	(mm^2)	current cross-sectional area
σ_c	(MPa)	true compressive stress
e		engineering strain
ϵ		natural or logarithmic strain
$\dot{e}$		engineering strain rate
$\dot{\epsilon}$		natural strain rate
σ_r	(MPa)	radial stress
ϵ_i		longitudinal strain
σ_i	(MPa)	longitudinal stress
ϵ_r	(micro)	radial strain
NSOH		non-shrinking oil hardening steel die
HCHC		high chromium high carbon steel die
C.I.		cast iron die
Cu		copper tube drawn without lubricant
SS		stainless steel tube drawn without lubricant
AL		aluminium steel tube drawn without lubricant
Br		annealed brass tube drawn without lubricant
CuL		copper tube drawn with lubricant

SSL	stainless steel tube drawn with lubricant
BrL	brass tube drawn with lubricant
ALL	aluminium tube drawn with lubricant
NSOH-Cu	specimen drawn through die

LIST OF FIGURES

		Page
Fig.1.1.	Mannesmann process	175
Fig.1.2.	Assel process	175
Fig.1.3.	Rotary Rolling process	175
Fig.1.4.	Methods of tube drawing	175
Fig.1.5.	Tube expanding	175
Fig.1.6.	Typical Aircraft Tank unit inner tube	176
Fig.1.7.	An aircraft fuel gauging unit.	177
Fig.4.10.	Initial Design of elemental dies with $\alpha = 7^{\circ}$, $R_T = 0.375$	182
Fig.4.11	Initial Design of elemental dies with $\alpha = 15^{\circ}$, $R_T = 0.375$	183
Fig.4.12.	Initial Design of elemental dies with $\alpha = 7^{\circ}$, $R_T = 0.250$	184
Fig.4.13.	Initial Design of elemental dies with$\alpha = 15^{\circ}$, $R_T = 0.250$	185
Fig.4.14.	Alternative design of elemental dies with$\alpha = 7^{\circ}$, $R_T = 0.375$	186
Fig.4.15.	Alternative design of elemental dies with $\alpha = 15^{\circ}$, $R_T = 0.375$	187
Fig.4.16.	Alternative design of elemental dies with $\alpha = 7^{\circ}$, $R_T = 0.250$	188
Fig.4.17.	Alternative design of elemental dies with $\alpha = 15^{\circ}$, $R_T = 0.250$	189
Fig.4.18.	A power press employed for pointing specimens	190
Fig.4.19.	A Die set and swaging tool removed from power press.	191
Fig.5.10.	Curves of True Compressive Stress - Natural Strain of annealed Brass	192
Fig.5.20.	Curves of True Compressive Stress - Natural Strain of Copper	193
Fig.5.30.	Curves of True Compressive Stress - Natural Strain of Stainless steel	194
Fig.5.40.	True Stress - Natural Strain Curves showing the effect of Redundant Deformation and die pass length on Yield Stress	195
Fig.6.01.	μ_e-R_e Curves for C.I. Elemental Dies with $\alpha = 7^{\circ}$, $R_T = 0.375$	219
Fig.6.02.	μ_e-R_e Curves for NSOH Elemental Dies with $\alpha = 7^{\circ}$, $R_T = 0.375$	220
Fig.6.03.	μ_e-R_e Curves for HCHC Elemental Dies with $\alpha = 7^{\circ}$, $R_T = 0.375$	221
Fig.6.04.	μ_{eL}-R_e Curves for C.I. Elemental Dies with $\alpha = 7^{\circ}$, $R_T = 0.375$	222
Fig.6.05.	μ_{eL}-R_e Curves for NSOH Elemental Dies with $\alpha = 7^{\circ}$, R_T =0.375	223

		Page
Fig.6.06.	μ_{eL}-R_e Curves for HCHC Elemental Dies with α = 7°, R_T =0.375	224
Fig.6.07.	μ_e-R_e Curves for C.I. Elemental Dies with α = 7°, R_T = 0.250	225
Fig.6.08.	μ_e-R_e Curves for NSOH Elemental Dies with α = 7°, R_T = 0.250	226
Fig.6.09.	μ_e-R_e Curves for HCHC Elemental Dies with α = 7°, R_T = 0.250	227
Fig.6.11.	μ_{eL}-R_e Curves for C.I. Elemental Dies with α = 7°, R_T = 0.250	228
Fig.6.12.	μ_{eL}-R_e Curves for NSOH Elemental Dies with α = 7°, R_T =0.250	229
Fig.6.13.	μ_{eL}-R_e Curves for HCHC Elemental Dies with α = 7°, R_T =0.250	230
Fig.6.14.	μ_e-R_e Curves for C.I. Elemental Dies with α = 15°, R_T = 0.375	231
Fig.6.15.	μ_e-R_e Curves for NSOH Elemental Dies with α = 15°, R_T =0.375	232
Fig.6.16.	μ_e-R_e Curves for HCHC Elemental Dies with α = 15°, R_T=0.375	233
Fig.6.16′	μ_{eL}-R_e Curves for C.I. Elemental Die with α = 15°,R_T=0.375	234
Fig.6.17.	μ_{eL}-R_e Curves for NSOH Elemental Dies with α = 15°, R_T=0.375	235
Fig.6.18.	μ_{eL}-R_e Curves for HCHC Elemental Dies with α = 15°,R_T=0.375	236
Fig.6.19.	μ_e-R_e Curves for C.I. Elemental Dies with α = 15°, R_T = 0.250	237
Fig.6.20.	μ_e-R_e Curves for NSOH Elemental Dies with α = 15°, R_T=0.250	238
Fig.6.21.	μ_e-R_e Curves for HCHC Elemental Dies with α = 15°, R_T=0.250	239
Fig.6.22.	μ_{eL}-R_e Curves for C.I. Elemental Dies with α = 15°, R_T =0.250	240
Fig.6.23.	μ_{eL}-R_e Curves for NSOH Elemental Dies with α = 15°, R_T=0.250	241
Fig.6.24.	μ_{eL}-R_e Curves for HCHC Elemental Dies with α = 15°, R_T=0.250	242
Fig.6.25.	Graphs of (μ_s-μ_{sL}) against Initial Hardness of Tubing Material for α = 7° and R_T = 0.375 dies.	243
Fig.6.26.	Graphs of (μ_s-μ_{sL}) against Initial Hardness of Tubing Material for α = 15° and R_T = 0.375 dies.	244
Fig.6.27.	Sets of 7° C.I. Elemental Dies with R_T = 0.250 & R_T = 0.375	293
Fig.6.28.	Sets of 7° NSOH Elemental Dies with R_T = 0.250 & R_T = 0.375	294
Fig.6.29.	Sets of 7° HCHC Elemental Dies with R_T = 0.250 & R_T = 0.375	295
Fig.6.30.	Sets of 15° C.I. Elemental Dies with R_T = 0.250 & R_T = 0.375	296
Fig.6.31.	Sets of 15° NSOH Elemental Dies with R_T = 0.250 & R_T = 0.375	297
Fig.6.32.	Sets of 15° HCHC Elemental Dies with R_T = 0.250 & R_T = 0.375	298
Fig.6.33.	Sets of new and used specimens	299

		Page
Fig.7.01.	Mechnaics of thick cylinder	
Fig.7.02.	Graphs of Strain against Pressure for calibration	308
Fig.7.03.	Curves of Strain against Fractional Reduction of Al Specimen drawn at 3 cm/min	300
Fig.7.04.	Curves of Strain - Elemental Fractional Reduction of Al Specimen drawn at 2 cm/min	301
Fig.7.05.	Elemental Radial Pressure against Fractional Reduction Graphs of Al drawn specimen at 3 cm/min	302
Fig.7.06.	Elemental Radial Pressure against Fractional Reduction of Al specimen drawn at 2 cm/min	303
Fig.7.07.	Elemental Frictional Force against Fractional Reduction Curves	304
Fig.7.08.	Set up of equipment for calibration.	314

LIST OF TABLES

		Page
4.10.	General Specification for Part I elemental die.	178
4.11.	Further details of sets of elemental dies with 0.375 total fractional reduction	179
4.12.	Further details of sets of elemental dies with 0.250 total fraction reduction	179
4.13.	Details of sets of elemental dies for 0.375 fractional reduction to prove redundant deformation	180
4.14.	Details of sets of elemental dies for 0.250 fractional reduction to prove redundant deformation	181
5.01 - 5.06.	Quasi-static axisymmetric compression test (Brass)	192-201
5.07 - 5.12.	Quasi-static axisymmetric compression test (Copper)	202-207
5.13 - 5.22.	Quasi-static axisymmetric compression test (Stainless steel)	208-217
6.01.	Experimental and Calculated results for R_T = 0.375, NSOH-AL α = 7°	245
6.02.	Experimental and Calculated results for R_T = 0.375, HCHC-AL α = 7°	245
6.03.	Experimental and Calculated results for R_T = 0.375, NSOH-Cu α = 7°	246
6.04.	Experimental and Calculated results for R_T = 0.375, HCHC-Cu α = 7°	246
6.05.	Experimental and Calculated results for R_T = 0.375, NSOH-SS α = 7°	247
6.06.	Experimental and Calculated results for R_T = 0.375, HCHC-SS α = 7°	247
6.07.	Experimental and Calculated results for R_T = 0.375, NSOH-Br α = 7°	248
6.08.	Experimental and Calculated results for R_T = 0.375, HCHC-Br α = 7°	248
6.09	Experimental and Calculated results for R_T = 0.375, CI-AL α = 7°	249
6.10.	Experimental and Calculated results for R_T = 0.375, CI-SS α = 7°	249
6.11.	Experimental and Calculated results for R_T = 0.375, CI-Br α = 7°	250

Page

6.12. Experimental and Calculated results for R_T = 0.375, CI-Cu $\alpha = 7^\circ$ 250

6.13. Experimental and Calculated results for R_T = 0.375, NSOH-ALL $\alpha = 7^\circ$ 251

6.14. Experimental and Calculated results for R_T = 0.375, HCHC-ALL $\alpha = 7^\circ$ 251

6.15. Experimental and Calculated results for R_T = 0.375, NSOH-BrL $\alpha = 7^\circ$ 252

6.16. Experimental and Calculated results for R_T = 0.375, HCHC-BrL $\alpha = 7^\circ$ 252

6.17. Experimental and Calculated results for R_T = 0.375, NSOH-SSL $\alpha = 7^\circ$ 253

6.18. Experimental and Calculated results for R_T = 0.375, HCHC-SSL $\alpha = 7^\circ$ 253

6.19. Experimental and Calculated results for R_T = 0.375, NSOH-CuL $\alpha = 7^\circ$ 254

6.20. Experimental and Calculated results for R_T = 0.375, HCHC-CuL $\alpha = 7^\circ$ 254

6.21. Experimental and Calculated results for R_T = 0.375, CI-ALL $\alpha = 7^\circ$ 255

6.22. Experimental and Calculated results for R_T = 0.375, CI-SSL $\alpha = 7^\circ$ 255

6.23. Experimental and Calculated results for R_T = 0.375, CI-BrL $\alpha = 7^\circ$ 256

6.24. Experimental and Calculated results for R_T = 0.375, CI-CuL $\alpha = 7^\circ$ 256

6.25. Experimental and Calculated results for R_T = 0.250, NSOH-Br $\alpha = 7^\circ$ 257

6.26. Experimental and Calculated results for R_T = 0.250, HCHC-Br $\alpha = 7^\circ$ 257

6.27. Experimental and Calculated results for R_T = 0.250, NSOH-AL $\alpha = 7^\circ$ 258

6.28. Experimental and Calculated results for R_T = 0.250, HCHC-AL $\alpha = 7^\circ$ 258

6.29. Experimental and Calculated results for R_T = 0.250, NSOH-SS $\alpha = 7^\circ$ 259

6.30. Experimental and Calculated results for R_T = 0.250, HCHC-SS $\alpha = 7^\circ$ 259

Page

6.31. Experimental and Calculated results for R_T = 0.250, NSOH-Cu $\alpha = 7^\circ$ 260

6.32. Experimental and Calculated results for R_T = 0.250, HCHC-Cu $\alpha = 7^\circ$ 260

6.33. Experimental and Calculated results for R_T = 0.250, CI-Br $\alpha = 7^\circ$ 261

6.34. Experimental and Calculated results for R_T = 0.250, CI-Cu $\alpha = 7^\circ$ 261

6.35. Experimental and Calculated results for R_T = 0.250, CI-AL $\alpha = 7^\circ$ 262

6.36. Experimental and Calculated results for R_T = 0.250, CI-SS $\alpha = 7^\circ$ 262

6.37. Experimental and Calculated results for R_T = 0.250, NSOH-ALL $\alpha = 7^\circ$ 263

6.38. Experimental and Calculated results for R_T = 0.250, HCHC-ALL $\alpha = 7^\circ$ 263

6.39. Experimental and Calculated results for R_T = 0.250, NSOH-SSL $\alpha = 7^\circ$ 264

6.40. Experimental and Calculated results for R_T = 0.250, HCHC-SSL $\alpha = 7^\circ$ 264

6.41. Experimental and Calculated results for R_T = 0.250, NSOH-CuL $\alpha = 7^\circ$ 265

6.42. Experimental and Calculated results for R_T = 0.250, HCHC-CuL $\alpha = 7^\circ$ 265

6.43. Experimental and Calculated results for R_T = 0.250, NSOH-BrL $\alpha = 7^\circ$ 266

6.44. Experimental and Calculated results for R_T = 0.250, HCHC-BrL $\alpha = 7^\circ$ 266

6.45. Experimental and Calculated results for R_T = 0.250, CI-BrL $\alpha = 7^\circ$ 267

6.46. Experimental and Calculated results for R_T = 0.250, CI-CuL $\alpha = 7^\circ$ 267

6.47. Experimental and Calculated results for R_T = 0.250, CI-ALL $\alpha = 7^\circ$ 268

6.48. Experimental and Calculated results for R_T = 0.250, CI-SSL $\alpha = 7^\circ$ 268

6.49. Experimental and Calculated results for R_T = 0.375, NSOH-Br $\alpha = 15^\circ$ 269

		Page
6.50.	Experimental and Calculated results for R_T = 0.375, HCHC-Br α = 15°	269
6.51.	Experimental and Calculated results for R_T = 0.375, NSOH-AL α = 15°	270
6.52.	Experimental and Calculated results for R_T = 0.375, HCHC-AL α = 15°	270
6.53.	Experimental and Calculated results for R_T = 0.375, NSOH-Cu α = 15°	271
6.54.	Experimental and Calculated results for R_T = 0.375, HCHC-Cu α = 15°	271
6.55.	Experimental and Calculated results for R_T = 0.375, NSOH-SS α = 15°	272
6.56.	Experimental and Calculated results for R_T = 0.375, HCHC-SS α = 15°	272
6.57.	Experimental and Calculated results for R_T = 0.375, CI-Br α = 15°	273
6.58.	Experimental and Calculated results for R_T = 0.375, CI-AL α = 15°	273
6.59.	Experimental and Calculated results for R_T = 0.375, CI-Cu α = 15°	274
6.60.	Experimental and Calculated results for R_T = 0.375, CI-SS α = 15°	274
6.61.	Experimental and Calculated results for R_T = 0.375, NSOH-CuL α = 15°	275
6.62.	Experimental and Calculated results for R_T = 0.375, HCHC-CuL α = 15°	275
6.63.	Experimental and Calculated results for R_T = 0.375, NSOH-BrL α = 15°	276
6.64.	Experimental and Calculated results for R_T = 0.375, HCHC-BrL α = 15°	276
6.65.	Experimental and Calculated results for R_T = 0.375, NSOH-SSL α = 15°	277
6.66.	Experimental and Calculated results for R_T = 0.375, HCHC-SSL α = 15°	277
6.67.	Experimental and Calculated results for R_T = 0.375, NSOH-ALL α = 15°	278
6.68.	Experimental and Calculated results for R_T = 0.375, HCHC-ALL α = 15°	278

Page

6.69. Experimental and Calculated results for R_T = 0.375, CI-ALL α = 15° 279

6.70. Experimental and Calculated results for R_T = 0.375, CI-BrL α = 15° 279

6.71. Experimental and Calculated results for R_T = 0.375, CI-CuL α = 15° 280

6.72. Experimental and Calculated results for R_T = 0.375, CI-SSL α = 15° 280

6.73. Experimental and Calculated results for R_T = 0.250, NSOH-AL α = 15° 281

6.74. Experimental and Calculated results for R_T = 0.250, HCHC-AL α = 15° 281

6.75. Experimental and Calculated results for R_T = 0.250, NSOH-SS α = 15° 282

6.76. Experimental and Calculated results for R_T = 0.250, HCHC-SS α = 15° 282

6.77. Experimental and Calculated results for R_T = 0.250, NSOH-Br α = 15° 283

6.78. Experimental and Calculated results for R_T = 0.250, HCHC-Br α = 15° 283

6.79. Experimental and Calculated results for R_T = 0.250, NSOH-Cu α = 15° 284

6.80. Experimental and Calculated results for R_T = 0.250, HCHC-Cu α = 15° 284

6.81. Experimental and Calculated results for R_T = 0.250, CI-AL α = 15° 285

6.82. Experimental and Calculated results for R_T = 0.250, CI-Br α = 15° 285

6.83. Experimental and Calculated results for R_T = 0.250, CI-Cu α = 15° 286

6.84. Experimental and Calculated results for R_T = 0.250, CI-SS α = 15° 286

6.85. Experimental and Calculated results for R_T = 0.250, NSOH-CuL α = 15° 287

6.86. Experimental and Calculated results for R_T = 0.250, HCHC-CuL α = 15° 287

6.87. Experimental and Calculated results for R_T = 0.250, NSOH-BrL α = 15° 288

		Page
6.88.	Experimental and Calculated results for R_T = 0.250, HCHC-BrL α = 15°	288
6.89.	Experimental and Calculated results for R_T = 0.250, NSOH-ALL α = 15°	289
6.90.	Experimental and Calculated results for R_T = 0.250, HCHC-ALL α = 15°	289
6.91.	Experimental and Calculated results for R_T = 0.250, NSOH-SSL α = 15°	290
6.92.	Experimental and Calculated results for R_T = 0.250, HCHC-SSL α = 15°	290
6.93.	Experimental and Calculated results for R_T = 0.250, CI-ALL α = 15°	291
6.94.	Experimental and Calculated results for R_T = 0.250, CI-BrL α = 15°	291
6.95.	Experimental and Calculated results for R_T = 0.250, CI-CuL α = 15°	292
6.96.	Experimental and Calculated results for R_T = 0.250, CI-SSL α = 15°	292
6.97a.	Summary and Comparison of elemental coefficient of friction related to NSOH-Die, α = 7° and R_T = 0.375	90
6.97b.	Summary and Comparison of elemental coefficient of friction related to HCHC-Die, α = 7° and R_T = 0.375	90
9.97c.	Summary and Comparison of elemental coefficient of friction related to Cast Iron-Die, α = 7° and R_T = 0.375	91
6.98a.	Summary and Comparison of elemental coefficient of friction related to NSOH-Die, α = 7° and R_T = 0.250	92
6.98b.	Summary and Comparison of elemental coefficient of friction related to HCHC-Die, α = 7° and R_T = 0.250	92
6.98c.	Summary and Comparison of elemental coefficient of friction related to Cast Iron-Die, α = 7° and R_T = 0.250	93
6.99a	Summary and Comparison of elemental coefficient of friction related to NSOH-Die, α = 15° and R_T = 0.375	94
6.99b.	Summary and Comparison of elemental coefficient of friction related to HCHC-Die, α = 15° and R_T = 0.375	94
6.99c.	Summary and Comparison of elemental coefficient of friction related to Cast Iron-Die, α = 15° and R_T = 0.375	95
6.100a	Summary and Comparison of elemental coefficient of friction related to NSOH-Die, α = 15° and R_T = 0.250	96

		Page
6.100b.	Summary and Comparison of elemental coefficient of friction related to HCHC-Die, α = 15° and R_T = 0.250	96
6.100c.	Summary and Comparison of elemental coefficient of friction related to Cast Iron-Die, α = 15° and R_T = 0.250	97
6.101.	Summary and Comparison of significant values of coefficient of friction for R_T = 0.375.	98
6.102.	Summary and Comparison of significant values of coefficient of friction for R_T = 0.250	98
6.103.	Comparison of Upper Bound Calculated Results with Experimental results	104
7.01.	Calibration Results at R_e = 0.075	305
7.02.	Calibration Results at R_e = 0.150	305
7.03.	Calibration Results at R_e = 0.225	306
7.04.	Calibration Results at R_e = 0.300	306
7.05.	Calibration Results at R_e = 0.375	307
7.06 - 7.16.	Experimental results for the aluminium specimens drawn at various speeds with different lubricant through a total fractional reduction, R_T = 0.375 with 7° semi-angle	310-313
7.17.	Results Summary	121
8.01 - 8.03.	Elemental strains due to redundant deformation with the mean value ϵ_{eu}'s for the set of 15° semi-angle elemental dies	317-318
8.04.	Summary of the strains due to redundant deformation, ϵ_{eu} for the annealed Brass specimens.	318
8.05.	Strains due to redundant deformation ϵ_{eu} with their equivalent drawing forces F_{Deu} calculated from equation (8.8) with their corresponding redundant strains for aluminium alloy specimen	320
8.06	Strains due to redundant deformation ϵ_{eu} with their equivalent drawing forces F_{Deu} calculated from equation (8.8) with their corresponding redundant strains for copper specimen	320
8.07 - 8.11.	Elemental strains due to redundant deformation with the mean value, ϵ_{eu}'s for the st of 7° semi-angle elemental dies	321-323
8.12.	Summary of the strains due to redundant deformation ϵ_{eu} with their corresponding drawing forces F_{Deu} for the annealed brass	323

Page

8.13 - 8.14. Strains due to redundant deformation ϵ_{eu} with their equivalent drawing forces F_{Deu} calculated from equation (8.9) with their corresponding redundant strains for aluminium and copper specimens respectively 325

8.15 - 8.18. Strain readings at various points (3) during a pass of an aluminium tube specimen through a 15° semi-angle die assembly with 10 mm exit diameter. 326-329

8.19 - 8.22. Typical strain readings, ϵ_e's from data logger at one pass of an aluminium tube specimen through 15° semi-angle elemental die assembly. 330-332

8.23 - 8.28. Strain readings at various points (3) during a pass of a copper tube specimen through a 15° semi-angle die assembly with 10 mm exit diameter. 333-338

8.29 - 8.31.. Typical strain readings, ϵ_e's from data logger at one pass of a copper tube specimen through 15° semi-angle elemental die assembly 339-341

8.32 - 8.37. Strain readings at various points (5) during a pass of an aluminium tube specimen through a 7° semi-angle die assembly with 10 mm exit diameter. 342-347

8.38 - 8.39. Typical strain readings, ϵ_e's from data logger at one pass of an aluminium tube specimen through 7° semi-angle elemental die assembly. 348-349

8.40 - 8.46. Strain readings at various points (5) during a pass of a copper tube specimen through a 7° semi-angle die assembly with 10 mm exit diameter. 350-356

8.47 - 8.49. Typical strain readings, ϵ_e's from data logger at one pass of a copper tube specimen through 7° semi-angle elemental die assembly. 357-359

8.50 - 8.52. Relevant experimental results for the analysis of the experimental redundant deformation strains, ϵ_{re*}'s of aluminium specimens drawn through 15° semi-angle elemental dies assembly. 360

8.53 - 8.55. Relevant experimental results for the analysis of the experimental redundant deformation strains, ϵ_{re*}'s of copper specimens drawn through 15° semi-angle elemental dies assembly. 361

8.56 - 8.60. Relevant experimental results for the analysis of the experimental redundant deformation strains, ϵ_{re*}'s of aluminium specimens drawn through 7° semi-angle elemental dies assembly. 362-363

8.61 - 8.65. Relevant experimental results for the analysis of the experimental redundant deformation strains, ϵ_{re*}'s of copper specimens drawn through 7° semi-angle elemental dies assembly. 364-365

Page

8.66 - 8.68. Resulting data from further analysis of the results (strains and forces) related to each elemental die of the die assembly (α = 15° and aluminium specimen) 366

8.69 - 8.71. Resulting data from further analysis of the results (strains and forces) related to each elemental die of the die assembly (α = 15° and Copper specimen) 367

8.72 - 8.81. Resulting data from further analysis of the results related to each elemental die of the 7° semi-angle die assembly for both aluminium and copper respectively, 368-372

8.82. Summary of forces for Aluminium (α = 7°) 150

8.83. Summary of forces for Copper (α = 7°) 150

8.84. Summary of forces for Aluminium (α = 15°) 151

8.85. Summary of forces for Copper (α = 15°) 151

8.86. Summary of overall error of the proposed elemental die theory 152

8.87 - 8.90. Mean values of related results of aluminium and copper specimens passed through each element of the 7° and 15° semi-angle proto-dies respectively. 153-154

8.91. Summary of the proposed correcting factor, C_f, for tube sinking force equation. 373

8.92. Unacceptable contact strain data 374

8.93. Specimen print-out of reliable contact strains

ACKNOWLEDGEMENTS

I would like to express my sincere thanks to Professor G.T.S. Done, Head of the Department of Mechanical Engineering, and Dr.R.S. Neve, the Postgraduate Tutor for making it possible for me to carry out this study.

My sincere thanks go to Professor W.A. Penny for his original and expertise ideas, and for his skillful and sympathetic guidance through all the stages of this project.

I am deeply indebted to my supervisor, Dr.A. Jebb, Head of Manufacturing Division, for his patience, tactful guidance, frequent valuable advice, encouragement and for his moral support all the time.

My further sincere thanks also go to the technical staff of the Mechanical Engineering Department, particularly [redacted] the Chief Technician of the Manufacturing Division of the Mechanical Engineering Department; [redacted] for their technical assistance throughout the time I spent on this study.

I would also like to extend my thanks to Smiths' Industries for their financial support during my study.

Finally, I would like to express my grateful thanks to [redacted], who was responsible for the typing of this thesis.

CHAPTER 1

INTRODUCTION

1.11. Friction

Frictional resistance is a redundant energy which engineers continuously strive to reduce. Only very few engineering situations occur in which friction does not play some part. In some cases, it is gainfully employed, as in clamping devices, and friction drives. More frequently, it exists as an integral part of the situation merely because it cannot be eradicated, and results in the dissipation of energy and the gradual erosion of material from the component involved. This erosion of material, or wear, due to friction represents a substantial economic loss in engineering. Because of this, a considerable amount of research has been undertaken in recent years aimed at a greater understanding of the processes involved and the development by which it may be reduced.

Rubbing a metal shaft on a metal bearing is not realistic simply because of surface damage and eventually seizure of the components. A lubricant is used to separate the components and its beneficial role is to provide low friction which is essential for efficiency and economy. As the ceiling for speed and load is raised, the choice of materials to provide the friction couple and the use of suitable lubricant becomes the task of specialists.

The enormous waste of energy through friction resistance is obvious but we tend to ignore the beneficial role that friction plays in our day to day activities. If our feet or the soles of our shoes did not have a high friction as they grip the road surface, it would be impossible for us to stand firm. Typically, on clay-rich soil in the rainy season in Africa or on icy roads in Europe, this difficulty is ever present. If we had not been able to grip roads with our feet, our evolutionary behaviour would probably have been different as far as mobility is concerned. The ideal mode for a dynamic system such as an automobile is that it should have sliding or rolling interfaces completely free of friction, in practice, an interfacial friction must be present in order to bring it to rest. A brake shoe relies entirely on the presence of friction for its efficiency. Examples are many but it is clear that from the tribological point of view an understanding of friction is very important because of both its positive and damaging roles in the relative motion of components.

1.12. Historical Background of Friction

Even though there is little evidence of tribological practices in the early Stone Age, but we may still speculate that the first fires made by humans were created by using the heat of friction. In fact, usefulness of friction must have been known to primitive man because it would appear that he was aware of the fact that a spherical object will move more readily than a flat one. However, one does not know if the act of rubbing pieces of wood together to produce fire was

discovered by accident or from some vague notion that rubbing generates heat since in cold climates, human beings rub their hands habitually to produce warmth.

In later times to the Stone Age, hand or mouth held bearings were developed for the spindle of drills, which were used to bore holes and start fires. These bearings were often made of wood , or bone; their recorded use cover some four Millenia. Among the earliest made bearings are door sockets which were first made of wood or stone and later lined with copper, and potter's wheels, such as one unearthed in Jerico and dated at 2000 B.C. It contained traces of bitumen which might have been used as a lubricant.

1.13. Lubricant

One of the earliest recorded uses of a lubricant, probably water was for transportation of the statue of Ti, ca. 2400 B.C. Lubricants were probably used on bearings of chariots which first appeared, ca. 3500 B.C. A considerable development of tribology took place in Greece and Rome at the beginning of the fourth century B.C. during and after the time of Aristotle. Evidence of advanced lubrication practices during Roman times was provided by two pleasure boats that sank in Lake Nemi in Italy, ca. A.D.50; they contained what might be considered prototypes of three kinds of modern rolling-element bearings. The Middle Ages saw a further improvement in the application of tribological principles, as evidenced by the development of machinery such as water mills.

1.14. History of Tubular Products

Tubular products are used over a wide range of industries and sciences in modern civilisation. The ability to constrain fluids and efficient structural properties of tubular section, permit a vast range of applications.

The existence of tubular products can be traced back to the history of ancient Egypt. In fact, evidence of such an early employment of tubular products even in metal can be seen from photographs of an ancient Egyptian copper water pipe dating from 2750 B.C. An example is illustrated in reference [2] of a tube approximately 75 mm inside diameter and 300 mm long. However, in spite of this use of tubular products, the rapid advances in tubular products did not take off until the 18th and 19th centuries, especially following the development of processes for producing hollows from which seamless tubes could be produced. Among the materials widely used during this development were wood, iron, stone, copper and lead.

1.15. Wooden Tubes

Wooden tubes were being produced all over the world at small expense. They were easily made, and joined together, but the greatest objection was their lack of strength to resist high pressure without breaking and their liability to decay. For water-works they were usually made from elm, or alder; oak, though far preferable, being too expensive.

They were best made from small trees of the proper size; and the bark thought to preserve them was left on [1]. The passage was bored out by a long auger, turned round by one or two men whilst the tree was supported in a convenient position on trestles, and bound fast down upon them by ropes to which weights were attached. In towns where water-works were established the demand for tubular products was such as to render this method too expensive and machines were used to bore them, driven by horses, water or steam engines. One of the early patents went to Eckhardt and Lyon in 1806 for a method of making wooden pipes by separate staves, resembling a barrel, but less curvature and greater proportional length, so as to approach near to a cylindrical form, particularly inside. They were to be bound by iron hoops, made fast either by driving them on from the ends, or by screwing the hoops together; the lengths were joined together by forming one end of each taper and enlarging the corresponding ends of others to receive them. The staves were to be fitted by torque, rabbiting, or dove-tailing. However, the Eckhardt and Lyon methods were not practised to a large extent because they were very expensive, being accompanied by all defects of wood tubes and were liable to speedy decay buried in the ground.

1.16. Iron Tubes

Iron tubes or pipes were cast at the iron-founderies to a wide range of dimensions. For durability and strength combined were greatly superior to any other material. They were procured in lengths of ten feet and united by nuts and screws passed through

flanges cast on their ends. Within a few years, cast-iron pipes were adopted by most of the great companies which supplied London water. However, within these few years, immense quantities of iron tubes had been laid in all parts of London for conveyance of water. Great prejudices were excited against them, under the idea that they would give the water a metallic taste which would be injurious to health of the inhabitants.

1.17. Stone Tubes

The prejudice the public at first entertained against iron tubes induced many projectors to find out other substances which possessed the strength and durability of metal. Sir George Wright proposed stone and invented a machine for cutting out cones from the hollow of the tube. Sir George first employed a boring or drilling machine to pierce a small hole through the centre of the block of stone in the axis of the intended pipe. Sir George obtained a patent for his invention in 1805 and his method was widely practiced for some time and many large stone pipes were laid but unfortunately great difficulties arose in making good joints [1].

1.18. Modern Manufacture of Tubular Products

The methods of tube manufacture continue to develop in two basic forms, namely, seamed and seamless.

1.19. Seamed Tube

Seamed tube is manufactured by the forming of sheet or strip and the application of a joining process. Present techniques include:

i) Forming strip of suitable width around a mandrel using form rollers and seaming by welding.

ii) Drawing through a bell shaped die and seamed in the axial direction by welding. Dies have been so shaped and the material characteristics selected such that butt welds are achieved during the drawing process.

iii) Strip wound on a mandrel in helical form and seamed by welding.

1.20. Seamless Tube

Seamless tube is produced either by rolling, casting, extrusion or drawing. The rolling, extrusion and drawing processes are initiated from hollows produced by piercing billets and continued by various methods of plastic deformation. Some of the methods of manufacture are described briefly as follows:

(i) Rolling Process:

Well developed techniques such as the Mannesmann and Assel processes use rolls with axes which are inclined obliquely relative to both each other and the workpiece. The workpiece is plastically deformed by being subjected to combined rotary and axial force relative to a piercing tool or mandrel. The Mannesmann process is used to pierce billets and produce seamless

hollows. The Assel process is used to provide elongation [21]. Also see Figures (1.1), (1.2) and (1.3) reference [22].

(ii) Drawing with a fixed mandrel or plug:

Drawing through a die with mandrel or plug positioned in the internal diameter. This process is used for simultaneous control of external and internal diameters, Figure (1.4b), reference [13].

(iii) Drawing with a floating plug:

Drawing through a die with a shaped plug retained in position relative to external diameter and die entrance by frictional forces, see Figure (1.4c), reference [13].

(iv) Drawing with a moving mandrel:

Drawing through a die with moving mandrel in the internal diameter such that it travels at approximately the same velocity as the drawn tube. The frictional resistance at the mandrel-tube interface is in the opposite direction to the frictional resistance at the die-workpiece interface, thus reducing the drawing force required due to frictional resistance. One disadvantage which can arise is the difficulty in removing the mandrel, see Figure (1.4a), reference [13].

(v) Expanding:

A conical plug is drawn through the tube, thus causing the internal diameter to be expanded. This process is used where the inside diameter is required to be precise and for tubes of large diameter and thin walls, see Figure (1.5), reference [13].

(v) Other methods:

Include rotating roller dies (usually for non-circular tube) and rotating ball dies which it is desirable to reduce drawing stress.

In all cases, tube drawing is initiated from hollows produced by piercing billets using hot rolling or from hollows produced by rolling and seaming.

CHAPTER 2

2.11. Objective of this Study

In the process of inward and outward plastic-elastic bending of a tube workpiece at both entrance and exit of a conical die respectively there is a considerable internal shear distortion of the workpiece in excess of that required to produce the desired change of shape, i.e. from D_1 at entrance to D_2 at the exit from the die. Energy is therefore dissipated in producing this shear deformation, which makes no useful contribution in effecting the desired change of shape. A number of methods for making an allowance for the drawing stress of this wasteful phenomenon, termed redundant deformation, have been proposed. Most are based upon velocity fields and shearing which assume either a thinning of the material during passage through the die, or a thickening of the material at the die entrance, followed by thinning at the die exit. Neither of these assumptions appear to be applicable from the evidence of experiment. Clarke and Swift showed by experiment [20] that bending occurred at die entrance and die exit. The proposed method for making allowance for redundant deformation in tube sinking thin walled tube made by Penny [12] appeared to have reduced the risk of under-estimation of total drawing force of a tube drastically. However, in the absence of experimental data to support either Penny's proposed theory or the bar drawing redundant deformation theory on which Penny based his proposed method, the scepticism on the validity of Penny's method remains.

In addition to uncertainty on the accuracy of redundant deformation theory, another fundamental weakness of the basic drawing force equation is lack of appropriate method of determining the values of coefficient of friction μ for various materials, die-configurations and tribological conditions. Several attempts were made by previous workers, working on the tube sinking process to develop a method of estimating μ but their theories were in marked disagreement over die radial pressure. It has been assumed that the frictional stress, τ, at die-tube interface cannot be greater than yield shear stress at the interface, i.e. $\tau = \mu p \leqslant k$, where p is the absolute radial pressure, and k is the yield stress in shear. Apart from the fact that the values of μ attained from this assumption does not define the profile of the coefficient of friction across a die-pass there has been doubt on the validity of the upper bound values of μ attained from the upper bound hypothesis based on plain strain theory, which is far from an ideal tube sinking process. Therefore the objects of this study include:

1) To devise an experimental method for proving and for accurate assessment of redundant deformation due to plastic-elastic deformation at the die entrance and the die exit respectively.

2) To observe differences between the redundant work at the entrance and exit of a conical die.

3) To determine a theoretical and an experimental method for the accurate assessment and analysis of the coefficient of friction at die-workpiece interface across the pass of a conical die.

4) To determine accurately values of the coefficient of friction required for accurate estimates of the total drawing force.

5) To determine the effect of die half-angle, α, tribological treatment, die materials and tube materials on the values of coefficient of friction.

6) To compare wherever possible the theoretical and experimental results of the study with the results of previous work.

7) To add the contents of this study to the existing knowledge of tubing sinking process and to identify the specific areas of work for further studies.

2.12. Review of Previous Work

2.13. Theories

Theories have been developed to estimate the stresses and strains which occur during the tube sinking process and methods have been proposed by a number of workers for estimating drawing stress for a given fractional reduction which are applicable to drawing thin walled tubes through straight conical dies. The theories proposed to date are based upon either differential equations of equilibrium or upper bound methods.

2.14. Differential Equations of Equilibrium

Sachs and Baldwin proposed a method based upon differential equations of equilibrium which make allowance for homogeneous deformation and frictional resistance. When verified by experiment, it was shown to provide a method from which estimates could be made of drawing stress for a given fractional reduction with accuracy adequate for most manufacturing purposes [5], [6]. For a method of deriving the equations for drawing stress and, hence, drawing force for a given fractional reduction, see reference [13]. Derivation of these equations is shown in an abbreviated form in Chapter 3.

The theory is based upon the following assumptions:

i) that a pressure normal to the die and workpiece interface operates on both die and workpiece.
ii) that friction at the interface causes a shear stress.
iii) that transverse sections are free of shear stresses.
iv) that the stress in a transverse section is uniformly distributed and is a principal stress.
v) that wall thickness remains constant.

2.15. Epsey and Sachs - Drawing with Moving Mandrel

Initially, Epsey and Sachs carried out their test on an almost constant stress flow material (no strain hardening) notably a cartridge brass (70 percent copper and 30 percent zinc) tube. They

later did further tests on commercially annealed cartridge brass tubing of the same dimensions as earlier material and finally extended their test onto a commercial annealed 0.02% carbon steel of about 13.87 mm outside diameter and 1.18 mm wall thickness. Having carried out similar tests with variations in mandrel diameter, angle of tapered dies, and variations in specimen material, Epsey and Sachs were able to show that tube drawing with moving mandrel can still be analysed in much the same manner as other forming processes in general and other drawing processes in particular [8].

Epsey and Sachs were able to show that friction coefficients derived in their analysis were relatively small compared with ones in the previous analysis and the reasons for the lower values, better coefficients of friction were attributed to the particular attention which they paid to polishing of the tools, preparation of the metal surfaces and also special selection of lubricant.

2.16. Upper Bound Estimates

The method of obtaining an upper bound estimate of drawing stress using kinematically admissible velocity field as proposed by Johnson [17] has been shown to be applicable to tube sinking by Moore and Wallace [5]. This assumes plain strain (no change in wall thickness) and provides an upper bound estimate. The concept is based upon development of an element of a conical surface such that plain strain is applicable. Lines of velocity discontinuity are then proposed whereby the work done is plastically deforming the element is

minimised. By considering a perfectly smooth and non-strain hardening material, an upper bound estimate for frictionless may be obtained.

Moore and Wallace also show that an upper bound estimate of drawing stress with allowance for friction can be obtained by deriving an expression for work done against friction between the workpiece and die face. This produces a factor by which the frictionless drawing stress can be multiplied to obtain an upper bound estimate with allowance for friction [11]. Both of these methods have been verified and show correlation between estimates and experiments which are adequate for most manufacturing process purposes [7].

Avitzur proposes a theory which is based upon an increase in wall thickness at the die entrance and a decrease in wall thickness at the die exit [18]. This arises from the consideration of velocity fields within the external and internal surfaces of a tube formed by two cones with apexes at a common point. This theory makes allowance for deformation which occurs at die entrance and die exit. Application of this theory to data from work published previously does not appear to show good correlation with experimental results.

2.17. Blazynski and Cole

With the use of Von Mises Criterion, Knights' empirical expression and Sachs' equation, in 1959 Blazynski and Cole were able

to show through the results of their experimental and theoretical investigation on plug drawing process that sinking has a considerable adverse effect on the magnitude of the redundant work and should therefore, where possible, be avoided. From their experimental and calculated results it was shown that mathematical formulae can be used successfully for the purpose of predicting the behaviour of a metal during plug drawing [9].

2.18. Wall thickness

Hill showed the relationship between wall thickness and fractional reduction in diameter [19].

Swift [10] and Moore and Wallace [11] have predicted wall thickness changes.

Swift's analysis was based upon assumptions that $D_o >> t_o$ and concluded that errors involved by neglecting thickness changes in stress calculations are remarkably small over the useful range of fractional reduction.

Moore and Wallace in their considerations included an effect due to the ratio of initial wall thickness to external diameter. They predicted that wall thickness increases with fractional reduction up to 0.5 and thinning occurs beyond this.

However, experimental evidence exists to suggest that thickening may occur in thin wall tube up to a fractional reduction of 1.0 [14].

The theory proposed by Moore and Wallace for the effect of strain hardening of the workpiece upon wall thickness changes, tends to agree with experiment. The effects of strain rate and temperature rise are neglected.

2.19. Flinn

Another prominent worker on wall thickness is J.E.Flinn of the Metallurgical Department, Washington State University. He did some experimental work on the parameters which influence the changes in the wall thickness and on the bulk strain behaviour of hollow drawn tubing. Flinn prepared his specimens from six different materials of commercial purity. Specimens of each material possessed various ratio wall to the tubes outer radius values and in some cases different outer diameters. The highly polished tungsten carbide drawing die used by Flinn possessed a conical geometry with die angles of 8 and 15 degrees.

From Flinn's experimental results, he was able to conclude that thick-wall tubes thin, and thin-wall tubes thicken with reducton. He concluded that alloying or material, die angle, and initial wall thickness were the influential parameters on wall thickness changes in tube drawing, that the reduction per pass or magnitude of draft had only negligible effect [14].

2.20. Others

At the same time as Flinn's experimental work on tube drawing, S.K. Misra, a senior research metallurgist and N.H. Polakowski, a Professor of the Metallurgical Department of Illinois Institute of Technology, directed their experimental work toward the development of a means for in-process control of residual stress during tube sinking. 304 and 321 stainless steels, Incoloy 800 and copper tubes were the main materials employed by Misra and Polakowski for their experiments.

All the three main classical methods (mandrel, plug, drawing and sinking) were used for their experiments. On their hydraulic drawbench was a bolster plate equipped with a holder which accommodates two dies in tandem, spaced 12.5 mm apart to provide a lubricant pocket for the second die. Strain gauge cells were used to measure drawing forces.

Misra and Polakowski demonstrated in their experiments that drastic in-process modifications of the residual stress patterns left in tubing after conventional drawing are possible in many important cases, by means of a second, low-reduction, or "skim-pass" die. They claimed that the effect was amplified when the normally cylindrical bearing portion of the die is given a slight taper form . Also in their conclusions, they claimed that the reorganisation of the stress is most pronounced in mandrel-drawn tubes where it results in

a large reduction of the pressure between the reduced tube and the mandrel inside it. This in turn lowers the reeling pressure required to free the mandrel for extraction, an effect that might be useful in the fabrication of low-ductility crack-prone tubing.

2.21. Folding Phenomenon

Prior to Epsey and Sachs experimental work on tube drawing with a moving mandrel, Sachs has done some experimental work with Lincus on the properties of drawn wire and on power consumption in wire drawing in Berlin around 1931; has also worked with Klinger on the flow of metal through tools of circular contour. He also then did some investigations with Baldwin into folding phenomenon in tube sinking.

For the analysis of folding, four different materials which included hard phosphorus deoxidised copper (Rockwell 30-T, 59-66); soft phosphorus-deoxidised copper (annealed 1 hour at 485°C in a forced convection furnace); soft tube brass (66.5 copper, 5% lead, balance zinc, annealed 1 hour at about 485°C); and soft aluminium (25, annealed 15 minutes at 285°C) were employed.

Baldwin and Sachs drew the tube specimens of approximately 980 mm long through three different sets of conical steel dies with half-die angles of 7°, 14° and 27° respectively. They imposed two types of points (folded point and a fold free point) on the tube.

They observed during their experimental work that it was impossible to collapse any tube with a fold-free point because the circular contour appeared to be highly resistible to buckling, even in tubes with thinnest wall and subjected to the maximum possible fractional reduction. However, it was emphasised that such fold-free tubes are only attainable if the tubing is free from any form of dents and seams. It was also observed that any lubricant entrapped between the die and tube surface resulted in folding.

Baldwin and Sachs concluded that the results of their investigation cannot be harmonised with conventional theory of buckling and collapsing. They claimed that the factors which determine the existence or elimination respectively of a fold in tube sinking are different from those which determine definite buckling phenomena, such as the collapsing of a tube. Baldwin and Sachs also made it clear in their conclusions that apart from small thickness-to-diameter ratio which is a conducive factor to both folding and collapsing formation, other factors, such as length along which pressure is applied, elasticity and plasticity of the metal, which play significant roles in collapsing, have very negligible influence in folding [16].

2.22. Redundant Deformation

Deformation occurs at the die entrance and die exit due to bending and unbending respectively. This deformation occurs in addition to that required to change the form of the workpiece from the initial to the final form.

A number of methods for making an allowance of drawing due to redundant deformation have been proposed. Most are based upon velocity fields and shearing which assume either a thinning of the material during passage through the die, or a thickening of the material at the die entrance followed by thinning at the die exit.

Neither of these assumptions appear to be applicable from the evidence of experiment. Clarke and Swift [20] showed by experiment that bending occurred at die entrance and die exit. Penny proposed a method of making an allowance for redundant deformation in 1977. Penny's theory which we have employed in this research work was based upon a method proposed for bar drawing [12].

CHAPTER 3

THEORY OF TUBE SINKING THROUGH A CONICAL DIE

The sinking of a thin-walled tube through a conical die of semi-angle, to reduce the mean diameter $D_1 = 2R_1$ to $D_2 = 2R_2$, is illustrated in Figure 3.1(a)

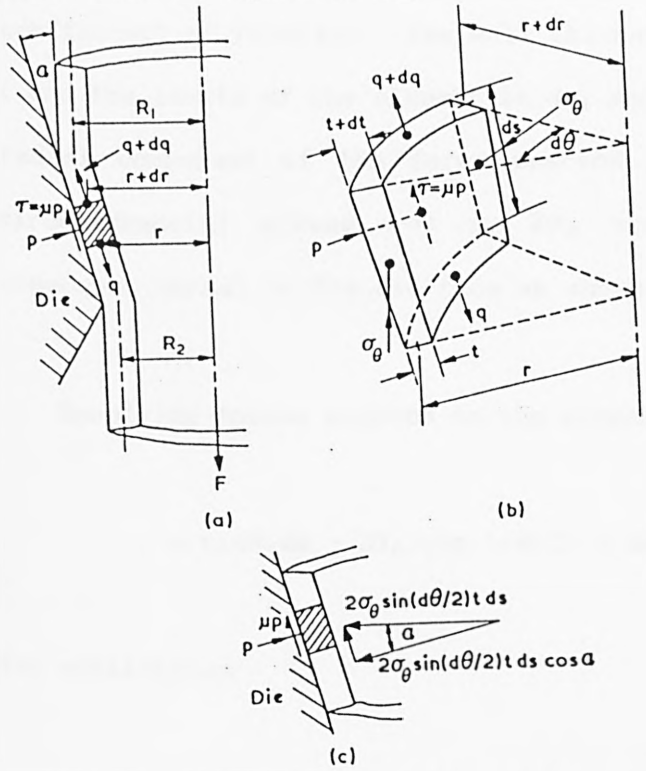

Figure 3.1

[after Slater [13]]

Fig.3.1. (a) Tube sinking through a conical die;
(b) Stress acting on an element of the tube;
(c) Component of the radial force due to circumferential stress, σ_θ exerted on the element in direction normal to the die face.

Assumptions:

(i) The wall of the tube is thin at any section compared with the diameter so that the effect of plastic bending is negligible and the variation in stress across the wall of the tube is insignificant.

(ii) Each part of the tube is subjected to the same deformation as it passes through the die, and

(iii) The length of the tube is such that steady deformation is established.

At any mean radius, r, within the die, the stresses acting on an element are as shown in Figure 3.1(b) where q is the longitudinal stress, that is the stress parallel to the die face, σ_θ is the circumferential stress, p is the normal die pressure and the frictional stress at the tube-die interface is $\tau = \mu p$ where μ is the coefficient of friction. The wall thickness at any mean radius r, is t and the length of the element is ds, parallel to the die face. The radial component of the force exerted on the element due to the circumferential stress, $\sigma\theta$ is $2\sigma_\theta \sin (d\theta/2)tds$, which has a component normal to the die face as shown in Figure 3.1(c).

Resolving forces exerted on the element normal to the die face:

$$p.r.d\theta.ds - 2\sigma_\theta \sin (d\theta/2).t.ds.\cos\alpha = 0 \qquad (1)$$

for equilibrium:

$$p.r.d\theta.ds - \sigma_\theta.d\theta.t.ds.\cos\alpha = 0$$

Therefore:

$$p = \sigma_\theta \cos\alpha/r \qquad (2)$$

Resolving forces exerted on the element parallel to the die face:

$$(q + dq)(r + dr)(t + dt)d\theta - q.r.d\theta.t + 2\sigma_\theta \sin(d\theta/2).t.ds.\sin\alpha + \mu p.r.d\theta.ds = 0 \qquad (3)$$

Simplifying and neglecting small quantities of the second order and dividing by $d\theta.dr$, equation (3) reduces to:

$$r.t.(dq/dr) + q.t.(dr/dr) + q.r(dt/dr) + \sigma_\theta.t + \mu.p.r/\sin\alpha = 0$$

Substituting for p from equation (2) gives:

$$r.t.(dq/dr) + q.t.(dr./dr) + q.r(dt/dr) + \sigma_\theta.t + \mu\sigma_\theta.t.\cot\alpha = 0$$

or

$$\{d(q.r.t)/dr\} + \sigma_\theta.t(1 - \mu\cot\alpha) = 0 \qquad (4)$$

Equation (4) is the differential equation of equilibrium for tube sinking. However, if the variation of tube wall thickness is negligible then $dt/dr \to 0$ and equation (4) therefore becomes:

$$r(dq/dr) + q + \sigma_\theta(1 - \mu\cot\alpha) = 0$$

or

$$r(dq/dr) + q + \sigma_\theta(1 + B) = 0 \qquad (5)$$

where $B = \mu\cot\alpha$.

For a thin-wall tube, $(t\cos\alpha/r)$ will be small compared with the circumferential stress, σ_θ.

Therefore:

$$q \gtrsim (p \to 0) \gtrsim \sigma_\theta$$

since q is tensile and considered as positive, then σ_θ is compressive and therefore negative.

The modified Tresca yield criterion gives:

$$q - (-\sigma_\theta) = m\bar{y} \text{ for a strain hardening material.} \qquad (6)$$

or

$$\sigma_\theta = m\bar{y} - q \qquad (7)$$

where m = 1.1 and $\bar{y}$ is the mean yield stress for a strain hardening material.

Combining equations (5) and (7) yields:

$$r(dq/dr) + q + (m.\bar{y} - q)(1 + B) = 0$$

or

$$r(dq/dr) - Bq + m\bar{y}\,(1 + B) = 0$$

Therefore:

$$dq/\{Bq - m\bar{y}(1 + B)\} = dr/r \qquad (8)$$

$$\int dq\{Bq - m\bar{y}(1 + B)\} = \int dr/r$$

Therefore:

$$(1/B)\ell n(Bq + C) = \ell nr + \ell nA$$

where $C = - m\bar{y}(1 + B)$

and ℓnA is a constant of integration.

Hence $(Bq + C)^{\frac{1}{B}} = rA.$

At the entrance to the die, where $r = R_1 = D_1/2$, $q = q_1 = 0$

Therefore:

$$C^{\frac{1}{B}} = R_1 A$$

or

$$A = C^{\frac{1}{B}}/R_1$$

Hence $(Bq + C)^{\frac{1}{B}} = (r/R_1)C^{\frac{1}{B}}$

$$Bq + C = (r/R_1)^B.C$$

Therefore

$$q = (C/B)\{(r/R_1)\}^B - 1\}$$

or

$$q = m\bar{v}\{(1 + B)/B\}\{1 - (r/R_1)^B\} \qquad (9)$$

At exit from the die where $r = R_2 = D_2/2$, $q = q_2$ the longitudinal stress parallel to the die face is:

$$q_2 = m\bar{v}\{(1 + B)/B\}\{1 = (R_2/R_1)^B\}$$

or

$$q_2 = m\bar{v}.\ (1 + B/B)\{1 - (D_2/D_1)^B\} \qquad (10)$$

The drawing stress σ_d in the axial direction is:

$$\sigma_d = q_2/\cos\alpha$$

Therefore:

$$\sigma_d = \{m\bar{y}/\cos\alpha\}\{(1 + B)/B\}\{1 - (D_2/D_1)^B\} \qquad (11)$$

Since the area of the drawn tube is given approximately by $\pi.D_2.t$, then the drawing force, F_d required in the axial direction is given by:

$$F_d = \{q_2.\pi.D_2.t\}/\cos\alpha$$

i.e.

$$F_d = \left\{\frac{\pi.D_2.t.m.\bar{y}}{\cos\alpha}\right\}\left\{\frac{1 + B}{B}\right\}\left\{1 - \left[\frac{D_2}{D_1}\right]\right\}^B$$

or

$$F_d = \left\{\frac{\pi.D_2.t.m.\bar{y}}{\cos\alpha}\right\}\left\{\frac{1 + \mu\cot\alpha}{\mu\cot\alpha}\right\}\left\{1 - \left[\frac{D_2}{D_1}\right]^{\mu\cot\alpha}\right\} \qquad (12)$$

3.11. Method of Making Allowance for Drawing Stress Due to Redundant Deformation in Tube Sinking Process [by Penny]

Having shown by Slater [3] that in the drawing of a bar through a conical die, the drawing stress due to redundant deformation is given by:

$$\sigma_{red} = 2\bar{y}\alpha/3 \qquad (13)$$

Penny then proposed that the drawing force due to redundant

TYPICAL THEORETICAL CURVES OF DRAWING STRESS AGAINST FRACTIONAL REDUCTION SHOWING ALLOWANCES FOR FRICTION AND REDUNDAN DEFORMATION
[$\alpha = 7^{\circ}$; $\mu = 0.2$, and $\bar{y} = 300$ MPa]

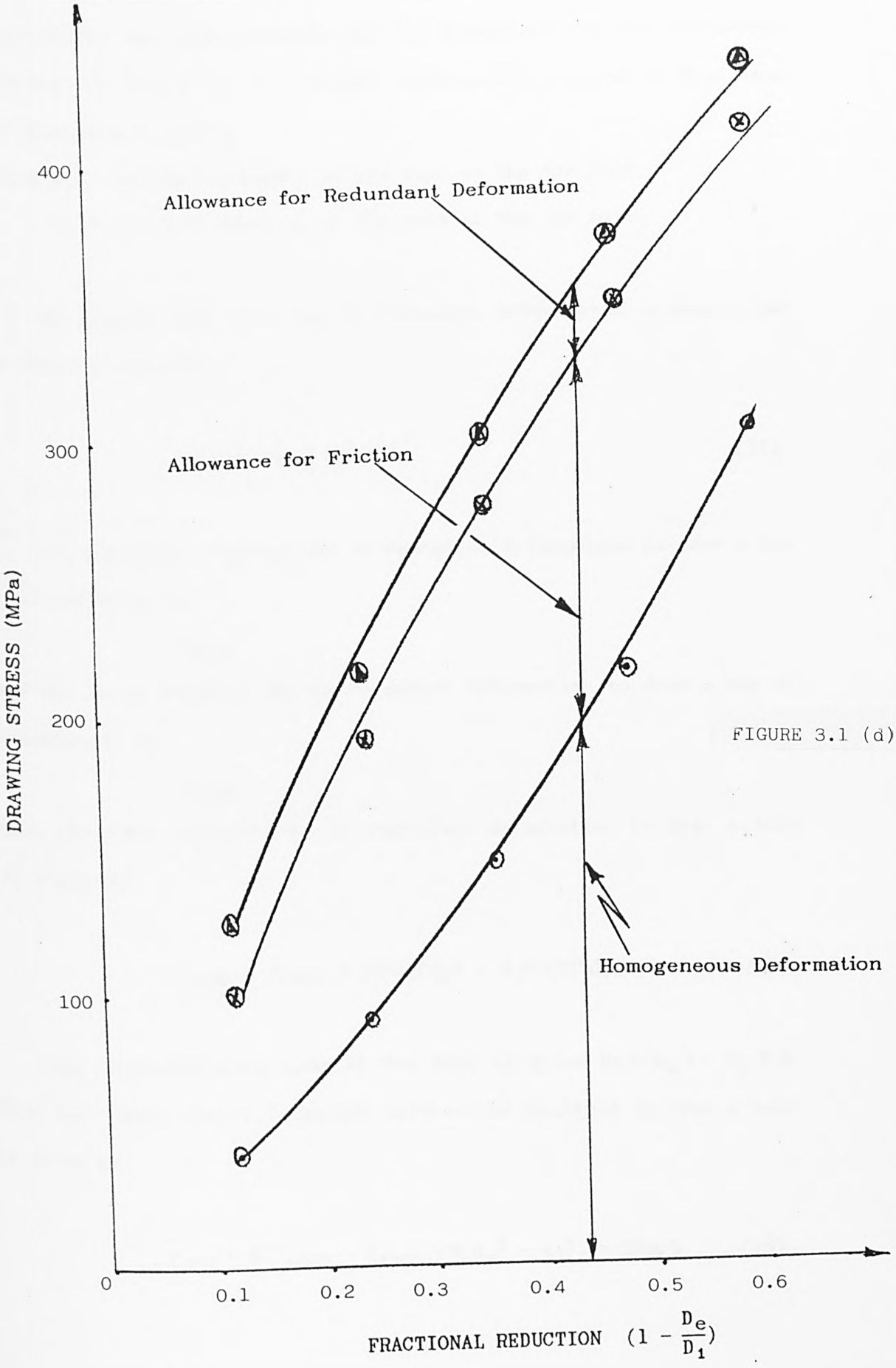

FIGURE 3.1 (d)

deformation for tube drawing may be considered as the difference between the forces due to redundant deformation required to draw bars of diameters d_e and d_i

where d_e = external diameter of the tube at the die exit,

d_i = internal diameter of the tube at the die exit.

Let F_{red} be the force due to redundant deformation to draw a bar of diameter d, then:

$$F_{red} \approx (\sigma_{red}\, \pi d^2)/4 \qquad (14)$$

Let the force required due to redundant deformation to draw a bar of diameter d_e be

$$F_{rede}$$

and the force required due to redundant deformation to draw a bar of diameter d_i be

$$F_{redi}$$

then the force required due to redundant deformation to draw a tube is given by:

$$F_{rede} - F_{redi} \approx (\pi/4)(d_e^2 - d_i^2)(2\bar{y}\alpha)/3 \qquad (15)$$

The cross-sectional area of the tube is given by $\pi(d_e^2 - d_i^2)/4$ thus the stress due to redundant deformation required to draw a tube is given by:

$$\sigma_{red} = 4(F_{rede} - F_{redi})/\pi(d_e^2 - d_i^2) = 2\bar{y}\alpha/3 \qquad (16)$$

The total force required due to redundant deformation to draw a tube is then given by:

$$F_{dT} \approx \left\{\frac{\pi D_2 t m \bar{y}}{\cos\alpha}\right\}\left\{\frac{1 + \mu\cot\alpha}{\mu\cot\alpha}\right\}\left\{1 - \left[\frac{D_2}{D_1}\right]^{\mu\cot\alpha}\right\} + \frac{2\pi D_1 t \bar{y}}{3} \qquad (17)$$

3.12. A Proposed Elemental Die Theory for the Analysis of Coefficient of Friction Across the Working Face and for the Analysis of Redundant Deformation at the Entry and Exit of a Typical Conical Die.

Equation (17) only estimates the total drawing force through a conical die but it does not show the distribution of the drawing force across the die pass, L_w and more importantly the value of coefficient of friction μ is the upper bound value which exists at the die exit.

Therefore, it is proposed that a typical conical die in Figure 3.2(a) can be divided into a number of elemental dies with elemental die pass, ℓ_e, and be used individually and progressively to draw a thin wall tube until the total fractional reduction achievable through the use of the typical conical die in Figure 3.2(b) is achieved.

$$L_w = \frac{R_1 - R_2}{\sin\alpha} = \frac{(D_1/2) - (D_2/2)}{\sin\alpha} \qquad (18)$$

$$\therefore \ell_e = \frac{(R_1 - R_2)/\sin\alpha}{n} = \frac{L_w}{n} \qquad (19)$$

where n is the number of equal elemental dies.

For an elemental die, equation (17) can be re-written as:

$$F_{Deu} = \frac{\pi D_{e2} t_1 m \bar{y}}{\cos\alpha} \left\{\frac{1 + \mu_e \cot\alpha}{\mu_e \cot\alpha}\right\}\left\{1 - \left[\frac{D_{e2}}{D_{e1}}\right]^{\mu_e \cot\alpha} + \frac{2\pi D_{e1} t \bar{y}\alpha}{3}\right. \quad (20)$$

where F_{Deu} is the uncorrected measured elemental drawing force (i.e. elemental drawing force with a full elemental redundant deformation).

Then:

$$F_{De} = F_{Deu} - R_{De} \quad (21)$$

where F_{De} is the corrected elemental drawing force and R_{De} is the elemental redundant deformation.

Assuming:

$$\Sigma F_{De} = F_{dT}$$

i.e. $F_{De1} + F_{De2} + F_{De3} + F_{De4} + \ldots\ldots + F_{Den} = F_{dT}$

then for a typical conical die represented by a set of elemental dies of n number to be used individually and progressively to draw a thin wall tube until the final reduction is achieved, equation (17) can be re-written as:

$$F_{dT} = \left[\left\{\frac{\pi D_{e21} t m \bar{y}}{\cos\alpha}\right\}\left\{\frac{1 + \mu_{e1}\cot\alpha}{\mu_{e1}\cot\alpha}\right\}\left\{1 + \left[\frac{D_{e21}}{D_{e11}}\right]^{\mu_{e1}\cot\alpha}\right\} + \left\{\frac{\pi D_{e11} t \bar{y}\alpha}{3}\right\}\right]$$

$$+ \left[\left\{\frac{\pi D_{e22} t m \bar{y}}{\cos\alpha}\right\}\left\{\frac{1 + \mu_{e2}\cot\alpha}{\mu_{e2}\cot\alpha}\right\}\left\{1 - \left[\frac{D_{e22}}{D_{e12}}\right]^{\mu_{e1}\cot\alpha}\right\} \pm \left\{\frac{2\pi D_{e12} t \bar{y}\alpha}{3}\right\}\right]$$

$$+\left[\left\{\frac{\pi D_{e23} t m \bar{y}}{\cos\alpha}\right\}\left\{\frac{1+\mu_{e3}\cot\alpha}{\mu_{e3}\cot\alpha}\right\}\left\{1-\left(\frac{D_{e23}}{D_{e13}}\right)^{\mu_{e3}\cot\alpha}\right\} \pm \left\{\frac{2\pi D_{e13} t \bar{y}\alpha}{3}\right\}\right]$$

$$+\left[\left\{\frac{\pi D_{e24} t m \bar{y}}{\cos\alpha}\right\}\left\{\frac{1+\mu_{e4}\cot\alpha}{\mu_{e4}\cot\alpha}\right\}\left\{1-\left(\frac{D_{e24}}{D_{e14}}\right)^{\mu_{e4}\cot\alpha}\right\} \pm \left\{\frac{2\pi D_{e14} t \bar{y}\alpha}{3}\right\}\right]$$

$$+.....+.....+$$

$$+.....+.....+$$

$$+\left[\left\{\frac{\pi D_{e2n} t m \bar{y}}{\cos\alpha}\right\}\left\{\frac{1+\mu_{en}\cot\alpha}{\mu_{en}\cot\alpha}\right\}\left\{1-\left(\frac{D_{e2n}}{D_{e1n}}\right)^{\mu_{en}\cot\alpha}\right\} + \left\{\frac{\pi D_{e1n} t \bar{y}\alpha}{3}\right\}\right] \quad (22)$$

where:

D_{e21} and D_{e11} = mean entry and exit diameters of the first elemental die of the set respectively.

D_{e2n} and D_{e1n} = mean entry and exit diameters of the last elemental die of the set respectively.

μ_{e1}, μ_{e2}, μ_{en} = the coefficient of friction of elemental dies or instantaneous coefficient of friction along the working face of the typical conical die during a pass of a tube specimen.

$\bar{y}$ = mean yield stress (but instantaneous yield stress, y_{en} values are called for the tubing materials (e.g.) stainless steel) with very large differences between the initial value of the yield stress at die entry and the yield stress value at the exit of the die during the drawing of the tube.

Alternatively, the short-hand form of equation (2) can be re-written as:

$$F_{dT} = \left[\left\{F_{Deu1} - \frac{R_{De1}}{2}\right\} + \left\{F_{Deu2} \overset{**}{-} R_{De2}\right\} + \left\{F_{Deu3} \overset{**}{-} R_{De3}\right\} + \left\{F_{Deu4} - R_{De4}\right\} + \ldots\ldots + \ldots\ldots\ldots + \ldots\ldots\ldots + \left\{F_{Deun} - \frac{R_{Den}}{2}\right\}\right] \quad (23)$$

However, when the elemental dies are assembled together as shown in Figure 3.2(c) to form a proto-type die, then the intermediate redundant deformation terms in equation (22) become zero, i.e.:

$$F_{dT} = \left[\left\{\frac{\pi D_{e21} t m \bar{y}}{\cos\alpha}\right\}\left\{\frac{1 + \mu_{e1}\cot\alpha}{\mu_{e1}\cot\alpha}\right\}\left\{1 - \left(\frac{D_{e21}}{D_{e11}}\right)^{\mu_{e1}\cot\alpha}\right\} + \left\{\frac{\pi D_{e11} t \bar{y}\alpha}{3}\right\}\right]$$

$$+ \left[\left\{\frac{\pi D_{e22} t m \bar{y}}{\cos\alpha}\right\}\left\{\frac{1 + \mu_{e2}\cot\alpha}{\mu_{e2}\cot\alpha}\right\}\left\{1 - \left(\frac{D_{e22}}{D_{e12}}\right)^{\mu_{e2}\cot\alpha}\right\}\right] +$$

$$+ \left[\left\{\frac{\pi D_{e23} t m \bar{y}}{\cos\alpha}\right\}\left\{\frac{1 + \mu_{e3}\cot\alpha}{\mu_{e3}\cot\alpha}\right\}\left\{1 - \left(\frac{D_{e23}}{D_{e13}}\right)^{\mu_{e3}\cot\alpha}\right\}\right]$$

$$+ \left[\left\{\frac{\pi D_{e24} t m \bar{y}}{\cos\alpha}\right\}\left\{\frac{1 + \mu_{e4}\cot\alpha}{\mu_{e4}\cot\alpha}\right\}\left\{1 - \left(\frac{D_{e24}}{D_{e13}}\right)^{\mu_{e4}\cot\alpha}\right\}\right]$$

$$+ \ldots\ldots\ldots\ldots + \ldots\ldots\ldots\ldots + \ldots\ldots\ldots$$

$$+ \left[\left\{\frac{\pi D_{e2n} t m \bar{y}}{\cos\alpha}\right\}\left\{\frac{1 + \mu_{en}\cot\alpha}{\mu_{en}\cot\alpha}\right\}\left\{1 - \left(\frac{D_{e2n}}{D_{e1n}}\right)^{\mu_{en}\cot\alpha}\right\} + \left\{\frac{\pi D_{en} t \bar{y}\alpha}{3}\right\}\right] \quad (24)$$

or

$$F_{dT} = \left[\left\{F_{deu1} - \frac{R_{De1}}{2}\right\} + F_{De2} + F_{De3} + F_{De4} + \ldots\ldots + \ldots\ldots\ldots + \left\{F_{Deun} - \frac{R_{Den}}{2}\right\}\right]$$

or

$$F_{dT} = \left[\left\{F_{De1} + \frac{R_{Den}}{2}\right\} + F_{De2} + F_{De3} + F_{De4} + \ldots\ldots + \ldots\ldots + \ldots\ldots\ldots + \left\{F_{Den} + \frac{R_{Den}}{2}\right\}\right] \quad (25)$$

** Redundant deformation occurs only at the entry and at exit of a typical conical die. But when each elemental die in a set employed to represent the proto-die is used individually and progressively to draw a specimen tube until the total achievable fractional reduction, R_T at one pass of the tube specimen through the proto-die is attained, the measurable elemental drawing force of each elemental die is inclusive of full elemental redundant deformation. Therefore the negative sign in equation (23) and (24) is necessary to eliminate the elemental redundant deformation of the intermediate dies in the set.

The total redundant deformation at entry and exit of the typical or proto-die is represented or approximately equal to the sum of the redundant deformation at entry and exit of the first and last elemental dies in the set respectively. That is:

$$R_{DT} = \frac{2\pi D_1 t\bar{y}\alpha}{3} = \frac{\pi D_{e11} t\bar{y}\alpha}{3} + \frac{\pi D_{e1n} t\bar{y}\alpha}{3}$$

or

$$R_{DT} = \frac{\pi\alpha}{3}\left\{D_{e11} t\bar{y} + D_{e1n} t_n \bar{y}\right\} \qquad (26)$$

From our quasi-static axisymmetric compression experimental results it has been shown that there is a large difference between the initial and the final values (i.e. at die entrance and exit) of the yield stress of tube material such as stainless steel. Therefore it will be inappropriate to employ mean values of yield stress for the elemental analysis of such highly strain hardening material. Instead of mean yield strain $\bar{y}$ instantaneous or elemental yield stress, y_{e1}, y_{e2}, y_{e3}, y_{e4} or y_{en} must be employed for the computation of instantaneous coefficient of friction μ_e and analysis of redundant deformation for the highly strain hardening materials.

3.13. Design of Dies for the Analysis of Coefficient of Friction and Redundant Deformation

(i)

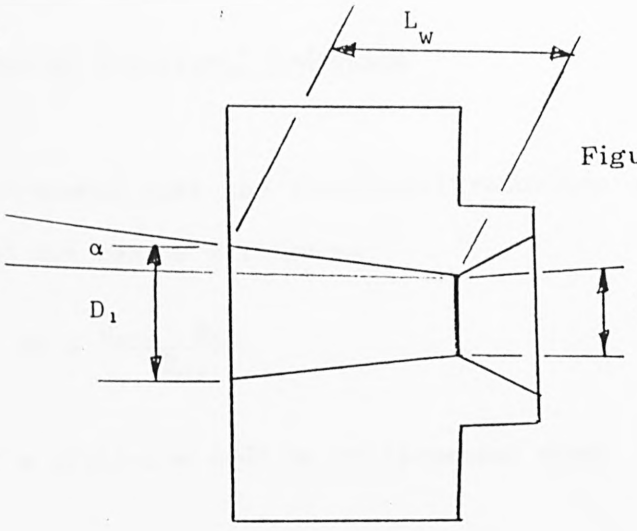

Figure (3.2(a)) A Typical Conical Die

(ii)

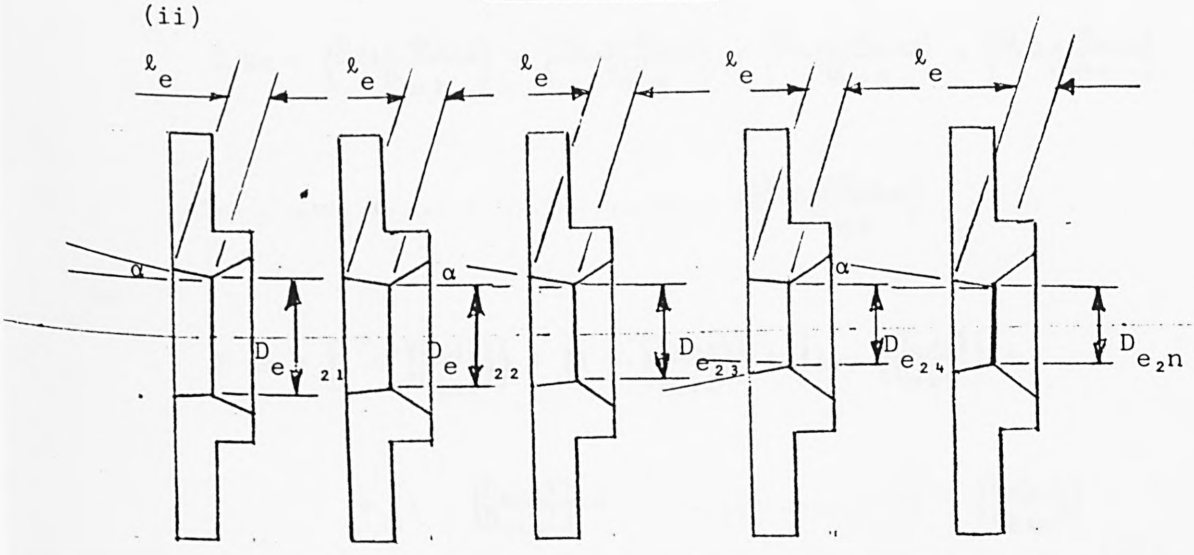

Figure (3.2.(b)) A set of Elemental Dies representing the Typical Conical Die in (i)

(iii)

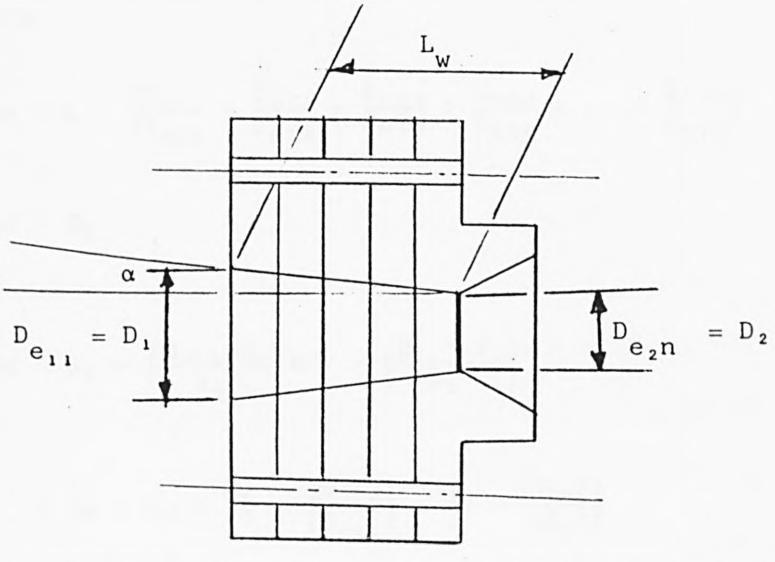

Figure (3.2.(c)) Assembly of the Modified Elemental Die from (ii)

3.14. Elemental Fractional Reduction

It is proposed that the fractional reduction attainable through an elemental die can be written as:

$$Re = \frac{D_{e1} - D_{e2}}{D_{e1}}$$

Now for a proto-die made up of elemental dies:

$$\Sigma Re = \left\{\frac{D_{e11}-D_{e21}}{D_{e11}}\right\} + \left\{\frac{D_{e12}-D_{e22}}{D_{e12}}\right\} + \left\{\frac{D_{e13}-D_{e23}}{D_{e13}}\right\} + \left\{\frac{D_{e14}-D_{e24}}{D_{e14}}\right\}$$

$$+.....+.....+ ..... +\left\{\frac{D_{e1n}-D_{e2n}}{D_{e1n}}\right\}$$

or

$$\Sigma Re = \left\{1 - \left\{\frac{D_{e21}}{D_{e11}}\right\}\right\} + \left\{1 - \left\{\frac{D_{e22}}{D_{e12}}\right\}\right\} + \left\{1 - \left\{\frac{D_{e23}}{D_{e13}}\right\}\right\} +$$

$$+ \left\{1 - \left\{\frac{D_{e24}}{D_{e14}}\right\}\right\} +.....+.....+\left\{1 - \left\{\frac{D_{e2n}}{D_{e1n}}\right\}\right\} \qquad (27)$$

Therefore:

$$\Sigma Re = n - \left\{\frac{D_{e21}}{D_{e11}} + \frac{D_{e22}}{D_{e12}} + \frac{D_{e23}}{D_{e13}} + \frac{D_{e24}}{D_{e14}} +....+ \frac{D_{e2n}}{D_{e1n}}\right\} \qquad (28)$$

But $\Sigma Re = R_T$

or

$$\Sigma Re = R_T = \left\{\frac{D_{e11}-D_{e2n}}{D_{e11}}\right\} = \left\{\frac{D_1 - D_2}{D_1}\right\}$$

Therefore $$\Sigma Re = R_T = \left\{1 - \left\{\frac{D_{e2n}}{D_{e11}}\right\} = \left\{1 - \left\{\frac{D_2}{D_1}\right\}\right\}\right. \qquad (29)$$

CHAPTER 4

DESIGN OF THE EXPERIMENT

4.11. Previous Work

From the study of previous work, and having taken into consideration the existing equipment available for the project, it was decided to conduct the experiment using different methods. Apart from the difficulties in measuring the radial pressure of conical dies, there were marked disagreements in the results attained from the previous work based on measurement of die pressure and the values of the coefficient of friction attained from the upper bound assumption, $\tau = \mu p \leq K$ are unreliable and often resulted in under or over estimation of total drawing force.

4.12. The Draw Bench

The existing draw bench which was designed and manufactured by Hille Engineering Company is capable of producing a drawing force up to 92.5 kN and its drawing velocity ranges from 0 - 15 m/s. The maximum draw length is 1.83 m. The force transducer installed has a range of 0 - 50 kN. The die holder is designed to accept dies of 55 mm outside diameter and provides a machined location recess and thrust face to suit. The exit diameter of the die holder is 27.5 mm. The die holder assembly is mounted on a pivoted arm and connected to the main frame through trunnions in a manner which causes drawing forces to be reacted upon a force transducer. The wedge box provided on the hydraulic ram head can accept specimens up to 25 mm diameter.

The draw bench is hydraulically operated and the drawing velocity is controlled via a flow valve with a calibrated scale to permit the velocity to be preset. A control lever is provided for start and stop, together with provision for controlling the direction of motion.

4.13. Materials for Specimen Workpiece

The objective of the project was to design a method for accurate assessment and prediction of the coefficient of friction along the die pass and also to provide an experimental method of determining and proving the redundant deformation at the entry and exit of a straight conical die for accurate calculation of the total drawing force. Thus the specimen material must be readily available, easy to cold work, must be suitable quality and at minimum cost.

A further consideration relating to the choice of material was given to the use of the existing materials in the Stores, aluminium alloy with 16 mm outside diameter and 0.82 mm wall thickness which has been employed for tentative experiment during the feasibility study of the project, it was therefore decided that any other specimen materials must be of the physical specifications in terms of outside diameter and wall thickness with the existing one which would be optimum for existing equipment constraints and economic consideration.

From the range of suitable specimen materials available, cold drawn seamless copper, brass and stainless steel were considered to

be the most economic and readily available with physical specifications commensurate with those of the existing material, aluminium alloy. They are described by British Standard Specifications B.S.2871 and EN58E. They describe a range of cold drawn seamless aluminium, copper, brass, stainless steel tubes which are suitable for cold working and available in the range of the diameters and wall thickness required.

To conduct the experiment at the sizes concluded reduces the problem related to size of tooling and force required in the pointing process which is necessary in specimen preparation.

4.14. Die Design

The proposed elemental die theory assumed that a normal straight conical die can be divided into a number of practicable elements depending on the geometry of the proto-die (i.e. the entry and exit diameters and the die semi-angle) which constitutes the length of the working face of the die.

The existing cast-iron proto-dies which were employed for the initial feasibility study of the project are of 7° semi-angle which is the smallest practicable angle which can be achieved giving consideration to the length of the die bore and method of manufacture when a fractional reduction of approximately 0.5 is required.

Also in previous work, and in the industries, dies with 15° semi-angle were and are employed respectively. Therefore in order

to enable direct comparison to be made between the results from the two semi-angles 7° and 15° and direct comparison with previous work, it was decided that 7° and 15° semi-angle would be employed in the elemental die design.

Except for covering the range of fractional reductions which are possible at one pass of the chosen specimen materials through a proto-conical die (to be made by assembly of elemental dies) and to maximise the use of the existing solid proto-die to minimise cost, there was no other special reasons for the employment of 0.375 and 0.25 total fractional reductions, R_T for the experiment.

Taking into consideration the total pass ≈25 mm of the 7° semi-angle conical die with 0.375 total fractional reduction, it was decided to produce 5 elemental dies with the same semi-angle (7°), the same working pass, 4.92 mm, and the same elemental fractional reduction of 0.075 which their sum constitute the total fractional reduction of the proto-die to be represented.

Also the 15° semi-angle conical die was to be represented with a set of 3 elemental dies of the equal pass length, 2.58 mm, and equal elemental fractional reduction, R_ℓ = 0.125 mm which their sum amount to the total fractional reduction R_T = 0.375.

The same considerations were given to the other proto-dies with total fractional reduction 0.25, with nominal exit diameter of 12 mm and with 7° and 15° semi-angle and it was decided to produce 5 and 3 elemental die sets to cover their working passes respectively.

In order to achieve an acceptable accurate representation of these proto-die profiles the proposed corresponding sets of elemental dies, it was considered necessary to produce the conical face (the semi-angle) of the elements in a set at a setting of the cross-slide of a lathe machine so that the semi-angle of the elemental dies in the set would remain the same.

Taking into consideration the constraints of the die box on the draw bench, it was decided that the outside diameter of the body and that the location of each elemental must not be greater than 54.5 mm and 27 mm respectively.

Considering the cost of the 12 sets of 3 and 5 elemental dies to be produced from 3 different die materials, it was decided that the sets of elemental dies to be employed for the coefficient of friction test must be readily adaptable for the redundant deformation experiment as well.

Since it was considered that the adaptation of the original elemental dies for redundant deformation test would require further manufacturing operations which would in involve the followings:

(1) reduction of each elemental die outside diameter to the size which would facilitate sensible strain readings from the strain gauges to be used to sense elemental drawing forces, F_{Deu} and F_{De} in terms of hoop strain,

(2) reduction of the length of the die location to less than 2 mm to avoid mass effect on the strain readings.

and (3) drilling and reaming of the holes for the accommodation of the identical pins used for the assembly of elemental dies for measuring corrected elemental strain (ϵ_{De}) (equivalent strain to the corrected elemental drawing force, F_{De}) it was decided that there should be no heat treatment of the elemental dies.

Longitudinal positioning of the strain gauges on the outer diameter of the elemental was given consideration and tested to sense strain in the axial direction as the elemental drawing forces, F_{Deu} and F_{De}. The drawback of this method of laying strain gauges was the restriction on the gauge and overall lengths of the strain gauges which can be successfully accommodated by the elemental dies with thin thickness. The strain readings attained during the tentative test were poor and considered unreliable, hence the decision to lay the strain gauges with longer gauge length circumferentially on the elemental dies.

In practice, the materials to be used for the die would be expected to be hard (50 - 60 Rockwell C) for abrasion resistance, since subsequent manufacturing operations such as turning and drilling were required to adapt the dies for the subsequent experiment (redundant deformation) and it was considered that heat treatment of the dies was uncalled for, therefore the degree of hardness was limited. The three common die materials considered appropriate to give a reasonable degree of hardness against abrasion and to give comparative results are Carr's 14 S, Extra Tough High Carbon High Chrome steel (C.2.15%, Ni.0.5%, Cr.14%, Mo.0.35%,

V.035%), Non-shrinking Oil Hardening Steel and Cast-Iron (grade 17 to BSS.1452).

The effect of friction upon both drawing forces and die wear are clearly important economic considerations in the tube manufacturing industry. The lubricants commonly used are namely: soap solutions and mineral oils. The lubricants often contain additives such as stearic acid or molybdenim disulphide. However, during our feasibility study on this project, several mineral oils were tested for their effect on drawing forces and wear of dies and among the ones with best results were Mobil Dromus 'B', Mobil Vactra '2' and Parafin.

It was decided to employ Mobil Dromus 'B' as the main lubricant for the experiment.

4.15. Preparation of Specimen Workpiece (Tube Pointing)

4.16. Method Used in Industry

The objective is to prepare the workpiece such that it can be fed through the die exit and gripped for the purpose of drawing.

The method used in industry for pointing are forging (hot and cold), swaging, or forced feed (pressing) of tube into the die. For smaller sizes with thin walls, a folding and forming technique is used. This consists of folding and forming such that the walls are in contact and the point is therefore solid.

The pressing of tube into the die demands that the external diameter of the tube is gripped at a distance small enough from the die entrance to obviate buckling. Force is then applied in the direction of drawing that sufficient tube emerges from the die exit for gripping purposes. Provision for this is made on many machines in use in industry.

4.17. Method Used for the Project

The Bliss 25 power press which is situated in the Manufacturing Processes Laboratory was the main equipment employed for this aspect of the experiment. This press (shown in Figure 4.19) manufactured by R.W. Bliss, Ltd., Serial No.AA-103-14875-1961, is capable of producing a force of 250 kN, with stroke adjustable over the range 6 mm to 90 mm at 135 strokes per minute.

An 82 mm diameter x 41 mm long mild steel mandrel with 55 mm diameter x 55 mm long spigot location was fitted to the operating ram of the press. The press was then adjusted such that the die set and swaging tool fully closed at the bottom of the operating stroke which was set at 12.7 mm. The die set with swaging tool was clamped to the bed of the press with its operating spigot hole co-axial approximately with the axis of the operating ram.

The screw adjustment on the die set was adjusted to provide a gap of 2 mm between the faces of the split swaging tool. The tube was fed manually through the hollow cylindrical plastic support which

facilitated the control of alignment of the specimen at a distance from the entrance to the swaging tool. The desired gauge length of specimen was cut off and the swaged end of each workpiece was plugged with mild steel rod for a length of 60 mm. This was done to prevent collapse when the specimen was gripped in the wedge box.

CHAPTER 5

QUASI-STATIC AXISYMMETRIC COMPRESSION TEST

5.11. Objective of the Experiment

This experiment is carried out to obtain yield stress - strain characteristics for various materials to provide necessary data to facilitate the analysis of redundant deformation and coefficient of friction across the pass of a conical die. From previous experience it is considered necessary to verify whenever possible the data provided by the supplier of such materials. For a strain hardening material such as stainless steel tube which strain hardened considerably when cold worked, the employment of its original value of yield stress in the analysis of the parameters which are dependent of this data becomes meaningless and unreliable. Therefore the objects of this experiment include:

(1) To estimate the elemental yield stress Y_e needed for the analysis of the elemental coefficient of friction and the redundant deformation of the highly strain-hardening tube material such as stainless steel during its slow drawing through a conical die.

(2) To estimate the mean yield stress $\bar{Y}$ needed for the analysis of the elemental coefficient of friction and redundant deformation of less strain hardening materials such as copper and aluminium during their slow drawing through a conical die.

(3) To investigate the effect of repeated redundant deformation and the effect of the die pass length on the yield stress of a tube material.

5.12. Theory

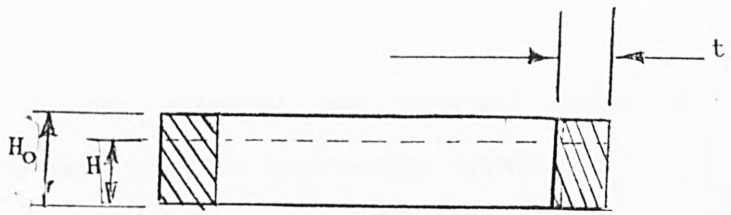

Let F = compressive axial force (N) exerted on specimen

A_o = initial cross-sectional area (mm^2) of specimen

A = current cross-sectional area (mm^2) of specimen

H_o = initial height of specimen (mm)

H = current height of specimen (mm).

Then the true compressive stress at any instant is:

$$\sigma_c = F/A \text{ (MPa)} \qquad (5.1)$$

For constancy of volume:

$$A_o H_o = AH$$

$$\therefore \quad A = (A_o/H_o)/H \qquad (5.2)$$

where

$A_o = \pi D_o t = \pi D_o H_o$ when t is very small when compared with D_o.

For the cases where t is considered large:

$$A_o = \pi(r_e^2 - r_i^2)$$

where r_e and r_i are external and internal radii of the tube respectively. Conventional or Engineering strain is:

$$e = (H - H_o)/H_o$$

$$= (H/H_o) - 1$$

or

$$H/H_o = 1 + e \tag{5.3}$$

A decrement, dH, in the deformed height gives an engineeing strain increment as:

$$de = dH/H_o \tag{5.4}$$

Also the increment of the logarithmic or natural strain, $d\epsilon$, introduced by Ludwick is based on the current gauge height and is defined as:

$$d\epsilon = dH/H \tag{5.5}$$

and the total logarithmic or natural strain, ϵ, when the initial gauge height, H_o, is compressed to a current height, H, is then defined as:

$$\epsilon = \int d\epsilon = \int_{H_o}^{H} (dH/H) = \ln H/H_o \tag{5.6}$$

But $H/H_o = 1 + e$

$$\therefore \epsilon = \ln (1 + e) \tag{5.7}$$

Hence:

$$e = \exp.(\epsilon) - 1 \tag{5.8}$$

For small compression, the values of both engineering and natural strains, e and ϵ, are almost identical but diverge as the compression increases.

5.13. Strain Rate in Unaxial Compression

The increment of engineering strain is:

$$de = dH/H_o$$

The engineering strain rate, $\dot{e}$ is:

$$\dot{e} = de/dt \tag{5.9}$$

Therefore:

$$\dot{e} = -\left[\frac{dH/H_o}{dt}\right] = -\left[\frac{dH/H_o}{dt}\right] = -\frac{v}{H_o}$$

$$\therefore \dot{e} = v/H_o \tag{5.10}$$

where $v = \frac{dH}{dt}$ (the velocity)

Also, the corresponding natural strain rate, $\dot{\epsilon}$, is:

$$\dot{\epsilon} = d\epsilon/dt = \frac{(dH/H)}{dt}$$

$$\therefore \dot{\epsilon} = -\left[\frac{1}{H}\right].\left[dH/dt\right] = -v/H$$

$$\therefore \dot{\epsilon} = -v/H \qquad (5.11)$$

5.14. Fractional Reduction, R

$$R = \frac{D_1 - D_2}{D_1} = 1 - \left[\frac{D_2}{D_1}\right] \qquad (5.12)$$

where D_1 and D_2 are the mean external diameters before and after drawing respectively.

5.15. Apparatus and Equipment

1. Avery Universal Testing Machine, 250 kN capacity, type 7110DCT, Serial No.E.70254, operated as a force indicating slow hydraulic press.

2. A sub-press fitted with rectilinear ball bearings on the guide pillars. Hardened ground and polished steel platens are fitted to the upper and lower internal faces of the die set.

3. A dial test indicator calibrated with 0.01 mm divisions with 50 mm plunger traverse, complete with adjustable stand and a base with provision for magnetic base.

4. Micrometer (0 - 25 mm).

5. A digital Vernier caliper.

6. Specimens from various fractonal reduction, Re and from different tube materials with the height of the specimens are approximately equal to their wall thickness.

(i) Batch 1: Aluminium Specimen Drawn with 7° semi-angle elemental die (5 in a set).

3 specimens at Re = 0.075, Re = 0.150, Re = 0.225, Re = 0.300 and Re = 0.375.

(ii) Batch 2: Copper tube Drawn with 7° semi-angle elemental dies as in (i)

3 specimens at each fractional reduction Re = 0.075, Re = 0.150, Re = 0.225, Re = 0.300, and Re = 0.375.

(iii) Batch 3: Brass tube Drawn with 7° semi-angle elemental dies as in (i)

3 specimens at each fractional reduction Re = 0.075, Re = 0.150, Re = 0.255, Re = 0.300 and Re = 0.375.

(iv) Batch 4: Stainless steel tube Drawn with 7° semi-angle elemental die as in (i)

3 specimens at each fractional reduction Re = 0.075, Re = 0.150, Re = 0.225, Re = 0.300, and Re = 0.375.

(v) Batch 5: Stainless steel, brass, copper and aluminium tubes

Drawn with 3 and 2 elemental dies.

3 specimens from each material at a total fractional reduction, $R_T = 0.375$.

5.16. Test Procedure

The Universal Testing Machine was set to read on the range 12.5 kN full-scale. The spigot of the die set consists of upper and lower platens in the operating ram of the Universal Testing Machine was located and clamped.

With the spherical end of the operating shaft of dial indicator in contact with the machine face at the lower end of the ram, the dial test indicator was clamped to the testing machine bed.

A specimen was cleaned with the degreasing agent and the diameter, height, and wall thickness of the specimen were cross-checked with micrometer and a Vernier caliper.

With the upper and lower deforming platens properly cleaned with degreasing agent, both faces were lightly coated with molykote lubricant. Then with the aid of a pair of tweezers, the specimen was placed with the axis vertical on the centre of the lower platen.

The ram was lowered until the gap between the upper platen and the specimen was reduced to approximately 0.1 mm. Through the use

of adjustment facility provided the load was adjusted to zero. By using the fine control valve, the speed of the ram was adjusted such that the indication of height on the dial indicator was reduced at approximately 0.01 mm in 30 seconds. This was assumed to produce a strain of 10^{-3}/sec. Readings of the compressive forces were taken at every 0.02 mm displacement of the dial indicator's pointer until almost the full-range of force, 12.5 kN was covered. The ram was fully raised, the deformed specimen was removed from the platen and cleaned with the degreasing agent. The final height of the specimen, after compression, was measured. Then the platens of the sub-press were cleaned with degreasing agent and the procedure was repeated for other specimens from different batches.

5.17. Results from the Experiment

1. The experimental results, force displacement tests are as shown in Tables (5.01) to (5.20). The compressive flow stress and the corresponding natural strains were calculated and the results attained are as shown in the same tables, (5.01) to (5.20).

2. Also shown in Tables (5.24) to (5.27) is the estimation of the experimental errors.

3. The graphs, Figures (5.10) to (5.13) show the comparison of the true compressive stress - natural compressive strain at different fractional reductions for the different tube materials tested.

4. Also Figure (5.4), the graphs of the true compressive stress against natural compressive strain of the stainless steel specimen drawn to a total fractional reduction, R_T = 0.375, at different number of passes and with 7° and 15° semi-angle dies show the effect of redundant deformation and die pass length on yield stress of the drawn specimen.

5. The specimens from aluminium tube material were not tested because an identical test has been carried out on the same material and an identical specimen at almost the same fractional reductions.

6. The summary of the estimated mean yield stress, $\bar{Y}$, and elemental yield stress, Y_e, for both less strain hardened material (such as Cu, Al, annealed brass), and highly strain hardened material (stainless steel) are as shown in Tables (5.21), (5.22) and (5.23) respectively.

5.18. Summary of the Elemental Yield Stress Y_e

STAINLESS STEEL

Elemental Fractional Reduction Re	Elemental Yield Stress Y_e (MPa)
0.00	400
0.075	475
0.150	500
0.225	750
0.300	755
0.375	823
	$\bar{y}$ = 617 (MPa)

Table (5.21)

BRASS

Re	Y_e (MPa)
0.00	249
0.075	387
0.150	310
0.225	425
0.300	441
0.350	439
	$\bar{y}$ = 375 (MPa)

Table (5.22)

COPPER

Re	Y_e (MPa)
0.00	146
0.075	194
0.150	210
0.225	230
0.300	235
0.375	229
	$\bar{y}$ = 207(MPa)

Table (5.23)

5.19 Estimation of Errors

ESTIMATION OF ERRORS

	(mm)	H_o(av) (mm)	ΔHT (mm)	ΔHT+H_f (mm)	E_a=[ΔHT+H_f]−H_o (mm)
S1H_fB2 =	0.44		0.60	1.04	0.048
S2H_fB2 =	0.45		0.60	1.05	0.058
S3H_fB2 =	0.40	0.992	0.64	1.04	0.048
S4H_fB2 =	0.35		0.66	1.01	0.018
S5H_fB2 =	0.38		0.66	1.04	0.048
S6H_fB2 =	0.45		0.60	1.05	0.058
S1H_fB3 =	0.46		0.60	1.06	0.068
S2H_fB3 =	0.44		0.60	1.04	0.048
S2H_fB3 =	0.46	0.992	0.60	1.06	0.068
S2H_fB3 =	0.45		0.60	1.05	0.058
S2H_fB3 =	0.43		0.60	1.03	0.038
S2H_fB3 =	0.43		0.62	1.05	0.058
S1H_fB4 =	0.46		0.60	1.06	0.068
S2H_fB4 =	0.45		0.60	1.05	0.058
S3H_fB4 =	0.45	0.992	0.60	1.05	0.058
S4H_fB4 =	0.46		0.60	1.06	0.068
S5H_fB4 =	0.46		0.60	1.06	0.068
S6H_fB4 =	0.45		0.60	1.05	0.058
S1H_fB5 =	0.45	1.00	0.58	1.03	0.03
S2H_fB5 =	0.46		0.58	1.04	0.04

Table (5.24)

Limit of Error for the Dial Gauge Used
(Scale Divisionof 0.01 mm)

Interval Reading	Error in Reading over stated Interval (mm)
Every 0.1 mm	0.005
Every half revolution	0.0075
Every one revolution	0.0100
Every two revolutions	0.0150
Every longer interval	0.0200

Table (5.25)

The Average Apparent Errors, E_{aa}

Batches	E_{aa} (mm)
2	0.046
3	0.056
4	0.063
5	0.035

Table (5.26)

Summary of Errors

E_{aa} (mm)	E_i (mm)	$E_o = [E_{aa}-E_i]$ (mm)	E_i	E_o
0.046	0.01	0.036	22	78
0.56	0.01	0.046	18	82
0.63	0.01	0.053	16	84
0.035	0.01	0.025	29	71

Table (5.27)

where E_i is the error due to dial gauge used

E_o is the other errors due to reading, friction, etc.

5.19. Discussion

Shown in Tables (5.21) to (5.23) are the estimated elemental and mean yield stresses (Y_e and $\bar{y}$) for the materials tested. The yield stress of copper, annealed brass, aluminium and stainless steel tubes rose from 146 MPa to 235 MPa, 249 MPa to about 439 MPa, 140 MPa to about 220 MPa and from about 400 MPa to 823 MPa respectively. The minute inconsistency in the progressive increase in the value of the elemental yield stress values shown in the result summary, Tables (5.22) and (5.23) for the soft materials (copper and annealed brass) may be due to roundness error encountered during the production of the ring specimens. With harder and tougher material like stainless steel, the production of the ring specimens was much easier and the resulting specimens are more accurate and reliable. As would be noticed in the result summary tables, the results for the stainless steel are much more consistent.

Another source of error in the rate of increase of the yield stress of the annealed brass tube in particular could be due to initial non-uniform heat treatment (annealing by simply heating the tube locally to a dull red state with a torch) this material underwent in order to facilitate its specimen pointing operation through swaging. Though the final specimens with pointed ends were subjected to a uniform subsequent heat treatment (annealinng) in a controlled system and atmosphere (electric furnace) but the effect of initial crude heating with a torch is likely to reflect in the final state of the specimen produced.

It must be borne in mind that all the above-mentioned results are related to the tube specimens drawn through 7° semi-angle elemental dies.

In order to ensure reliable results from the analysis of redundant deformation and coefficient of friction across the die pass, it was decided that the employment of the mean values of the yield stress $\bar{Y}$ of the softer materials would be appropriate whilst the elemental or instantaneous yield stress was recommended for the same analysis across the same die pass for the highly strain hardening material, stainless steel.

Shown in Figure (5.4) are the resulting curves of the True Compressive Stress and Natural Strain data recorded for the stainless steel tube specimens subjected to a total fractional reduction of 0.375 with dies of different semi-angle (7° and 15°). As would be noticed from the result, Figure (5.4) there is only little difference between the yield stress of the specimens drawn through the 15° semi-angle dies at two and three passes respectively. With a closer look into the curves in Figure (5.4) a difference of about 100 MPa between yield stress of the specimen drawn progressively through the set of 7° semi-angle 5 elemental dies the yield stress value of the ones drawn with 2 and 3 elemental dies with 15° semi-angle to the same final diameter, 10 mm (R_T = 0.375) would be noticed.

During the process of drawing, the subjection of one specimen to 0.375 fractional reduction through 5 elemental dies with 7° semi-angle and total pass length of 24.6 mm was accompanied by a

total elemental redundant deformation force of about 7.52 kN whilst that drawn through element dies with 15° semi-angle and a total pass length of 11.6 mm for the same fractional reduction of 0.375 underwent a total elemental redundant deformation force of about 7.96 kN.

From the results attained, it can be concluded that the longer the pass length of a die, the higher the enhancement of the yield stress of the tube material being drawn through it. Also from the results, it was shown that repeatedly subjecting the tube material to elemental redundant deformation has got little or no effect on the final yield stress.

However, it must be borne in mind that at very high fractional reduction, tubing material like aluminium would start to strain soften due to the self annealing process taking place at this higher degree of cold working process. This phenomenon of strain-softening was experienced during a similar test on the same aluminium specimens at 0.606 fractional reduction [27] attained through the use of 7° semi-angle conical dies. In this particular case, the original yield stress, 225 MPa of the aluminium workpiece at 0.375 fractional reduction was drastically reduced to about 160 MPa at further reduction, 0.606. From the results attained, it could also be concluded that the point of instability (i.e. fractional reduction at which strain-softening commences) can be improved through the employment of 15° semi-angle dies from the drawing of the materials which suffer from the strain-softening phenomenon.

5.20. Conclusions

1. Both the elemental and mean yield stress of the materials were successfully estimated and it is concluded that mean yield stress $\bar{Y}$ would be appropriate for the analysis of the redundant deformation force and the coefficient of friction across a die pass for the less strain hardening materials whilst elemental or instantaneous yield stress, Ye is considered more appropriate for the analysis of the same parameters of the highly strain hardening tube materials drawn through a conical die.

2. The effect of repeated redundant deformation (as shown by the results) is less important than the length of die pass on the maximum yield stress of any tube materials drawn through a conical die.

3. The yield stress of a tube material enhanced by the length of the die pass which is a function of the total frictional work done on the workpiece across the die pass. It is therefore concluded that 7° semi-angle die (with longer pass) would be employed when maximum strain hardening of the tube material is desirable.

4. For tube material which strain-soften at higher fractional reduction, the use of the 15° semi-angle die is recommended (die with shorter pass length) in order to prolong the point of initiation of strain softening when higher fractional reduction and maximum yield stress are very important.

CHAPTER 6
EXPERIMENTAL ANALYSIS OF COEFFICIENT OF FRICTION IN TUBE SINKING PROCESS

6.11. Objects of the Experiment

1) To devise a method of estimating the values of coefficient of friction needed for accurate estimation of drawing forces in tube sinking process.

2) To determine the profile of the coefficient of friction across the pass (from the entry to the exit of the die) of a conical die.

3) To determine the effect of die material on the value of the coefficient of friction.

4) To assess the improvement contributed by the employment of a lubricant over the value of coefficient of friction when different tube materials are drawn through a conical die.

5) To determine the influence of the die semi-angle on the values of the coefficient of friction across the die pass.

6) To employ the results of the experiment to assess the validity of the upper bound theorem based on plain strain deformation as applied to tube sinking process analysis.

6.12. Theory

It has been shown in Chapter (2) that for a typical conical die to be represented by a set of elemental dies of n number to be used individually and progressively to draw a thin wall tube until the final reduction is achieved, the total drawing force, F_{dT}, is given by:

$$F_{dT} \approx \left[\left\{\frac{\pi D_{e21} t m \bar{y}}{\cos\alpha}\right\}\left\{\frac{1+\mu_{e1}\cot\alpha}{\mu_{e1}\cot\alpha}\right\}\left\{1 - \left\{\frac{D_{e21}}{D_{e11}}\right\}^{\mu_{e1}\cot\alpha}\right\} + \left\{\frac{\pi D_{e11} t \bar{y}\alpha}{3}\right\}\right]$$

$$+ \left[\left\{\frac{\pi D_{e22} t m \bar{y}}{\cos\alpha}\right\}\left\{\frac{1+\mu_{e2}\cot\alpha}{\mu_{e2}\cot\alpha}\right\}\left\{1 - \left\{\frac{D_{e22}}{D_{e12}}\right\}^{\mu_{e2}\cot\alpha}\right\} - \left\{\frac{2\pi D_{e12} t \bar{y}\alpha}{3}\right\}\right]$$

$$+ \left[\left\{\frac{\pi D_{e23} t m \bar{y}}{\cos\alpha}\right\}\left\{\frac{1+\mu_{e3}\cot\alpha}{\mu_{e3}\cot\alpha}\right\}\left\{1 - \left\{\frac{D_{e23}}{D_{e13}}\right\}^{\mu_{e3}\cot\alpha}\right\} - \left\{\frac{2\pi D_{e13} t \bar{y}\alpha}{3}\right\}\right]$$

$$+ \ldots\ldots\ldots + \ldots\ldots\ldots\ldots + \ldots\ldots\ldots\ldots$$

$$+ \ldots\ldots\ldots + \ldots\ldots\ldots\ldots\ldots + \ldots\ldots\ldots\ldots\ldots$$

$$+ \left[\left\{\frac{\pi D_{e2n} t m \bar{y}}{\cos\alpha}\right\}\left\{\frac{1+\mu_{en}\cot\alpha}{\mu_{en}\cot\alpha}\right\}\left\{1 - \left\{\frac{D_{e2n}}{D_{e1n}}\right\}^{\mu_{en}\cot\alpha}\right\} + \left\{\frac{\pi D_{e1n} t \bar{y}\alpha}{3}\right\}\right]$$

where μ_{e1}, μ_{e2}, μ_{e3}, μ_{en} are the elemental coefficients of friction across the pass of the typical conical die and the values of μ_e's are computed from the employment of Newton-Raphson iteration (see the basic programme under the Appendix).

6.13. Equipment

1) Hille 100 kN hydraulic draw bench equipped with 50 kN load transducer, Serial No. SZ-E-5223, calibration of 4.38 kN/cm. When used with amplifier Serial No.SG.905, Channel II, set at attenuation scale reading 45 and galvanometer type B-450, Serial No.9-4317.

2) A U.V. recorder with minature galvanometer and U.V. sensitive recording paper to record an analogue of the drawing force throughout the drawing operation, Calibration 1 cm = 4.38 kN.

3) Sets of elemental dies with conical profiles to represent proto-dies with 0.375 and 0.250 total fractional reductions respectively, details as follows:

(i) 3 sets of elemental dies with semi-angle 7°: Each set consists of 5 elemental dies with exit diameters, 14.80 mm, 13.60 mm, 12.40 mm, 11.20 mm and 10 mm to provide a total fractional reduction, R_T = 0.375 of a proto-die with 10 mm nominal exit diameter and 7° semi-angle.

(ii) 3 sets of elemental dies with semi-angle of 7°: Each set consists of 5 elemental dies with exit diameters 15.20 mm, 14.40 mm, 13.60 mm, 12.80 mm, and 12 mm, to provide a total fractional reduction, R_T = 0.250 of a proto-die with 12 mm nominal exit diameter and with 7° semi-angle.

(iii) 3 sets of elemental dies with 15° semi-angle: Each set consists of 3 elemental dies with exit diameters 14 mm, 12 mm, and 10 mm to provide a total fractional reduction, R_T = 0.375 of

a proto-die with 15° semi-angle and with 10 mm nominal exit diameter.

(iv) 3 sets of elemental dies with 15° semi-angle: Each set consists of 3 elemental dies with exit diameters 14.67 mm, 13.33 mm, and 12 mm, to provide a total fractional reduction, R_T = 0.250 of a proto-die with 15° semi-angle and with 12 mm nominal exit diameter.

Each 3 sets of elemental dies were manufactured from Non-Shrinking Oil Harddening (NSOH) Steel, High Carbon High Chromium Steel (HCHC) and Cast Iron, Surface finish $\leqslant$ 0.5 μm.

4) Specimen workpieces for 16 mm nominal external diameter, 0.82 mm nominal wall thickness copper, aluminium, annealed brass and stainless steel cold drawn seamless tube, approximately 30 cm total length, with ends pointed by swaging and fitted with solid plugs suitable for leading through the elemental die exits.

5) Lubricant - Mobil "Dromus B".

6) "Genkelene" proprietary degreasing agent.

7) A micrometer capable of measuring 0 - 26 mm with a spherical attachment for filament to anvil.

6.14. Procedure

1) The dies and specimens were cleaned with degreasing agent and allowed to dry. Cleanliness of die housing was ensured.

2) The external diameters of the specimens were measured (mean of five readings) using the micrometer.

3) The wall thickness (mean of six readings) was measured using the micrometer with a spherical adaptor on the anvil.

4) The U.V. paper speed was adjusted to 5 mm/sec and the galvanometer spot set to the desired position. Correct function of the force recording system was checked by switching attenuation to setting 12 and applying a manual force in the direction of the sinking force. The attenuation switch was then positioned at setting 45. The recorder paper feed was switched on just prior to commencement of drawing.

5) The 5 elemental dies of a set of 7° semi-angle element dies with a total fractional reduction 0.375 were arrangeed and placed in a progressive order of use at the reach of the operator.

6) A specimen lead end was inserted through the first elemental die (with largest exit diameter) in the set and located in the die housing on the hydraulic draw bench. The specimen was then gripped in the wedge box grips by closing the jaws.

7) The drawing speed was set by positioning the control valve at 2 cm/min and drawing was commenced by operation of the control lever and continued until the specimen was drawn through its entire gauge length. The recorder paper drive was stopped.

8) The wedge box grip was released and the specimen was withdrawn.

9) Procedures 6 to 8 were repeated for the same specimen with the rest of the elemental dies in the set until the final diameter (10 mm) of the specimen was achieved.

10) From the U.V. recorder traces, the mean ordinates of the elemental drawing forces analogue F_{Deu} (mm) were established and with the calibration of the force transducer known, the mean elemental drawing forces F_{Deu}((N) were determined.

11) With drawing operation continued without the use of lubricant on the dies and the specimen procedures 6 - 10 were repeated with same set of elemental dies for other specimens of different materials (copper, brass and stainless steel).

12) The procedures 5 to 11 were repeated with the other sets of 7° semi-angle elemental dies made from different die material.

13) Then procedures 5 to 12 were repeated with other sets of elemental dies with 15° semi-angle.

6.15 Analysis of Results

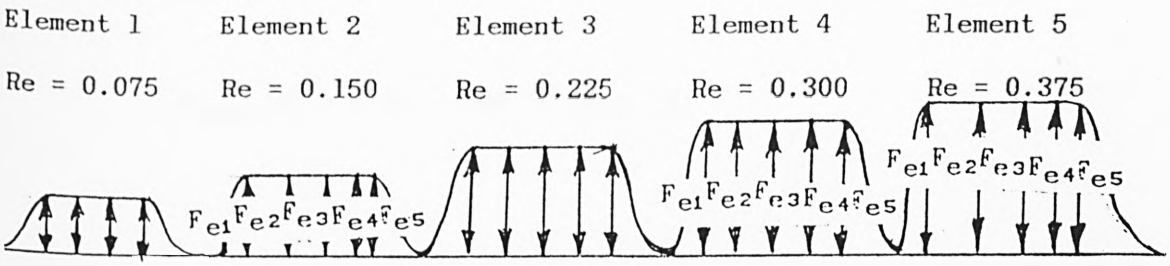

Analogue of Elemental Drawing forces of a Set of Elemental Dies (with $\alpha = 7^{\circ}$ and $R_T = 0.375$.

$$F_{Deu}(mm) = \frac{(F_{e1} + F_{e2} + F_{e3} + F_{e4} + F_{e5})}{n} \quad (mm)$$

i.e. $$F_{Deu}\ (mm) = \frac{\Sigma F_e}{n} \quad (mm)$$

$$F_{Deu}(N) = \left[\frac{\Sigma F_e}{n}\right] \times C$$

where F_{Deu} is the elemental drawing force due to full elemental redundant deformation

n is the number of analogue results taken per trace for an elemental die

C is the force calibrating factor, 438 ≡ 10 mm.

Examples

From tables 6.01(a) and 6.01(b)

At Re = 0.075

$$F_{Deu1}\ (mm) = \frac{[5.1 + .5 + 5 + 5 + 5]}{5} = 5.02\ (mm)$$

$$\therefore F_{Deu}\ (N) = 5.02 \times 438 = \underline{2199\ (N)}$$

At Re = 0.150

$$F_{Deu2}\ (mm) = \frac{[5.8 + 5.9 + 5.9 + 5.9 + 5.7]}{5} = 5.84\ (mm)$$

$$\therefore F_{Deu2}(N) = 5.84 \times 438 = \underline{2558\ (N)}$$

At Re = 0.225

$$F_{Deu3}\ (mm) = \frac{[6.0 + 6.0 + 5.7 + 5.8 + 5.7]}{5} = 5.86\ (mm)$$

$$\therefore F_{Deu3}(N) = 5.86 \times 438 = \underline{2567\ (N)}$$

At Re = 0.300

$$F_{Deu4}\ (mm) = \frac{[7.0 + 6.7 + 6.2 + 6.2 + 6.2]}{5} = 6.46\ (mm)$$

$$\therefore F_{Deu4}\ (N) = 6.46 \times 438 = \underline{2830\ (N)}$$

At Re = 0.375

$$F_{Deu5}\ (mm) = \frac{[7.4 + 7.0 + 7.4 + 6.3 + 6.2]}{5} = 6.86\ (mm)$$

$$\therefore F_{Deu5}(N) = 6.86 \times 438 = \underline{3005\ (N)}$$

SUMMARY AND COMPARISON TABLE OF ELEMENTAL COEFFICIENT OF FRICTION [UNDER DIFFERENT TRIBOLOGICAL TREATMENT] AT VARIOUS POINTS ALONG THE WORKING FACE OF A NSOH-DIE WITH 7° SEMI-ANGLE REPRESENTED BY A SET OF ELEMENTAL DIES (TOTAL FRACTIONAL REDUCTION R_T = 0.375)

Re	ALUMINIUM NSOH DIE				COPPER NSOH DIE				BRASS NSOH DIE				STAINLESS STEEL NSOH DIE			
	μ_e	μ_{eL}	$\Delta\mu_e$	%I	μ_e	μ_{eL}	$\Delta\mu_e$	%I	μ_e	μ_{eL}	$\Delta\mu_e$	%I	μ_e	μ_{eL}	$\Delta\mu_e$	%I
0.075	0.27	0.11	0.16	59	0.18	0.08	0.10	56	0.09	3.2×10^{-7}	0.09	≈100	0.08	0.04	0.04	50
0.150	0.30	0.14	0.16	53	0.16	0.07	0.09	56	0.08	0.02	0.06	75	0.13	0.09	0.04	31
0.225	0.31	0.16	0.15	48	0.22	0.09	0.13	59	0.16	0.12	0.04	25	0.08	0.02	0.06	75
0.300	0.42	0.19	0.23	55	0.28	0.17	0.17	39	0.20	0.18	0.02	10	0.13	0.11	0.02	15
0.350	0.60	0.27	0.33	55	0.58	0.26	0.32	55	0.23	0.19	0.04	17	0.20	0.13	0.07	35

Table 6.97(a)

SUMMARY AND COMPARISON TABLE OF ELEMENTAL COEFFICIENT OF FRICTION [UNDER DIFFERENT TRIBOLOGICAL TREATMENT] AT VARIOUS POINTS ALONG THE WORKING FACE OF AN HCHC-DIE WITH 7° SEMI-ANGLE REPRESENTED BY A SET OF ELEMENTAL DIES (TOTAL FRACTIONAL REDUCTION R_T = 0.375)

Re	ALUMINIUM HCHC DIE				COPPER HCHC DIE				BRASS HCHC DIE				STAINLESS STEEL HCHC DIE			
	μ_e	μ_{eL}	$\Delta\mu_e$	%I	μ_e	μ_{eL}	$\Delta\mu_e$	%I	μ_e	μ_{eL}	$\Delta\mu_e$	%I	μ_e	μ_{eL}	$\Delta\mu_e$	%I
0.075	0.27	0.10	0.17	63	0.17	0.08	0.09	53	0.08	3×10^{-7}	0.08	≈100	0.08	0.04	0.04	50
0.150	0.31	0.14	0.17	55	0.16	0.07	0.09	56	0.08	0.04	0.04	50	0.13	0.09	0.04	31
0.225	0.30	0.16	0.14	47	0.22	0.09	0.13	59	0.16	0.11	0.05	31	0.08	0.02	0.06	25
0.300	0.41	0.19	0.22	54	0.28	0.17	0.11	39	0.20	0.19	0.01	5	0.13	0.11	0.02	15
0.350	0.64	0.27	0.37	58	0.61	0.26	0.35	57	0.23	0.20	0.03	13	0.20	0.14	0.06	30

Table 6.97(b)

SUMMARY AND COMPARISON TABLE OF ELEMENTAL COEFFICIENT OF FRICTION [UNDER DIFFERENT TRIBOLOGICAL TREATMENT] AT VARIOUS POINTS ALONG THE WORKING FACE OF A CAST IRON DIE WITH 7° SEMI-ANGLE REPRESENTED BY A SET OF ELEMENTAL DIES (TOTAL FRACTIONAL REDUCTION R_T = 0.375)

Re	ALUMINIUM CAST IRON DIE				COPPER CAST IRON DIE				BRASS CAST IRON DIE				STAINLESS STEEL CAST IRON DIE			
	μ_e	μ_{eL}	$\Delta\mu_e$	%I	μ_e	μ_{eL}	$\Delta\mu_e$	%I	μ_e	μ_{eL}	$\Delta\mu_e$	%I	μ_e	μ_{eL}	$\Delta\mu_e$	%I
0.075	0.17	0.17	0.0	0	0.14	0.11	0.03	21	7.6×10^{-8}	6.7×10^{-8}	0.9×10^{-8}	12	0.05	0.05	0.0	0
0.150	0.23	0.23	0.0	0	0.19	0.17	0.02	11	0.06	0.05	0.01	17	0.10	0.10	0.0	0
0.225	0.23	0.23	0.0	0	0.21	0.20	0.01	5	0.12	0.12	0.0	0	0.09	0.09	0.0	0
0.300	0.31	0.31	0.0	0	0.29	0.28	0.01	4	0.20	0.20	0.0	0	0.15	0.15	0.0	0
0.350	0.46	0.44	0.02	4	0.36	0.36	0.0	0	0.37	0.30	0.07	19	0.24	0.24	0.0	0

Table 6.97(c)

SUMMARY AND COMPARISON TABLE OF ELEMENTAL COEFFICIENT OF FRICTION [UNDER DIFFERENT TRIBOLOGICAL TREATMENT] AT VARIOUS POINTS ALONG THE WORKING FACE OF A NSOH-DIE WITH 7° SEMI-ANGLE REPRESENTED BY A SET OF ELEMENTAL DIES (TOTAL FRACTIONAL REDUCTION R_T = 0.250)

Re	ALUMINIUM NSOH DIE				COPPER NSOH DIE				BRASS NSOH DIE				STAINLESS STEEL NSOH DIE			
	μ_e	μ_{eL}	$\Delta\mu_e$	%I	μ_e	μ_{eL}	$\Delta\mu_e$	%I	μ_e	μ_{eL}	$\Delta\mu_e$	%I	μ_e	μ_{eL}	$\Delta\mu_e$	%I
0.05	0.23	0.09	0.14	61	0.18	0.10	0.08	44	0.04	1.4×10^{-7}	0.04	0	0.06	0.05	0.01	17
0.10	0.31	0.13	0.18	58	0.09	0.04	0.05	56	1.1×10^{-7}	1×10^{-7}	0.1×10^{-7}	9	0.09	0.04	0.05	56
0.15	0.44	0.17	0.27	61	0.16	0.11	0.05	31	0.07	0.03	0.04	57	0.05	0.02	0.03	60
0.20	0.48	0.19	0.29	60	0.18	0.12	0.06	33	0.14	0.07	0.07	50	0.10	0.08	0.02	20
0.25	0.55	0.29	0.26	47	0.25	0.20	0.05	25	0.20	0.08	0.12	60	0.14	0.12	0.02	14

Table 6.98(a)

SUMMARY AND COMPARISON TABLE OF ELEMENTAL COEFFICIENT OF FRICTION [UNDER DIFFERENT TRIBOLOGICAL TREATMENT] AT VARIOUS POINTS ALONG THE WORKING FACE OF A HCHC-DIE WITH 7° SEMI-ANGLE REPRESENTED BY A SET OF ELEMENTAL DIES (TOTAL FRACTIONAL REDUCTION R_T = 0.250)

Re	ALUMINIUM HCHC DIE				COPPER HCHC DIE				BRASS HCHC DIE				STAINLESS STEEL HCHC DIE			
	μ_e	μ_{eL}	$\Delta\mu_e$	%I	μ_e	μ_{eL}	$\Delta\mu_e$	%I	μ_e	μ_{eL}	$\Delta\mu_e$	%I	μ_e	μ_{eL}	$\Delta\mu_e$	%I
0.05	0.23	0.09	0.14	61	0.17	0.09	0.08	47	0.04	10^{-7}	0.04	0	0.06	0.05	0.01	17
0.10	0.36	0.10	0.26	72	0.09	0.04	0.05	56	1.1×10^{-7}	1.4×10^{-7}	0.4×10^{-7}	27	0,09	0.04	0.05	56
0.15	0.41	0.17	0.24	59	0.17	0.11	0.06	35	0.07	0.02	0.05	71	0.05	0.12	0.03	60
0.20	0.43	0.20	0.23	55	0.18	0.12	0.06	33	0.14	0.06	0.08	57	0.10	0.07	0.03	30
0.25	0.48	0.20	0.28	58	0.26	0.20	0.06	23	0.20	0.07	0.13	65	0.14	0.12	0.02	14

Table 6.98(b)

SUMMARY AND COMPARISON TABLE OF ELEMENTAL COEFFICIENT OF FRICTION [UNDER DIFFERENT TRIBOLOGICAL TREATMENT] AT VARIOUS POINTS ALONG THE WORKING FACE OF A CAST IRON-DIE WITH 7° SEMI-ANGLE REPRESENTED BY A SET OF ELEMENTAL DIES (TOTAL FRACTIONAL REDUCTION R_T = 0.250)

Re	ALUMINIUM C.I. DIE				COPPER C.I. DIE				BRASS C.I. DIE				STAINLESS STEEL C.I. DIE			
	μ_e	μ_{eL}	$\Delta\mu_e$	%I	μ_e	μ_{eL}	$\Delta\mu_e$	%I	μ_e	μ_{eL}	$\Delta\mu_e$	%I	μ_e	μ_{eL}	$\Delta\mu_e$	%I
0.05	0.08	0.20	0.12	60	0.14	0.13	0.01	7	10^{-7}	10^{-7}	0.0	0	0.06	0.05	0.01	17
0.10	0.15	0.12	0.03	20	0.12	0.11	0.01	8	10^{-7}	10^{-7}	0.0	0	0.03	0.02	0.01	33
0.15	0.17	0.13	0.04	24	0.19	0.13	0.06	32	0.05	0.04	0.01	20	0.10	0.09	0.01	10
0.20	0.16	0.15	0.01	6	0.19	0.15	0.04	21	0.12	0.09	0.03	25	0.12	0.12	0.0	0
0.25	0.26	0.24	0.02	8	0.31	0.28	0.03	10	0.25	0.25	0.0	0	0.18	0.18	0.0	0

Table 6.98(c)

SUMMARY AND COMPARISON TABLE OF ELEMENTAL COEFFICIENT OF FRICTION [UNDER DIFFERENT TRIBOLOGICAL TREATMENT] AT VARIOUS POINTS ALONG THE WORKING FACE OF A NSOH-DIE WITH 15° SEMI-ANGLE REPRESENTED BY A SET OF ELEMENTAL DIES (TOTAL FRACTIONAL REDUCTION R_T = 0.375)

Re	ALUMINIUM NSOH DIE				COPPER NSOH DIE				BRASS NSOH DIE				STAINLESS STEEL NSOH DIE			
	μ_e	μ_{eL}	$\Delta\mu_e$	%I	μ_e	μ_{eL}	$\Delta\mu_e$	%I	μ_e	μ_{eL}	$\Delta\mu_e$	%I	μ_e	μ_{eL}	$\Delta\mu_e$	%I
0.125	0.13	0.11	0.02	15	0.06	0.06	0.0	0	6.7×10^{-8}	4.8×10^{-8}	2×10^{-8}	28	0.06	0.06	0.0	0
0.250	0.07	0.05	0.02	29	0.24	0.02	0.22	92	0.05	6.8×10^{-6}	0.50	100	6×10^{-8}	10^{-8}	5×10^{-8}	83
0.375	0.19	0.17	0.02	12	0.17	0.14	0.03	18	0.14	0.13	0.01	7	0.12	0.11	0.01	8

Table 6.99(a)

SUMMARY AND COMPARISON TABLE OF ELEMENTAL COEFFICIENT OF FRICTION [UNDER DIFFERENT TRIBOLOGICAL TREATMENT] AT VARIOUS POINTS ALONG THE WORKING FACE OF A HCHC-DIE WITH 15° SEMI-ANGLE REPRESENTED BY A SET OF ELEMENTAL DIES (TOTAL FRACTIONAL REDUCTION R_T = 0.375)

Re	ALUMINIUM HCHC DIE				COPPER HCHC DIE				BRASS HCHC DIE				STAINLESS STEEL HCHC DIE			
	μ_e	μ_{eL}	$\Delta\mu_e$	%I	μ_e	μ_{eL}	$\Delta\mu_e$	%I	μ_e	μ_{eL}	$\Delta\mu_e$	%I	μ_e	μ_{eL}	$\Delta\mu_e$	%I
0.125	0.13	0.11	0.02	15	0.05	0.06	-0.01	20	5.5×10^{-7}	5×10^{-7}	$.5\times10^{-7}$	9	0.06	0.06	0.0	0
0.250	0.07	0.05	0.02	28	0.03	0.02	0.01	33	0.002	7×10^{-4}	1.3×10^{-3}	65	5.7×10^{-8}	5.7×10^{-8}	0.0	0
0.375	0.19	0.16	0.03	16	0.20	0.14	0.06	30	0.14	0.14	0.0	0	0.12	0.10	0.02	17

Table 6.99(b)

SUMMARY AND COMPARISON TABLE OF ELEMENTAL COEFFICIENT OF FRICTION [UNDER DIFFERENT TRIBOLOGICAL TREATMENT] AT VARIOUS POINTS ALONG THE WORKING FACE OF A CAST IRON-DIE WITH 15° SEMI-ANGLE REPRESENTED BY A SET OF ELEMENTAL DIES (TOTAL FRACTIONAL REDUCTION R_T = 0.375)

Re	ALUMINIUM CAST IRON DIE				COPPER CAST IRON DIE				BRASS CAST IRON DIE				STAINLESS STEEL CAST IRON DIE			
	μ_e	μ_{eL}	$\Delta\mu_e$	%I	μ_e	μ_{eL}	$\Delta\mu_e$	%I	μ_e	μ_{eL}	$\Delta\mu_e$	%I	μ_e	μ_{eL}	$\Delta\mu_e$	%I
0.125	0.22	0.19	0.03	14	0.12	0.09	0.03	25	0.11	0.08	0.03	27	0.08	0.07	0.01	13
0.250	0.15	0.10	0.05	33	0.06	0.04	0.02	33	0.04	0.03	0.01	25	0.09	0.07	0.02	22
0.375	0.23	0.20	0.03	13	0.22	0.17	0.05	23	0.20	0.18	0.02	10	0.13	0.12	0.01	8

Table 6.99(c)

SUMMARY AND COMPARISON TABLE OF ELEMENTAL COEFFICIENT OF FRICTION [UNDER DIFFERENT TRIBOLOGICAL TREATMENT] AT VARIOUS POINTS ALONG THE WORKING FACE OF A NSOH-DIE WITH 15° SEMI-ANGLE REPRESENTED BY A SET OF ELEMENTAL DIES (TOTAL FRACTIONAL REDUCTION R_T = 0.250)

Re	ALUMINIUM NSOH DIE				COPPER NSOH DIE				BRASS NSOH DIE				STAINLESS STEEL NSOH DIE			
	μ_e	μ_{eL}	$\Delta\mu_e$	%I	μ_e	μ_{eL}	$\Delta\mu_e$	%I	μ_e	μ_{eL}	$\Delta\mu_e$	%I	μ_e	μ_{eL}	$\Delta\mu_e$	%I
0.083	0.22	0.19	0.03	14	0.09	0.07	0.02	22	10^{-7}	10^{-7}	0.0	0	0.02	0.02	0.0	0
0.166	0.09	0.06	0.03	33	10^{-7}	3.5×10^{-8}	6.5×10^{-8}	65	5.7×10^{-8}	5.6×10^{-8}	0.1×10^{-8}	2	10^{-8}	10^{-8}	0.0	0
0.250	0.24	0.20	0.04	17	0.10	0.09	0.01	10	0.11	0.09	0.02	18	0.08	0.07	0.01	13

Table 6.100(a)

SUMMARY AND COMPARISON TABLE OF ELEMENTAL COEFFICIENT OF FRICTION [UNDER DIFFERENT TRIBOLOGICAL TREATMENT] AT VARIOUS POINTS ALONG THE WORKING FACE OF A HCHC-DIE WITH 15° SEMI-ANGLE REPRESENTED BY A SET OF ELEMENTAL DIES (TOTAL FRACTIONAL REDUCTION R_T = 0.250)

Re	ALUMINIUM HCHC DIE				COPPER HCHC DIE				BRASS HCHC DIE				STAINLESS STEEL HCHC DIE			
	μ_e	μ_{eL}	$\Delta\mu_e$	%I	μ_e	μ_{eL}	$\Delta\mu_e$	%I	μ_e	μ_{eL}	$\Delta\mu_e$	%I	μ_e	μ_{eL}	$\Delta\mu_e$	%I
0.083	0.23	0.19	0.04	17	0.09	0.07	0.02	22	1×10^{-7}	10^{-7}	0.0	0	0.02	0.02	0.0	0
0.166	0.10	0.11	0.01	10	8.7×10^{-6}	3×10^{-8}	8.7×10^{-6}	50	5.6×10^{-8}	5×10^{-8}	0.6×10^{-8}	11	10^{-8}	10^{-8}	0.0	0
0.250	0.24	0.21	0.03	13	0.13	0.09	0.04	3	0.11	0.09	0.02	18	0.08	0.07	0.01	13

Table 6.100(b)

SUMMARY AND COMPARISON TABLE OF ELEMENTAL COEFFICIENT OF FRICTION [UNDER DIFFERENT TRIBOLOGICAL TREATMENT] AT VARIOUS POINTS ALONG THE WORKING FACE OF A CAST IRON-DIE WITH 15° SEMI-ANGLE REPRESENTED BY A SET OF ELEMENTAL DIES (TOTAL FRACTIONAL REDUCTION R_T = 0.250)

Re	ALUMINIUM CAST IRON DIE				COPPER CAST IRON DIE				BRASS CAST IRON DIE				STAINLESS STEEL CAST IRON DIE			
	μ_e	μ_{eL}	$\Delta\mu_e$	%I	μ_e	μ_{eL}	$\Delta\mu_e$	%I	μ_e	μ_{eL}	$\Delta\mu_e$	%I	μ_e	μ_{eL}	$\Delta\mu_e$	%I
0.083	0.21	0.20	0.01	5	0.12	0.12	0.0	0	0.003	2.5×10^{-7}	0.003	=0	0.05	0.05	0.0	0
0.166	0.19	0.07	0.12	63	0.10	0.10	0.0	0	10^{-7}	10^{-7}	0.0	0		10^{-8}	0.0	0
0.250	0.34	0.18	0.16	47	0.16	0.13	0.3	19	0.14	0.12	0.02	14	0.10	0.07	0.03	30

Table 6.100(c)

SUMMARY AND COMPARISON TABLE OF THE SIGNIFICANT VALUES OF COEFFICIENT OF FRICTION (μ_e AND μ_{eL} AT DIE EXIT) AT TOTAL FRACTIONAL REDUCTION, R_T = 0.375 FOR DIFFERENT TUBE MATERIALS AND DIFFERENT DIE MATERIALS WITH 7° AND 15° SEMI-ANGLES

DIES	ALUMINIUM SPECIMENS				COPPER SPECIMENS				BRASS SPECIMENS				STAINLESS STEEL SPECIMENS			
	7°		15°		7°		15°		7°		15°		7°		15°	
	μ_e	μ_{eL}	μ_e	μ_{eL}	μ_e	μ_{eL}	μ_e	μ_{eL}	μ_e	μ_{eL}	μ_e	μ_{eL}	μ_e	μ_{eL}	μ_e	μ_{eL}
NSOH	0.60	0.27	0.19	0.17	0.58	0.26	0.17	0.14	0.23	0.19	0.14	0.13	0.20	0.13	0.12	0.11
HCHC	0.64	0.27	0.19	0.16	0.61	0.26	0.20	0.14	0.23	0.20	0.14	0.14	0.20	0.14	0.12	0.10
CAST IRON	0.46	0.44	0.23	0.20	0.36	0.36	0.22	0.17	0.37	0.30	0.20	0.18	0.24	0.24	0.13	0.12

Table (6.101)

SUMMARY AND COMPARISON TABLE OF THE SIGNIFICANT VALUES OF COEFFICIENT OF FRICTION (μ_e AND μ_{eL} AT DIE EXIT) AT TOTAL FRACTIONAL REDUCTION, R_T = 0.250 FOR DIFFERENT TUBE MATERIALS AND DIFFERENT DIE MATERIALS WITH 7° AND 15° SEMI-ANGLES

DIES	ALUMINIUM SPECIMENS				COPPER SPECIMENS				BRASS SPECIMENS				STAINLESS STEEL SPECIMENS			
	7°		15°		7°		15°		7°		15°		7°		15°	
	μ_e	μ_{eL}	μ_e	μ_{eL}	μ_e	μ_{eL}	μ_e	μ_{eL}	μ_e	μ_{eL}	μ_e	μ_{eL}	μ_e	μ_{eL}	μ_e	μ_{eL}
NSOH	0.55	0.29	0.24	0.20	0.25	0.20	0.10	0.09	0.20	0.08	0.11	0.09	0.14	0.12	0.08	0.07
HCHC	0.48	0.20	0.24	0.21	0.26	0.20	0.13	0.09	0.20	0.07	0.11	0.09	0.14	0.12	0.08	0.07
CAST IRON	0.26	0.24	0.34	0.18	0.31	0.28	0.16	0.13	0.25	0.25	0.14	0.12	0.18	0.18	0.10	0.07

Table (6.102)

6.16. Results from the Experiment

1) Shown in Tables 6.01(a) to 6.12(a) are the measured analogue values of the uncorrected elemental drawing forces, Fe's (mm) [elemental drawing force due to full elemental redundant deformation] with their mean values F_{Deu} (mn) for 0.375 total fractional reduction, R_T, of aluminium, copper, brass and stainless steel specimens drawn through the sets of N.S.O.H; H.C.H.C. and Cast Iron elemental dies with 7° semi-angle without application of lubricant.

2) In Tables 6.01(b) to 6.12(b) are the resulting data from Tables 6.01(a) to 6.12(a) of uncorrected elemental drawing forces, F_{Deu} (mm) and (N), calculated applicable redundant deformation forces, R_{De} (N), corrected elemental drawing forces F_{De} (N), and the calculated elemental coefficient of friction, μ_e.

3) Also shown in Tables 6.13(a) to 6.24(a) are the measured analogue values of the uncorrected elemental drawing forces, Fe's (mm) [elemental drawing forces with full elemental redundant deformation] with their mean values, F_{Deu} (mm) for 0.375 total fractional reduction, R_T, of aluminium, copper, brass and stainless steel through the sets of N.S.O.H, H.C.H.C. and Cast Iron elemental dies with 7° semi-angle respectively with application of lubricant.

4) The resulting data of the uncorrected elemental drawing forces (mm) and (N), calculated redundant deformation forces, R_{De} (N), corrected elemental drawing forces, F_{De} (N), and the calculated

elemental coefficient of friction, μ_e, from Tables 6.13(a) to 6.26(a) are as shown in Tables 6.13(b) to 6.26(b).

5) The data in Tables 6.25(a) to 6.36(a) are the measured analogue of the uncorrected elemental drawing forces, Fe's (mm) with their mean values, F_{Deu} (mm) for 0.250 total fractional reduction, R_T, of aluminium, copper, brass and stainless steel specimens drawn through the sets of N.S.O.H, H.C.H.C. and Cast Iron elemental dies with 7° semi-angle without lubricant.

6) In Tables 6.25(b) to 6.36(b) are the resulting data from Tables 6.25(a) to 6.36(a) of the uncorrected elemental drawing forces, F_{Deu} (mm) and (N), calculated applicable elemental redundant deformation forces, R_{De} (N), corrected elemental drawing forces, F_{De} (N), and the calculated elemental coefficient of friction, μ_e.

7) Similar data to the ones in (5) and (6) for the same total fractional reduction R_T (0.25), the same specimens, the same sets of elemental dies mentioned in (5) and (6) but with application of lubricant are as shown in Tables 6.37(a) to 6.48(a) and Tables 6.37(b) to 6.48(b).

8) Shown in Tables 6.49(a) to 6.60(a) are the measured analogue values of the uncorrected elemental drawing forces, Fe's (mm) with their mean values, F_{Deu} (mm) for 0.375 total fractional reduction, R_T of aluminium, copper, brass and stainless steel specimens drawn without lubricant through sets of N.S.O.H. H.C.H.C. and Cast Iron elemental dies with 15° semi-angle.

9) Also in Tables 6.49(b) to 6.60(b) are the resulting data from Tables 6.49(a) to 6.60(a) of the uncorrected elemental drawing forces, F_{Deu} (mm) and (N), calculated related elemental redundant deformation forces, R_{De} (N), corrected elemental drawing forces, F_{De} (N) and the calculated elemental coefficient of friction, μ_e.

10) Also similar data to the ones in (8) and (9) for the same total fractional reduction R_T (0.375), the same specimens, and the same sets of elemental dies mentioned in (8) but with application of lubricant are as shown in Tables 6.61(a) to 6.72(a) and Tables 6.61(b) to 6.72(b).

11) In Tables 6.73(a) to 6.84(a) are the measured analogue values of the uncorected elemental drawing forces, Fe's (mm), with their mean values, F_{Deu} (mm) for 0.250 total fractional reduction, R_T of aluminium, copper, brass, and stainless steel drawn through the sets of (15° semi-angle) N.S.O.H., H.C.H.C, and Cast Iron elemental dies without lubricant.

12) Also in Tables 6.73(b) to 6.84(b) are the resulting data from Tables 6.73(a) to 6.84(a) of the uncorrected elemental drawing forces, F_{Deu} (mm) and (N), calculated related elemental redundant deformation forces, R_{De} (N), and corrected elemental drawing forces, F_{De} (N) and the calculated elemental coefficient of friction, μ_e.

13) Shown in Tables 6.85(a) to 6.96(a) and Tables 6.85(b) to 6.96(b) are the data similar to cases (11) and (12) for the same total

fractional reduction, R_T = 0.250, the same specimens and the same set of elemental dies with 15° semi-angle, but employed with application of lubricant.

14) The results in Tables 6.97(a) to 61.100(a) are the summaries and comparison of the elemental coefficients of friction, μ_e and μ_{eL} for the two tribological conditions (drawing of the different tubes with and without lubricant progressively through the sets of N.S.O.H, H.C.H.C. and Cast Iron elemental dies with 7 and 15 semi-angles to attain total fractional reductions of 0.375 and 0.250 respectively tested.

Also shown in the same tables are the differences, $\Delta\mu_e$ between the two values, μ_e and μ_{eL} with the improvement 'I' (due to the use of lubricant) expressed as a percentage of the coefficient of friction without lubricant.

15) The resulting data in Tables 61.101 and 61.102 are the summaries of the elemental coefficient of friction at the exit of all the 7° and 15° semi-angle of the die set employed to draw all the different specimens with and without lubricant. These coefficients of friction at the exits are defined as the significant (μ_s and μ_{sL}) values of coefficients of friction needed for calculation of the total drawing froces of the tubes due to redundant deformation through a proto-die at one pass to attain 0.375 and 0.25 fractional reductions respectively.

16) The curves shown in Figures 6.01 to 6.13 and Figures 6.14 to 6.24 are the graphs of the elemental coefficients of friction against elemental fractional reductions of the N.S.O.H., H.C.H.C and Cast Iron dies with 0.375 and 0.250 total fractional reduction and with 7° and 15° semi-angles employed to draw the different tube materials with and without lubricant respectively.

6.17 Correlating Upper Bound Theorem with the Experimental Results

From Upper Bound hypothesis:

$$\tau_R = \mu_e p_e \leqslant k$$

where τ is the elemental shear stress due to friction

μ_e is the die-workpiece interface elemental coefficient of friction

k is the yield stress in shear of the workpiece.

From Tresca Yield Criterion: $k = Y/2$

where Y is the yield stress in uniaxial tension or compression.

Also from [Sach's]

$$F_e = \pi D_e \mu_e \int_0^x p_e dx$$

Table 61.103

COMPARISON TABLE FOR CALCULATED RESULTS EMPLOYING UPPER BOUND THEOREM WITH THE EXPERIMENTAL RESULTS FOR AN ALUMINIUM SPECIMEN WITH $\bar{Y}$ = 197 MPa

Re	μ_e	De (mm)	$\int_0^x dx$ (mm)	Pe(e) (MPa)	Fe(e) (kN)	Pe(u) = k/μ_e (MPa)	Fe(u) (kN)
0.075	0.27	14.8	4.92	7.31	0.452	364.8	15.24
0.150	0.30	13.6	4.92	8.94	0.564	328.3	17.10
0.225	0.31	12.4	4.92	11.58	0.712	317.7	18.90
0.300	0.42	11.2	4.92	19.50	1.419	234.5	20.69
0.375	0.60	10.0	4.92	23.36	2.168	164.2	22.57

ΣFe(e) = 5.313 (kN) ΣFe(u)= 94.5 (kN)

Note:

μ_e The experimental elemental coefficient of friction of NSOH-AL from Table 6.97(a).

Pe(e) The experimental elemental radial pressure estimated for NSOH-AL from Table 7.07, Appendix 7.

Fe(e) The experimental frictional force based on Pe(e)

Pe(u) The unacceptable, calculated elemental radial pressure using upper bound theorem based on plain strain deformation.

Fe(u) The corresponding unacceptable elemental frictional forces based on Pe(u).

6.18 Discussion

The most striking point one would notice at the first glance through the results of the elemental drawing forces, F_{Deu} due to the full elemental redundant deformation is the inequality of the elemental forces, F_{Deu} across each element which makes up a set of the elemental dies that constitute a proto-die even though each

elemental die in a set contributes the same elemental fractional reduction, Re, to the total fraction reduction R_T ($Re_1 = Re_2 = Re_3 = R_n$ and $\Sigma Re = R_T$) of the proto-die. The elemental force, F_{Deu}, increases progressively across the pass of a proto-die because the workpiece strain-hardening and increase of yield stress across the die pass vary from material to material depending on the nature of the tubing material. For example, across the 24.62 mm total pass of the 7° semi-angle (0.375 total fractional reduction, R_T) set of elemental dies, the yield stress of copper specimen increased from its initial value of 146 MPa to about 230 MPa whilst that of stainless steel increased sharply to 874 MPa from 310 MPa, its initial value. The strain hardening and increase in yield stresses of these two materials seemed to have provided a succinct elucidation on the reason for the increase of elemental drawing forces across the die pass. From the result tables: (2085 N, 2286 N, 2532 N, 2838 N and 3320 N) and (3215 N, 4730 N, 6027 N, 7104 N and 7674 N) are the sets of elemental drawing forces, F_{Deu}, due to redundant deformation recorded for both copper and stainless steel specimens drawn through the same set of dies without lubricant respectively. With this variation of the drawing force across the die pass, the variation of the coefficient of friction across the pass becomes less surprising.

However, it must be borne in mind that while increase in yield stress constitutes increase in the drawing force across the die pass, its influence on the coefficient of friction according to the results attained could be in the negative direction. For example, at the die exit where fractional reduction, $R_T = 0.375$ (die with $\alpha = 7°$) the

values of coefficient of friction recorded for aluminium, copper and stainless steel specimens with 197 MPa (mean yield stress) 185 MPa (mean yield stress) and 874 MPa (elemental yield stress) are 0.60, 0.58 and 0.20 respectively. Another major influential mechanical property on coefficient of friction between the die-workpiece face is the hardness which also being enhanced by the increase in yield stress of the tube material. As has been shown by Figures 6.25 and 6.26 (the graphs of the significant coefficient of friction μ_s against initial hardness of the tube material) the coefficient of friction goes down with high initial tube material hardness. These graphs of the initial material hardness against the significant coefficient of friction μ_s is a generalised and conclusive data deduced from the experimental results for any tube material with the same wall thickness intended to be subjected to any fractional reduction within the range covered by the experiment.

Looking into the effect of die material on the values of the coefficient of friction, it would be noticed from the results obtained that the differences between the values of coefficient of friction recorded for the tube materials drawn through non-shrinking oil hardening and high carbon chromium (NSOH and H.C.H.C) dies are very small and negligible. The small differences could be attributed wholly to general experimental errors. Therefore, with almost identical results recorded for the two die materials, NSOH and H.C.H.C., the preference for their practical or industrial use would depend on the cost, machineability and durability. The results show that the use of lubricant during the employment of both die-material,

NSOH and H.C.H.C. resulted in the same drastic reduction in the values of the coefficient of friction. Both die materials responded well to the use of lubricant. Up to 60% reductions in the values of the coefficient of friction were recorded for both die materials with 7° and 15° semi-angles.

However, turning to the Cast Iron die case, the die material (Cast Iron) responded to the tube materials and lubricant differently when compared with the cases of H.C.H.C. and NSOH dies. Without the use of lubricant there was a sharp drop in the values of coefficient of friction recorded for Cast Iron - AL (aluminium specimen drawn through Cast Iron die) when compared with the cases of NSOH-AL and HCHC-AL. For the 7° semi-angle case (testing aluminium specimen without lubricant), 0.60 and 0.46 significant coefficient of friction, μ_s, were recorded for either H.C.H.C. or NSOH and Cast Iron dies respectively. This gives a reduction of about 23% for the significant value, μ_s recorded for the Cast Iron die case. Also a reduction of about 38% over the other die materials (NSOH and HCHC) was recorded for the Cast Iron-Cu (copper specimen tested through Cast Iron dies). Surprisingly, however, Cast Iron dies responded in the reverse direction with tubing material with higher hardness (i.e. increase in coefficient of friction compared with the other die materials, HCHC and NSOH). Up to about 20% increase in coefficient of friction values was recorded for Cast Iron-Stainless steel (tube) over the values recorded for HCHC-SS and NSOH-SS cases.

Cast Iron die material has a very hard grain structure and with such a hard and tough material as stainless steel being drawn against the hard grains of the Cast Iron dies, the higher values of coefficient of friction over other softer die materials (HCHC and NSOH) appear to be justified. However, a closer look into the result summaries would reveal that the Cast Iron dies have got little or no affinity for the use of lubricant. As shown by the results, there was little or negligible difference between the values of coefficient of friction recorded for both cases (with and without lubricant). The simple reason for this is that the graphite structure of the Cast Iron die acts as lubricant between the die and the workpiece face hence the reduction in the coefficient of friction values over the values attained for other die materials employed under the same tribological condition (i.e. used without lubricant) and eventually when lubricant is applied to the specimen and the working face of the Cast Iron, the application of the lubricant becomes less significant in terms of the reduction in the coefficient of friction.

Thoroughly studying the results in the summary table (comparing the significant values of coefficient of friction of 7° andd 15° semi-angle for the same fractional reduction) comparing 7° and 15° semi-angle significant values, μ_S and μ_{SL} would reveal that up to 70% drop over the significant values recorded for soft and ductile materials tested through 7° semi-angle dies was recorded for the same materials using 15° semi-angle dies (e.g. for NSOH-Al [α = 7°], μ_S = 0.60; for NSOH-AL [α = 15°] μ_S = 0.19). For harder materials such as

brass and stainless steel the drop attained in the significant values of coefficient of friction through the use of 15° semi-angle dies (when compared with the case of dies with α = 7°) for the same fractional reduction is about 40% (e.g. for NSOH-SS [α = 7°], μ_s = 0.12 at 0.375 total fractional reduction).

However, it must not be forgotten that the high reduction in the significant values of the coefficient of friction of 15° semi-angle die is at the expense of higher redundant deformation work as has been shown in the general result tables.

For example, for the 0.375 total fractional reduction at the die exits (for both 7° and 15° semi-angle), the redundant deformation forces for aluminium and stainless steel tubes, employing dies with semi-angle of 7° are 243 N and 1014 N respectively while the redundant forces for the same materials using dies with 15° semi-angle are about 545 N and 1750 N respectively. In spite of this higher redundant work encountered in the use of 15° semi-angle dies, it has been demonstrated under redundant deformation experiment that for the same fractional reduction of a tube material, due to lower coefficient of friction, less total drawing force is needed when a die with 15° semi-angle is in use.

Studying the curves of elemental coefficient of friction and that of elemental radial pressure (against elemental fractional reduction Re), one would realise that the exponential form of the radial pressure variation across the proto-die pass is a connotation of how

much the two parameters depend on one another. The results show that the radial pressure increases as the coefficient of friction across the die pass.

However, as shown in Table (61.103), the data from the experimental results are in contrast with the hypothesis of the upper bound theorem. As shown the results Table (61.103) the experimental die pressure, Pe(e), increases from its minimum value, 7.31 MPa at the die entry to 23.36 MPa at the exit whilst the radial pressure calculated from the upper bound theorem, $\tau = \mu p \leq k$ decreases from its unacceptable maximum value 364.8 MPa at the entry to 164.2 MPa at the die exit.

From the calculation based on the radial pressure attained through the upper bound assumption a total (ΣFe(u)) frictional force of 22.5 kN which is almost four times the actual measured total drawing force, F_d (5.95 kN) due to redundant deformation was recorded. Comparing this frictional force value, 22.5 kN with that of experimental friction force (ΣFe(e)), 4.603 kN [about 77% of the total drawing force] the apparent conclusion which can be drawn from the result is invalidity of upper bound assumption application to tube sinking analysis.

The only apparent reason for this invalid result is the theorem of the plain strain deformation situation being imposed on a somewhat rather different situation of tube sinking analysis.

6.19. Conclusions

1) The coefficient of friction across a die pass varies approximately in an exponential form as the accompanied radial pressure.

2) In spite of the variation of the coefficient of friction across the die pass, the useful value defined as the significant value of coefficient of friction for calculation of the total drawing force due to friction is the value attained at the die exit, μ_s or μ_{sL}.

3) A generalised and conclusive graphical data deduced from the experimental results (based on the initial hardness of the workpiece specimen) can be employed for the estimation of the appropriate value of coefficient of friction for the calculation of the total drawing forces for any fractional reductions of tubes which fall within the range covered by the experiment.

4) The method employed for the experiment and its analysis (the proposed elemental die theory) has eliminated the problem of unreliable results from the upper bound assumption as applied to tube sinking analysis.

5) With more than 50% improvement or reduction recorded in most cases (except for Cast Iron dies) for the coefficient of friction over the test carried out without lubricant, the results of the test have clearly defined the importance of the use of lubricant in tube sinking.

6) Except for prolonging the die life from wear, it is concluded from the results attained that lubrication of the Cast Iron die contributes only little improvement in the reduction of coefficient of friction along the working face of the die.

CHAPTER 7

RADIAL PRESSURE EXPERIMENT

7.11. Objective of the Experiment

Several attempts were made by previous workers working on the tube sinking process to develop a method of estimating the coefficient of friction, μ, but their theories were in marked disagreement over the die radial pressure. In most cases no attempts were made to analyse the profile of this pressure across the entire pass of the dies employed; instead only a rough estimate of the average radial pressure at the die exit was made - perhaps due to lack of appropriate instruments and equipment.

In order to enable us to correlate the results of our present work on coefficient of friction with the estimates from the upper bound theory, i.e. $\tau = \mu p \leq k$, it is considered necessary to provide an appropriate and reliable data of the die radial pressure through a fresh experiment with one of our dies and the tubing materials being employed in the coefficient of friction analysis. Therefore, the object of this experiment is to determine the radial pressure across the pass of a conical die and to compare the results of the experiment with the resulting data from the coefficient of friction analysis across the pass of the conical die.

7.12. Theory

Lame's Theory

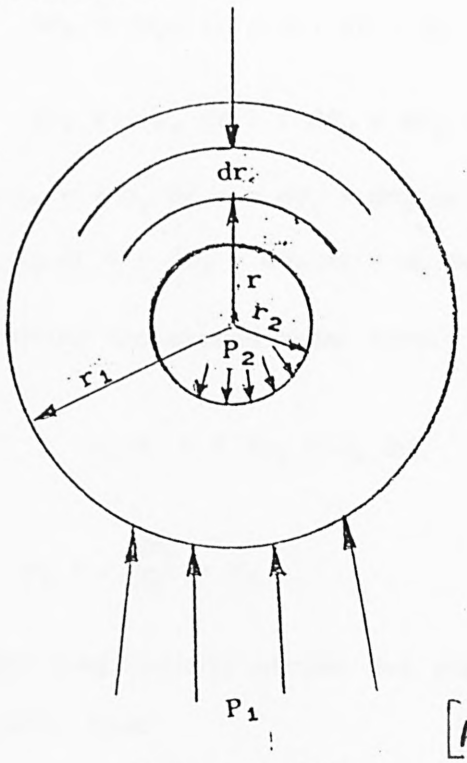

Figure (7.01a)

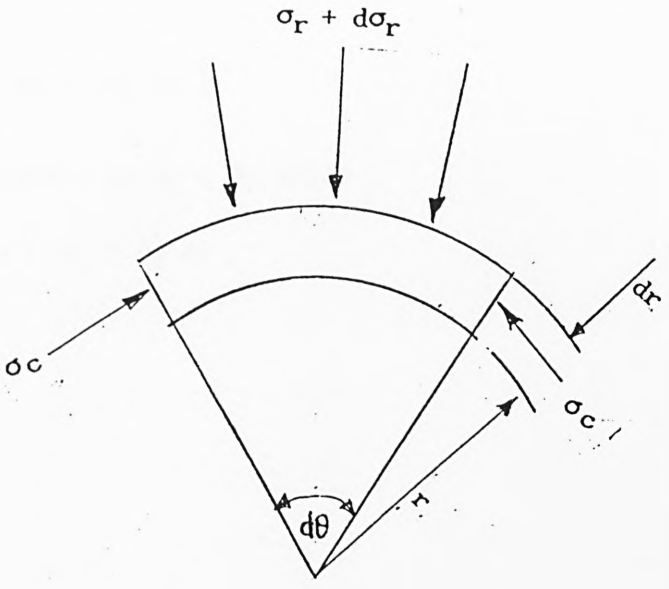

Figure (7.01b)

[After Stephens] [27]

Though a conical die with a very small semi-angle is still not a true ideal straight cylinder, however if the die is divided into a number of elements across its entire pass, each element on its own can be regarded as a small straight thick cylinder.

Figure (7.01a) shows a thick cylinder of external and internal radii, r_1 and r_2 respectively, with external and internal pressures, p_1 and p_2, and Figure (7.01b) shows the stresses acting on an element of radius r and thickness dr, subtending an angle $d\theta$ at the centre. The radial and circumferential stresses, σ_r and σ_c have both been assumed to be compressive, which is considered positive.

If the radial stress varies from σ_r to $\sigma_r + d\sigma_r$ over the thickness dr, then resolving forces on the element radially over a unit length of cylinder, [Reference 27]

$$(\sigma_r + d\sigma_r)\ (r + dr)\ d\theta = \sigma_r\ r\ d\theta + 2\sigma_c\ dr\ \frac{d\theta}{2}$$

$$\{\sigma_r\ r + \sigma_r\ dr + r\ d\sigma_r + d\sigma_r\ dr\}d\theta = \{r\ \sigma_r + \sigma_c\ dr\}d\theta$$

$$\therefore \sigma_r\ r + \sigma_r\ dr + r\ d\sigma_r + d\sigma_r\ dr = r\ \sigma_r + \sigma_c\ dr$$

$$\sigma_r\ dr + r\ d\sigma_r + d\sigma_r\ dr = \sigma_c\ dr$$

Neglecting the second order term:

$$\therefore \quad \sigma_r\ dr + r\ d\sigma_r = \sigma_c\ dr$$

or

$$\sigma_r + r\ \frac{d\sigma_r}{dr} = \sigma_c \qquad (7.1)$$

If the longitudinal stress and strain are denoted by σ_i and ϵ_i respectively, then:

$$\epsilon_\ell = \frac{\sigma_\ell}{E} = \nu\left(\frac{\sigma_r + \sigma_c}{E}\right)$$

It is assumed that ϵ_ℓ is constant across the thickness, i.e. that a plane cross-section of the cylinder remains plane after the application of pressure, and that σ_ℓ is also uniform across the thickness, both assumptions being reasonable on planes remote from the ends of the cylinder.

It therefore follows from these assumptions that $\sigma_r + \sigma_c$ is a constant, which will be denoted by 2a.

Thus:

$$\sigma_c = 2a - \sigma_r \qquad (7.2)$$

Substituting in equation (6):

$$\sigma_r + r\frac{d\sigma_r}{dr} = 2a - \sigma_r$$

or $$2\sigma_r\, r + r^2\frac{d\sigma_r}{dr} - 2a\, r = 0 \text{ multiplying through by r:}$$

i.e. $$\frac{d}{dr}(\sigma_r r^2 - a r^2) = 0$$

$$\therefore \quad \sigma_r r^2 - a r^2 = b$$

$$\sigma_r = a + \frac{b}{r^2} \qquad (7.3)$$

Therefore from equation (7.2),

$$\sigma_c = a - \frac{b}{r^2} \qquad (7.4)$$

Equations (7.3) and (7.4) are known as Lame's equations.

For a cylinder with internal pressure only:

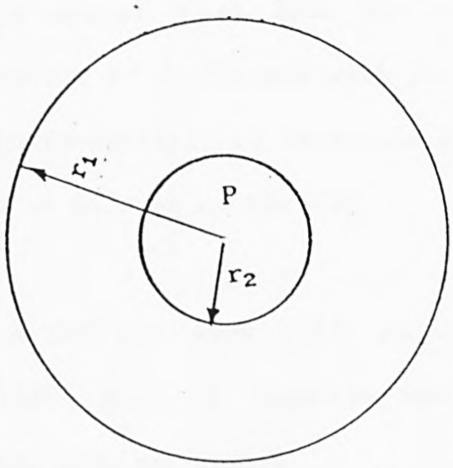

$\sigma_r = P$ when $r = r_2$

and $\sigma_r = 0$ when $r = r_1$

$$\therefore \quad P = a + \frac{b}{r_2^2}$$

$$\text{and } 0 = a + \frac{b}{r_1^2}$$

from which $a = -P \frac{r_2^2}{r_1^2 - r_2^2}$

and $$b = P \frac{r_1^2 \, r_2^2}{r_1^2 - r_2^2}$$

$$\therefore \sigma_r = a + \frac{b}{r^2}$$

$$\therefore \sigma_r = -P \frac{r_2^2}{r_1^2 - r_2^2} \left(1 - \frac{r_1^2}{r^2}\right) \qquad (7.5)$$

and $$\sigma_c = a - \frac{b}{r^2}$$

$$\therefore \sigma_c = -P \frac{r_2^2}{r_1^2 - r_2^2} \left(1 + \frac{r_1^2}{r^2}\right)$$

The maximum and circumferential stress occur at $r = r_2$, when $\sigma_r = P$

and

$\sigma_c = -P \frac{r_1^2 + r_2^2}{r_1^2 - r_2^2}$, the negative sign indicating tension.

7.13. Apparatus and Equipment

1) A conical Cast Iron die with 7° semi-angle, total fractional reduction of 0.375 and with 5, 120 Ω resistance strain gauges laid circumferentially at intervals of approximately 5 mm across the total pass of 24.6 mm of the die.

2) A CROPICO Apex Unit and Selector Switch: Type SM10, Serial No.15463 with 10 channels into which leads from the five strain gauges were connected.

3) A Wheatstone Bridge.

4) A Phillips meter, Serial No.PR.9307: Voltage range of 0 V to 10 V and output range between 0 to 5000 (micros).

5) A digital voltmeter to facilitate strain readings.

6) A hydraulic hand pump with 3000 lb/in^2 capacity.

7) Hille 100 kN hydraulic draw bench equipped with 50 kN load transducer.

8) 16 mm external diameter aluminium alloy specimens.

9) A 9 mm threaded plug of approximately 100 mm length with central hole of 1 mm diameter, connected to a threaded cylindrical base of 20 mm diameter, connected to the connection of the hand hydraulic pump, (see Figure (7.08)).

7.14 Procedure

7.15 Part 1

1) With the digital voltmeter connected to the voltage output connection of the Phillips meter and the voltage reading set to 1 V range, the strain gauge leads were connected to the Apex Unit and selector switch and to the Wheatstone Bridge.

2) With the operating voltage of the Phillips meter set to 2 V, the switch at the back of the Phillips meter was turned to half-bridge operation because we were dealing with one active and one dummy gauge.

3) To balance the meter, the sensitivity knob was switched to low region, and the balance knob was turned to the direction desired to achieve zero deflection of the indicating needle arm.

4) For coarse adjustment of the needle towards zero position, the potentiometer knob of the meter was turned and the needle arm was finally adjusted to zero position with the meter fine adjustment knob.

5) With the core of the die and an aluminium specimen properly coated with one of the lubricants, the specimen was plugged into the die and the assembly (die and specimen) were carefully and gently located in the die box of the hydraulic draw bench and the pointed end of the specimen was clamped to the clamp provided on the draw bench.

6) The needle arm of the Phillips meter was readjusted to zero position.

7) In order to attain 100 micros full-scale deflection to enable calibration of the Phillips meter reading with DVM voltage readout, the Phillips meter sensitivity voltage was adjusted to 1 mV. With the DVM voltage range re-ensured at 1 V position, a calibration of 0.01 V ≡ 1 micro was achieved.

8) With the ram speed of the draw bench set to 2 cm/min. while the 100 cm long aluminium specimen was being drawn through the die, 3 readings of strain were recorded for each gauge on the dies before the drawing of the specimen was completed through its entire length.

9) Then the procedures were repeated for other ram speeds, 3 cm/min., 4 cm/min. and different lubricants.

7.16 Part 2 - Calibration

i) With the screw plug properly sealed and fitted onto the die, the threaded cylindrical base nut was fitted onto the manually operated hydraulic pump. The set up was as shown in Figure (7.08) except with the data logger replaced by the Apex Switch Selector, Phillips meter and the DVM.

ii) Having ensured that there was no leakage either from the plug-die assembly and the pump connection, then the procedures (1), (2), (3), (4) and (7) of Part 1 were repeated.

iii) While the pressure of the oil was being pumped progressively from zero to the maximum capacity, 3000 lb/in^2 of the hydraulic pump, 4 strain readings were taken at every 200 lb/in^2 interval of pressure for strain gauge No.1 (i.e. strain gauge located at the die entrance).

iv) The pressure was pumped up to the maximum, 3000 lb/in^2 and reduced progressively and readings checked at every 200 lb/in^2 to cross check the readings taken in (iii) but in reverse direction.

Estimation of Frictional Force for Two Die Materials Lubricated with the Same Lubricant

$$F_e = \pi\ D_e\ \mu_e \int_0^x P_e\ dx \qquad \text{[Sachs]}$$

where D_e is the mean external elemental diameter

μ_e is the elemental coefficient of friction

P_e is the absolute elemental radial pressure

$\int_0^x dx$ is elemental die length

and F_e is the elemental frictional force.

Results Summary Table

Re	D_e (mm)	$\int_0^x dx$ (mm)	P_e (MPa)	CAST IRON μ_{eL}	CAST IRON F_e (N)	NSOH DIE μ_{eL}	NSOH DIE F_e (N)
0.075	14.8	4.92	3.82	0.17	149	0.11	97
0.150	13.6	4.92	4.60	0.23	223	0.14	136
0.225	12.4	4.92	7.56	0.23	334	0.16	232
0.300	11.2	4.92	11.54	0.31	620	0.19	380
0.375	10.2	4.92	17.77	0.46	1264	0.27	742
					2590 (N)*		1587(N)*

Table (7.17)

u_{eL}'s are value of the elemental coefficient of friction for the 7° semi-angle, Cast Iron and NSOH dies (lubricated with Dromus "B") from Tables (6.97(c) and (6.97(a)

* Sum of the elemental friction force, ΣF_e.

v) Then procedures (iii) and (iv) were repeated for the rest of the 4 strain gauges, and the average strain readings for the individual gauges at every pressure of 200 lb/in^2 were calculated.

vi) Because there was little or no difference in the set of the average strain readings for the five gauges employed, only 3 sets of average strain readings were plotted against the pressure.

7.17. Results from the Experiment

1) Shown in Tables (7.01), (7.02), (7.03), (7.04) and (7.05) are the results of the 4 strain readings with their average values, ϵ_{1av}, ϵ_{2av}, ϵ_{3av}, etc., recorded between zero and 3000 lb/in^2 at intervals of 200 lb/in^2 for the 5 strain gauges respectively.

2) Figure (7.02) is the plot of the set of average strain readings against pressure of 3 channels of the 5 strain gauges employed for the test to provide calibration for the strain readings recorded when the specimens were drawn through the die.

3) Shown in Tables (7.06) to (7.16) are the strain readings with their average values and their equivalent radial pressure calculated from the calibration equation (equation (7.6)) at various fractional reductions across the die pass, at different drawing speeds under different tribological treatments.

4) The curves shown in Figures (7.03) to (7.06) are the plots of the elemental radial strain against elemental fractional reduction and

the plots of elemental radial pressure against elemental fractional reduction for the specimens drawn at 3 cm/min. and 2 cm/min. of the draw bench speed with the use of different lubricants respectively.

5) In Table (7.17) is the results summary showing the elemental frictional force estimated for both Cast Iron and Non-Shrinking Oil hardening die material lubricated with the same lubricant, while aluminium tube is drawn through them, and the resulting curves of elemental frictional force against elemental fractional reduction for both dies are as shown in Figure (7.07) .

7.18. Discussion

At the first glance through the plots of the radial pressure against elemental fractional reduction, it would be noticed that the radial pressure varies exponentially from the entrance to the exit of the die as the coefficient of friction across the die pass. However, it must be borne in mind that a high coefficient of friction does not necessarily imply a higher radial pressure. As has been demonstrated in the results of the coefficient of friction test, higher coefficient of friction values were recorded for soft tube materials. The coefficient of friction itself depends on how much ploughing effect can the die working surface have on the tube materials. With increase in yield stress of the tube material, the frictional shear stess at workpiece-die interface increases hence the increase in the radial pressure as the tube material strain hardened across the die pass.

From the results shown in Table (7.15) a slight drop in the values of radial pressure across the die pass would be noticed when Mobil Dromus 'B' was employed as lubricant. This implies that there was a slight reduction of frictional shearing effect at workpiece-die interface across the die pass.

As has been discussed under coefficient of friction analysis, the correlation of the measured radial pressure with the theoretical values attained through the employment of upper bound hypothesis is very difficult because of the very marked disagreement between the two values. The upper bound predicted values are much larger than the measured radial pressure. The employment of the two values of radial pressure to assess the frictional force across a die pass exposed the extent of invalidity of the use of upper bound assumption based on plain strain theory for the estimation of upper bound value of coefficient of friction in tube sinking process, (see Table (61.103).

7.19 Conclusions

1) The radial pressure varies exponentially as the frictional force across the die pass.

2) The variation of drawing speed has negligible or no effect on the radial pressure across the die pass.

3) With better lubricant, the radial pressure across the die pass can be reduced slightly.

4) Due to marked disagreement between the measured radial pressure values and the values of the radial pressure predicted by upper bound assumption based on plain strain theory, it is concluded that the plain strain situation cannot be completely harmonised with an ideal tube sinking process.

CHAPTER 8

EXPERIMENT TO VERIFY AND TO ASSESS REDUNDANT DEFORMATION DUE TO PLASTIC AND ELASTIC WORK AND ELASTIC RECOVERY AT ENTRY AND EXIT RESPECTIVELY DURING DRAWING OF A THIN WALLED TUBE SLOWLY THROUGH A CONICAL DIE

8.11. Objective of the Experiment

1) To verify the existence of redundant work due to plastic-elastic work and elastic recovery at the entry and exit respectively during the drawing of a thin walled tube at a slow speed through a conical die.

2) To observe differences between the redundant work at the entry and exit of a conical die.

3) To test for correlation between theoretical redundant work predicted by Penny's proposed redundant deformation theory and results from experiment on thin walled tube drawn through a conical die.

4) To verify the validity of the proposed elemental die theory employed to determine the variation of coefficient of friction along the working face of a conical die using a set of elemental dies to represent approximately the profile of a conical die.

8.12. Theories

It has been shown in Chapter (3) that the elemental drawing force due to full elemental redundant deformation is given by:

$$F_{Deu} = \left\{\frac{\pi D_{e2} t m \bar{y}}{\cos\alpha}\right\}\left\{\frac{1 + \mu_e \cot\alpha}{\mu_e \cot\alpha}\right\}\left\{1 - \left[\frac{D_{e2}}{D_{e1}}\right]^{\mu_e \cot\alpha}\right\}$$

$$+ \frac{2\pi D_{e1} t \bar{y}\alpha}{3} \qquad (8.1)$$

For a typical conical die to be represented by a set of elemental dies when the elemental dies are used individually or progressively to draw a tube specimen until the achievable total fractional reduction, R_T, is attained, the total drawing force, F_{dT} is given by:

$$F_{dT} = \left\{F_{De1} + \frac{R_{De1}}{2}\right\} + \left\{F_{Deu2} - R_{De2}\right\} + \left\{F_{Deu3} - R_{De3}\right\}$$

$$+ \ldots\ldots\ldots\ldots + \ldots\ldots\ldots\ldots + \left\{F_{Deun} + \frac{R_{Den}}{2}\right\} \qquad (8.2)$$

When the drawing forces are measured in terms of strains, then (8.2) becomes:

$$\epsilon_{DT} = \left\{\epsilon_{De1} + \frac{\epsilon_{re1}}{2}\right\} + \left\{\epsilon_{eu2} - \epsilon_{re2}\right\} + \left\{\epsilon_{eu3} - \epsilon_{re3}\right\}$$

$$+ \ldots\ldots\ldots + \ldots\ldots\ldots + \left\{\epsilon_{Den} + \frac{\epsilon_{ren}}{2}\right\} \qquad (8.3)$$

where F_{De1} = elemental drawing force with exclusion of redundant deformation

R_{De1}, R_{De2}, R_{Den} are the elemental redundant deformation related to each elemental die

ϵ_{DT} = the hoop strain equivalent to F_{dT}, total drawing force

ϵ_{De} = hoop strain equivalent to elemental drawing force without redundant deformation

ϵ_{re} = hoop strain equivalent to elemental redundant deformation, R_{De}.

Also, for a typical conical die made of an assembly of elemental dies and then employed to draw the tube at one pass to the desired fractional reduction, R_T, then equations (8.2) and (8.3) become:

$$F_{dT} = \left\{F_{De1} + \frac{R_{De1}}{2}\right\} + F_{De2} + F_{De2} + F_{De4} + \cdots\cdots$$

$$+\cdots\cdots\cdots+ \left\{F_{Den} + \frac{R_{Den}}{2}\right\} \qquad (8.4)$$

and

$$\epsilon_{DT} = \left\{\epsilon_{De1} + \frac{\epsilon_{re1}}{2}\right\} + \epsilon_{De2} + \epsilon_{De3} + \epsilon_{De4} + \cdots\cdots$$

$$+ \cdots\cdots\cdots+ \cdots\cdots\cdots\left\{\epsilon_{Den} + \frac{\epsilon_{ren}}{2}\right\} \qquad (8.5)$$

For both cases:

$$\Sigma R_{De} = F_{red} = \frac{\pi D_{e11} t_1 \bar{y}\alpha}{3} + \frac{\pi D_{e1n} t_n \bar{y}\alpha}{3}$$

or

$$\Sigma R_{De} = F_{red} = \frac{\pi\alpha\bar{y}}{3}\left\{D_{e11}t_1 + D_{e1n}t_n\right\} \qquad (8.6)$$

Also,

$$\Sigma \epsilon_{re} = \frac{\epsilon_{re1}}{2} + \frac{\epsilon_{ren}}{2} = \frac{\epsilon_{re1} + \epsilon_{ren}}{2} \qquad (8.7)$$

8.13. Equipment

i) Hille 100 kN hydraulic draw bench equipped with 50 kN load transducer, Serial No.SZ-E-5223, Calibration of 4.38 kN/cm when used with amplifier Serial No.SG.905, Channel I, set at attenuation 80 and galvanometer, type B-450, Serial No.9-43177.

ii) A U.V. recorder with miniature galvanometer and U.V. sensitive (Kodak) recording paper to record an analogue of the drawing force, F_{Deu}, calibration 1 cm = 4.38 kN.

iii) A Phillips meter, Serial No.PR.9307 for measuring relative impedance variations in Wheatstone half or full-bridge arrangements. The meter is equipped with measuring ranges which employs attenuation with 11 steps: ±0.1mV/0.2mV/0.5mV/1mV/2mV/5mV/10mV/20mV/50mV/100mV/ 200mV similar to ±50 μ strain/100 μ strain/250 μ strain/500 μ strain, etc.

iv) A Modulog data logger type ML800 with the following features: Single channel (single shot), single channel (repeat), Auto scan (continuous) and scan speed ranging between 2 to 10 channels per second. The data logger is connected to an IBM typewriter for direct recording of the readings of the individual channels.

v) A strain gauge calibration box type M1C1-5000 microstrain with gauge factor of 2.

vi) A digital voltmeter to provide direct digital readout of the output from the Phillips meter and to facilitate readings.

vii) A 0 - 25 mm micrometer.

viii) A digital Vernier caliper.

ix) A steel rule.

x) Lubricating oil (Mobil "Dromus B").

xi) Nylon hand gloves to prevent the use of oily hands to operate the equipment in (ii), (iii) and (iv) whenever there was need for their operational adjustment.

xii) Specimen workpieces from 16 mm external diameter, 0.82 mm wall thickness stainless steel, annealed 70/30 brass, copper and aluminium alloy (N4), cold drawn seamless tubes. Each specimen with gauge length of approximately 8 cm, ends pointed by swaging and fitted with solid plugs suitable for leading the die's exits.

xiii) Dies with conical profile details as follows:

a) Sets of elemental dies to be used individually and progressively to draw the specimens and provide equivalent hoop strains, ϵ_{eu} to the individual elemental drawing forces F_{Deu} due to redundant deformation for the calibration of the strain readings, ϵ_{De} from the assembled elemental dies to be used as prototype in the second part of the experiment.

i) A set of 7° semi-angle elemental dies [5 in number] with a 120 Ω strain gauge laid circumferentially at the exit of each die and the strain gauge terminals connected to two banana plugs with 2 m cables. Nominal exit diametes - 14.80 mm, 13.60 mm, 12.40 mm, 11.20 mm and 10 mm respectively.

ii) A set of 15° semi-angle elemental dies [3 in number] with a 120 Ω strain gauge laid circumferentially at the exit of each die and the strain gauge terminals connected to two banana plugs

with 2 m cables. Nominal exit diameters, 14 mm, 12 mm and 10 mm respectively.

(iii) A set of 7° semi-angle elemental dies [5 in number] with a 120 Ω strain gauge laid circumferentially at the exit of each die and the strain gauge terminal connected to two banana plugs with 2 m cables. Nominal exit diametes, 15.20 mm, 14.4 mm, 13.60 mm, 12.80 mm, and 12 mm respectively.

(iv) A set of 15° semi-angle elemental dies [3 in number] with a 120 Ω strain gauge laid circumferentially at the exit of each die and terminal of the gauge connected to two banana plugs with 2 m cables.

b) Prototype dies (assembly of elemental dies) to draw specimen at one pass and to provide hoop strains, ϵ_{De} equivalent to the drawing forces. Without redundant deformation, F_{De}, at various points of the proto-dies.

i) Two prototype 7° semi-angle dies made up of the assembly of the elemental dies in a(i) and a(iii) with nominal exit diameters of 10 mm and 12 mm respectively. Terminals of the strain gauge on each element in each assembly are connected to a ten-channel point din plug for direct connection of the gauges to the data logger in (iv).

ii) Two prototype 15° semi-angle dies made up of the assembly of the elemental dies in a(ii) and a(iv) with nominal exit diameters of 10 mm and 12 mm respectively. Terminals of the strain gauge on each element in each assembly are connected to a ten-channel point din plug to the data logger in (iv).

xiv) Avery Universal Testing machine 250 KN capacity, type 7110 DEJ, Serial No.E.70254 operated as a force indicating slow hydraulic press.

xv) A sub-press, fitted with linear ball bearings on the guide pillars. Hardened ground and polished steel platens are fitted to the upper and lower internal faces of the die set.

xvi) A dial test indicator, calibrated with 0.01 mm divisions with 50 mm plunger traverse, complete with adjustable stand and a base with provision for magnetic clamping.

8.14. Test Procedure

The tests were carried out in 3 stages which included:

i) The use of elemental dies [in sets] individually and progressively to draw specimens for measurement of elemental strains, ϵ_{eu}, and their equivalent elemental drawing forces, F_{Deu}, due to redundant deformation to provide calibration for elemental strain readings, ϵ_{De}, equivalent to the elemental drawing forces, F_{De} (without redundant deformation) which their analogue cannot be measured simultaneously with the available transducer provided with the draw bench.

ii) The use of proto-dies [assemblies of elemental dies in (i)] to draw specimen at one pass for measurement of elemental strains, ϵ_{De} equivalent to the elemental drawing forces, F_{De} (without

redundant deformation) of each element in its respective assembly.

iii) The measurement of contact strains, ϵ_c, between the elements of the dies' assemblies in (ii).

8.15 Stage I(A)

1) The elemental dies in a set were arranged in the order of their nominal exit diameters for the progressive drawing of a specimen to the final diameter at a convenient reach.

2) The switch at the back of the Phillips meter was turned to half bridge position because we were dealing with one active and one dummy gauge.

3) The two banana plugs of the strain gauge of the first elemental die in the set were connected together with the terminal of the dummy to the Wheatstone bridge provided with the Phillips meter.

4) The output of the Phillips meter was connected to a digital voltmeter to facilitate readings.

5) Then the operating voltage of the Phillips meter was set to 2V.

6) To balance the meter, the sensitivity knob was turned to low region and the balance knob was turned to the direction desired to achieve zero deflection of the indicating needle.

7) For coarse adjustment of the needle towards zero position, the potentiometer knob of the meter was employed and the final adjustment of the needle to zero position was achieved by simply turning the fine adjustment knob.

8) Having properly coated the working face of the elemental die with lubricating oil (Mobil Dromus "B") the die was carefully and gently located in the die box of the hydraulic draw bench.

9) With the elemental die properly located in the die box, one of the annealed brass tube specimens was plugged into the elemental die and the pointed end of the specimen was firmly clamped to the clamp provided on the moving head of the hydraulic ram.

10) The indicating needle of the Phillips meter was readjusted to zero position.

11) Then the sensitivity of the meter was adjusted to 1 mV to achieve 100 micro strains full scale deflection which could be read directly in terms of mV from the Digital Voltmeter connected to the output of the Phillips meter.

12) With the ram speed of the hydraulic draw bench set to 1 cm/min, the aluminium specimen was drawn through its length and repetitive four readings of strains, ϵ_{u11}, ϵ_{u12}, ϵ_{u13}, and ϵ_{u14} were taken during the pass of tube through the die and the residual strain at the end of the pass was noted.

13) Then the procedures (3) to (13) were repeated for the rest of the elemental dies in the set, progressively with the original specimen until the desired final fractional reduction equal to that of proto-die at one pass was achieved.

14) Procedures (3) to (13) were repeated for another 5 annealed brass specimens.

15) Then procedures (3) to (14) were repeated for the remaining sets of elemental dies.

8.16. Stage I(B)

1) With the U.V. paper speed adjusted to 5 mm/sec and the galvanometer spot set to the desired position, the correct function of the force recording system was checked by switching attenuation to setting 12 and applying a manual force in the direction of the sinking force. The attenuation switch was then positioned at setting 90. Then the recorder paper feed was switched on just prior to commencement of drawing at 2 cm/min until the completion of the pass of each specimen progressively through individual elemental dies in each die set.

2) Only two specimens from each tubing material (aluminium, copper and brass) were drawn through the individual elemental dies in their respective sets which represent each dies' assembly employed in the Stages II and III of the tests because the measurement of the

elemental drawing force (analogue) F_{Deu}, for these materials has already been carried out under previous experiment (variation of coefficient of friction) with the same dies.

8.17. Stage II

The procedure for the second stage of the tests was as follows:

1) The bridge bank calibration unit was plugged into the 0 - 9 channel at the back of the data logger.

2) Having set the supply voltage to 2 V and the typewriter switch to stand-by position, the main of the logger was switched on.

3) The lower limit was set to zero while the upper limit was set to 1 above the required limit.

4) With mode set to single channel repeat, the start button was pressed and the zero reading was attained through the potentiometer provided.

5) The calibration button was depressed and reading displayed was adjusted to the desired calibration figure (in this case 4695 micro strain) with the scaling potentiometer appropriate to the channel 0 to 9 which was in use.

6) The calibration unit was unplugged from the logger and then replaced with one of the dies' assemblies gauges plug.

7) The upper limit was set to one above the number of gauges of the dies' assemblies.

8) Having pressed the start button of the logger, each channel of each gauge was either adjusted to zero or a convenient achievable reference, e.g. 100, 200 or 600 by pressing the incremental and the use of the potentiometer provided on the system.

9) Then the upper limit to the highest number of gauges of the dies' assembly and the lower limit button was depressed.

10) When the typewriter line length button was pressed to the number of gauges in the dies' assembly, the mode was set to single auto scan, the typewriter was set to carriage return and its switch on the logger was turned from stand-by to run position.

11) Then the start button was pressed to reference readings for the strain output from each channel.

12) With the working face of the elemental dies' assembly properly lubricated with lubricatin oil (Dromus "B") the proto-die (elemental assembly) was gently and carefully located in the die box of the hydraulic draw bench.

13) One of the aluminium specimens was properly coated with the oil (Dromus "B"), the specimen was plugged into the assembly of elemental dies and the pointed end firmly clamped with hydraulic draw bench clamp.

14) The hydraulic ram speed was set to 1 cm/min with the oil flow control valve of the draw bench.

15) Then the start button of the data logger was again pressed to print out the current references of each channel after the clamping of the specimen.

16) While drawing of the specimen continued at the preset speed of the ram, repetitive readings, ϵ_{es} (as many as possible) were taken by either using single auto scan or repeat auto scan modes provided on the logger.

17) As soon as enough consistent readings were taken for the pass, the speed of the ram was increased to draw the remaining part of the specimen through the die at a fast rate and immediately the passage of the tube was completed a few readings were taken to record the residual strains, ϵ_r, in each elemental die in the assembly after the drawing operation has been completed.

18) Procedures (11) to (17) were repeated for another six aluminium specimens which will constitute another six passes of specimens through the die assembly.

19) Procedures (11 to (18) were then repeated for copper specimens with the same proto-die (elemental die assembly).

20) Finally, procedures (1) to (19) were repeated for other proto-dies (elemental die assemblies).

8.18. Stage III(A)

1) With the same settings of the drawing speed and the U.V. paper employed in Stage I(B), the analogue values (at 1 cm = 4.38 kN) of the total drawing forces were taken at which each specimen of aluminium and copper was being drawn in one pass, through each proto-die (elemental die assembly) in the preceding stage).

2) Now the Universal Testing machine ws set to read on 12.5 kN full-scale.

4) With one of the dies' assembly properly located in the hole of a rotary forging tool holder and placed on the lower platen of the sub-press, the operating ram was lowered by operation of controls until a gap of about 20 mm existed between the die and the top anvil of the press.

5) Then procedures (1) to (11) of the preceding stage, (Stage II) were repeated.

6) The ram was then lowered until the gap between the upper pressing anvil and the back end of the elemental die assembly was reduced to approximately 0.1 mm.

7) By using the adjustment facility provided, the load scale was adjusted to zero.

8) Through the use of fine control valve, the speed of the ram was adjusted such that the indication of height on the dial indicator employed was reducing at approximately 0.16 mm/sec at which the elemental drawing forces, F_{De}, equivalent strains, ϵ_{De} were measured under Stage II.

9) Readings of contact strains between extreme die and pressing anvil, and readings of the contact strains, ϵ_c between the elemental die in the assembly were taken via typewriter equipped with data logger, at every 0.5 kN load until the maximum drawing force load, F_{dT} was reached.

10) Then, finally, procedures (2) to (9) were repeated for other die assemblies with the equivalent applicable total drawing forces, F_{dT}.

8.19 Stage III(B)

1) Now the procedures (1) to (7) of Stage I(A) were repeated while an elemental die in the set was properly located in the rotary forging tool holder.

2) Then the ram was lowered until the gap between the upper pressing anvil and the elemental die was about 0.1 mm.

3) The needle arm of the Phillips meter was readjusted to zero.

4) With the Digitial Voltmeter connected to the voltage output of the Phillips meter, the sensitivity of the meter was adjusted to 1 mV to give 100 micro strains full-scale deflection.

5) Through the use of the fine control valve provided, the ram speed was adjusted such that the indication height on the dial indicator in use was reducing at approximately 0.16 mm/sec to achieve drawing speed condition of 1 cm/min at which the elemental drawing forces, F_{De}, strain ϵ_{De}, equivalent were measured in each assembly of elemental dies in which the individual elemental dies were represented.

6) Readings of contact strain, ϵ_c between the elemental die and the pressing anvil were taken every 0.5 kN load until the maximum compressing load equal to the total drawing force, F_{dT}, to which the prototype (assembly) which the elemental die under test belonged to was subjected to Stage III(A).

7) Procedures (1) to (6) were repeated for the rest of the elemental dies in the same set.

8) Finally, procedures (1) to (7) were repeated for individual elemental dies in their respective sets.

8.20 Results Analysis

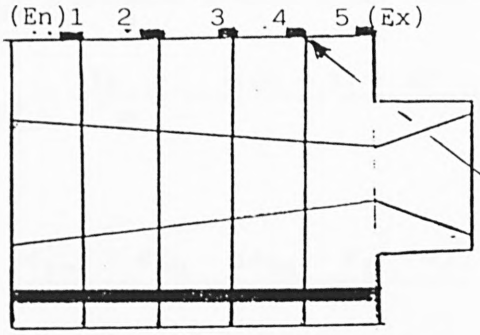

Assembly of 7° semi-angle
5 Elemental Dies

Figure (8.01)

Strain gauges

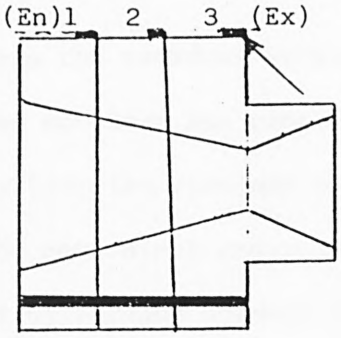

Assembly of 15° semi-angle
3 Elemental Dies

Strain gauges

Figure (8.02)

(i) $$\epsilon_{ea} = \frac{|\Sigma\epsilon_e|}{n}$$

where ϵ_{ea} is the average of the modulus of the uncorrected strain readings (ϵ_e's) of a particular element in its respective assembly. n is the number of uncorrected strain readings (ϵ_e's) taken per pass of the specimen through the assembly.

Examples:

From Table (8.15)

(1) $$\epsilon_{ea1} = \frac{|\Sigma\epsilon_{e1}|}{n} = |(46 + 55 + 54 + 54 + 53 + 53 + 53 + 53 + 53 + 53 + 53 + 53 + 53 + \ldots + \ldots + +)/|/23$$

i.e. $$\epsilon_{ea1} = \frac{|(\quad)|}{n} = \underline{53.46 \text{ (micro)}}$$

(2) $\epsilon_{ea2} = \frac{|\Sigma\epsilon_{e2}|}{n} = \frac{|(60 + 61 + 61 + 61 + \ldots + \ldots +)|}{23} = \underline{61.52 \text{ (micro)}}$

(3) $\epsilon_{ea3} = \frac{|\Sigma\epsilon_{e3}|}{n} = \frac{|(69 - 67 + 66 + 66 + \ldots + \ldots +)|}{23} = \underline{66.70 \text{ (micro)}}$

(ii) $\underline{\epsilon_{re*} = \epsilon_{eu} - [\epsilon_{ea} - \epsilon_r - \epsilon_c]}$

where ϵ_r's are the residual strain readings taken immediately after the specimen has completely passed through the dies assembly [see the specimen print-out].

ϵ_{res*} are the equivalent redundant deformation strains attained from the difference between the strain readings (ϵ_{eu1}, ϵ_{eu2}, ϵ_{eu3} etc.) of individual elemental dies (employed individually and progressively as mini-proto-dies) and the corrected strain readings, ϵ_{De*}'s ($\epsilon_{ea} - \epsilon_r - \epsilon_c$) of the elements in their respective assemblies (Proto-dies).

ϵ_c's are the strains due to contact forces between the elemental dies when specimen is drawn through their assemblies.

Examples:

From Tables (8.50), (8.51) and (8.52)

(1) $\epsilon_{re1*} = \epsilon_{eu1} - [\epsilon_{ea1} - \epsilon_{r1} - \epsilon_{c1}]$

$\therefore \epsilon_{re1*} = 51.373 - [53.46 - 17 - 0] = \underline{14.913 \text{ (micro)}}$

(2) $\epsilon_{re2*} = \epsilon_{eu2} - [\epsilon_{ea2} - \epsilon_{r2} - \epsilon_{c2}]$

$$\therefore \epsilon_{re2*} = 51.96 - [61.52 - 19 - 17] = \underline{26.44 \text{ (micro)}}$$

(3) $\epsilon_{re3*} = \epsilon_{eu3} - [\epsilon_{ea3} - \epsilon_{r3} - \epsilon_{c3}]$

$$\therefore \epsilon_{re3*} = 51.99 - [66.70 - 10 - 17] = \underline{12.29 \text{ (micro)}}$$

(iii) $\Delta\epsilon_r = [\epsilon_{re*} - \epsilon_{re}]$

where $\Delta\epsilon_r$'s are the difference between theoretically predicted elemental redundant strains, ϵ_{re}'s (based on Penny's theory) and that of experimentally attained redundant strains, ϵ_{re*}'s.

Examples:

From Tables (8.66), (8.67) and (8.68):

1) $\Delta\epsilon_{r1} = [\epsilon_{re1*} - \epsilon_{re1}] = [14.913 - 13.93] = \underline{0.993 \text{ (micros)}}$

2) $\Delta\epsilon_{r2} = [\epsilon_{re2*} - \epsilon_{re2}] = [26.44 - 24.03] = \underline{2.41 \text{ (micros)}}$

3) $\Delta\epsilon_{r3} = [\epsilon_{re3*} - \epsilon_{re3}] = [12.19 - 10.54] = \underline{1.75 \text{ (micros)}}$

(iv) $R_{De*} = \left[\frac{R_{De}}{\epsilon_{re}} \times \epsilon_{re*}\right]$

where R_{De}'s and ϵ_{re}'s are the theoretical elemental redundant forces and strains respectively

R_{De*}'s and ϵ_{re*}'s are the experimental redundant forces and strains respectively.

Examples:

From Tables (8.66), (8.67) and (8.68):

(1) $R_{De1*} = \left[\frac{R_{De}}{\epsilon_{re}} \times \epsilon_{re*}\right]_1 = \left[\frac{691}{13.92} \times 14.913\right] = \underline{740\ (N)}$

(2) $R_{De2*} = \left[\frac{R_{De}}{\epsilon_{re}} \times \epsilon_{re*}\right]_2 = \left[\frac{1240}{24.03} \times 26.44\right] = \underline{1364\ (N)}$

(3) $R_{De3*} = \left[\frac{R_{De}}{\epsilon_{re}} \times \epsilon_{re*}\right]_3 = \left[\frac{545}{10.54} \times 12.29\right] = \underline{636\ (N)}$

(v) $\Delta R_D = [R_{De*} - R_{De}]$

where ΔR_D's are the differences between theoretical and experimental redundant forces, R_{De} and R_{De*}.

Examples:

From Tables (8.66), (8.67) and (8.68):

(1) $\Delta R_{D1} = [R_{De1*} - R_{De1}] = [740 - 691] = \underline{49\ (N)}$

(2) $\Delta R_{D2} = [R_{De2*} - R_{De2}] = [1364 - 1240] = \underline{124\ (N)}$

(3) $\Delta R_{D3} = [R_{De3*} - R_{De3}] = [636 - 545] = \underline{91\ (N)}$

(vi) $\left\{\frac{\Delta\epsilon_r}{\epsilon_{re}}\right\} = \left\{\frac{\Delta R_D}{R_{De}}\right\} = \Delta$

These are the differences between experimental and theoretical strains and forces expressed as the fractions and the percentage of the theoretical values respectively.

Examples:

From Tables (8.66), (8.67) and (8.68):

(1) $\left[\frac{\Delta\epsilon_r}{\epsilon_{re}}\right]_1 = \left[\frac{\Delta R_D}{R_{De}}\right]_1 = \Delta_1 = \left[\frac{0.993}{13.92}\right] = \left[\frac{49}{691}\right] = \underline{0.071 \text{ or } 7.1\%}$

(2) $\left[\frac{\Delta\epsilon_r}{\epsilon_{re}}\right]_2 = \left[\frac{\Delta R_D}{R_{De}}\right]_2 = \Delta_2 = \left[\frac{2.41}{24.03}\right] = \left[\frac{124}{1240}\right] = \underline{0.10 \text{ or } 10\%}$

(3) $\left[\frac{\Delta\epsilon_r}{\epsilon_{re}}\right]_3 = \left[\frac{\Delta R_D}{R_{De}}\right]_3 = \Delta_3 = \left[\frac{1.75}{10.54}\right] = \left[\frac{91}{545}\right] = \underline{0.166 \text{ or } 16.6\%}$

8.21. Results Summary

(vii) $\epsilon_{rem} = \frac{\Sigma\epsilon_{re}}{s}$; $\epsilon_{rem*} = \frac{\Sigma\epsilon_{re*}}{s}$

where: ϵ_{rem}'s and ϵ_{rem*}'s are the mean values of the sum of the theoretical and experimental redundant strains for the number of specimens (or passes) s, made through the elemental dies in their respective assemblies.

Examples:

From Table (8.66):

(1) $\epsilon_{rem(1)}[En]** = \frac{\Sigma\epsilon_{re1}}{s} = \frac{(13.92 + 13.92 + 13.92 + 13.92)}{4}$

$\therefore \epsilon_{rem(1)}[En] = \underline{13.92 \text{ (micros)}}$

(2) $\epsilon_{rem(2)} = \frac{\Sigma\epsilon_{re2}}{s} = \frac{(24.03 + 24.03 + 24.03 + 24.03)}{4}$

$\therefore \epsilon_{rem(2)} = \underline{24.03 \text{ (micros)}}$

(3) $\epsilon_{rem(3)}[Ex]** = \frac{\Sigma\epsilon_{re3}}{s} = \frac{(10.54 + 10.54 + 10.54 + 10.54)}{4}$

$\therefore \epsilon_{rem(3)}[Ex] = \underline{10.54 \text{ (micros)}}$

(1) $\epsilon_{rem*(1)}[En] = \frac{\Sigma\epsilon_{re1*}}{s} = \frac{(14.913 + 15.203 + 14.773 + 15.153)}{4}$

$\therefore \epsilon_{rem1*}[En] = \underline{15.01 \text{ (micros)}}$

(2) $\epsilon_{rem*(2)} = \frac{\Sigma\epsilon_{re*2}}{s} = \frac{(26.44 + 26.61 + 26.74 + 26.44)}{4}$

$\therefore \epsilon_{rem*(2)} = \underline{26.56 \text{ (micros)}}$

(3) $\epsilon_{rem*(3)}[Ex] = \frac{\Sigma\epsilon_{re*3}}{s} = \frac{(12.29 + 12.51 + 12.82 + 13.42)}{4}$

$\therefore \epsilon_{rem*(3)}[Ex] = \underline{12.76 \text{ (micros)}}$

(viii) $\Delta\epsilon_{rm} = [\epsilon_{rem*} - \epsilon_{rem}]$

where: $\Delta\epsilon_{rm}$'s are the differences between the mean values of the experimental and theoretical redundant strains for the number of passes or specimens s, passed through the elemental dies in their respective assemblies.

Examples:

From the results summary Table (8.89):

(1) $\Delta\epsilon_{rm(1)}[Ex] = [\epsilon_{rem*} - \epsilon_{rem}]_{(1)} = [15.01 - 13.92] = \underline{1.091 \text{ (micro)}}$

(2) $\Delta\epsilon_{rm(2)} = [\epsilon_{rem*} - \epsilon_{rem}]_{(2)} = [26.56 - 24.03] = \underline{2.53 \text{ (micros)}}$

(3) $\Delta\epsilon_{rm(3)}[Ex] = [\epsilon_{rem*} - \epsilon_{rem}]_{(3)} = [12.76 - 10.54] = \underline{2.22 \text{ (micros)}}$

** En and Ex refer to the entry and exit of the proto-die (elemental die assembly) respectively.

(ix) $R_{Dem*} = \left[\frac{R_{Dem}}{\epsilon_{rem}} \times \epsilon_{rem*}\right]$

where: R_{Dem*} and R_{Dem} are defined as the mean values of the

experimental and theoretical redundant deformation forces for the number of specimens or passes s, made through each element in its respective assembly.

Examples:

From the results summary Table (8.89):

(1) $R_{Dem*(1)}[En] = \left[\frac{R_{Dem1}}{\epsilon_{rem}} \times \epsilon rem*\right]_{(1)} = \left[\frac{691}{13.92} \times 15.01\right] = \underline{745\ (N)}$

(2) $R_{Dem*(2)} = \left[\frac{R_{Dem}}{\epsilon_{rem}} \times \epsilon_{rem*}\right]_{(2)} = \left[\frac{1240}{24.03} \times 26.56\right] = \underline{1370\ (N)}$

(3) $R_{Dem*(3)}[Ex] = \left[\frac{R_{Dem}}{\epsilon_{rem}} \times \epsilon_{rem*}\right]_{(3)} = \left[\frac{545}{10.54} \times 12.76\right] = \underline{659\ (N)}$

(x) $\Delta R_{Dm} = [R_{Dem*} - R_{Dem}]$

ΔR_{Dm}'s are defined as the difference between the experimental and theoretical redundant forces for the number of passes or specimens, s, through the elements in their respective assemblies.

Examples:

From the results summary Table (8.89):

(1) $\Delta R_{Dm(1)}[En] = [R_{Dem*} - R_{Dem}]_{(1)} = [745 - 691] = \underline{54\ (N)}$

(2) $\Delta R_{Dm(2)} = [R_{Dem*} - R_{Dem}]_{(2)} = [1370 - 1240] = \underline{131\ (N)}$

(3) $\Delta R_{Dm(3)}[Ex] = [R_{Dem*} - R_{Dem}]_{(3)} = [659 - 545] = \underline{115\ (N)}$

(xi) $\left[\frac{\Delta \epsilon_{rm}}{\epsilon_{rem}}\right] = \left[\frac{\Delta R_{Dm}}{R_{Dem}}\right] = \Delta_m$

Examples:

From the results summary Table (8.89):

(1) $\left[\frac{\Delta\epsilon_{rm}}{\epsilon_{rem}}\right]_{(1)} = \left[\frac{\Delta R_{Dm}}{R_{Dem}}\right]_{(1)} = \Delta_{m(1)} \left[\frac{1.091}{13.92}\right] = 0.078 = 7.8\%$

(2) $\left[\frac{\Delta\epsilon_{rm}}{\epsilon_{rem}}\right]_{(2)} = \left[\frac{\Delta R_{Dm}}{R_{Dem}}\right]_{(2)} = \Delta_{m(2)} = \left[\frac{2.53}{24.03}\right] = 0.105 = 10.5\%$

(3) $\left[\frac{\Delta\epsilon_{rm}}{\epsilon_{rem}}\right]_{(3)} = \left[\frac{\Delta R_{Dm}}{R_{Dem}}\right]_{(3)} \Delta_{m(3)} = \left[\frac{2.22}{10.54}\right] = 0.21 = 21\%$

8.22. Checking Validity of the Proposed Elemental Die Theory

Table (8.82)

Summary of Forces for Aluminium ($\alpha = 7^{\circ}$)

Elemental No.	F_{De} (N)	R_{Dem}* (N)	R_{Dem} (N)	ΔR_{Dm} (N)	$F_{Dec} = (F_{De} - \Delta R_{Dm})$ (N)
1	1122	333	323	46	1076
2	1286	713	597	116	1170
3	1374	687	562	125	1249
4	1534	607	525	82	1452
5	1886	297	243	54	1832

$\Sigma F_{De} = 7202$ (N) $\Sigma F_{Dec} = 6779$ (N)

$ee = \Sigma F_{Dec} - F_{dT}$

where $F_{dT} = 5957$ (N). (The total drawing force measured).

$\therefore$ ee (6779 - 5957) = 822 (N)

$$\% \text{ ee} = \frac{(\Sigma F_{Dec} - F_{dT})}{\Sigma F_{Dec}}$$

$$\therefore \% \text{ ee} = \frac{822}{6779} \times 100 = 12\%$$

$\therefore$ % ee = 12%

Table (8.83)

Summary of Forces for Copper ($\alpha = 7^{\circ}$)

Elemental No.	F_{De} (N)	R_{Dem}* (N)	R_{Dem} (N)	ΔR_{Dm} (N)	$F_{Dec} = (F_{De} - \Delta R_{Dm})$ (N)
1	1196	378	372	28	1168
2	1117	739	688	59	1058
3	1227	701	648	71	1156
4	1690	651	605	55	1635
5	2155	328	280	68	2087

$\Sigma F_{De} = 7385$ (N) $\Sigma F_{Dec} = 7104$ (N)

$$ee = \Sigma F_{Dec} - F_{dT}$$

where F_{dT} = 6789 (N). (The total drawing force measured).

$\therefore$ ee (7104 - 6789) = 315 (N)

$$\% \text{ ee} = \frac{(\Sigma F_{Dec} - F_{dT})}{\Sigma F_{Dec}} = \frac{315}{7104} = 0.044 = 4.4\%$$

$\therefore$ % ee = 4.4%

Table (8.84)

Summary of Forces for Aluminium (α = 15°)

Elemental No.	F_{De} (N)	R_{Dem}* (N)	R_{Dem} (N)	ΔR_{Dm} (N)	$F_{Dec} = (F_{De} - \Delta R_{Dm})$ (N)
1	1859	745	691	54	1805
2	1441	1370	1240	131	1310
3	2144	659	545	115	2029

ΣF_{De} = 5444 (N) ΣF_{Dec} = 5144 (N)

$$ee = \Sigma F_{Dec} - F_{dT}$$

where F_{dT} = 5125 (N). (The total drawing force measured).

$\therefore$ ee (5144 - 5125) = 19 (N)

$$\% \text{ ee} = \frac{(\Sigma F_{Dec} - F_{dT})}{\Sigma F_{Dec}} = \frac{19}{5144} = 0.37\%$$

$\therefore$ % ee = 0.37%

Table (8.85)

Summary of Forces for Copper (α = 15°)

Elemental No.	F_{De} (N)	R_{Dem}* (N)	R_{Dem} (N)	ΔR_{Dm} (N)	$F_{Dec} = (F_{De} - \Delta R_{Dm})$ (N)
1	1829	745	650	74	1755
2	1647	1370	1165	112	1535
3	2495	659	510	92	2403

ΣF_{De} = 5971 (N) ΣF_{Dec} = 5693 (N)

$$ee = \Sigma F_{Dec} - F_{dT}$$

where F_{dT} = 5913 (N). (The total drawing force measured).

$\therefore$ ee |(5693 - 5913)| = 220 (N)

$$\% \text{ ee} = \frac{(\Sigma F_{Dec} - F_{dT})}{\Sigma F_{Dec}} = \frac{220}{5693} = 3.86\%$$

$\therefore$ % ee = 3.86%

Table (8.86)

Summary of the Overall Error, ee (%) of the Proposed Elemental Die Theory

Die Semi-angle	Aluminium	Copper
(α °)	ee (%)	ee (%)
7°	12.00	4.4
15°	0.37	3.86

The Mean Values of the Related Results of the Six Aluminium Specimens Passed Through Each Element of the Proto-die with 7° Semi-Angle [5 Elements in the Assembly]

ELEMENTAL No.	ϵ_{rem}	ϵ_{rem*}	$\Delta\epsilon_{rm}$ $[\epsilon_{rem*}-\epsilon_{rem}]$	R_{Dem*} $\left[\frac{R_{Dem}}{\epsilon_{rem}} \times \epsilon_{rem*}\right]$	ΔR_{Dm} $[R_{Dem*}-R_{Dem}]$	$\frac{\Delta\epsilon_r}{\epsilon_{rem}} = \frac{\Delta R_{Dm}}{R_{Dem}} =$	Δ_m
		(micros)		(N)	(N)	(N)	%
1 (En)	3.95	4.08	0.475	333	46	0.141	14.1
2	5.96	7.12	1.155	713	116	0.194	19.4
3	5.56	6.80	1.232	687	125	0.222	22.2
4	5.10	5.65	0.795	607	82	0.156	15.6
5 (Ex)	2.34	2.86	0.526	297	54	0.225	22.5

Table (8.87)

From the Table: $C_n = 0.141$, $C_x = 0.255$

$$C_{nx} = (C_n + C_x) = (0.141 + 0.225) = 0.366$$

$\therefore C_{nx} = 0.366$

The Mean Values of the Related Results of the Seven Copper Specimens Passed Through Each Element of the Proto-die with 7° Semi-Angle [5 Elements in the Assembly]

ELEMENTAL No.	ϵ_{rem}	ϵ_{rem*}	$\Delta\epsilon_{rm}$ $[\epsilon_{rem*}-\epsilon_{rem}]$	R_{Dem*} $\left[\frac{R_{Dem}}{\epsilon_{rem}} \times \epsilon_{rem*}\right]$	ΔR_{Dm} $[R_{Dem*}-R_{Dem}]$	$\frac{\Delta\epsilon_r}{\epsilon_{rem}} = \frac{\Delta R_{Dm}}{R_{Dem}} =$	Δ_m
		(micros)		(N)	(N)	(N)	%
1 (En)	3.95	3.40	0.30	378	28	0.077	7.7
2	6.96	7.48	0.601	739	59	0.086	8.6
3	6.48	7.01	0.706	701	71	0.109	10.9
4	5.70	6.13	0.432	651	55	0.091	9.1
5 (Ex)	2.59	3.10	0.537	328	68	0.241	24.1

Table (8.88)

From the Table: $C_n = 0.077$, $C_x = 0.241$

$$C_{nx} = (C_n \times C_x) = (0.077 + 0.241) = 0.32$$

$\therefore C_{nx} = 0.32.$

The Mean Values of the Related Results of the Four Aluminium Specimens Passed Through Each Element of the Proto-die with 15° Semi-Angle [3 Elements in the Assembly]

ELEMENTAL No.	ϵ_{rem}	ϵ_{rem*}	$\Delta\epsilon_{rm}$ $[\epsilon_{rem*}-\epsilon_{rem}]$	R_{Dem*} $\left[\frac{R_{Dem}}{\epsilon_{rem}} \times \epsilon_{rem*}\right]$	ΔR_{Dm} $[R_{Dem*}-R_{Dem}]$	$\frac{\Delta\epsilon_r}{\epsilon_{rem}} = \frac{\Delta R_{Dm}}{R_{Dem}} =$	Δ_m
	(micros)			(N)	(N)	(N)	%
1 (En)	13.92	15.01	1.091	745	54	0.078	7.8
2	24.03	26.56	2.53	1370	131	0.105	10.5
3 (Ex)	10.54	12.76	2.22	659	115	0.21	21.0

Table (8.89)

From the Table: $C_n = 0.078$, $C_x = 0.21$

$$C_{nx} = (C_n + C_x) = (0.078 + 0.21) = 0.288$$

$\therefore C_{nx} = 0.288$

The Mean Values of the Related Results of the Six Copper Specimens Passed Through Each Element of the Proto-die with 15° Semi-Angle [3 Elements in the Assembly]

ELEMENTAL No.	ϵ_{rem}	ϵ_{rem*}	$\Delta\epsilon_{rm}$ $[\epsilon_{rem*}-\epsilon_{rem}]$	R_{Dem*} $\left[\frac{R_{Dem}}{\epsilon_{rem}} \times \epsilon_{rem*}\right]$	ΔR_{Dm} $[R_{Dem*}-R_{Dem}]$	$\frac{\Delta\epsilon_r}{\epsilon_{rem}} = \frac{\Delta R_{Dm}}{R_{Dem}} =$	Δ_m
	(micros)			(N)	(N)	(N)	%
1 (En)	13.39	14.91	1.52	724	74	0.1137	11.37
2	21.77	23.87	2.10	1277	112	0.097	9.7
3 (Ex)	9.06	10.69	1.63	602	92	0.180	18.0

Table (8.90)

From the Table: $C_n = 0.1137$, $C_x = 0.18$

$$C_{nx} = (C_n + C_x) = (0.1137 + 0.18) = 0.294$$

$\therefore C_{nx} = 0.294$

Summary of the Proposed Correcting Factor, C_f, For Tube Sinking Force Equation

Die Semi-Angle (α)	Aluminium	Copper	Mean Factor	Actual Correcting Factor, $C_f = [1 + mC_{nx}]$
	C_{nx}	C_{nx}	mC_{nx}	
7	0.366	0.32	0.343	1.343
15	0.288	0.294	0.291	1.291

Table (8.91)

Proposed new form of drawing force equation:

$$F_{dT} = \frac{\pi D_2 t m \bar{\gamma}}{\cos\alpha} \left\{\frac{1 + \mu\cot\alpha}{\mu\cot\alpha}\right\} \left\{1 - \left[\frac{D_2}{D_1}\right]^{\mu\cot\alpha}\right\} + \frac{2\pi D_1 t \bar{\gamma}\alpha . C_f}{3}$$

8.23. Results from the Experiment

1) The data resulting from the procedure discussed under Stage I of the experiment, i.e. using individual elemental dies to measure elemental hoop strains ϵ_{eu}'s and their equivalent drawing forces, F_{Deu}, due to redundant deformation to provide calibration for the strain readings for the prototype dies (elemental die assemblies) are as shown in Tables (8.01) to (8.04) and Tables (8.07) to (8.12).

2) The graphs of the elemental strains, ϵ_{eu}'s, against the elemental drawing forces, F_{Deu}'s due to redundant deformation for annealed brass to provide general expressions between the two parameters, ϵ_{eu} and F_{Deu} for other tubing materials employed for the experiment for calibration purposes are as shown in Figures (8.03) and (8.04) for 15° and 7° die semi-angles respectively.

3) The data resulting from the employment of the expressions attained from the two graphs, Figures (8.03) and (8.04) to provide calibration for the strain readings attained when other materials, aluminium and copper, are drawn through proto-dies (assemblies of elemental dies) employed in Stage II of the experiment are as shown in Tables (8.05), (8.06), (8.13) and (8.14).

4) Shown in Tables (8.15) to (8.18) and Tables (8.23) to (8.28) are the uncorrected strain readings, ϵ_e's (strain readings with inclusion of residual strains, ϵ_r, and contact strains ϵ_c) recorded during a pass of each specimen of aluminium and copper through the proto-die

(assembly of 3 elemental dies with 15° semi-angle) respectively. At the bottom of each table of results are the mean values ϵ_{ea}'s of the uncorrected strains and the residual strains, ϵ_r's. Also accompanying these results tables are a few specimens of the direct print-out of the uncorrected strains with the residual strain from the data logger employed.

5) For the same proto-die (assembly of 3 elemental dies with 15° semi-angle) the results shown in Tables (8.50) to (8.52) amd Tables (8.53) to (8.55) are the relevant experimental results required for the analysis of the experimental redundant deformation strains, ϵ_{re*}, for the four aluminium and six copper specimens employed respectively.

6) Also shown in Tables (8.66) to (8.68) and Tables (8.69) to (8.71) are the resulting data from further analysis of the strains and forces related to each elemental die of the proto-die (assembly of 3 elemental dies with 15° semi-angle) through which both four aluminium and six copper specimens were drawn to constitute four and six passes respectively.

7) The results in Tables (8.82) and (8.83) for the 15° semi-angle proto-die are the condensed or mean values of the results in Tables (8.66) to (8.68) and Tables (8.69) to (8.71) for the four aluminium and six copper specimens respectively.

8) Also the uncorrected strain readings, ϵ_e's (strain readings with inclusion of residual, ϵ_r, and contact, ϵ_c, strains) together with

mean values recorded for both six aluminium and seven copper specimens tested using 7° semi-angle proto-die (assembly of 5 elemental dies) are as shown in Tables (8.32) to (8.37) and Tables (8.40) to (8.46) respectively.

9) For the same proto-die (assembly of 5 elemental dies with 7° semi-angle) the results shown in Tables (8.56) to (8.60) and Tables (8.61) to (8.65) are the relevant experimental results required for the calculation of the experimental redundant deformation strains, ϵ_{re*}'s for the six aluminium and seven copper specimens employed respectively.

10) With the same die in employment (assembly of 5 elemental dies with α = 7°) shown in Tables (8.72) to (8.76) and Tables (8.77) to (8.81) are the resulting data from further analysis of strains and forces related to each elemental die of the proto-die employed for drawing both six aluminium and seven copper specimens which constituted six and seven passes respectively.

11) Under Summary of Results in Tables (8.87) and (8.88) are the condensed or mean values of the data in Tables (8.72) to (8.76) and Tables (8.77) to (8.81) based on the number of specimens, 5 employed in each case (see Specimen Calculations) for the test through the proto-die (assembly of 5 elements with α = 7°).

12) Checking the validity and accuracy of the proposed elemental die theory employed for the analysis of the results, under Results

Summary, Tables (8.82) to (8.85), with their data were employed for the assessment of the general error, ee, which could be expected in the proposed elemental die theory and the conclusions of the assessment for both 7° and 15° die semi-angle are as shown in Table (8.86) for both aluminium and copper tubing materials.

13) Finally, using the mean deviation, Δ_m, between Pennyj's proposed theoretical and the experimental redundant deformation at the die entry and exit as correction factors, C_n and C_x related to the die entry and exit respectively, two values of a general correction factor, C_f, for both 7° and 15° semi-angle proto-die deduced and proposed for any tubing materials are as shown in the Conclusions Table (8.91) under Summary of Results.

8.24. Discussion

The results presented exclude data from annealed brass and stainless steel tube specimens. The reason for the exclusion of these materials was to avoid damage of the proto-die (assemblies of elemental dies). The dies were not heat-treated, therefore they were considered not suitable for drawing harder materials like brass and stainless steel at one pass for 0.375 fractional reduction. Apart from damaging the working face of the dies due to strength and hardness of the materials, particularly the stainless steel, the "pointed" ends of the specimens which suffered from non-homogeneous strain during the swaging operation are weak and therefore cannot withstand the total drawing forces needed to draw the stronger gauge lengths of the specimens at one pass.

The problems encountered during the tests were connected mainly with instrumentation. Study of the Results Tables of uncorrected strain readings, ϵ_e's, (strain readings with inclusion of residual and contact strains, ϵ_r and ϵ_c) reveals cases where the residual strains, ϵ_r, were almost higher than the desired strain values. Reasons for this could be attributed to (i) the nature and quality of the gauges employed, (ii) the quality of bonding material used, (iii) the amount of bonding material between the gauges and the surface, (iv) positioning of the die in the tooling compartment of the draw bench. The gauge lengths of the specimens were designed to be as short as possible in order to avoid unnecessary "wriggling" of the specimens which could lead to eccentricity of the specimen during the drawing operation. Any slight dislocation of the die in the tool compartment of the draw bench would affect the orientation of the drawing force which could induce further strain into the elements of the proto-die and thereby constitute residual strains which take some time to die away on completion of the drawing operation of the specimens. Also in addition to the above mentioned problems, the draw bench hydraulic ram speed was set to run at a very low speed in order to maintain a constant and steady speed for all the passes of the specimens tested. There was likely to be a slight variation of the preset speed due to changes in the viscosity of the hydraulic fluid as the system became warmer. In fact a very large fan was employed to blow cold air on to the hydraulic sump and the electric motor because of the damaging heat generated after running the system at low speed for about ten to fifteen minutes. The reason for this was that the drawing speed was being controlled by the opening and

closing of the oil flow valve of the system. At a very low speed (say 1 cm/min, at which the test was carried out) the hydraulic oil was being forced through a very small opening which resulted in heat generation and adversely affected the viscosity of the fluid as the system became hot.

As discussed under the test procedure, the timing of taking the readings of residual strains is very important as the readings taken too early or too late on completion of the drawing pass would result in overestimation or underestimation of the residual strain, ϵ_r respectively. For these reasons, the rest of the drawing of the specimens (when enough readings have been taken) were done at higher drawing speed (10 cm/min) and the maximum auto scan speed was employed to take a couple of readings of the residual strains, ϵ_r, immediately after each pass was completed.

Of the two methods employed for the compression test to determine approximately the contact strains, ϵ_c, due to the contact forces between the elemental dies when a specimen is drawn through the assembly, the later method (subjection of individual elemental dies individually to the push of the maximum drawing force due to redundant deformation required to draw a specimen at one pass to the final diameter through the proto-die) was abandoned because the results attained for the elemental dies tested were meaningless. In most cases, the strain readings due to the contact between the pushing anvil of the hydraulic press and the elemental dies were more than five times the value of the actual average uncorrected strains, ϵ_{ea} (see the results Table (8.92)).

The other method (subjection of the whole die assembly slowly to the maximum drawing force) gave sensible results and was employed for the tests. Contact strains in the first columns of the direct specimen print-out from the data logger accompanied with Table (8.93) was ignored because in practice, during drawing operations through an assembly of the elemental dies, there is no contact force experienced by the first die in the assembly. The contact strain readings shown in the specimen print-out were due to contact between the first elemental die of the assembly and the pushing anvil of the hydraulic press employed for the tests.

Looking through the results, one would notice the exclusion of the data from 12 mm exit diameter dies. The reason for this was due to thickness effects, which render the strain readings recorded for both 7° and 15°, 12 mm exit diameter dies less accurate and unacceptable. As shown in the proposed elemental theory (in Chapter 2), the maximum number of elements into which a proto-die can be divided depends on the total working length of the proto-die which is a function of the entry and exit diameter and the sine of the die half-angle, α. With a very thin element, the width of the strain gauge which can be laid on it circumferentially is restricted (see discussions on alternative design of the die in Chapter 4). When these thin elemental dies are clamped together, parts of width of the gauges were either not sitting properly on the die surface but overlapping and sitting on the small gap between the elements which constitute the assembly (proto-die). Also, a high number of elemental dies representing a 12 mm exit diameter proto-die implies very small fractional reduction which may not generate

enough hoop strains in each element to produce a sensible strain reading. However, it must be borne in mind that there was no special reason for the employment of 12 mm exit diameter dies for the test other than maximising the use of the available material and equipment (especially the dies) when tentative experiments were being carried out to test the feasibility of this project at the initial stage.

The 10 mm exit diameter dies which cover between 0 and 0.375 fractional reduction range actually cover the 12 mm nominal exit diameter dies' mission as well.

From the results shown in Tables (8.72) and (8.77) we would notice the situation where the difference between the experimental and theoretical redundant forces, R_{De*} and R_{De} tend to negative which resulted to negative deviation Δ. In both cases, the occurrences of the negative deviation, Δ, were recorded at the die entry when aluminium and copper specimens were tested. Though the negative sign of the deviations were ignored and their modulus values were considered when the mean values of the deviations recorded for all the specimens tested, were being analysed. In most cases, (for the 7° and 15 half die angle cases) the deviations from the originally predicted values by Penny's redundant deformation theory were minimum at the die entry while higher values of deviation were recorded for the exits. It must be borne in mind that the basic energy equation from which the original redundant deformation term $[2\pi D_i t\bar{\gamma}\alpha/3]$ was derived was based on the hypothesis of constant volume of the tube material passing through any point on the working face of the die.

However, the thickness of the tube wall which was assumed constant does vary slightly as the drawing progresses depending on the nature of the tubing material. Also the redundant deformation term at the die exit was originally based on the initial outside diameter D_1 of the tube was based on instantaneous exit elemental diameter in the elemental die theory. Therefore these two parameters, variation or slight increase in wall thickness at the die exit and the difference between the instantaneous diameter of the tube at the exit and the original tube outside diameter would account for the higher value of redundant deviation at the exit.

As has been shown in the proposed elemental die theory, only halves of the redundant deformation work of the first and the last dies in an assembly of elemental dies (proto-die) constitute full redundant deformation work of the proto-die. Therefore the general correction factor, C_f, $(C_{nx} + 1)$ attained for the original total drawing force equation due to redundant deformation was deduced from the local correction factors at entry and exit (C_n and C_x) of the elemental dies assembly.

The total local correction factor, C_{nx}, $(C_n + C_x)$ is the total underestimation of the redundant work by Penny's proposed theory revealed by these experimental results. As has been shown in the results conclusions, (Table 8.91), 0.343 and 0.291 underestimation were recorded for the conical dies with 7° and 15° semi-angles respectively.

From the results summary, Table (8.86) the overall error, ee, of the proposed elemental die theory for aluminium specimens are 12% and 0.37% while those of copper specimens are more consistent (4.4% and 3.86%) for the 7° and 15° semi-angled dies employed respectively. The overall error, ee, is largely dependent on accurate determination of the mean yield stress, $\bar{y}$, of the tube material between the entry and exit of the die. Other small errors which are very difficult to divorce from the overall error, ee, include errors due to instrumentation, measurement, calculation and homogeneuity of the tube material. In spite of this error which cannot be completely eliminated, looking generally into the results attained, it is reasonable to conclude that the proposed elemental die theory is accurate enough for the assessment of the coefficient of friction along the working face of a straight conical die.

8.25 Conclusions

1) The experimental results show that during the drawing of thin walled tube at a low speed through a straight conical die, redundant deformation work due to plastic-elastic and elastic recovery does exist at the entry and exit of the die respectively.

2) The results not only connoted the existence of the redundant deformation as predicted by Penny's proposed theory, it shows the degree of underestimation by Penny's proposed theory and general correction factors, C_f, to eliminate the risk of underestimation of

the total drawing force due to redundant deformation for both 7° and 15° semi-angled dies for any tubing material were deduced from the experimental results.

3) The results show small differences between the redundant work at die entry and exit because the assumption of the constant volume at any instant in the die pass becomes less valid as the tube wall thickens at higher fractional reduction.

4) The proposed elemental die theory employed for the experiment is very good and reliable provided the elemental or instantaneous yield stress, Y_i, (in case of materials which strain hardened largely between the die entry and exit, e.g. stainless steel) or mean yield stress, $\bar{y}$, (for less strain hardening tube material) are carefully and accurately determined.

CHAPTER 9

9.11. Summary Conclusions

In accordance with the original objectives of this study, the summary conclusions which can be drawn include:

1) An elemental die theory to facilitate the analysis of the elemental drawing force across the pass of a conical die has been devised and developed.

2) Provided t+he values of instantaneous or elemental yield stress, γ_e, of the highly strain hardening materials or the mean yield stress, $\bar{\gamma}$, of less strain hardening materials can be accurately determined for the workpiece across the die pass, it is proposed that the elemental die theory can be employed for the accurate estimation of the coefficient of friction across the conical die pass.

3) It also concluded that the proposed elemental die theory is very good and reliable for the analysis of redundant deformation phenomenon at both entry and exit of a conical die.

4) From both the experimental results and the analysis of the coefficient of friction through the employment of the proposed elemental die theory, it has been shown that the coefficient of friction (or the frictional effect) varies exponentially as the normal die pressure across the pass of a conical die.

5) In spite of the variation of the coefficient of friction across the die pass, the useful value, defined as the significant value of coefficient of friction, μ_s or μ_{sL}, desirable for the accurate and acceptable calculation of the total drawing force due to friction is the value attained at the die exit. This finding is in agreement with the original conventional employment of the upper bound value of coefficient of friction proposed by previous workers.

6) Though the data attained through the employment of the proposed elemental die theory connoted the validity of application of the upper bound value of coefficient of friction for the calculation of the drawing force due to friction, the results from this study also reveal the unacceptable extent of the unreliability of the upper bound assumption as applied to tube sinking analysis.

7) It is concluded that the use of the elemental theory has eliminated the problem of the unreliable results which often constituted by either overestimation or underestimation of the drawing force due to friction.

8) Also, due to marked disagreement between the measured radial pressure values and the values of the radial pressure predicted by upper bound assumption based on a plain strain theory, it is concluded that a plain strain situation cannot be completely harmonised with an ideal tube sinking process.

9) With more than 50% improvement or reduction recorded in most cases (except for the Cast Iron dies) for the coeficient of friction over the test carried out without lubricant, it is concluded that the results of the tests have clearly defined the importance of the use of lubricant in tube sinking process.

10) From the results of the coefficient of friction analysis, it is concluded that except for prolonging the die life from wear, the lubrication of the Cast Iron die contributes only little improvement in the reduction of coefficient of friction along the working face of the die since the graphite structure of the Cast Iron across the working face would negate the effect of the applied lubricant.

11) The results of this study not only connoted the existence of redundant deformation due to plastic-elastic deformation and elastic recovery at the entry and exit of the conical die during the drawing of thin walled tube at a low speed as predicted by Penny's proposed elemental deformation theory, the results show the degree of under-estimation by Penny's proposed theory and general correction factors, C_f, to eliminate the risk of underestimation of the total drawing force due to redundant deformation for both 7° and 15° semi-angle dies for any tubing materials were deduced from the results of the study.

12) From our experimental data, it is concluded that small differences do exist between the redundant work at the entry and exit of a conical die because the assumption of the constant volume of the work material at any instant across the die pass becomes less valid as the tube wall thickness at higher fractional reduction.

13) In addition to the findings during the pursuance of the primary objectives of this study, it is concluded from the results of our secondary experiments that:-

i) The yield stress of a tube material is enhanced by the length of the die pass which is a function of the total frictional work done on the workpiece across the die pass. It is therefore concluded that 7° semi-angle die (die with longer pass) would be employed when maximum strain hardening of the tube material is desirable.

ii) For tube materials which strain softening at higher fractional reduction, the use of 15° semi-angle die would be desirable (die with shorter pass) in order to prolong the point of initiation of strain softening when higher fractional reduction and maximum yield stress are very important.

9.12. Suggestions for Further Work

From the work to date on tube drawing generally to the status described in this thesis, it is suggested that further work should proceed on the following:

1) Extension of elemental die theory to the analysis of the coefficient of friction across the die pass in moving and fixed mandrel tube drawing processes.

2) Investigation of redundant deformation in the drawing processes in (1).

3) Effect of variation of die semi-angle on radial pressure in tube sinking process.

4) Further investigation into the effect of die geometry, particularly variation of die semi-angle and the length of die pass on the yield stress of the workpiece materials in tube sinking process.

5) Improvement into the existing tedious, laborious, and time-consuming method of pointing tubes prior to sinking operation.

REFERENCES

1 DAVID AND CHARLES — Rees's Manufacturing Industry (1819-1820) Vol.4., pp.136-140.

2. — Copper Development Association Publication 25.

3. DERRY, T.K. & WILLIAMS, T.I. — A short History of Technology from the Earliest Times to A.D. 1900. pp.498-593.

4. SACHS, G. & BALDWIN, W.M. — Stress Analysis of Analysis of Tube Sinking, Trans. A.S.M.E., 68.647, (1946).

5. MOORE, G.G. & WALLACE, J.F. — Theories and Experiments on Tube Sinking Through Conical Dies. Procs. I.Mech.E., 182, Pt.1, 867, 1967-1968.

6. BLAZYNKSI, T.Z. & COLE, I.M. — An Investigation of the Sinking and Mandrel Drawing Process. Procs. I.Mech.E., Vol.178, Pt.1, 33, p.894.

7. CHUN, S.Y. & SWIFT, H.W. — A Theory of Tube Sinking. J. Iron Steel Inst., (1952).

8. ESPEY, G. & SACHS, G. — Experimentation on Tube Drawing with a Moving Mandrel. J.Appl. Mech., 14.81 (1947).

9. BLAZYNSKI, T.Z. & COLE, I.M. — An Investigation of the Plug Drawing Process. Procs. I.Mech.E., 174.797, (1960).

10. SWIFT, H.W. — Stresses and Strains in Tube Drawing. Phil. Mag., Ser. 7.11 (308).883 (1949).

11. MOORE, G.G. & WALLACE, J.F. — Theoretical study of Tube Sinking through Conical Dies. J.Mech.Engng. Sci., 3, No.3, 225 (1961).

12. PENNY, W.A. — Development of 100 kN Draw Bench for Tube Drawing (1977).

13. SLATER, R.A.C. — Engineering Plasticity Macmillan Press

14. FLINN, J.E. — Parametric Influence on the Wall Thickness Changes and Bulk Strain Behaviour of Hollow Drawn Tubing. Trans. A.S.M.E., p.792 (1969).

15. AVITZUR, B. — Tube Sinking and Expanding. Trans. A.S.M.E. (1965).

16. SACHS, G. & BALDWIN, W.M. "Folding" in Tube Sinking. Trans. A.S.M.E., 68.655 (1946).

17. JOHNSON, W. Estimation of Upper Bound Loads for Extrusion and Coining Operation. Procs. I.Mech.E.,173, 173, Pt.1.61 (1959).

18. JOHNSON, W. & MELLOR, P.B. Engineering Plasticity Van Nostrand Reinhold Company

19. HILL, R. The Mathematical Theory of Plasticity, Chapter X, p.271, Oxford University Press. (1950).

20. CLARK, W.G. & SWIFT, H.W. Strain in Sunk and Drawn Tubes. Mot. Indust. Res. Assoc. Rep. 1945/R/5 (1945).

21 BLAZYNSKI, T.Z. Metal Forming Tool Profiles and Flow. Chapter 4, pp.72/73, Macmillan Press (1976)

22. EDGAR, C. Fundamentals of Manufacturing Processes and Materials. Addison Wesley. pp.422-423, (1965).

23. ASHAJU, D.I. "Quasi-static Axisymmetric Compression Tests to Predict Mechanical Propeties of Various Aircraft Tank Units Inner Tubes"

24. MOORE, F.D. Principles and Applications of Tribology, Pergamon Press.

25. SARKAR, A.D. Friction and Wear. Academic Press.

26. SZERI, A.Z. Tribology. Hemisphere Publishing Corp.

27. STEPHENS, R.C. Strengths of Materials (Theory & Examples). Edward Arnold Publishing Co.

28. TUVE/DOMHOLDT Engineering Experimentation. International Student Edition.

29. SCHAUM Strength of Mateials, 2nd Edition, McGraw-Hill.

30. BRITISH STANDARDS INSTITUTION IN ASSOCIATION WITH HUTCHINSON Manual of British Standards in Engineering Metrology.

31. HONEYCOMBE, R.W.K. Plastic Deformation of Metal.

32. ROZOV, N.V. Cold drawing of Tubes (Trans.from Russian) National Lending Library for Science & Technology

APPENDIX

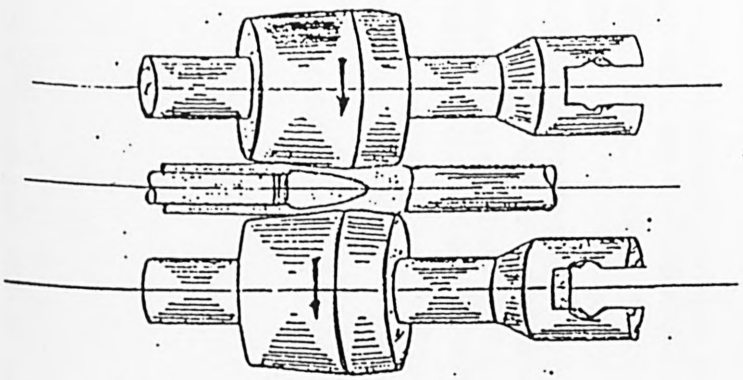

Figure (1.1) Mannesmann process
After Edgar [22]

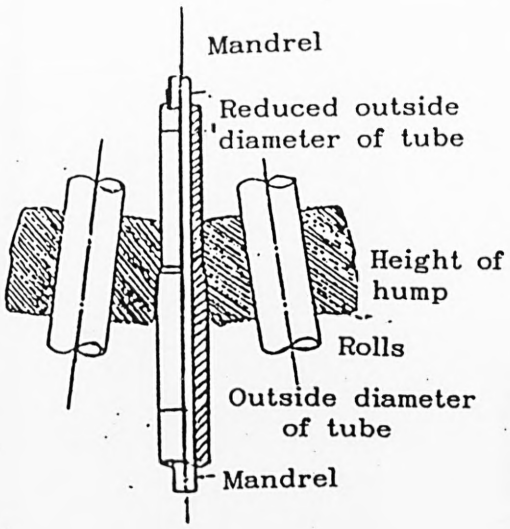

Figure (1.2) Assel process
After Edgar [22]

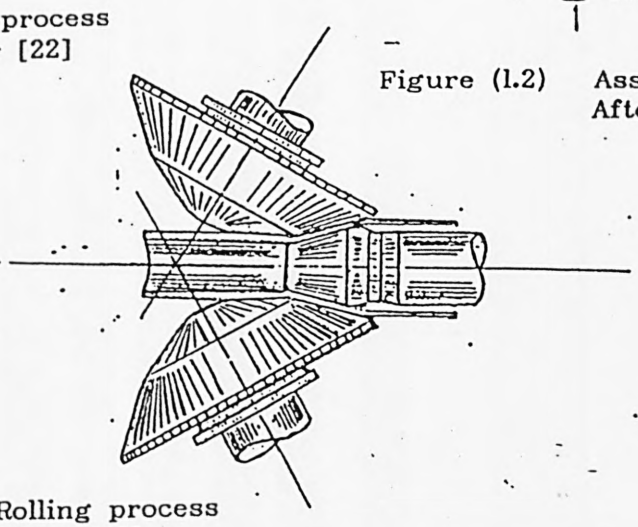

Figure (1.3) Rotary Rolling process
After Edgar [22]

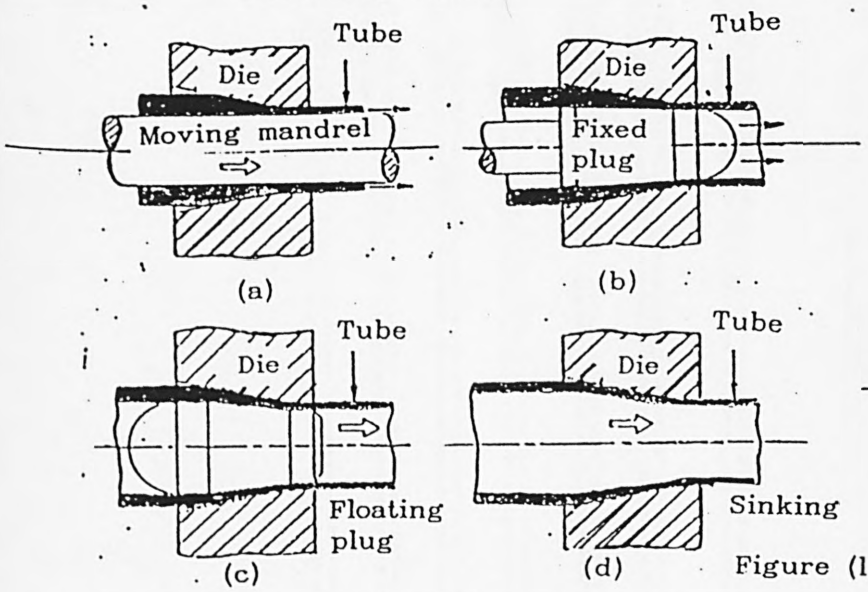

Figure (1.4) Methods of Tube drawing
After Slater [13]

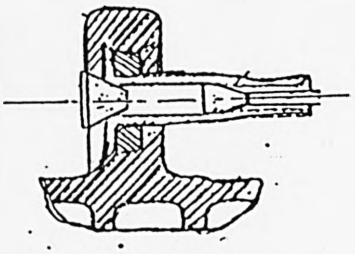

Figure (1.5) Tube expanding
After Rozov [32]

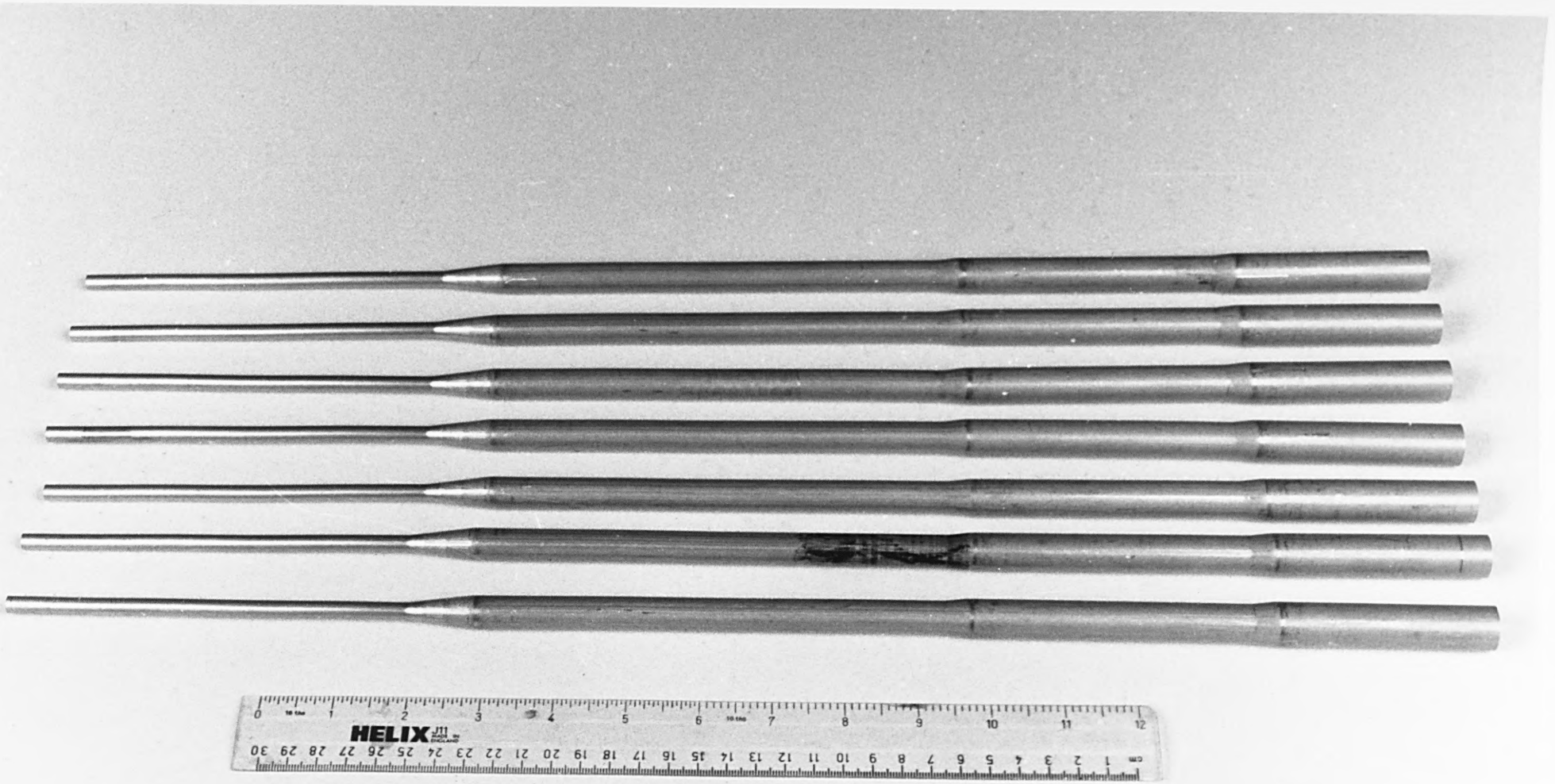

Fig.(1.6)

TYPICAL AIRCRAFT TANK UNIT INNER TUBES FOR
FUEL GAUGING SYSTEM PRODUCED BY TUBE SINKING PROCESS

Fig.1.7. An Aircraft Fuel Gauging Unit.

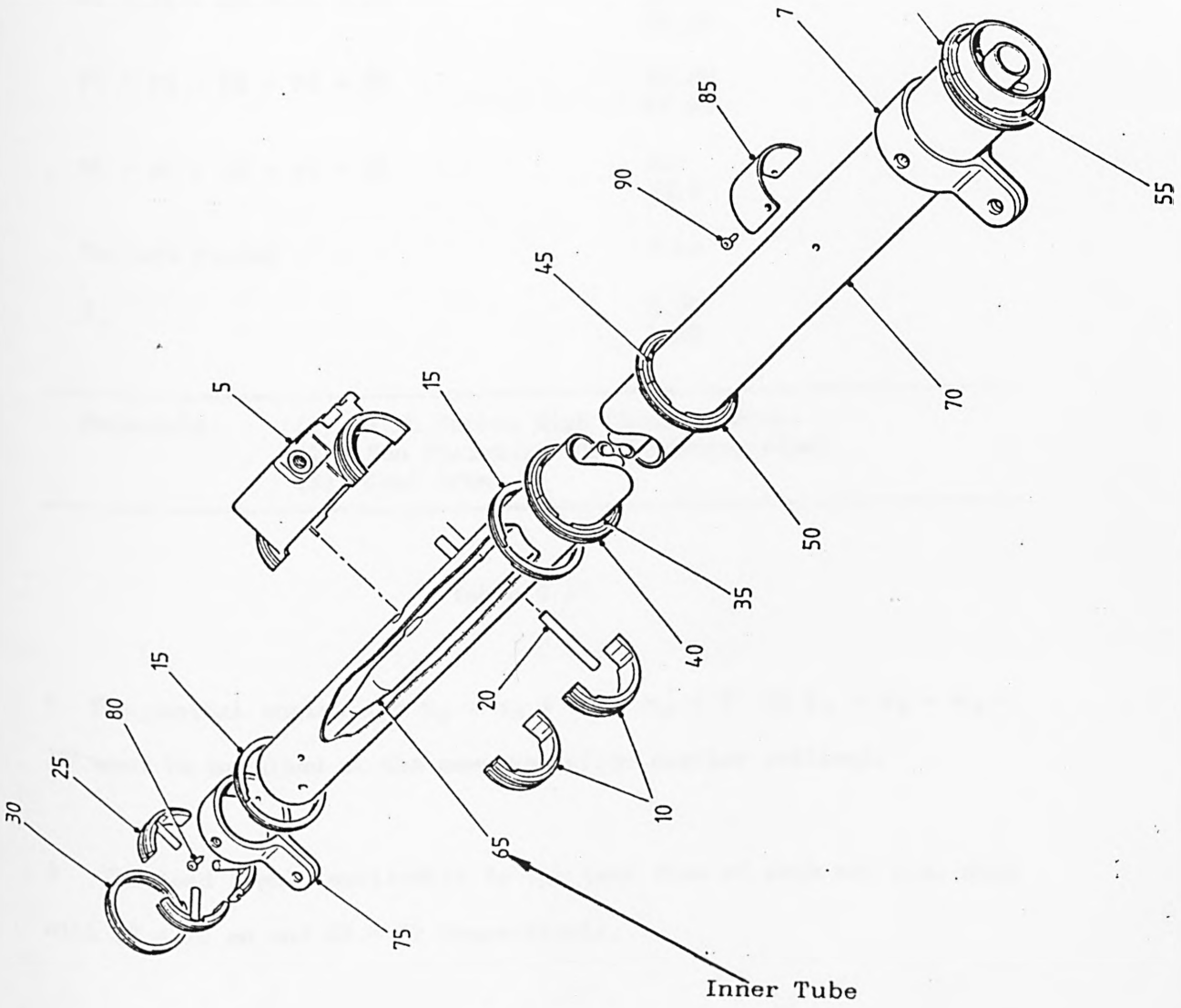

GENERAL SPECIFICATIONS FOR THE PART ONE ELEMENTAL DIES	
A1 = A2 = A3 = A4 = A5	10.00 9.95
B1 = B2 = B3 = B4 = B5	10.00 9.95
J1 = J2 = J3 = J4 = J5	27.00 26.95
F1 = F2 = F3 = F4 = F5	48.00 47.95
$\theta 1 = \theta 2 = \theta 3 = \theta 4 = \theta 5$	30° 29.9°
Surface Finish	5 μm
I	2.00 1.50
Materials: (1) High Carbon High Chromium Steel (2) Non Shrinking Oil Hardening Steel (3) Cast Iron	

Table 4.10.

* The conical angles $\alpha_1 = \alpha_2 = \alpha_3 = \alpha_4 = \alpha_5 = 7°$ OR $\alpha_1 = \alpha_2 = \alpha_3 = 15°$ must be machined at the same top slide angular settings.

* The load I only applicable to the last dies of each set i.e. dies with EX = 10 mm and EX = I2 respectively.

FURTHER DETAILS OF SETS OF ELEMENTAL DIES
(PART ONE - INITIAL DESIGN) WITH FRACTIONAL REDUCTION OF 0.375

5 PIECES WITH 7° CONICAL ANGLE		3 PIECES WITH 15° CONICAL ANGLE	
EX1	14.80	EX1	14.00
EX2	13.60	EX2	12.00
EX3	12.40	EX3	10.00
EX4	11.20		
EX5	10.00		
$\alpha_1 = \alpha_2 = \alpha_3 = \alpha_4 = \alpha_5$	7°	$\alpha_1 = \alpha_2 = \alpha_3$	15°
I	1.50	I	1.50
	1.40		1.40

Table 4.11.

FURTHER DETAILS OF SETS OF ELEMENTAL DIES
(PART ONE - INITIAL DESIGN) WITH FRACTIONAL REDUCTION OF 0.250

5 PIECES WITH 7° CONICAL ANGLE		3 PIECES WITH 15° CONICAL ANGLE	
EX1	15.20	EX1	14.67
EX2	14.40	EX2	13.33
EX3	13.60	EX3	12.00
EX4	12.80		
EX5	12.00		
$\alpha_1 = \alpha_2 = \alpha_3 = \alpha_4 = \alpha_5$	= 7°	$\alpha_1 = \alpha_2 = \alpha_3$	= 15°
I	1.50	I	1.50
	1.40		1.40

Table 4.12.

DETAILS OF SETS OF ELEMENTAL DIES FOR 0.375 FRACTIONAL REDUCTION TO PROOF AND TO ELIMINATE ELEMENTL REDUNDANT DEFORMATION

5 PIECES WITH 7° CONICAL ANGLE		3 PIECES WITH 15° CONICAL ANGLE	
EX1	14.80	EX1	14.00
EX2	13.60	EX2	12.00
EX3	12.40	EX3	10.00
EX4	11.20		
EX5	10.00		
I	1.50	I	1.50
	1.40		1.40
A1	10.00	A1	10.00
	9.95		9.95
A2	4.93	A2	3.87
	4.92		3.86
A3	4.93	A3	3.87
	4.92		3.86
A4	4.93	B	10.00
	4.92		9.95
A5	4.93	J	27.00
	4.92		26.95
B	10.00	F	48.00
	9.95		47.95
J	27.00		
	26.95		
F	48.00		
	47.95		
$\alpha_1 = \alpha_2 = \alpha_3 = \alpha_4 = \alpha_5 = 7°$		$\alpha_1 = \alpha_2 = \alpha_3 = 15°$	

Table 4.13.

DETAILS OF SETS OF ELEMENTAL DIES FOR 0.250 FRACTIONAL REDUCTION TO PROOF AND TO ELIMINATE ELEMENTL REDUNDANT DEFORMATION

5 PIECES WITH 7° CONICAL ANGLE		3 PIECES WITH 15° CONICAL ANGLE	
EX1	15.20	EX1	14.67
EX2	14.40	EX2	13.33
EX3	13.60	EX3	12.00
EX4	12.80		
EX5	12.00		
I	1.50	I	1.50
	1.40		1.40
A1	10.00	A1	10.00
	9.95		9.95
A2	3.282	A2	2.58
	3.280		2.57
A3	3.282	A3	2.58
	3.280		2.57
A4	3.282	B	10.00
	3.280		9.95
A5	3.282	J	27.00
	3.280		26.95
B	10.00	F	48.00
	9.95		47.95
J	48.00		
	47.95		
$\alpha_1 = \alpha_2 = \alpha_3 = \alpha_4 = \alpha_5 = 7°$		$\alpha_1 = \alpha_2 = \alpha_3 = 15°$	

Table 4.14

INITIAL DESIGN OF ELEMENTAL DIE WITH 7° CONICAL ANGLE FOR 0.375 FRACTIONAL REDUCTION

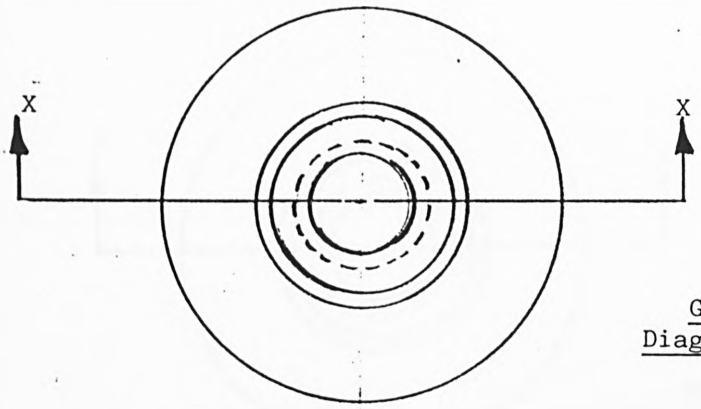

Generalised and Diagramatic Plan

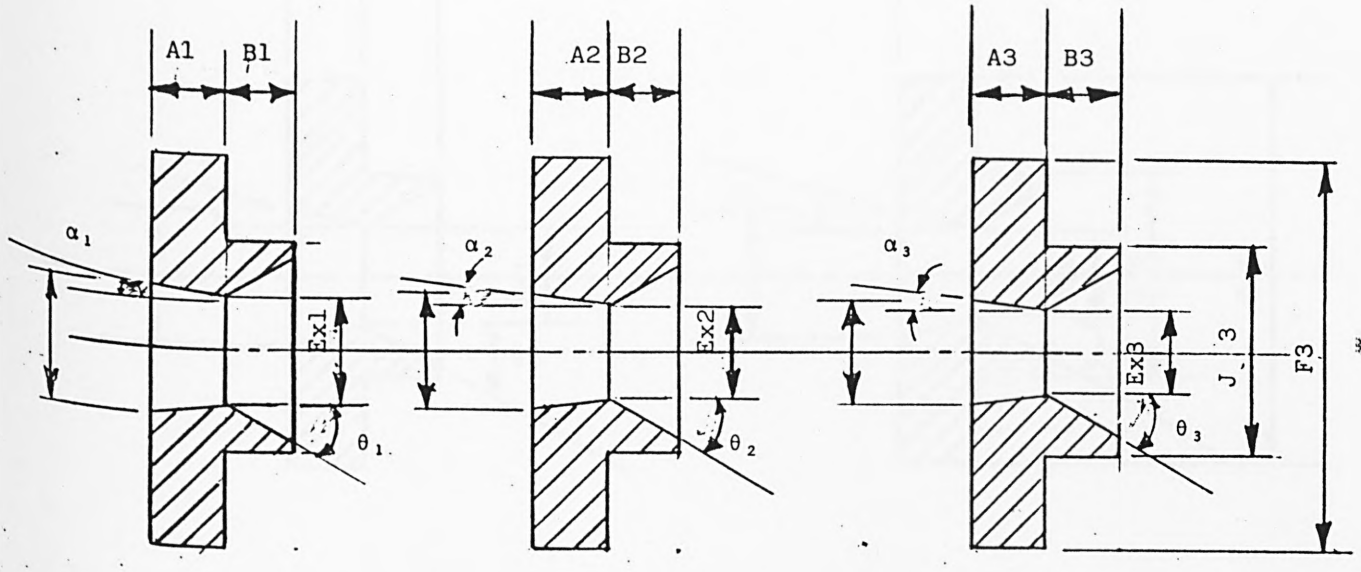

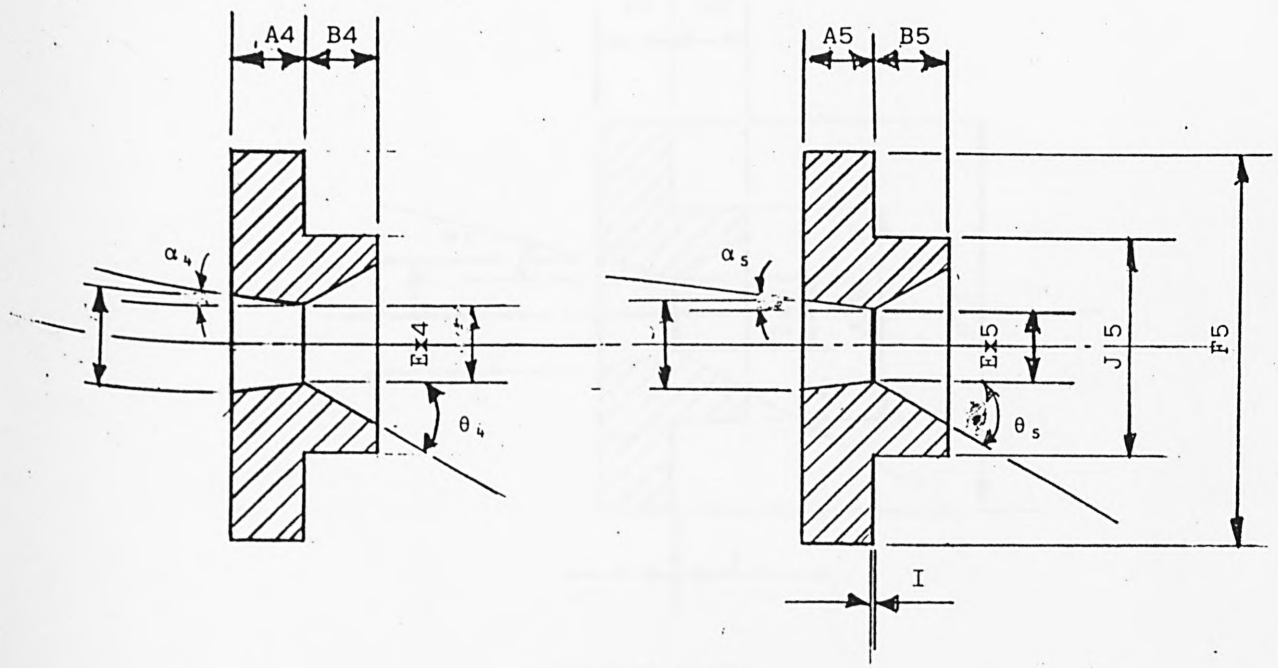

FIGURE (4.10)

INITIAL DESIGN OF ELEMENTAL DIE WITH 15° CONICAL ANGLE FOR 0.375 FRACTIONAL REDUCTION

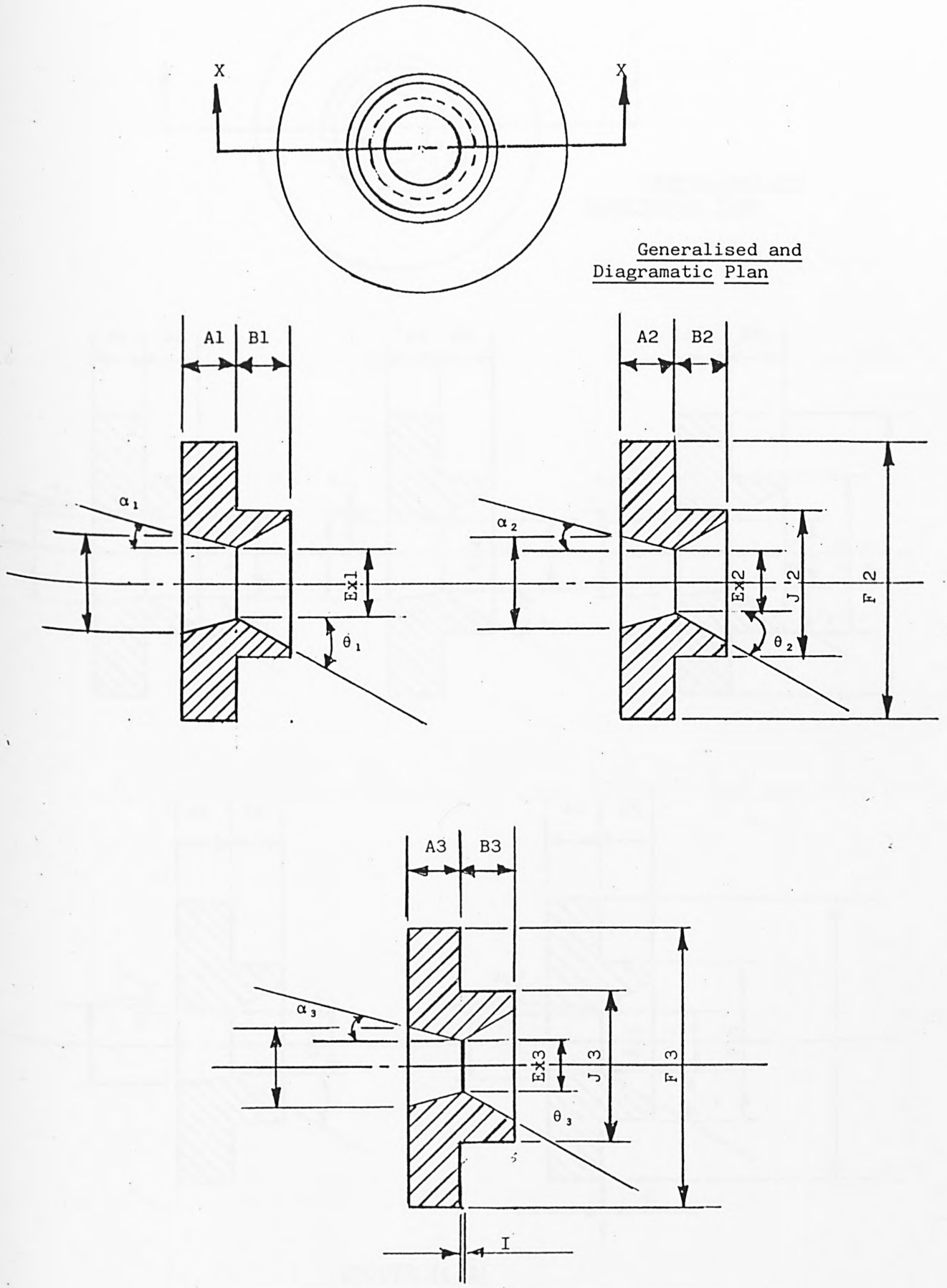

FIGURE (4.11)

INITIAL DESIGN OF ELEMENTAL DIE WITH 7° CONICAL ANGLE FOR 0.250 FRACTIONAL REDUCTION

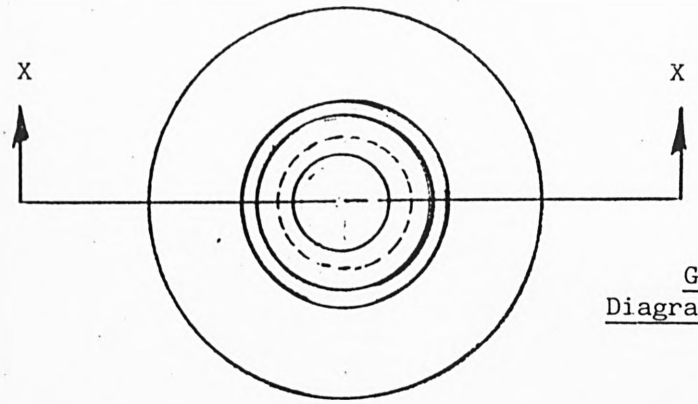

Generalised and Diagramatic Plan

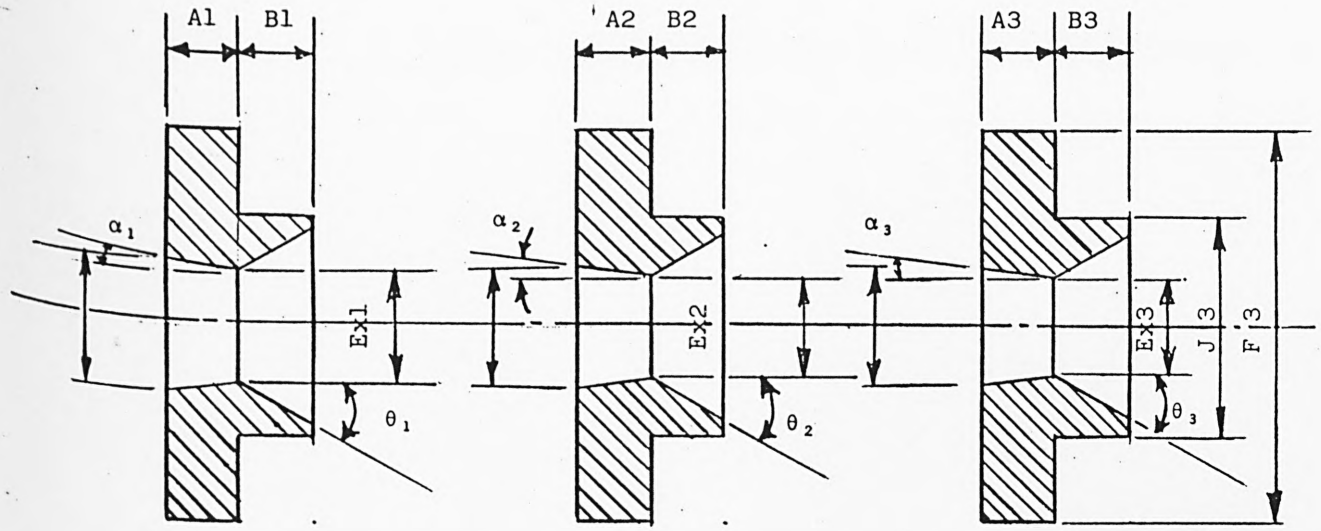

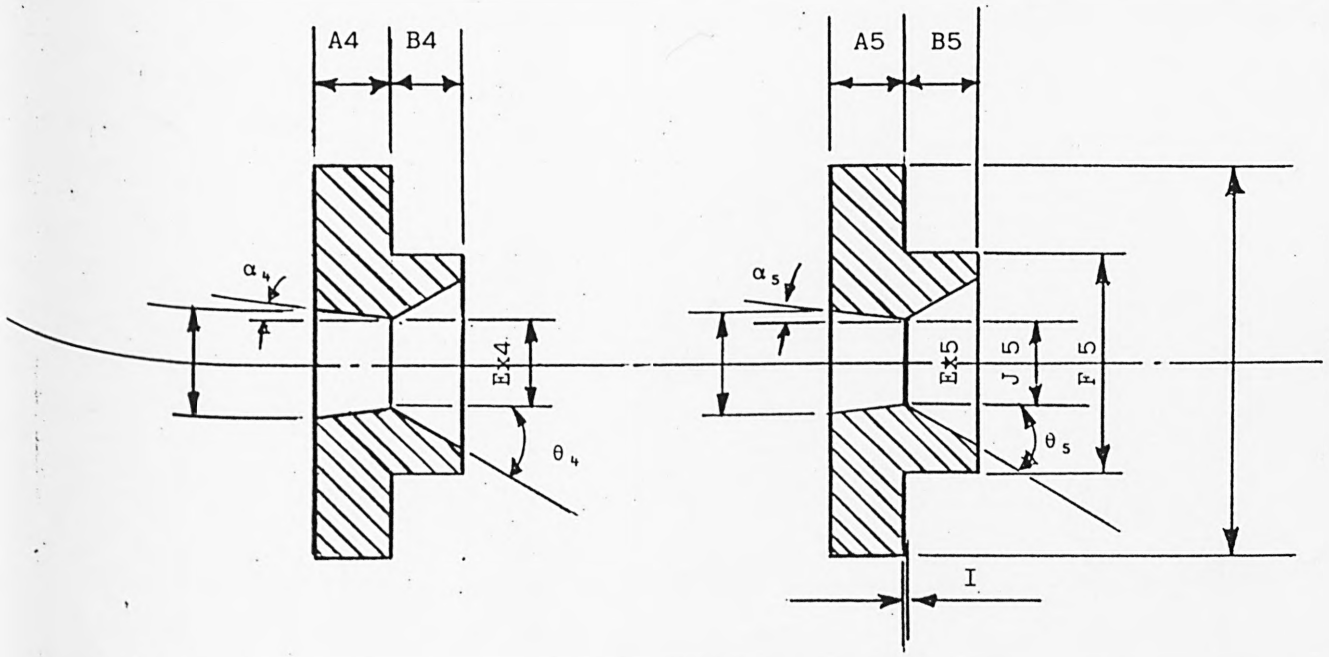

FIGURE (4.12)

INITIAL DESIGN OF ELEMENTAL DIE WITH 15° CONICAL ANGLE FOR 0.250 FRACTIONAL REDUCTION

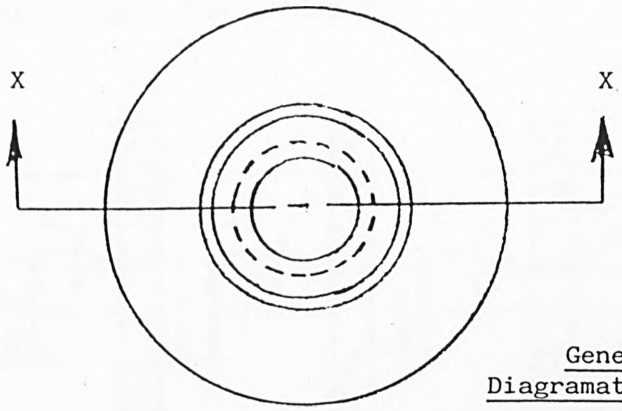

Generalised and Diagramatic Plan

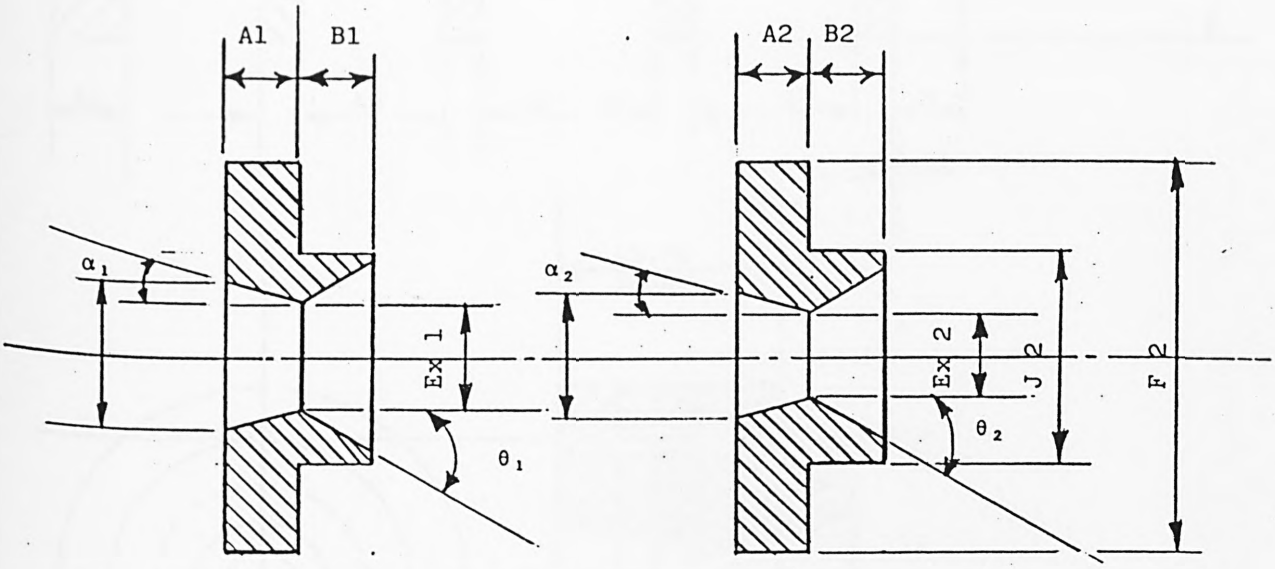

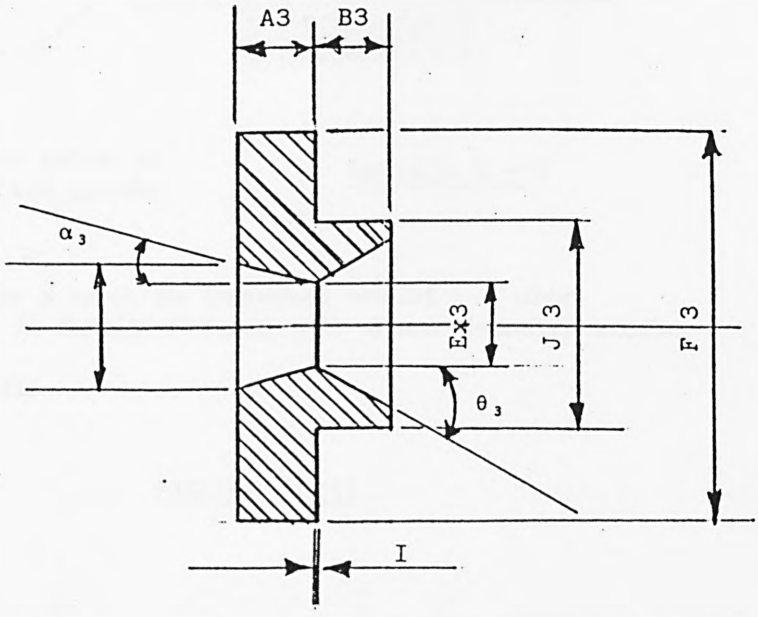

FIGURE (4.13)

ALTERNATIVE DESIGN OF ELEMENTAL DIE (FOR 0.375)
TO PROOF AND TO ELIMINATE ELEMENTAL
REDUNDANT DEFORMATION ($\alpha = 7^{\circ}$)

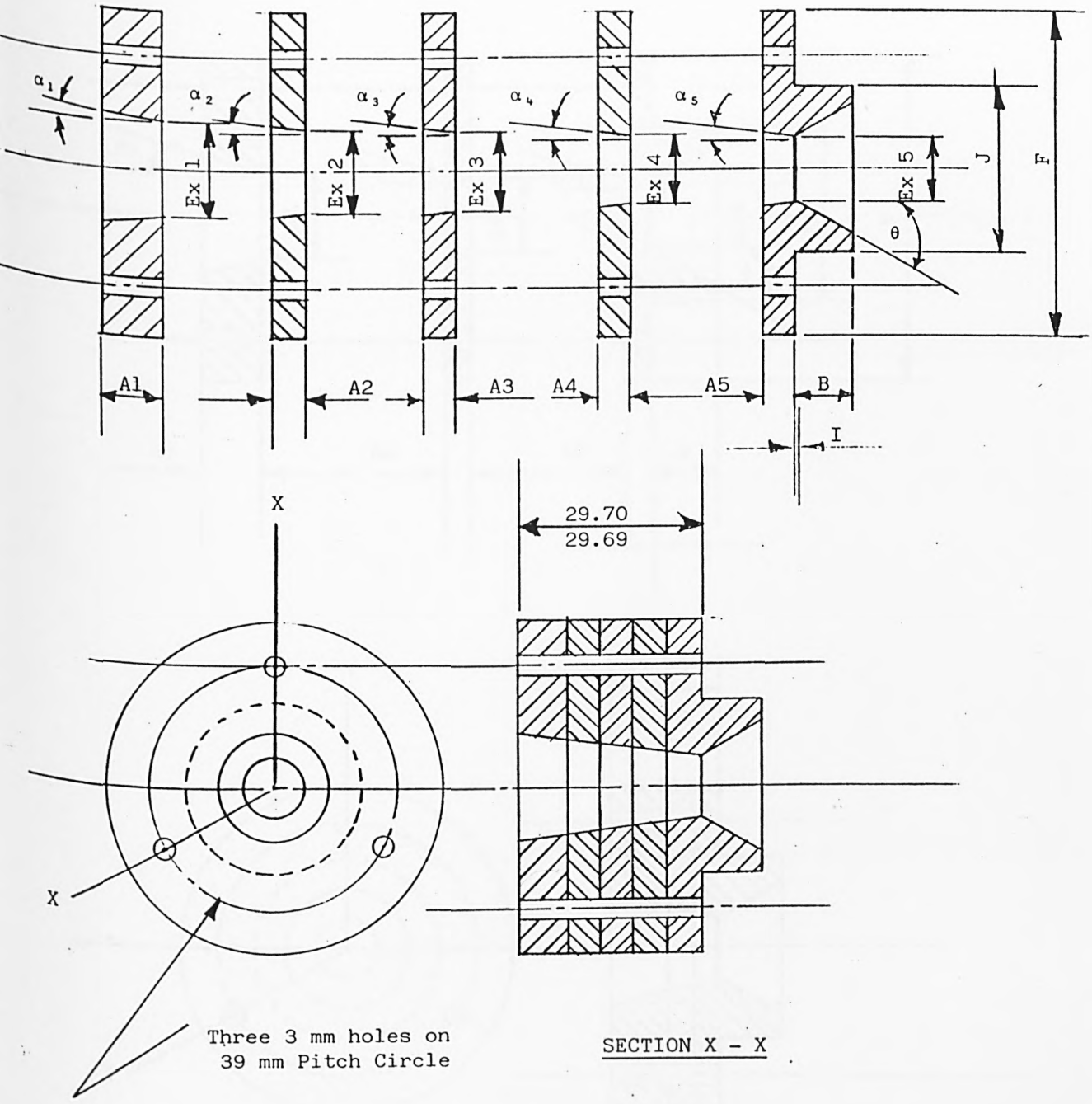

The Conical angle α must be machined whilst the dies' blanks assembly is firmly clamped with 3 mm diameter studs.

Scale: Diagramatic

FIGURE (4.14)

ALTERNATIVE DESIGN OF ELEMENTAL DIE (FOR 0.375) TO PROOF AND TO ELIMINATE ELEMENTAL REDUNDANT DEFORMATION (α = 15°)

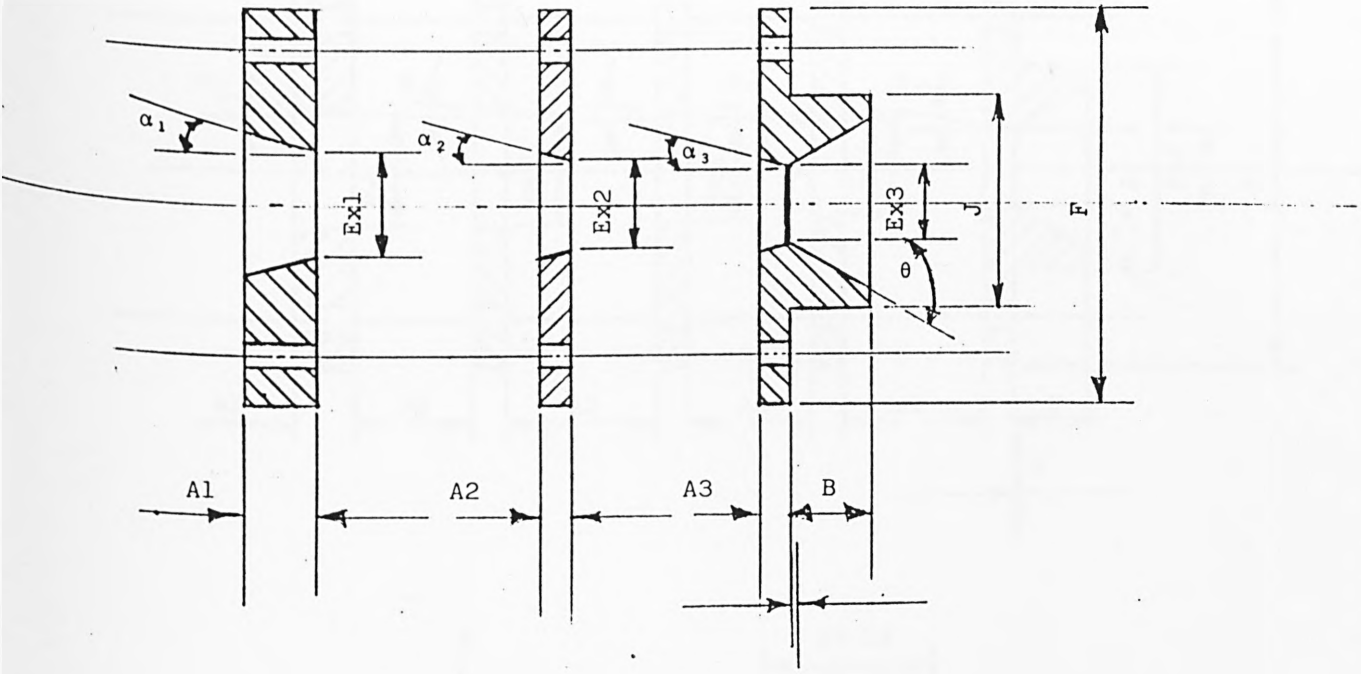

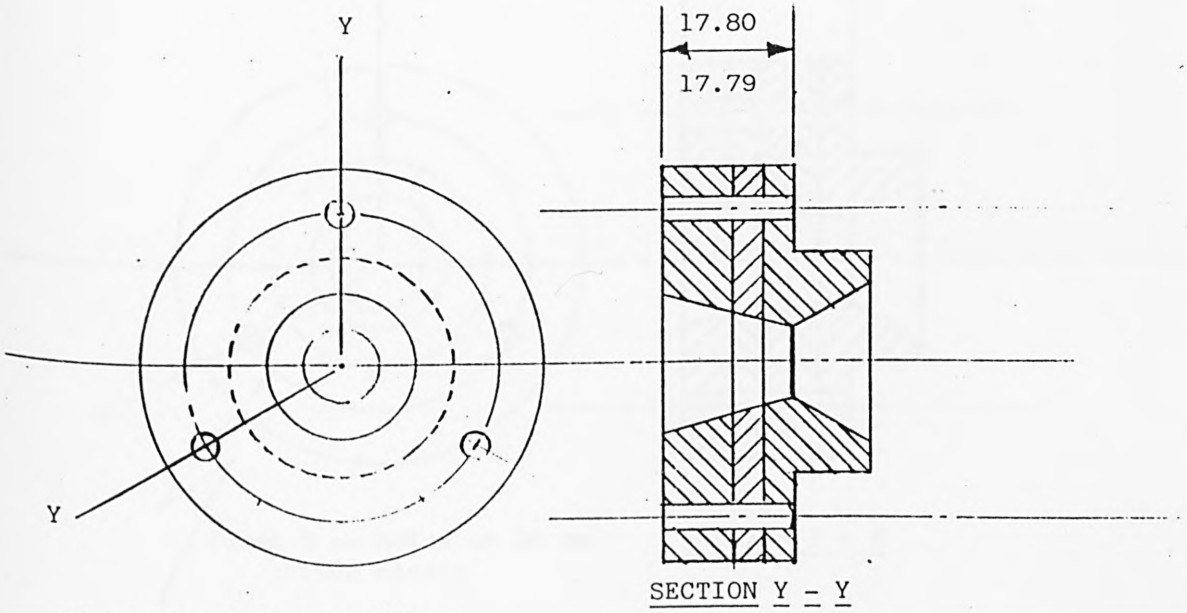

FIGURE (4.15)

ALTERNATIVE DESIGN OF ELEMENTAL DIE (FOR 0.250) TO PROOF AND TO ELIMINATE ELEMENTAL REDUNDANT DEFORMATION (α = 7°)

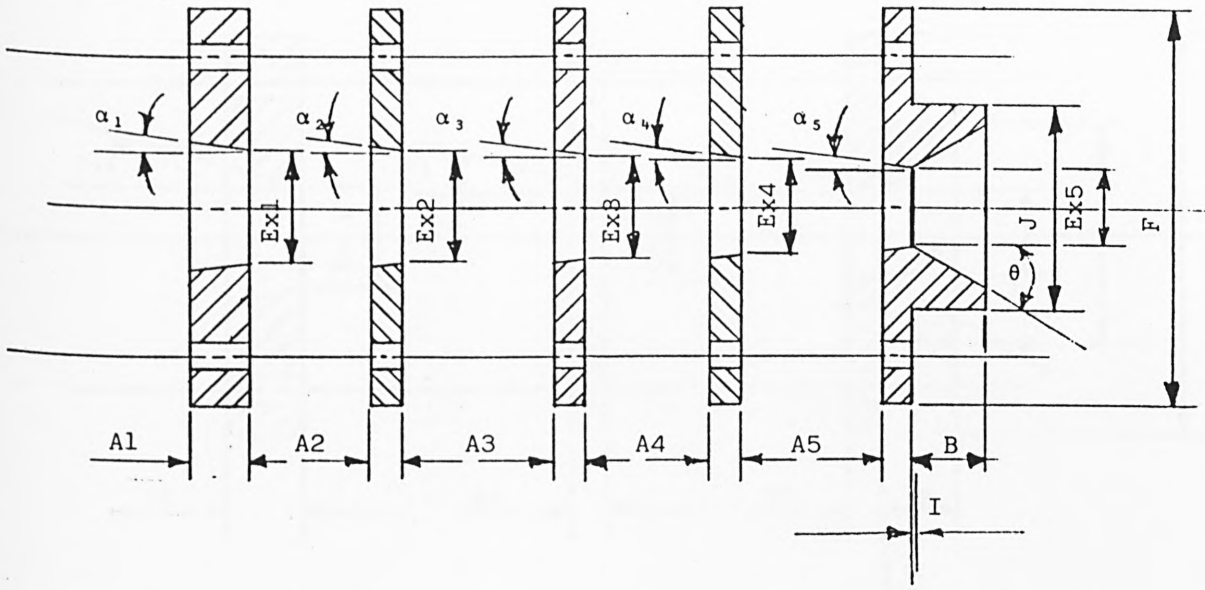

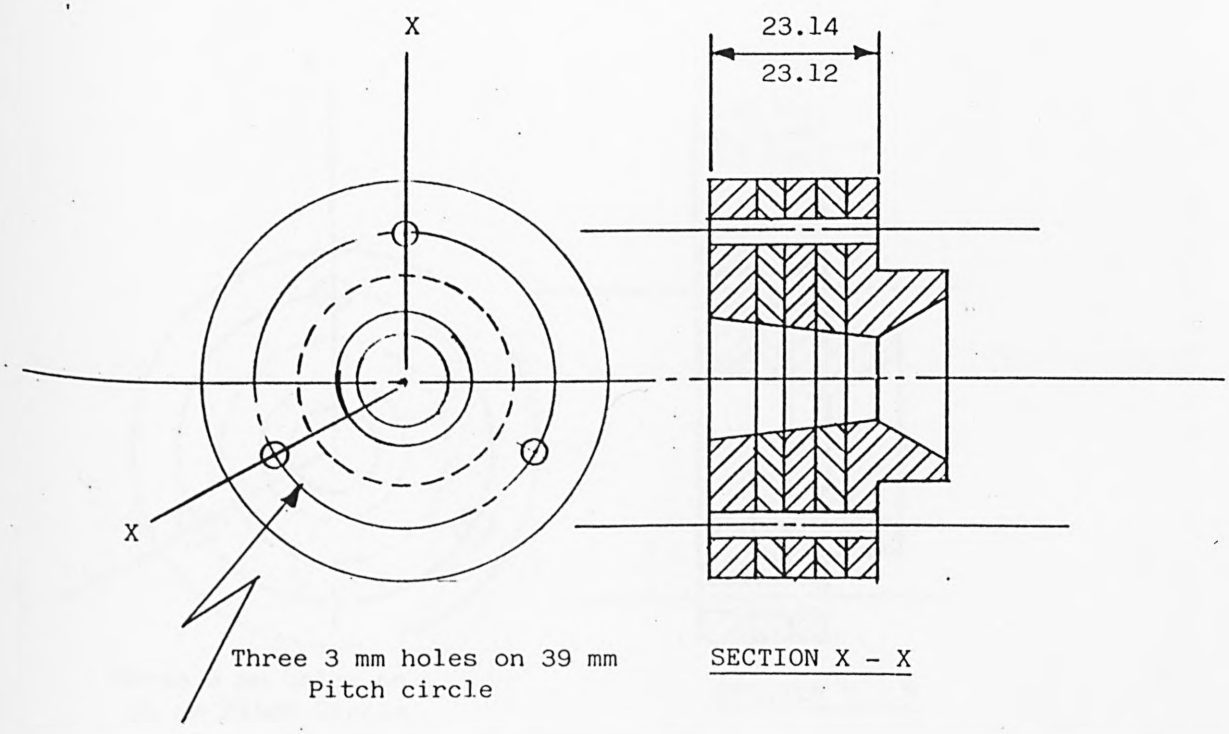

The Conical angle α must be machined whilst the dies' blanks assembly is firmly clamped with 3 mm diameter studs.

Scale: Diagramatic

FIGURE (4.16)

ALTERNATIVE DESIGN OF ELEMENTAL DIE (FOR 0.250) TO PROOF AND TO ELIMINATE ELEMENTAL REDUNDANT DEFORMATION (α = 15°)

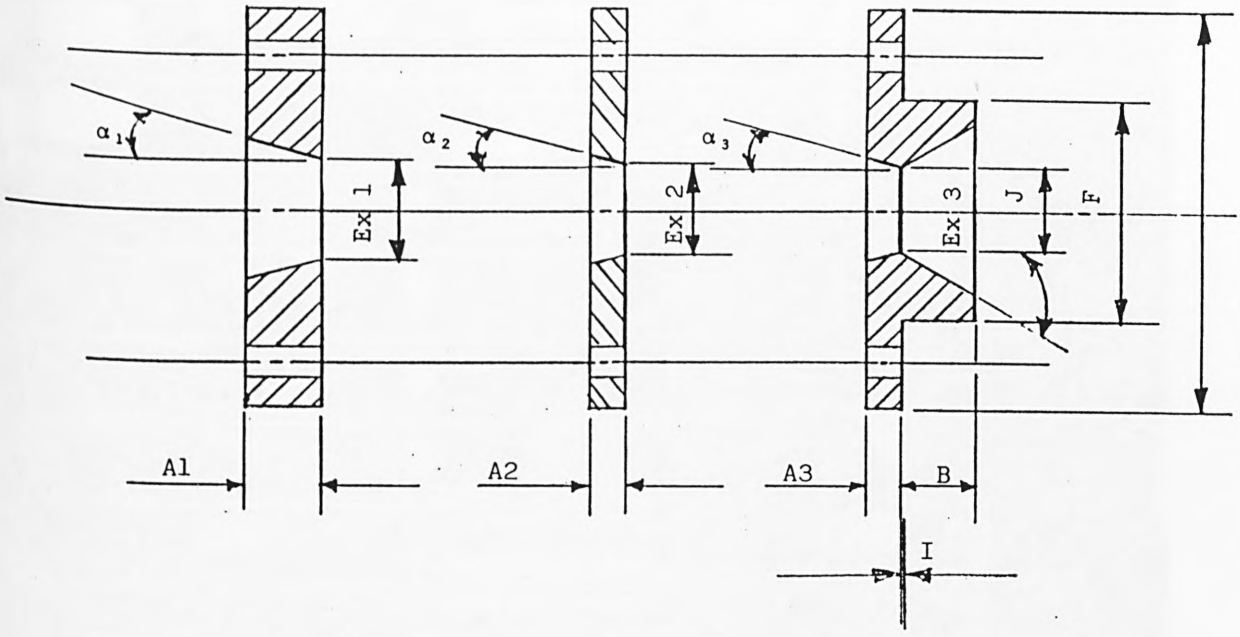

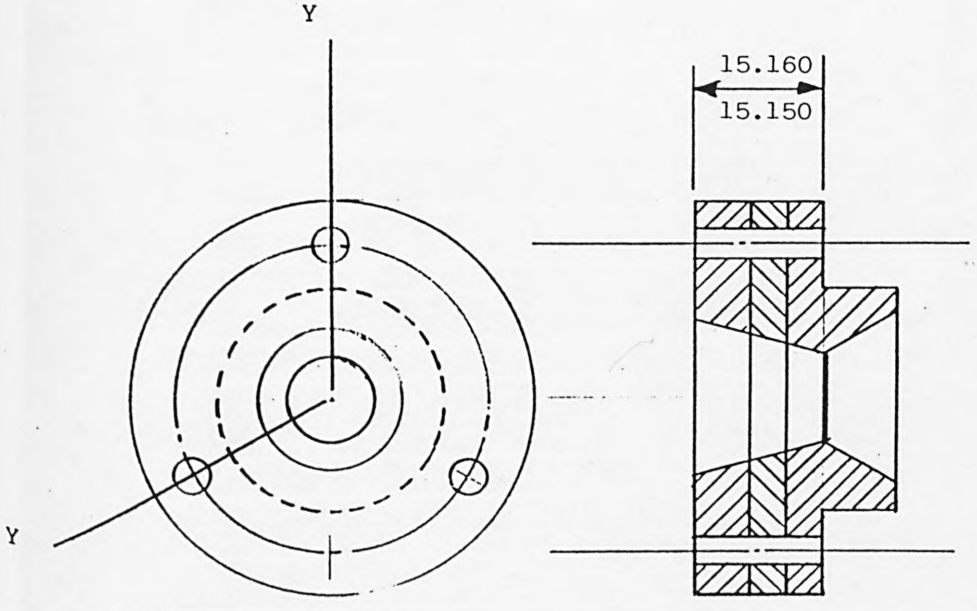

Three 3 mm holes on 39 mm Pitch Circle

SECTION Y - Y

FIGURE (4.17)



Fig.(4.18)

A POWER PRESS EMPLOYED FOR POINTING TUBE SPECIMENS

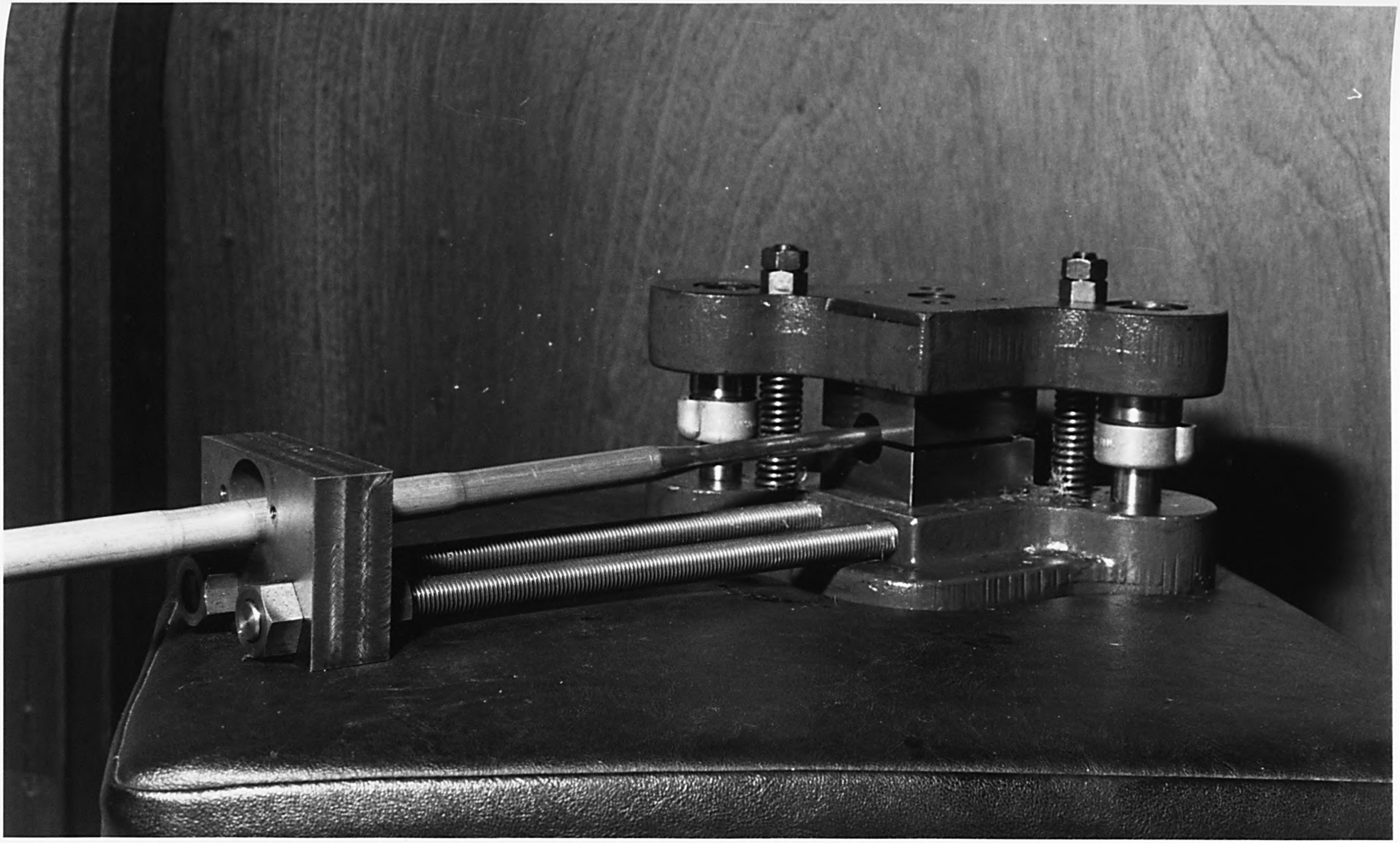

Fig.(4.19)

A DIE SET AND SWAGING TOOL REMOVED FROM POWER PRESS

Curves of Compressive Stress against Natural Strain for Brass Specimen

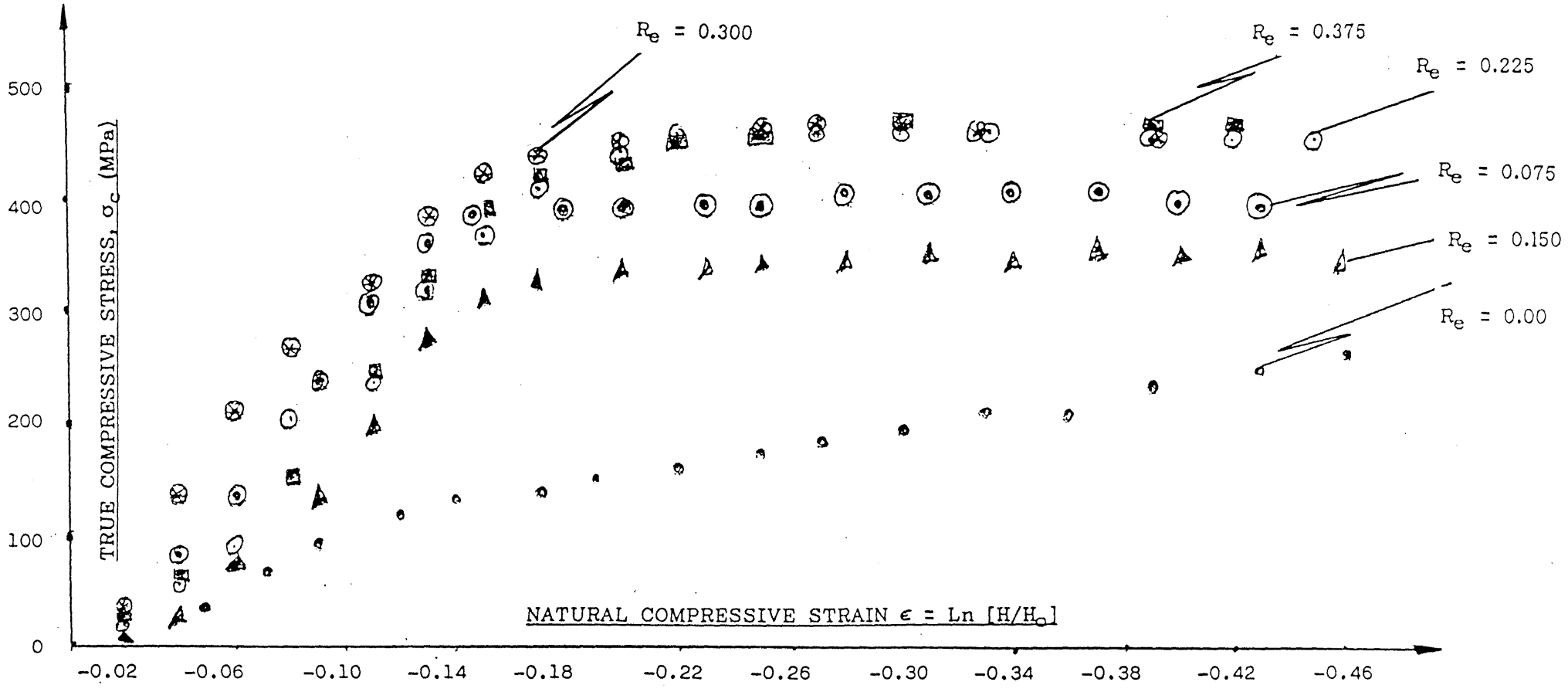

FIGURE (5.1)

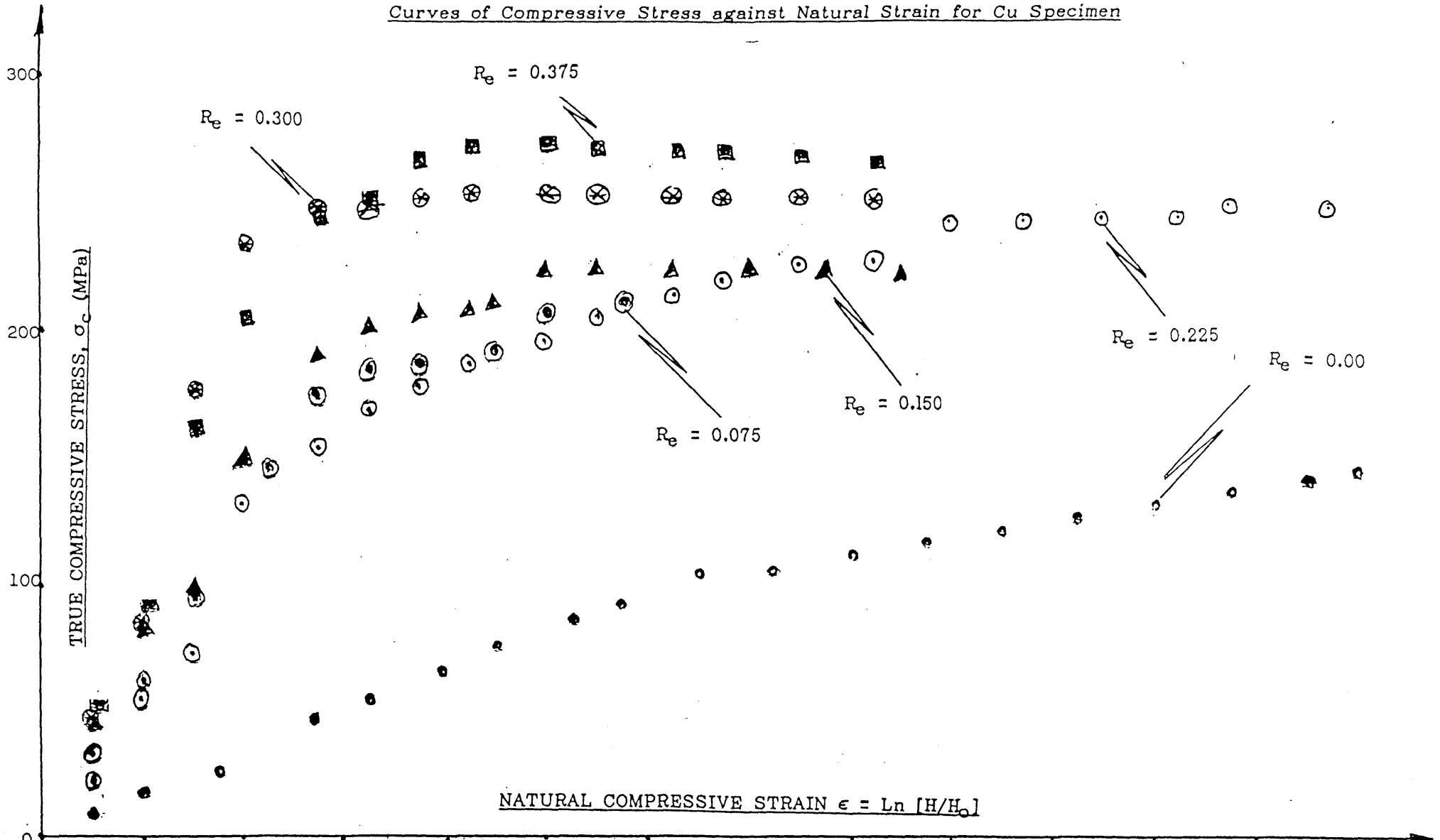
Curves of Compressive Stress against Natural Strain for Cu Specimen
300
200
100
0
TRUE COMPRESSIVE STRESS, σ_c (MPa)
R_e = 0.375
R_e = 0.300
R_e = 0.225
R_e = 0.00
R_e = 0.150
R_e = 0.075
NATURAL COMPRESSIVE STRAIN ϵ = Ln [H/H_o]
-0.04
-0.08
-0.12
-0.16
-0.20
-0.24
-0.28
-0.32
-0.36
-0.40
-0.44
-0.48
-0.52

FIGURE (5.2)

Curves of Compressive Stress against Natural Strain for Stainless Steel Specimen

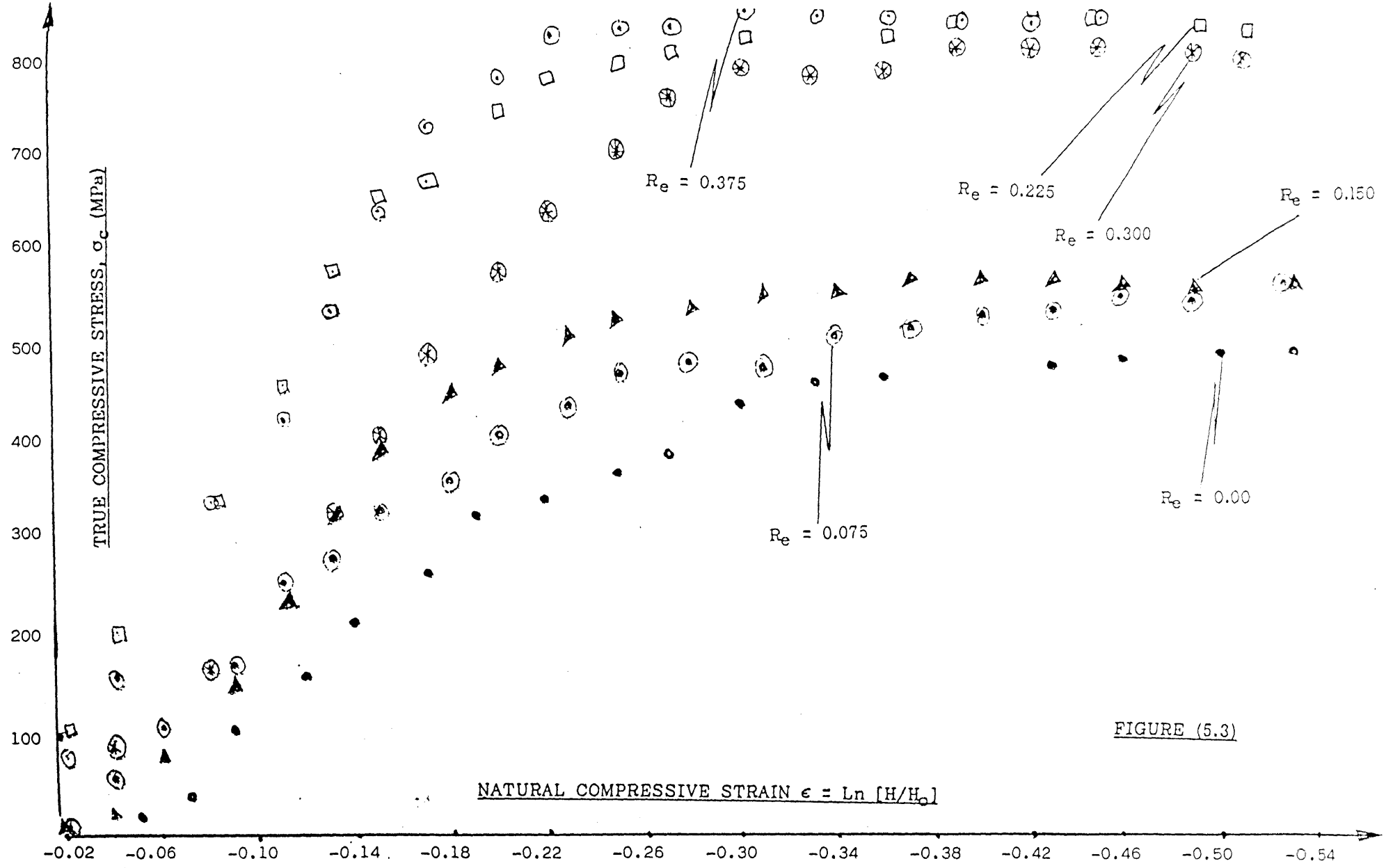

FIGURE (5.3)

Curves of Compressive Stress Against Natural Strain for Stainless Steel at R_T = 0.375 Showing the Effect of Redundant Deformation and Die Pass Length on Yield Stress

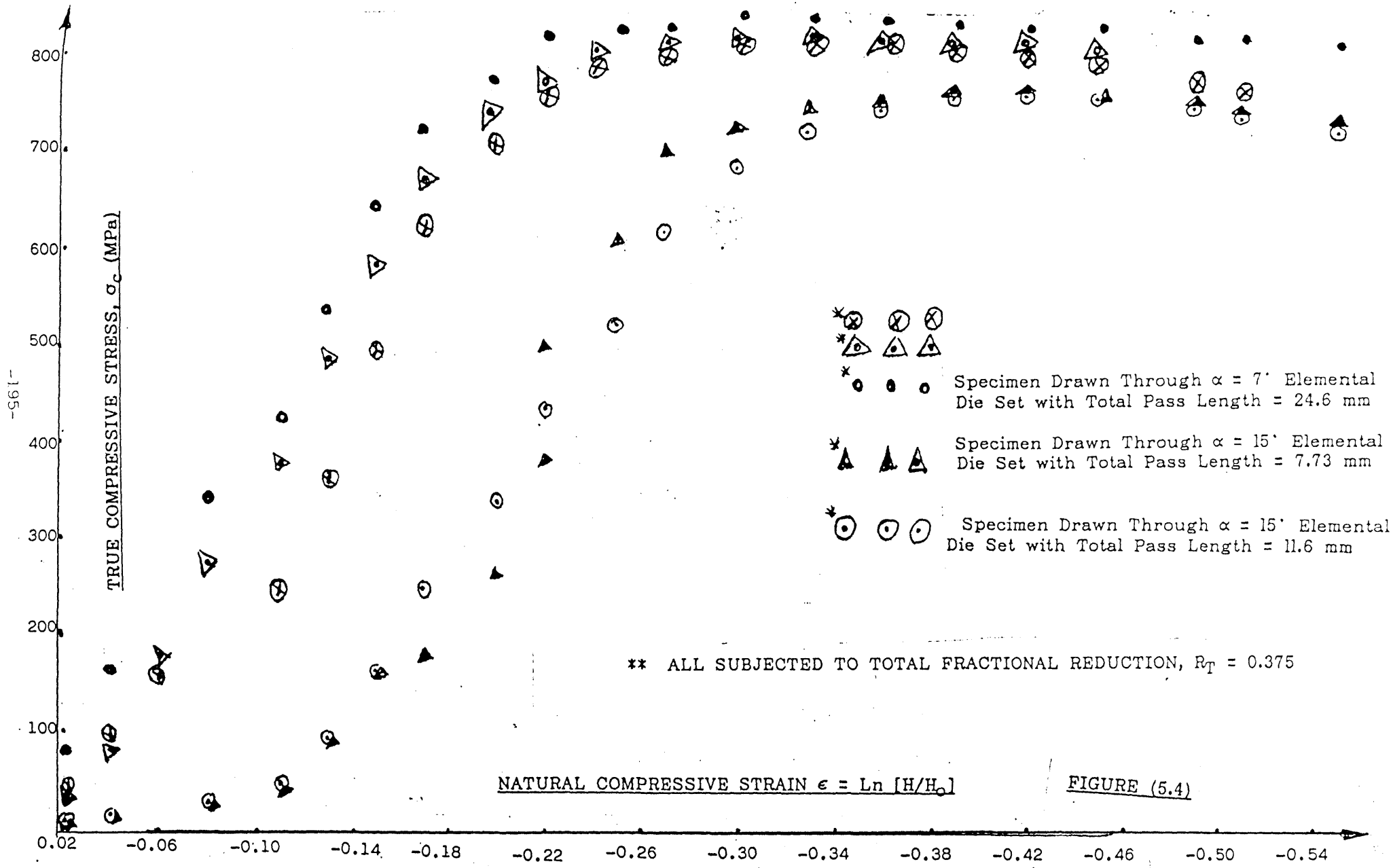

FIGURE (5.4)

QUASI-STATIC AXISYMMETRIC COMPRESSION TEST
SPECIMEN: BRASS

Height = 1.0 mm, Thickness: 0.98 mm, Diameter: 10.0 mm, Re: 0.375

ΔH (mm)	F_c (kN)	H (mm)	A (mm^2)	ϵ	σ_c (MPa)
0.02	0.60	0.98	32.1	-0.02	19
0.04	1.80	0.96	32.7	-0.04	55
0.06	3.00	0.94	33.4	-0.06	90
0.08	7.00	0.92	34.2	-0.08	205
0.10	8.20	0.90	34.9	-0.11	235
0.12	11.30	0.88	35.7	-0.13	317
0.14	13.30	0.86	36.5	-0.15	364
0.16	15.10	0.84	37.4	-0.17	404
0.18	16.80	0.82	38.3	-0.20	439
0.20	17.80	0.80	39.3	-0.22	453
0.22	18.60	0.78	40.3	-0.25	462
0.24	19.10	0.76	41.3	-0.27	463
0.26	19.60	0.74	42.5	-0.30	461
0.28	20.05	0.72	43.6	-0.33	460
0.30	20.40	0.70	44.9	-0.36	454
0.32	20.80	0.68	46.2	-0.39	450
0.34	21.40	0.66	47.6	-0.42	450
0.36	22.10	0.64	49.1	-0.45	450
0.38	22.50	0.62	50.7	-0.49	444
0.40	23.30	0.60	52.4	-0.51	445
0.42	24.10	0.58	54.2	-0.55	445
0.44	24.90	0.56	56.1	-0.58	444
0.46	25.60	0.54	58.2	-0.62	440
0.48	26.25	0.52	60.4	-0.65	435
0.50	27.10	0.50	62.8	-0.69	448
0.52	26.70	0.48	65.5	-0.73	423
0.54	28.60	0.46	68.3	-0.78	419
0.56	29.50	0.44	71.4	-0.82	413
0.58	30.60	0.42	74.8	-0.87	409
0.60	31.60	0.40	78.5	-0.92	403

Table (5.01)

QUASI-STATIC AXISYMMETRIC COMPRESSION TEST
SPECIMEN: BRASS

Height = 1.0 mm, Thickness: 0.96 mm, Diameter: 11.20 mm, Re: 0.300

ΔH (mm)	F_c (kN)	H (mm)	A (mm^2)	ϵ	σ_c (MPa)
0.02	1.40	0.98	32.1	-0.02	44
0.04	4.60	0.96	32.7	-0.04	141
0.06	7.20	0.94	33.4	-0.06	216
0.08	9.20	0.92	34.2	-0.08	269
0.10	11.40	0.90	34.9	-0.11	327
0.12	13.80	0.88	35.7	-0.13	387
0.14	15.50	0.86	36.5	-0.15	425
0.16	16.50	0.84	37.4	-0.17	441
0.18	17.30	0.82	38.3	-0.20	452
0.20	17.90	0.80	39.3	-0.22	456
0.22	18.50	0.78	40.3	-0.25	459
0.24	18.90	0.76	41.3	-0.27	458
0.26	19.50	0.74	42.5	-0.30	459
0.28	19.90	0.72	43.6	-0.33	456
0.30	20.20	0.70	44.9	-0.36	450
0.32	20.90	0.68	46.2	-0.39	452
0.34	21.40	0.66	47.6	-0.42	450
0.36	22.50	0.64	49.1	-0.45	458
0.38	23.20	0.62	50.8	-0.49	457
0.40	23.80	0.60	52.4	-0.51	454
0.42	24.50	0.58	54.2	-0.55	452
0.44	25.30	0.56	56.1	-0.58	451
0.46	26.10	0.54	58.2	-0.62	449
0.48	26.80	0.52	60.4	-0.65	444
0.50	27.60	0.50	62.8	-0.69	440
0.52	28.40	0.48	65.5	-0.73	434
0.54	29.00	0.46	68.3	-0.78	425
0.56	29.90	0.44	71.4	-0.82	419
0.60	30.80	0.42	74.8	-0.87	412

Table (5.02)

QUASI-STATIC AXISYMMETRIC COMPRESSION TEST
SPECIMEN: BRASS

Height = 1.0 mm, Thickness: 0.95mm, Diameter: 12.3 mm, Re: 0.225

ΔH (mm)	F_c (kN)	H (mm)	A (mm^2)	ϵ	σ_c (MPa)
0.02	1.00	0.98	32.1	-0.02	31
0.04	2.00	0.96	32.7	-0.04	61
0.06	5.00	0.94	33.4	-0.08	150
0.08	8.50	0.92	34.2	-0.11	249
0.10	11.60	0.90	34.9	-0.13	332
0.12	14.00	0.88	35.7	-0.15	392
0.14	15.40	0.86	36.5	-0.17	422
0.16	16.40	0.84	37.4	-0.20	439
0.18	17.30	0.82	38.3	-0.22	452
0.20	18.05	0.80	39.3	-0.25	459
0.22	18.80	0.78	40.3	-0.30	467
0.24	19.30	0.76	41.3	-0.33	467
0.26	19.80	0.74	42.5	-0.36	466
0.28	20.30	0.72	43.6	-0.39	466
0.30	20.80	0.70	44.9	-0.42	463
0.32	21.30	0.68	46.2	-0.45	461
0.34	21.70	0.66	47.6	-0.49	456
0.36	22.30	0.64	49.1	-0.51	454
0.38	22.80	0.62	50.7	-0.55	450
0.40	23.40	0.60	52.4	-0.58	447
0.42	24.00	0.58	54.2	-0.62	443
0.44	24.80	0.56	56.1	-0.65	442
0.46	25.60	0.54	58.2	-0.69	440
0.48	26.40	0.52	60.4	-0.73	437
0.50	27.10	0.50	62.8	-0.78	432
0.52	28.00	0.48	65.5	-0.82	428
0.54	29.00	0.46	68.3	-0.87	425
0.56	29.60	0.44	71.4	-0.92	415
0.58	30.40	0.42	74.8	-0.97	406
0.60	31.60	0.40	78.5	-1.02	403

Table (5.03)

QUASI-STATIC AXISYMMETRIC COMPRESSION TEST
SPECIMEN: BRASS

Height = 1.0 mm, Thickness: 0.935 mm, Diameter: 13.6 mm, Re: 0.150

ΔH (mm)	F_c (kN)	H (mm)	A (mm^2)	ϵ	σ_c (MPa)
0.02	0.50	0.96	42.7	-0.02	12
0.04	1.40	0.94	43.7	-0.04	32
0.06	3.50	0.92	44.6	-0.06	79
0.08	6.30	0.90	45.6	-0.09	138
0.10	9.40	0.88	46.6	-0.11	202
0.12	13.00	0.86	47.7	-0.13	273
0.14	15.20	0.84	48.9	-0.15	311
0.16	16.20	0.82	50.0	-0.18	324
0.18	17.20	0.80	51.3	-0.20	335
0.20	17.80	0.78	52.6	-0.23	338
0.22	18.50	0.76	54.0	-0.25	343
0.24	19.20	0.74	55.5	-0.28	346
0.26	20.00	0.72	57.0	-0.31	351
0.28	20.40	0.70	58.6	-0.34	348
0.30	21.40	0.68	60.3	-0.37	355
0.32	21.80	0.66	62.2	-0.40	351
0.34	22.40	0.64	64.1	-0.43	350
0.36	22.80	0.62	66.2	-0.46	344
0.38	23.10	0.60	68.2	-0.49	338
0.40	23.40	0.58	70.8	-0.53	331
0.42	24.00	0.56	73.3	-0.56	327
0.44	24.50	0.54	76.0	-0.60	322
0.46	25.50	0.52	78.9	-0.63	323
0.48	25.90	0.50	82.1	-0.67	315
0.50	26.60	0.48	85.5	-0.71	311
0.52	27.60	0.46	89.2	-0.76	310
0.54	28.50	0.44	93.3	-0.80	306
0.56	29.40	0.42	97.7	-0.85	301
0.58	20.40	0.40	103.0	-0.90	295
0.60	31.40	0.38	108.0	-0.95	291

Table (5.04)

QUASI-STATIC AXISYMMETRIC COMPRESSION TEST
SPECIMEN: BRASS

Height = 1.0 mm, Thickness: 0.93 mm, Diameter: 14.8 mm, Re: 0.075

ΔH (mm)	F_C (kN)	H (mm)	A (mm^2)	ϵ	σ_C (MPa)
0.02	1.10	0.96	42.7	-0.02	26
0.04	3.40	0.94	43.7	-0.04	78
0.06	6.30	0.92	44.6	-0.06	141
0.08	10.80	0.90	45.6	-0.09	237
0.10	14.60	0.88	46.6	-0.11	313
0.12	17.40	0.86	47.7	-0.13	365
0.14	18.90	0.84	48.9	-0.15	387
0.16	19.80	0.82	50.0	-0.18	396
0.18	20.20	0.80	51.3	-0.20	394
0.20	21.00	0.78	52.6	-0.23	399
0.22	21.50	0.76	54.0	-0.25	398
0.24	22.60	0.74	55.5	-0.28	407
0.26	23.00	0.72	57.0	-0.31	404
0.28	23.60	0.70	58.6	-0.34	403
0.30	24.05	0.68	60.3	-0.37	403
0.32	24.40	0.66	62.2	-0.40	392
0.34	24.70	0.64	64.1	-0.43	385
0.36	25.00	0.62	66.2	-0.46	378
0.38	25.40	0.60	68.4	-0.49	371
0.40	25.80	0.58	70.8	-0.53	364
0.42	26.50	0.56	73.3	-0.56	362
0.44	27.10	0.54	76.0	-0.60	357
0.46	28.40	0.52	78.9	-0.63	360
0.48	29.00	0.50	82.1	-0.67	349
0.50	29.80	0.48	85.5	-0.71	349
0.52	30.80	0.46	89.2	-0.76	345
0.54	31.70	0.44	93.2	-0.80	340
0.56	32.70	0.42	97.7	-0.85	335
0.58	33.60	0.40	103.0	-0.90	326
0.60	34.80	0.38	108.0	-0.95	322

Table (5.05)

QUASI-STATIC AXISYMMETRIC COMPRESSION TEST
SPECIMEN: BRASS

Height = 1.0 mm, Thickness: 0.92 mm, Diameter: 16.0 mm, Re: 0.00

ΔH (mm)	F_C (kN)	H (mm)	A (mm^2)	ϵ	σ_C (MPa)
0.02	1.00	0.90	47.27	-0.02	21.0
0.04	1.60	0.88	48.35	-0.05	33.0
0.06	3.40	0.86	49.47	-0.07	69.0
0.08	4.80	0.84	50.65	-0.09	95.0]
0.10	5.90	0.82	51.88	-0.12	114
0.12	7.00	0.80	53.18	-0.14	132
0.14	7.80	0.78	54.55	-0.17	143
0.16	8.50	0.76	55.98	-0.19	152
0.18	9.30	0.74	57.49	-0.22	162
0.20	10.20	0.72	59.10	-0.25	173
0.22	11.30	0.70	60.78	-0.27	186
0.24	12.30	0.68	62.6	-0.30	197
0.26	13.80	0.66	64.5	-0.33	214
0.28	14.00	0.64	66.5	-0.36	210
0.30	16.30	0.62	68.6	-0.39	238
0.32	17.68	0.60	70.9	-0.43	249
0.34	19.10	0.58	73.4	-0.46	260
0.36	20.20	0.56	76.0	-0.50	266
0.38	21.10	0.54	78.8	-0.53	268
0.40	21.80	0.52	81.8	-0.57	266
0.42	23.60	0.50	85.1	-0.61	277
0.44	24.60	0.48	88.6	-0.65	278
0.46	25.20	0.46	92.5	-0.69	273
0.48	26.00	0.44	96.7	-0.74	273
0.50	26.40	0.42	101	-0.78	261
0.52	27.10	0.40	106	-0.83	255
0.54	28.80	0.38	112	-0.88	257
0.56	29.30	0.36	118	-0.94	240
0.58	30.30	0.34	125	-1.00	242
0.60	31.00	0.32	133	-1.06	233
0.62	32.00	0.30	142	-1.12	226

Table (5.06)

QUASI-STATIC AXISYMMETRIC COMPRESSION TEST
SPECIMEN: Cu

Height = 1.0 mm, Thickness: 0.98 mm, Diameter: 10.0 mm, Re: 0.375

ΔH (mm)	F_c (kN)	H (mm)	A (mm^2)	ϵ	σ_c (MPa)
0.02	1.10	0.98	32.06	-0.02	34
0.04	1.80	0.96	32.72	-0.04	55
0.06	2.45	0.94	33.42	-0.06	73
0.08	4.50	0.92	34.15	-0.08	132
0.10	5.40	0.90	34.91	-0.11	155
0.12	6.00	0.88	35.70	-0.13	168
0.14	6.50	0.86	36.53	-0.15	178
0.16	7.00	0.84	37.40	-0.17	187
0.18	7.50	0.82	38.31	-0.20	196
0.20	8.10	0.80	39.27	-0.22	206
0.22	8.60	0.78	40.28	-0.25	214
0.24	9.10	0.76	41.43	-0.27	220
0.26	9.60	0.74	42.45	-0.30	226
0.28	10.0	0.72	43.63	-0.33	229
0.30	10.9	0.70	44.88	-0.36	243
0.32	11.2	0.68	46.20	-0.39	242
0.34	11.6	0.66	47.60	-0.42	244
0.36	12.1	0.64	49.09	-0.45	244
0.38	12.6	0.62	50.67	-0.49	249
0.40	13.0	0.60	52.36	-0.51	248
0.42	13.5	0.58	54.17	-0.55	249
0.44	14.0	0.56	56.10	-0.58	250
0.46	14.5	0.54	58.18	-0.62	249
0.48	15.1	0.52	60.42	-0.65	250
0.50	15.7	0.50	62.83	-0.69	250
0.52	16.3	0.48	65.45	-0.73	249
0.54	17.0	0.46	68.30	-0.78	249
0.56	17.6	0.44	71.40	-0.82	247
0.60	18.6	0.42	74.80	-0.87	249
0.62	21.2	0.40	78.54	-0.92	270
0.64	24.0	0.38	82.67	-0.97	290
0.66	27.0	0.36	87.27	-1.02	309

Table (5.07)

QUASI-STATIC AXISYMMETRIC COMPRESSION TEST
SPECIMEN: Cu

Height = 1.0 mm, Thickness: 0.96 mm, Diameter: 11.20 mm, Re: 0.300

ΔH (mm)	F_C (kN)	H (mm)	A (mm^2)	ϵ	σ_C (MPa)
0.02	0.90	0.98	32.06	-0.02	28
0.04	2.80	0.96	32.72	-0.04	86
0.06	5.90	0.94	33.42	-0.06	177
0.08	8.00	0.92	34.15	-0.08	234
0.10	8.70	0.90	34.91	-0.11	249
0.12	8.95	0.88	35.70	-0.13	251
0.14	9.20	0.86	36.53	-0.15	252
0.16	9.50	0.84	37.40	-0.17	254
0.18	9.70	0.82	38.30	-0.20	253
0.20	9.95	0.80	39.27	-0.22	253
0.22	10.2	0.78	40.28	-0.25	253
0.24	10.4	0.76	41.34	-0.27	252
0.26	10.65	0.74	42.45	-0.30	251
0.28	10.96	0.72	43.63	-0.33	251
0.30	11.20	0.70	44.88	-0.36	250
0.32	11.40	0.68	46.20	-0.39	247
0.34	11.70	0.66	47.60	-0.42	246
0.36	12.15	0.64	49.09	-0.45	248
0.38	12.50	0.62	50.67	-0.49	247
0.40	12.90	0.60	52.36	-0.51	246
0.42	13.25	0.58	54.17	-0.55	245
0.44	13.70	0.56	56.10	-0.58	244
0.46	14.20	0.54	58.18	-0.62	244
0.48	14.60	0.52	60.42	-0.65	242
0.50	15.00	0.50	62.83	-0.69	239
0.52	15.60	0.48	65.45	-0.73	238
0.54	16.10	0.46	68.30	-0.78	236
0.56	16.70	0.44	71.40	-0.82	234
0.58	17.20	0.42	74.80	-0.87	230
0.60	17.80	0.40	78.54	-0.92	227
0.64	18.40	0.38	82.67	-0.97	223
0.66	19.20	0.36	87.27	-1.02	220

Table (5.08)

QUASI-STATIC AXISYMMETRIC COMPRESSION TEST
SPECIMEN: Cu

Height = 1.0 mm, Thickness: 0.95 mm, Diameter: 12.40 mm, Re: 0.225

ΔH (mm)	F_C (kN)	H (mm)	A (mm^2)	ϵ	σ_C (MPa)
0.02	1.00	0.98	32.06	-0.02	31
0.04	3.00	0.96	32.72	-0.04	92
0.06	5.40	0.94	33.42	-0.06	162
0.08	7.00	0.92	34.15	-0.08	205
0.10	8.20	0.90	34.91	-0.11	245
0.12	9.00	0.88	35.70	-0.13	252
0.14	9.80	0.86	36.53	-0.15	268
0.16	10.20	0.84	37.40	-0.17	273
0.18	10.50	0.82	38.30	-0.20	274
0.20	10.70	0.80	39.27	-0.22	272
0.22	10.90	0.78	40.28	-0.25	271
0.24	11.20	0.76	41.34	-0.30	271
0.26	11.50	0.74	42.45	-0.33	271
0.28	11.70	0.72	43.63	-0.36	268
0.30	12.00	0.70	44.88	-0.39	267
0.32	12.30	0.68	46.20	-0.42	266
0.34	12.60	0.66	47.60	-0.45	265
0.36	12.90	0.64	49.09	-0.49	263
0.38	13.20	0.62	50.67	-0.51	261
0.40	13.60	0.60	52.36	-0.55	260
0.42	14.00	0.58	54.17	-0.58	259
0.44	14.40	0.56	56.10	-0.62	257
0.46	15.00	0.54	58.18	-0.65	258
0.48	15.40	0.52	60.42	-0.69	255
0.50	15.80	0.50	62.83	-0.73	252
0.52	16.20	0.48	65.45	-0.78	248
0.54	17.40	0.46	68.30	-0.82	255
0.56	17.90	0.44	71.40	-0.87	251
0.58	18.50	0.42	74.80	-0.92	247
0.60	19.20	0.40	78.54	-0.97	245
0.62	19.90	0.38	82.67	-1.02	241
0.64	20.60	0.36	87.27	-1.08	236

Table (5.09)

QUASI-STATIC AXISYMMETRIC COMPRESSION TEST
SPECIMEN: Cu

Height = 1.0 mm, Thickness: 0.94 mm, Diameter: 13.60 mm, Re: 0.150

ΔH (mm)	F_C (kN)	H (mm)	A (mm^2)	ϵ	σ_C (MPa)
0.02	1.10	0.96	42.74	-0.02	26
0.04	3.60	0.94	43.65	-0.04	83
0.06	5.40	0.92	44.60	-0.06	121
0.08	7.00	0.90	45.60	-0.09	154
0.10	9.00	0.88	46.63	-0.11	193
0.12	9.60	0.86	47.71	-0.13	201
0.14	10.20	0.84	48.85	-0.15	209
0.16	10.60	0.82	50.04	-0.18	212
0.18	11.60	0.80	51.29	-0.20	226
0.20	11.90	0.78	52.61	-0.23	226
0.22	12.20	0.76	53.99	-0.25	226
0.24	12.40	0.74	55.45	-0.28	224
0.26	12.80	0.72	56.99	-0.31	225
0.28	13.00	0.70	58.62	-0.34	222
0.30	13.50	0.68	60.34	-0.37	224
0.32	13.90	0.66	62.17	-0.40	224
0.34	14.30	0.64	64.12	-0.43	223
0.36	15.10	0.62	66.18	-0.46	228
0.38	15.60	0.60	68.39	-0.49	228
0.40	16.10	0.58	70.75	-0.53	228
0.42	16.60	0.56	73.28	-0.56	226
0.44	17.20	0.54	75.99	-0.60	226
0.46	19.60	0.52	78.91	-0.63	223
0.48	18.20	0.50	82.07	-0.67	222
0.50	18.70	0.48	85.49	-0.71	219
0.52	19.40	0.46	89.20	-0.76	218
0.54	20.00	0.44	93.26	-0.80	215
0.56	20.70	0.42	97.70	-0.85	212
0.58	21.50	0.40	102.6	-0.90	210
0.60	22.40	0.38	108.0	-0.95	207

Table (5.10)

QUASI-STATIC AXISYMMETRIC COMPRESSION TEST
SPECIMEN: Cu

Height = 1.0 mm, Thickness: 0.935 mm, Diameter: 14.80 mm, Re: 0.075

ΔH (mm)	F_C (kN)	H (mm)	A (mm^2)	ϵ	σ_C (MPa)
0.02	0.60	0.96	42.74	-0.02	14
0.04	1.80	0.94	43.65	-0.04	41
0.06	4.40	0.92	44.60	-0.06	99
0.08	6.80	0.90	45.60	-0.09	149
0.10	8.20	0.88	46.63	-0.11	176
0.12	8.80	0.86	47.71	-0.13	185
0.14	9.20	0.84	48.85	-0.15	188
0.16	9.70	0.82	50.04	-0.18	194
0.18	10.70	0.80	51.29	-0.20	209
0.20	11.10	0.78	52.61	-0.23	211
0.22	11.50	0.76	53.99	-0.25	213
0.24	11.90	0.74	55.45	-0.28	215
0.26	12.30	0.72	56.99	-0.31	216
0.28	12.60	0.70	58.62	-0.34	215
0.30	13.00	0.68	60.34	-0.37	216
0.32	13.40	0.66	62.17	-0.40	216
0.34	13.70	0.64	64.12	-0.43	214
0.36	14.20	0.62	66.18	-0.46	215
0.38	14.40	0.60	68.39	-0.49	211
0.40	15.00	0.58	70.75	-0.53	212
0.42	15.40	0.56	73.28	-0.56	210
0.44	15.90	0.54	75.99	-0.60	209
0.46	16.40	0.52	78.91	-0.63	208
0.48	17.00	0.50	82.07	-0.67	207
0.50	17.60	0.48	85.49	-0.71	206
0.52	18.20	0.46	89.20	-0.76	205
0.54	18.70	0.44	93.26	-0.80	201
0.56	19.40	0.42	97.70	-0.85	199
0.58	20.00	0.40	102.6	-0.90	195
0.60	20.60	0.38	108.0	-0.95	191

Table (5.11)

QUASI-STATIC AXISYMMETRIC COMPRESSION TEST
SPECIMEN: Cu

Height = 1.0 mm, Thickness: 0.92 mm, Diameter: 16.0 mm, Re: 0.00

ΔH (mm)	F_c (kN)	H (mm)	A (mm^2)	ϵ	σ_c (MPa)
0.02	0.50	0.94	47.23	-0.02	11
0.04	0.90	0.92	48.26	-0.04	19
0.06	1.40	0.90	49.33	-0.07	28
0.08	1.90	0.88	50.45	-0.09	38
0.10	2.50	0.86	51.62	-0.11	48
0.12	2.95	0.84	52.85	-0.13	56
0.14	3.70	0.82	54.14	-0.16	68
0.16	4.40	0.80	55.50	-0.18	79
0.18	5.00	0.78	56.92	-0.21	88
0.20	5.50	0.76	58.41	-0.23	94
0.22	6.10	0.74	60.00	-0.26	102
0.24	6.60	0.72	61.66	-0.29	107
0.26	7.10	0.70	63.42	-0.32	112
0.28	7.70	0.68	65.29	-0.35	118
0.30	8.20	0.66	67.26	-0.38	122
0.32	8.90	0.64	69.37	-0.41	128
0.34	9.50	0.62	71.60	-0.44	133
0.36	10.30	0.60	73.99	-0.47	139
0.38	10.90	0.58	76.54	-0.50	142
0.40	11.60	0.56	79.28	-0.54	146
0.42	12.20	0.54	82.21	-0.58	148
0.44	12.70	0.52	85.37	-0.61	149
0.46	13.40	0.50	88.79	-0.65	151
0.48	13.90	0.48	92.49	-0.69	150
0.50	14.60	0.46	96.51	-0.74	151
0.52	15.20	0.44	100.9	-0.78	151
0.54	15.5	0.42	105.7	-0.83	147
0.56	15.90	0.40	111.0	-0.88	143
0.58	16.70	0.38	116.8	-0.93	143
0.60	17.5	0.36	123.3	-0.98	142

Table (5.12)

QUASI-STATIC AXISYMMETRIC COMPRESSION TEST
SPECIMEN: STAINLESS STEEL

Height = 1.0 mm, Thickness: 0.98 mm, Diameter: 10.0 mm, Re: 0.375

ΔH (mm)	F_C (kN)	H (mm)	A (mm^2)	ϵ	σ_C (MPa)
0.02	2.50	0.98	32.1	-0.02	78
0.04	5.30	0.96	32.7	-0.04	162
0.06	11.50	0.94	33.4	-0.08	344
0.08	14.50	0.92	34.2	-0.11	424
0.10	18.70	0.90	34.9	-0.13	536
0.12	23.00	0.88	35.7	-0.15	644
0.14	26.50	0.86	36.5	-0.17	726
0.16	29.00	0.84	37.4	-0.20	775
0.18	31.50	0.82	38.3	-0.22	823
0.20	32.50	0.80	39.3	-0.25	827
0.22	33.40	0.78	40.3	-0.27	829
0.24	35.00	0.76	41.3	-0.30	848
0.26	35.60	0.74	42.5	-0.33	838
0.28	36.50	0.72	43.6	-0.36	837
0.30	37.50	0.70	44.9	-0.39	835
0.32	38.50	0.68	46.2	-0.42	833
0.34	39.50	0.66	47.6	-0.45	830
0.36	40.00	0.64	49.1	-0.49	815
0.38	41.50	0.62	50.7	-0.51	819
0.40	42.50	0.60	52.4	-0.55	811
0.42	43.50	0.58	54.2	-0.58	803
0.44	44.60	0.56	56.1	-0.62	795
0.46	45.50	0.54	58.2	-0.65	782
0.48	47.30	0.52	60.4	-0.69	783
0.50	49.00	0.50	62.8	-0.73	780
0.52	50.50	0.48	65.5	-0.78	771
0.54	52.00	0.46	68.3	-0.82	761
0.56	54.00	0.44	71.4	-0.87	756
0.58	55.00	0.42	74.8	-0.92	735
0.60	57.00	0.40	78.5	-0.97	726

Table (5.13)

QUASI-STATIC AXISYMMETRIC COMPRESSION TEST
SPECIMEN: STAINLESS STEEL

Height = 1.0 mm, Thickness: 0.96 mm, Diameter: 11.20 mm, Re: 0.300

ΔH (mm)	F_c (kN)	H (mm)	A (mm^2)	ϵ	σ_c (MPa)
0.02	0.57	0.98	32.1	-0.02	18
0.04	3.00	0.96	32.7	-0.04	92
0.06	5.70	0.94	33.4	-0.06	171
0.08	8.50	0.92	34.2	-0.08	249
0.10	11.50	0.90	34.9	-0.11	330
0.12	14.70	0.88	35.7	-0.13	412
0.14	17.80	0.86	36.5	-0.15	488
0.16	21.50	0.84	37.4	-0.17	575
0.18	24.50	0.82	38.3	-0.20	640
0.20	27.50	0.80	39.3	-0.22	700
0.22	30.40	0.78	40.3	-0.25	754
0.24	32.50	0.76	41.3	-0.27	787
0.26	33.00	0.74	42.5	-0.30	777
0.28	34.00	0.72	43.6	-0.33	780
0.30	36.40	0.70	44.9	-0.36	811
0.32	37.50	0.68	46.2	-0.39	812
0.34	38.70	0.66	47.6	-0.42	813
0.36	39.50	0.64	49.1	-0.45	805
0.38	40.70	0.62	50.8	-0.49	801
0.40	41.70	0.60	52.4	-0.51	796
0.42	43.00	0.58	54.2	-0.55	793
0.44	44.00	0.56	56.1	-0.58	784
0.46	45.00	0.54	58.2	-0.62	773
0.48	46.00	0.52	60.4	-0.65	762
0.50	47.40	0.50	62.8	-0.69	755
0.52	48.40	0.48	65.5	-0.73	739
0.54	50.00	0.46	68.3	-0.78	732
0.56	51.50	0.44	71.4	-0.82	721
0.58	53.20	0.42	74.8	-0.87	711
0.60	54.70	0.40	78.5	-0.92	697

Table (5.14)

QUASI-STATIC AXISYMMETRIC COMPRESSION TEST
SPECIMEN: STAINLESS STEEL

Height = 1.0 mm, Thickness: 0.945 mm, Diameter: 12.40 mm, Re: 0.225

ΔH (mm)	F_C (kN)	H (mm)	A (mm^2)	ϵ	σ_C (MPa)
0.02	3.50	0.98	32.1	-0.02	109
0.04	6.70	0.96	32.7	-0.04	205
0.06	11.40	0.94	33.4	-0.08	341
0.08	15.70	0.92	34.2	-0.11	459
0.10	20.20	0.90	34.9	-0.13	579
0.12	23.30	0.88	35.7	-0.15	653
0.14	25.50	0.86	36.5	-0.17	699
0.16	28.00	0.84	37.4	-0.20	749
0.18	29.70	0.82	38.3	-0.22	776
0.20	31.20	0.80	39.3	-0.25	794
0.22	32.50	0.78	40.3	-0.30	807
0.24	33.80	0.76	41.3	-0.33	818
0.26	35.00	0.74	42.5	-0.36	824
0.28	36.40	0.72	43.6	-0.39	835
0.30	38.00	0.70	44.9	-0.42	846
0.32	38.50	0.68	46.2	-0.45	833
0.34	39.50	0.66	47.6	-0.49	830
0.36	40.40	0.64	49.1	-0.51	823
0.38	41.50	0.62	50.7	-0.55	819
0.40	43.00	0.60	52.4	-0.58	821
0.42	44.40	0.58	54.2	-0.62	819
0.44	46.20	0.56	56.1	-0.65	824
0.46	47.90	0.54	58.2	-0.69	823
0.48	49.70	0.52	60.4	-0.73	823
0.50	52.00	0.50	62.8	-0.78	828
0.52	55.8	0.48	65.5	-0.82	852
0.54	58.00	0.46	68.3	-0.87	849
0.56	60.30	0.44	71.4	-0.92	845
0.58	62.5	0.42	74.8	-0.97	836
0.60	66.0	0.40	78.5	-1.02	846

Table (5.15)

QUASI-STATIC AXISYMMETRIC COMPRESSION TEST
SPECIMEN: STAINLESS STEEL

Height = 1.0 mm, Thickness: 0.94 mm, Diameter: 13.60 mm, Re: 0.150

ΔH (mm)	F_C (kN)	H (mm)	A (mm^2)	ϵ	σ_C (MPa)
0.02	0.50	0.96	42.7	-0.02	12
0.04	1.00	0.94	43.7	-0.04	23
0.06	3.60	0.92	44.6	-0.06	81
0.08	7.00	0.90	45.6	-0.09	154
0.10	11.50	0.88	46.6	-0.11	247
0.12	15.60	0.86	47.7	-0.13	327
0.14	19.30	0.84	48.9	-0.15	395
0.16	22.50	0.82	50.0	-0.18	450
0.18	24.50	0.80	51.3	-0.20	478
0.20	26.50	0.78	52.6	-0.23	504
0.22	28.40	0.76	54.0	-0.25	526
0.24	30.00	0.74	55.5	-0.28	541
0.26	31.50	0.72	57.0	-0.31	553
0.28	32.50	0.70	58.6	-0.34	555
0.30	34.50	0.68	60.3	-0.37	572
0.32	35.50	0.66	62.2	-0.40	571
0.34	36.50	0.64	64.1	-0.43	569
0.36	37.50	0.62	66.2	-0.46	565
0.38	38.30	0.60	68.4	-0.49	560
0.40	40.00	0.58	70.8	-0.53	565
0.42	41.00	0.56	73.3	-0.56	559
0.44	41.50	0.54	76.0	-0.60	546
0.46	42.50	0.52	78.9	-0.63	539
0.48	43.50	0.50	82.1	-0.67	530
0.50	45.5	0.48	85.5	-0.71	532
0.52	46.50	0.46	89.2	-0.76	521
0.54	48.50	0.44	93.3	-0.80	520
0.56	50.70	0.42	97.7	-0.85	519
0.58	52.50	0.40	103.0	-0.90	510
0.60	54.50	0.38	108.0	-0.95	504

Table (5.16)

QUASI-STATIC AXISYMMETRIC COMPRESSION TEST
SPECIMEN: STAINLESS STEEL

Height = 1.0 mm, Thickness: 0.93 mm, Diameter: 14.0 mm, Re: 0.075

ΔH (mm)	F_c (kN)	H (mm)	A (mm^2)	ϵ	σ_c (MPa)
0.02	0.55	0.96	42.7	-0.02	13
0.04	2.50	0.94	43.7	-0.04	57
0.06	5.00	0.92	44.6	-0.06	112
0.08	8.00	0.90	45.6	-0.09	175
0.10	11.80	0.88	46.6	-0.11	253
0.12	13.50	0.86	47.7	-0.13	283
0.14	16.00	0.84	48.9	-0.15	327
0.16	18.00	0.82	50.0	-0.18	360
0.18	28.8	0.80	51.3	-0.20	406
0.20	23.00	0.78	52.6	-0.23	437
0.22	25.40	0.76	54.0	-0.25	470
0.24	26.50	0.74	55.5	-0.28	478
0.26	27.00	0.72	57.0	-0.31	474
0.28	30.00	0.70	58.6	-0.34	512
0.30	31.30	0.68	60.3	-0.37	519
0.32	33.00	0.66	62.2	-0.40	531
0.34	34.40	0.64	64.1	-0.43	537
0.36	36.50	0.62	66.2	-0.46	551
0.38	37.50	0.60	68.4	-0.49	548
0.40	39.50	0.58	70.8	-0.53	558
0.42	40.50	0.56	73.3	-0.56	553
0.44	41.70	0.54	76.0	-0.60	549
0.46	43.00	0.52	78.9	-0.63	545
0.48	44.50	0.50	82.1	-0.67	542
0.50	46.00	0.48	85.5	-0.71	538
0.52	47.40	0.46	89.2	-0.76	531
0.54	49.00	0.44	93.3	-0.80	525
0.56	51.00	0.42	97.7	-0.85	522
0.58	52.80	0.40	103.0	-0.90	513
0.60	55.33	0.38	108.0	-0.95	512

Table (5.17)

QUASI-STATIC AXISYMMETRIC COMPRESSION TEST
SPECIMEN: STAINLESS STEEL

Height = 1.0 mm, Thickness: 0.92 mm, Diameter: 16.0 mm, Re: 0.00

ΔH (mm)	F_c (kN)	H (mm)	A (mm^2)	ϵ	σ_c (MPa)
0.02	0.40	0.90	47.3	-0.02	9
0.04	0.96	0.88	48.4	-0.05	20
0.06	2.20	0.86	49.5	-0.07	44
0.08	5.20	0.84	50.7	-0.09	103
0.10	8.60	0.82	51.9	-0.12	166
0.12	11.80	0.80	53.2	-0.14	222
0.14	14.80	0.78	54.6	-0.17	271
0.16	18.20	0.76	56.0	-0.19	325
0.18	19.80	0.74	57.5	-0.22	344
0.20	21.8	0.72	59.1	-0.25	369
0.22	24.00	0.70	60.8	-0.27	395
0.24	27.60	0.68	62.0	-0.30	445
0.26	30.00	0.66	64.5	-0.33	465
0.28	31.20	0.64	66.5	-0.36	469
0.30	32.80	0.62	68.6	-0.43	478
0.32	34.40	0.60	70.9	-0.46	485
0.34	36.00	0.58	73.4	-0.50	491
0.36	37.60	0.56	76.0	-0.53	495
0.38	38.45	0.54	78.8	-0.57	488
0.40	40.00	0.52	81.8	-0.61	489
0.42	41.30	0.50	85.1	-0.65	485
0.44	43.00	0.48	88.6	-0.69	485
0.46	44.60	0.46	92.5	-0.74	482
0.48	45.70	0.44	96.7	-0.78	473
0.50	47.70	0.42	101.	-0.83	472
0.52	49.60	0.40	106	-0.88	468
0.54	51.40	0.38	112	-0.94	459
0.56	54.20	0.36	118	-1.00	459
0.58	55.80	0.34	125	-1.06	446
0.60	58.10	0.32	133	-1.12	437

Table (5.18)

QUASI-STATIC AXISYMMETRIC COMPRESSION TEST
SPECIMEN: STAINLESS STEEL DRAWN AT 3 PASSES

Height = 1.0 mm, Thickness: 0.98 mm, Diameter: 10.0 mm, R_T = 0.375, α = 15°

ΔH (mm)	F_C (kN)	H (mm)	A (mm^2)	ϵ ($\ell n[H/H_o]$	σ_C (MPa)
0.02	0.13	0.98	32.1	-0.02	4
0.04	0.48	0.96	32.7	-0.04	15
0.06	0.82	0.94	33.4	-0.06	25
0.08	1.41	0.92	34.2	-0.08	41
0.10	3.13	0.90	34.9	-0.11	90
0.12	5.80	0.88	35.7	-0.13	163
0.14	6.70	0.86	36.5	-0.15	184
0.16	10.00	0.84	37.4	-0.17	267
0.18	14.80	0.82	38.3	-0.20	386
0.20	19.80	0.80	39.3	-0.22	504
0.22	24.60	0.78	40.3	-0.25	610
0.24	29.00	0.76	41.3	-0.27	702
0.26	31.00	0.74	42.5	-0.33	729
0.28	32.60	0.72	43.6	-0.36	748
0.30	33.86	0.70	44.9	-0.39	754
0.32	35.20	0.68	46.2	-0.42	762
0.34	36.20	0.66	47.6	-0.45	760
0.36	37.15	0.64	49.1	-0.49	757
0.38	38.00	0.62	50.7	-0.51	750
0.40	40.45	0.60	52.4	-0.55	740
0.42	41.40	0.58	54.2	-0.58	729
0.44	42.60	0.56	56.1	-0.62	721
0.42	44.00	0.54	58.2	-0.65	711
0.48	42.60	0.52	60.4	-0.69	705
0.50	44.00	0.50	62.8	-0.73	701
0.52	45.60	0.48	65.5	-0.78	696
0.54	47.20	0.46	68.3	-0.82	691
0.56	47.20	0.44	71.4	-0.87	661
0.58	48.70	0.42	74.8	-0.92	651

Table (5.19)

QUASI-STATIC AXISYMMETRIC COMPRESSION TEST
SPECIMEN: STAINLESS STEEL DRAWN AT 2 PASSES

Height = 1.0 mm, Thickness: 0.98 mm, Diameter: 10.0 mm, R_T = 0.375, α = 15°

ΔH (mm)	F_c (kN)	H (mm)	A (mm^2)	ϵ ($\ln[H/H_o]$	σ_c (MPa)
0.02	0.16	0.98	32.1	-0.02	5
0.04	0.50	0.96	32.7	-0.04	15
0.06	0.92	0.94	33.4	-0.06	28
0.08	1.66	0.92	34.2	-0.08	49
0.10	3.40	0.90	34.9	-0.11	97
0.12	5.90	0.88	35.7	-0.13	165
0.14	9.10	0.86	36.5	-0.15	249
0.16	12.70	0.84	37.4	-0.17	340
0.18	16.70	0.82	38.3	-0.20	436
0.20	20.60	0.80	39.3	-0.22	524
0.22	24.90	0.78	40.3	-0.25	618
0.24	28.30	0.76	41.3	-0.27	685
0.26	30.70	0.74	42.5	-0.33	722
0.28	32.60	0.72	43.6	-0.36	748
0.30	34.00	0.70	44.9	-0.39	757
0.32	35.00	0.68	46.2	-0.42	758
0.34	35.90	0.66	47.6	-0.45	754
0.36	36.90	0.64	49.1	-0.49	752
0.38	37.80	0.62	50.7	-0.51	746
0.40	38.40	0.60	52.4	-0.55	733
0.42	39.10	0.58	54.2	-0.58	721
0.44	39.90	0.56	56.1	-0.62	711
0.46	40.70	0.54	58.2	-0.65	699
0.48	41.60	0.52	60.4	-0.69	689
0.50	43.00	0.50	62.8	-0.73	685
0.52	44.35	0.48	65.5	-0.78	677
0.54	45.80	0.46	68.3	-0.82	671
0.56	47.30	0.44	71.4	-0.87	663
0.58	48.90	0.42	74.8	-0.92	654

Table (5.20)

QUASI-STATIC AXISYMMETRIC COMPRESSION TEST
SPECIMEN: STAINLESS STEEL DRAWN AT 5 PASSES

Height = 1.0 mm, Thickness: 0.98 mm, Diameter: 10.0 mm, R_T = 0.375, α = 7°

ΔH (mm)	F_c (kN)	H (mm)	A (mm^2)	ϵ ($\ln[H/H_o]$)	σ_c (MPa)
0.02	1.00	0.98	32.1	-0.02	31
0.04	2.50	0.96	32.7	-0.04	77
0.06	5.20	0.94	33.4	-0.08	156
0.08	8.50	0.92	34.2	-0.11	249
0.10	12.60	0.90	34.9	-0.13	361
0.12	17.65	0.88	35.7	-0.15	494
0.14	22.70	0.86	36.5	-0.17	622
0.16	26.40	0.84	37.4	-0.20	706
0.18	29.10	0.82	38.3	-0.22	760
0.20	30.90	0.80	39.3	-0.25	786
0.22	32.20	0.78	40.3	-0.27	799
0.24	33.50	0.76	41.3	-0.30	811
0.26	34.60	0.74	42.5	-0.33	814
0.28	35.70	0.72	43.6	-0.36	819
0.30	36.60	0.70	44.9	-0.39	815
0.32	37.00	0.68	46.2	-0.42	801
0.34	37.40	0.66	47.6	-0.45	786
0.36	37.80	0.64	49.1	-0.49	770
0.38	38.35	0.62	50.7	-0.51	756
0.40	39.00	0.60	56.1	-0.55	695
0.42	39.80	0.58	58.2	-0.58	684
0.44	40.80	0.56	60.4	-0.62	755
0.46	42.00	0.54	62.8	-0.65	669
0.48	43.3	0.52	65.5	-0.69	661

Table (5.21)

QUASI-STATIC AXISYMMETRIC COMPRESSION TEST
SPECIMEN: STAINLESS STEEL DRAWN AT 5 PASSES

Height = 1.0 mm, Thickness: 0.98 mm, Diameter: 10.0 mm, R_T = 0.375, α = 7°

ΔH (mm)	F_C (kN)	H (mm)	A (mm^2)	ϵ ($\ell n[H/H_o]$	σ_C (MPa)
0.02	1.00	0.98	32.1	-0.02	31
0.04	2.90	0.96	32.7	-0.04	89
0.06	5.80	0.94	33.4	-0.09	174
0.08	9.40	0.92	34.2	-0.11	275
0.10	13.10	0.90	34.9	-0.13	375
0.12	17.50	0.88	35.7	-0.15	490
0.14	21.30	0.86	36.5	-0.17	584
0.16	25.00	0.84	37.4	-0.20	669
0.18	28.30	0.82	38.3	-0.22	739
0.20	30.50	0.80	39.3	-0.25	776
0.22	32.50	0.78	40.3	-0.27	807
0.24	33.80	0.76	41.3	-0.30	818
0.26	34.80	0.74	42.5	-0.33	819
0.28	35.80	0.72	43.6	-0.36	821
0.30	36.80	0.70	44.9	-0.39	820
0.32	37.60	0.68	46.2	-0.42	814
0.34	38.45	0.66	47.6	-0.45	808
0.36	39.20	0.64	49.1	-0.49	798
0.38	39.90	0.62	50.7	-0.51	787
0.40	40.70	0.60	56.1	-0.55	726
0.42	41.50	0.58	58.2	-0.58	713
0.44	42.40	0.56	60.4	-0.62	702
0.42	43.4	0.54	62.8	-0.65	691

Table (5.22)

```
10      REM  EXPERIMENTAL AND THEORETICAL ANALYSIS OF COEFFICIENT
20      REM  OF  FRICTION  WITH  SPECIFIC  APPLICATION  IN  THE  TUBE
30      REM  SINKING  PROCESS
50      PI=3.1416
51      A = .1222
52      M = 1.1
53     INPUT  "TYPE IN THE ELEMENTAL YIED STRESS"; Y
60      REM  M  IS  THE  MODIFYING  TRESCA  FOR  UPPER  BOUND
70      REM  A  "HALF  DIE ANGLE  IN  DEGREE"
80      REM  Y  "THE  YIELD  STRESS  OF  TUBE  MATERIAL"
90      INPUT  "TYPE  IN THE  DRAWING  FORCE"; FD
100     INPUT  "TYPE  IN  THE  WALL  THICKNESS"; T
110     INPUT  "TYPE  IN  THE  EXIT  DIAMETER"; D2
120     INPUT  "TYPE  IN  THE  ENTRY  DIAMETER"; D1
130     X1=PI*D2*T
140     X2=X1/COS(A)
170     R=D2/D1
180     REM  D1 "DIAMETER  OF TUBE  AT  DIE  ENTRY"
190     REM  D2 "DIAMETWR  OF  TUBE  AT  DIE  EXIT"
200     REM  R  "DIAMETER  RATIO"
210     X4=M*Y
220     P=1/TAN(A)
230     X5=X2*X4
240     REM "CALCULATION OF COEFFICIENT OF FRICTION BY NEWTON RAPHSON"
250     REM BY SOLVING F(U)=1/UP-1/UP*R**P-R**P+1-FD/X5=0
260     REM  FIRST ACCEPT  AN  ESTIMATE  OF  THE  ANSWER
270     INPUT "TYPE IN GUESSED COEFFICIENT OF FRICTION";U1
280     REM  U1  THE  FIRST  ESTIMATE OF  COEFFICIENT  OF  FRICTION
290     LET  A1=P*U1
300     LET   A2=R^A1
310     LET  A3=FD/X5
330     LET  A4=LOG(R)
331     LET  A5=1/(P*(U1^2))
332     LET  A6=1/A1
333     LET  X7= A6 - (A6*A2) - A2+1-A3
335     LET  X8= A5-(A5*A2)+(A6*A2*A4)-(A2*A4)
360     REM   X8  DIFFERENTIAL  OF  X7
370     REM   X7  SIMPLIFIED  DRAWING  FORCE  EQUATION
380     REM   NOW  CALCULATE  AN  IMPROVED  ESTIMATE  U2
390     LET  U2=U1-X7/X8
400     PRINT "AT "U1" F(U)  IS "X7" SLOPE "X8" NEW  ESTIMATE" U2
410     REM  USE THE NEW ESTIMATE AS DATA FOR A NEW ITERATION
420     LET  E=(U2-U1)/U1
421     PRINT " ERROR E = (U2-U1)/U1 IS ";E
430     REM  E AN EXPRESSION INVOLVING NORMALISED ABS. VALUE OF CHANGE
440     IF ABS(E) <=.0001  THEN 930
445     U1=U2
450      GOTO 290
930   PRINT  "COEFFICIENT  OF  FRICTION"
940     PRINT  "U2=", U2;"
941     INPUT "DO YOU WISH TO CONTINUE? Y(1)/N(2)";AP
942     IF AP = 1 THEN 90
960     END
```

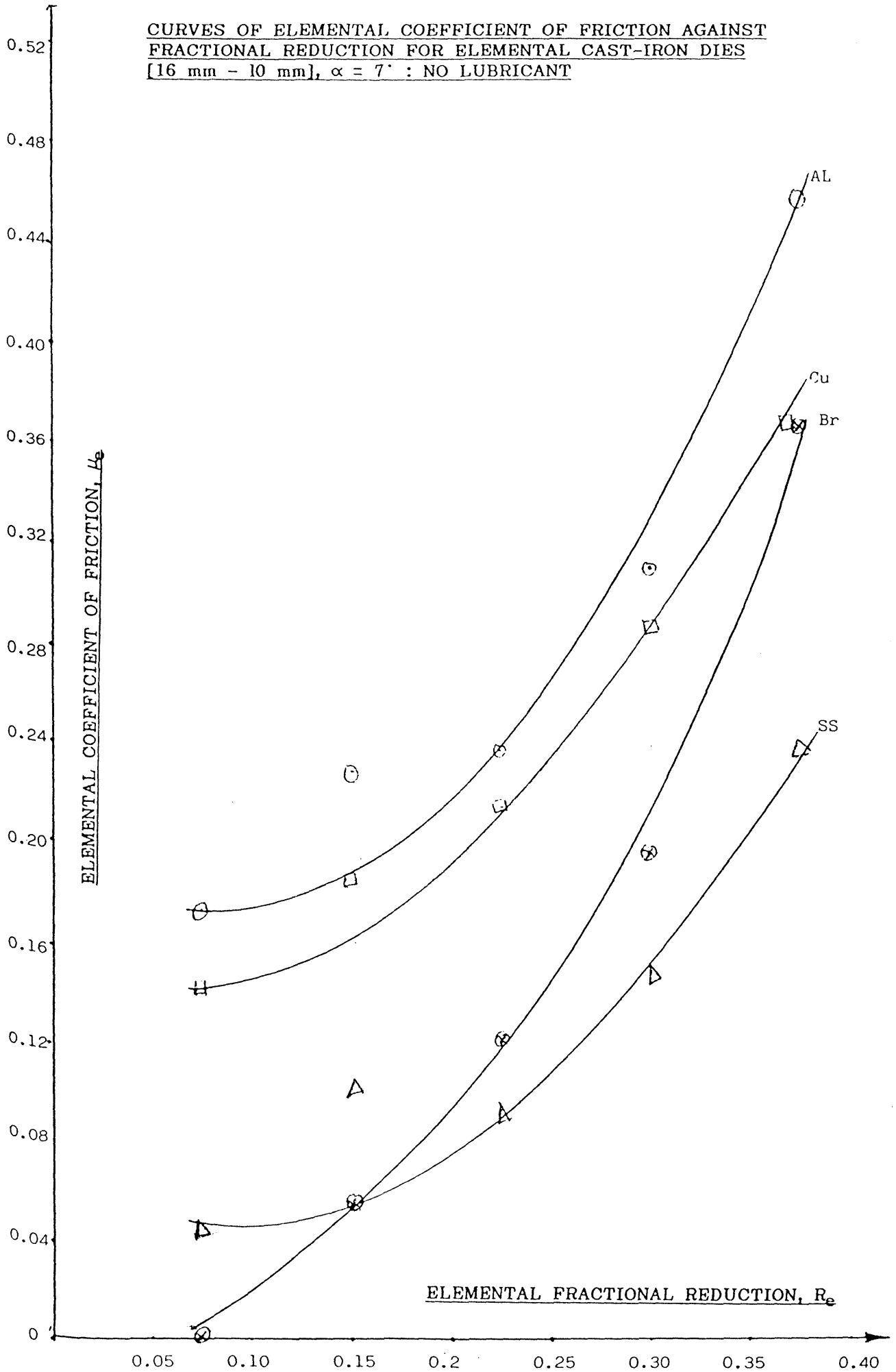
CURVES OF ELEMENTAL COEFFICIENT OF FRICTION AGAINST FRACTIONAL REDUCTION FOR ELEMENTAL CAST-IRON DIES [16 mm - 10 mm], α = 7° : NO LUBRICANT
ELEMENTAL COEFFICIENT OF FRICTION, μe
ELEMENTAL FRACTIONAL REDUCTION, Re
0.52
0.48
0.44
0.40
0.36
0.32
0.28
0.24
0.20
0.16
0.12
0.08
0.04
0
0.05
0.10
0.15
0.2
0.25
0.30
0.35
0.40
AL
Cu
Br
SS

FIGURE (6.01)

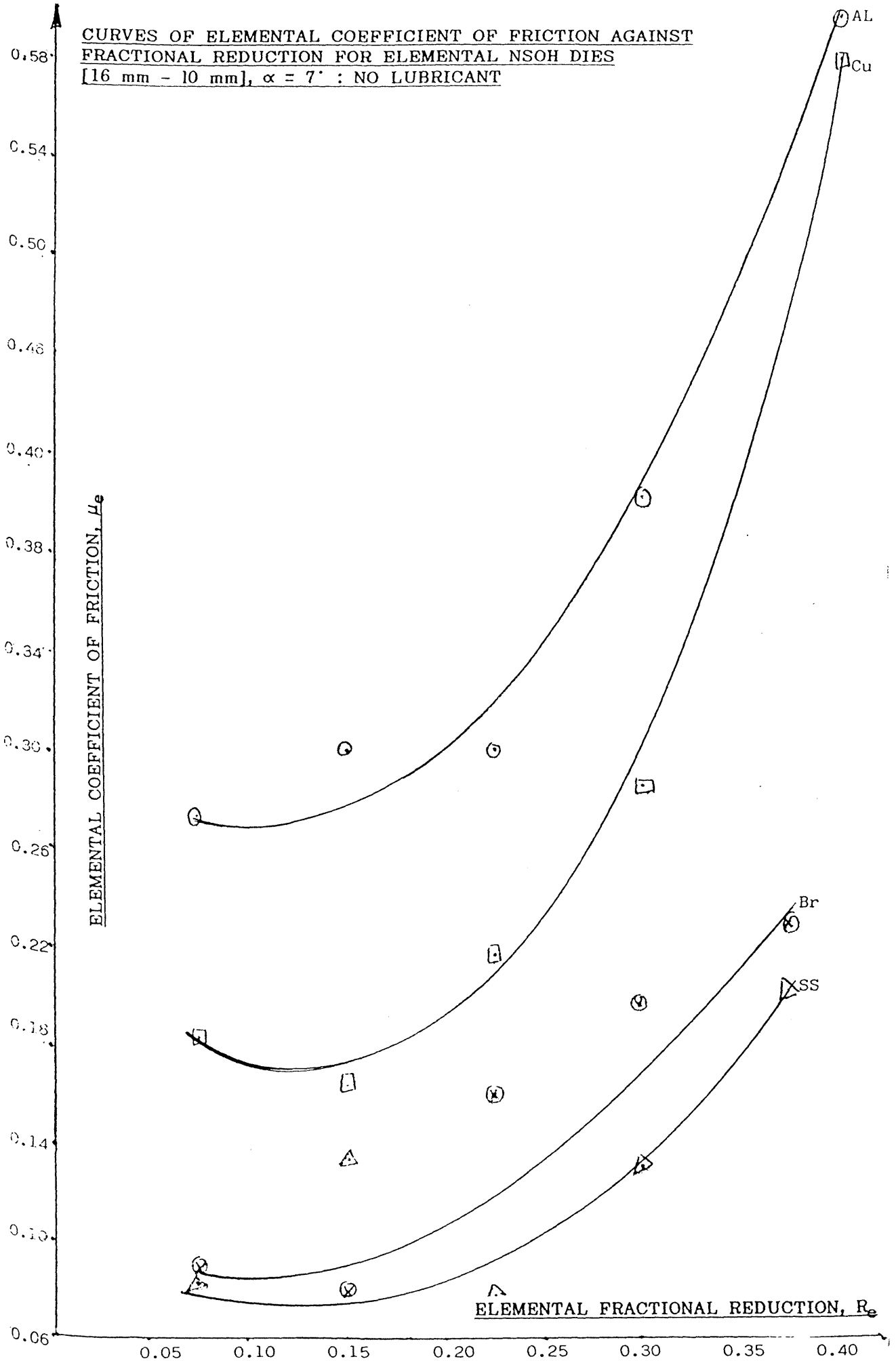
CURVES OF ELEMENTAL COEFFICIENT OF FRICTION AGAINST FRACTIONAL REDUCTION FOR ELEMENTAL NSOH DIES [16 mm - 10 mm], α = 7° : NO LUBRICANT
AL
Cu
Br
SS
ELEMENTAL COEFFICIENT OF FRICTION, μ_e
ELEMENTAL FRACTIONAL REDUCTION, R_e
0.58
0.54
0.50
0.46
0.40
0.38
0.34
0.30
0.26
0.22
0.18
0.14
0.10
0.06
0.05
0.10
0.15
0.20
0.25
0.30
0.35
0.40

FIGURE (6.02)

CURVES OF ELEMENTAL COEFFICIENT OF FRICTION AGAINST FRACTIONAL REDUCTION FOR ELEMENTAL HCHC DIES [16 mm - 10 mm], $\alpha = 7^{\circ}$: NO LUBRICANT

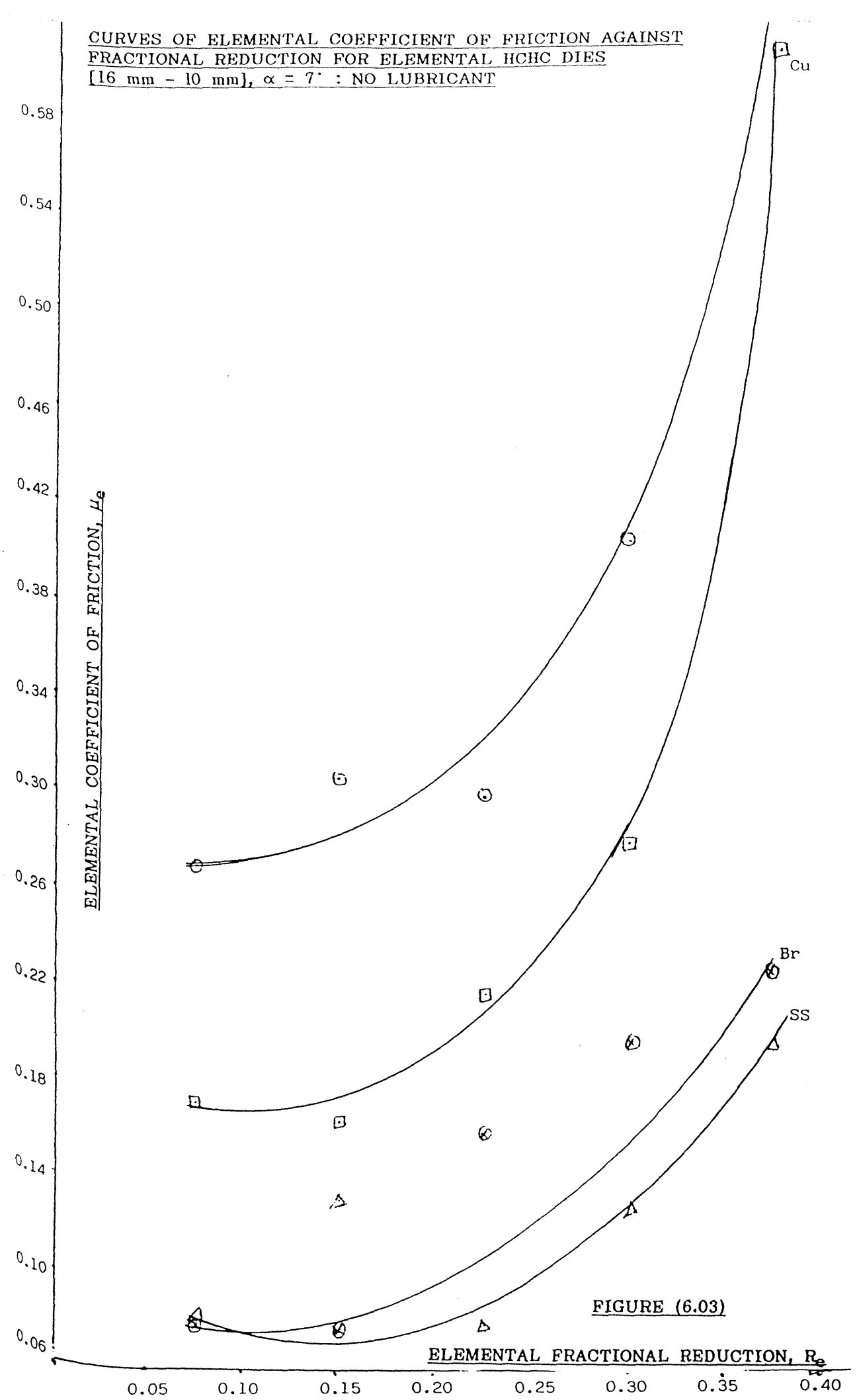

FIGURE (6.03)

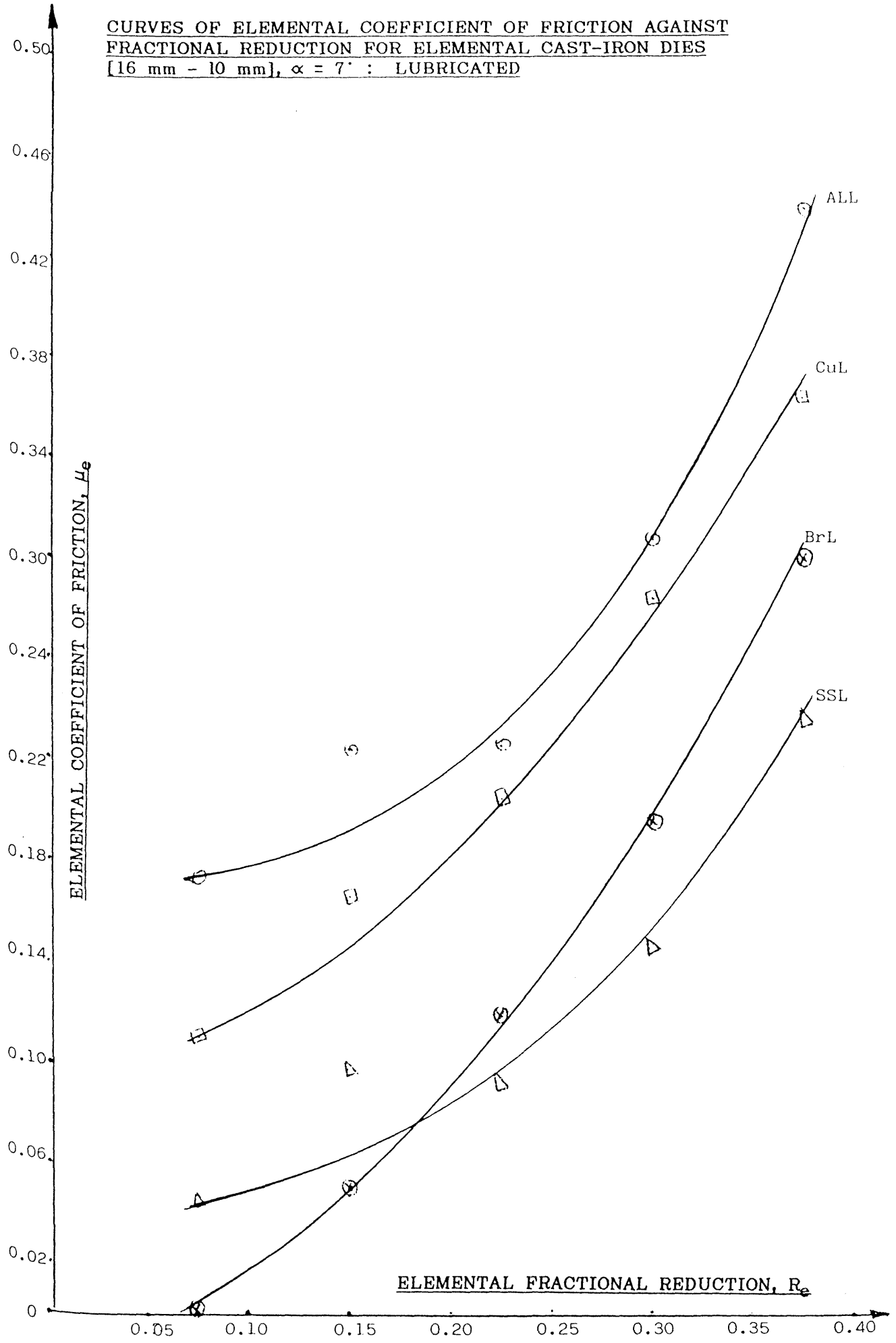
CURVES OF ELEMENTAL COEFFICIENT OF FRICTION AGAINST FRACTIONAL REDUCTION FOR ELEMENTAL CAST-IRON DIES [16 mm - 10 mm], α = 7° : LUBRICATED
ELEMENTAL COEFFICIENT OF FRICTION, μ_e
0.50
0.46
0.42
0.38
0.34
0.30
0.24
0.22
0.18
0.14
0.10
0.06
0.02
0
ALL
CuL
BrL
SSL
ELEMENTAL FRACTIONAL REDUCTION, R_e
0.05
0.10
0.15
0.20
0.25
0.30
0.35
0.40

FIGURE (6.04)

CURVES OF ELEMENTAL COEFFICIENT OF FRICTION AGAINST FRACTIONAL REDUCTION FOR ELEMENTAL NSOH DIES [16 mm - 10 mm], α = 7° : LUBRICATED

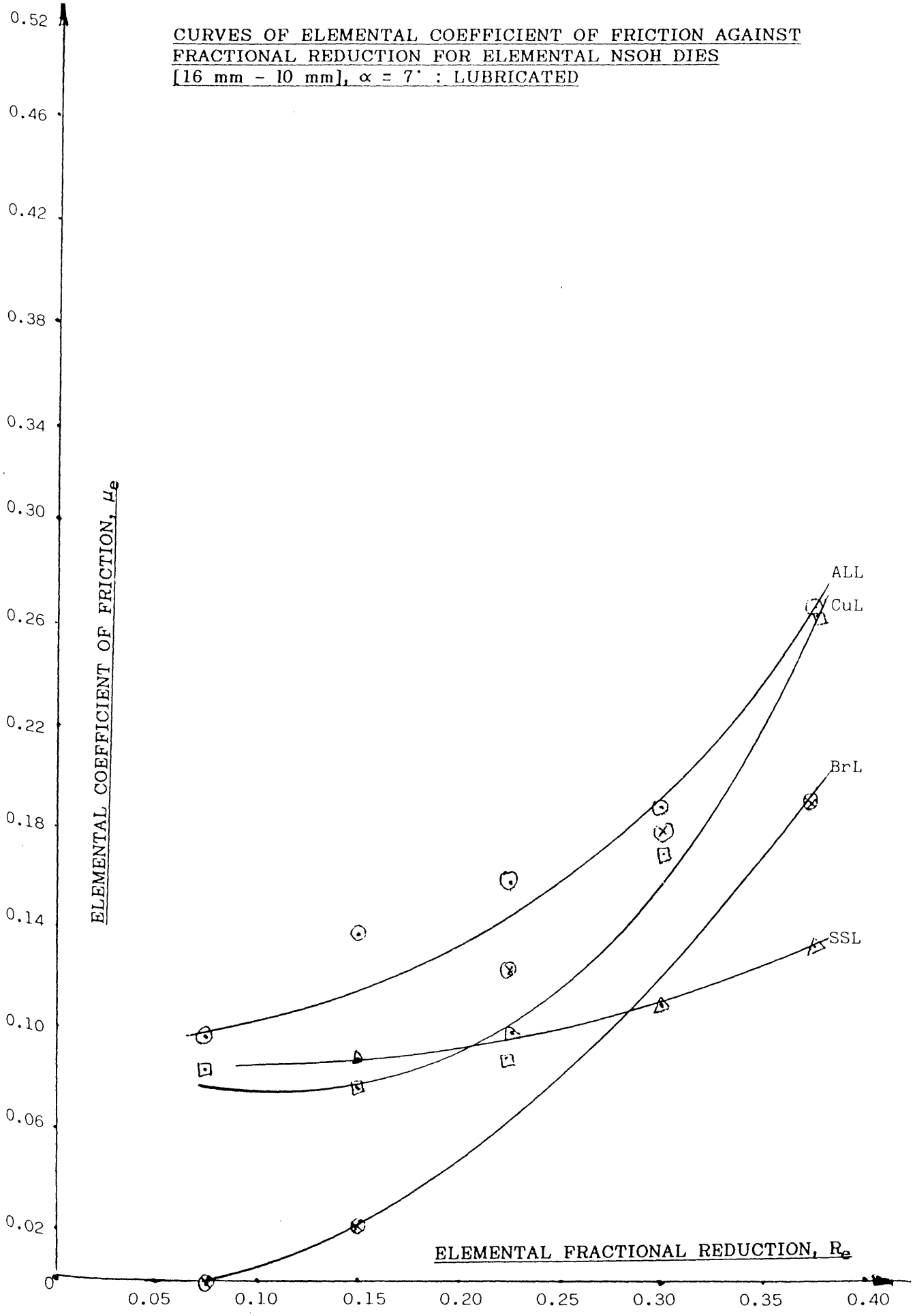

FIGURE (6.05)

CURVES OF ELEMENTAL COEFFICIENT OF FRICTION AGAINST FRACTIONAL REDUCTION FOR ELEMENTAL HCHC DIES [16 mm - 10 mm], $\alpha = 7^{\circ}$: LUBRICATED

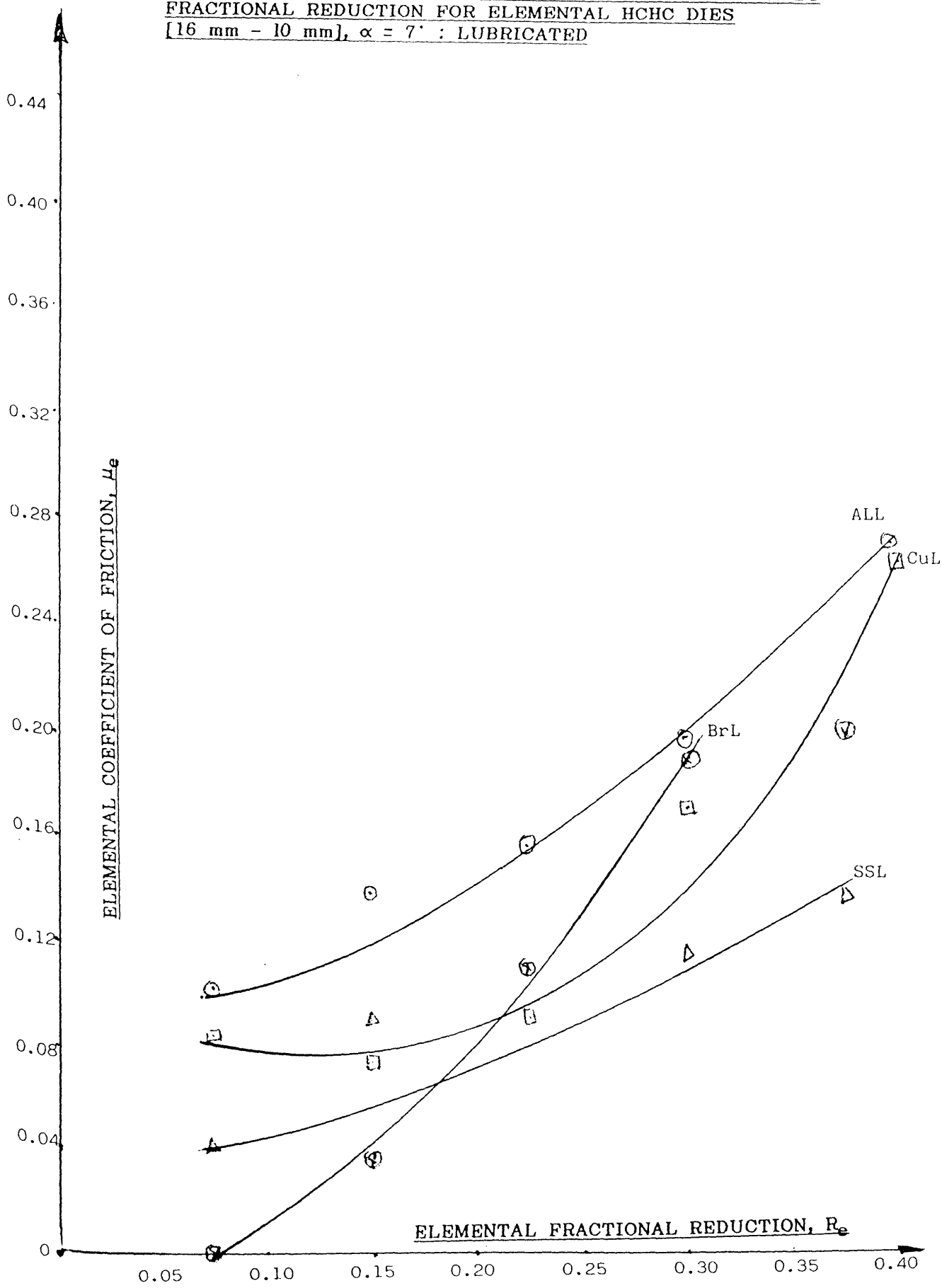

FIGURE (6.06)

CURVES OF ELEMENTAL COEFFICIENT OF FRICTION AGAINST FRACTIONAL REDUCTION FOR ELEMENTAL CAST-IRON DIES [16 mm - 12 mm], $\alpha = 7^{\circ}$: NO LUBRICANT

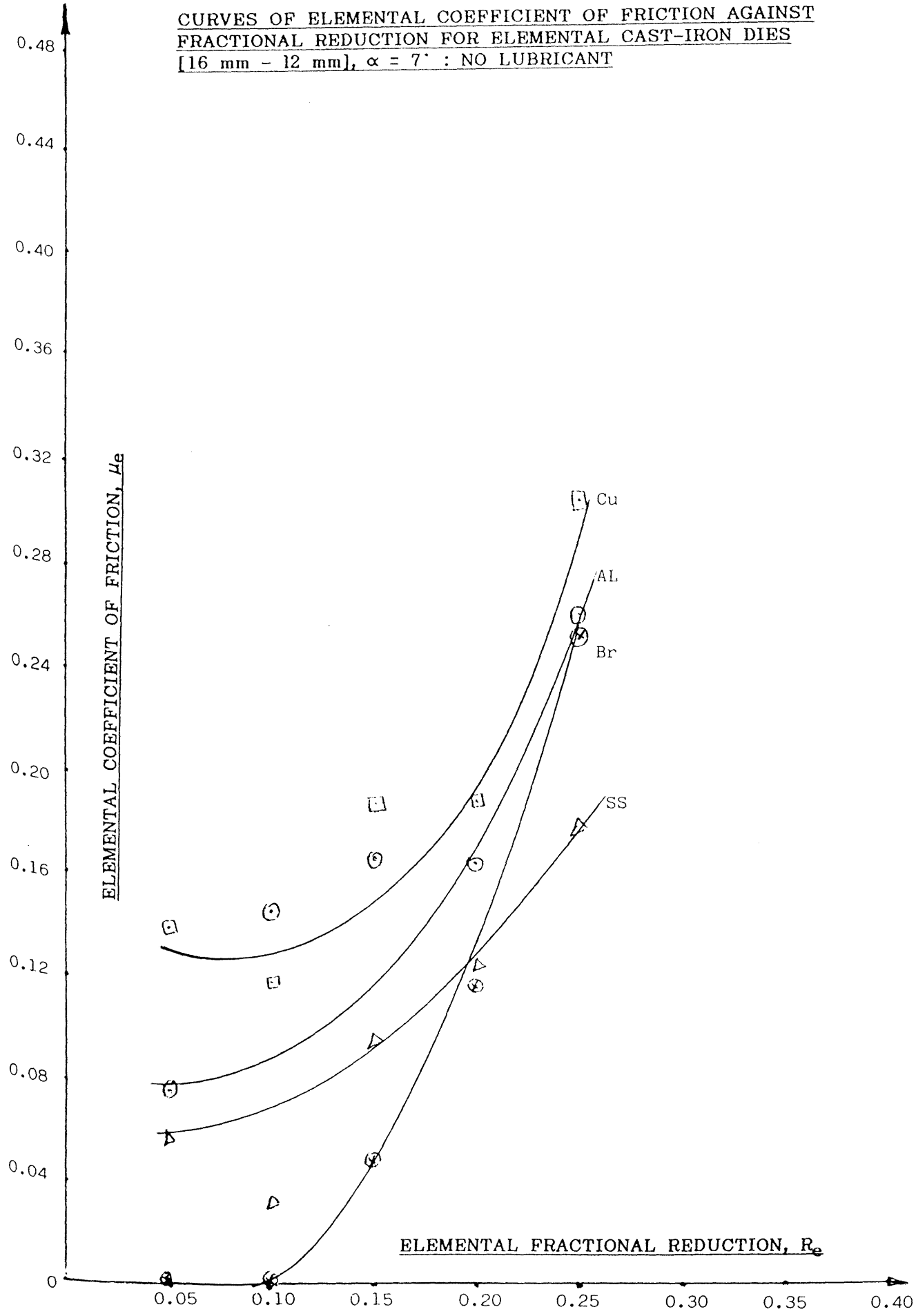

FIGURE (6.07)

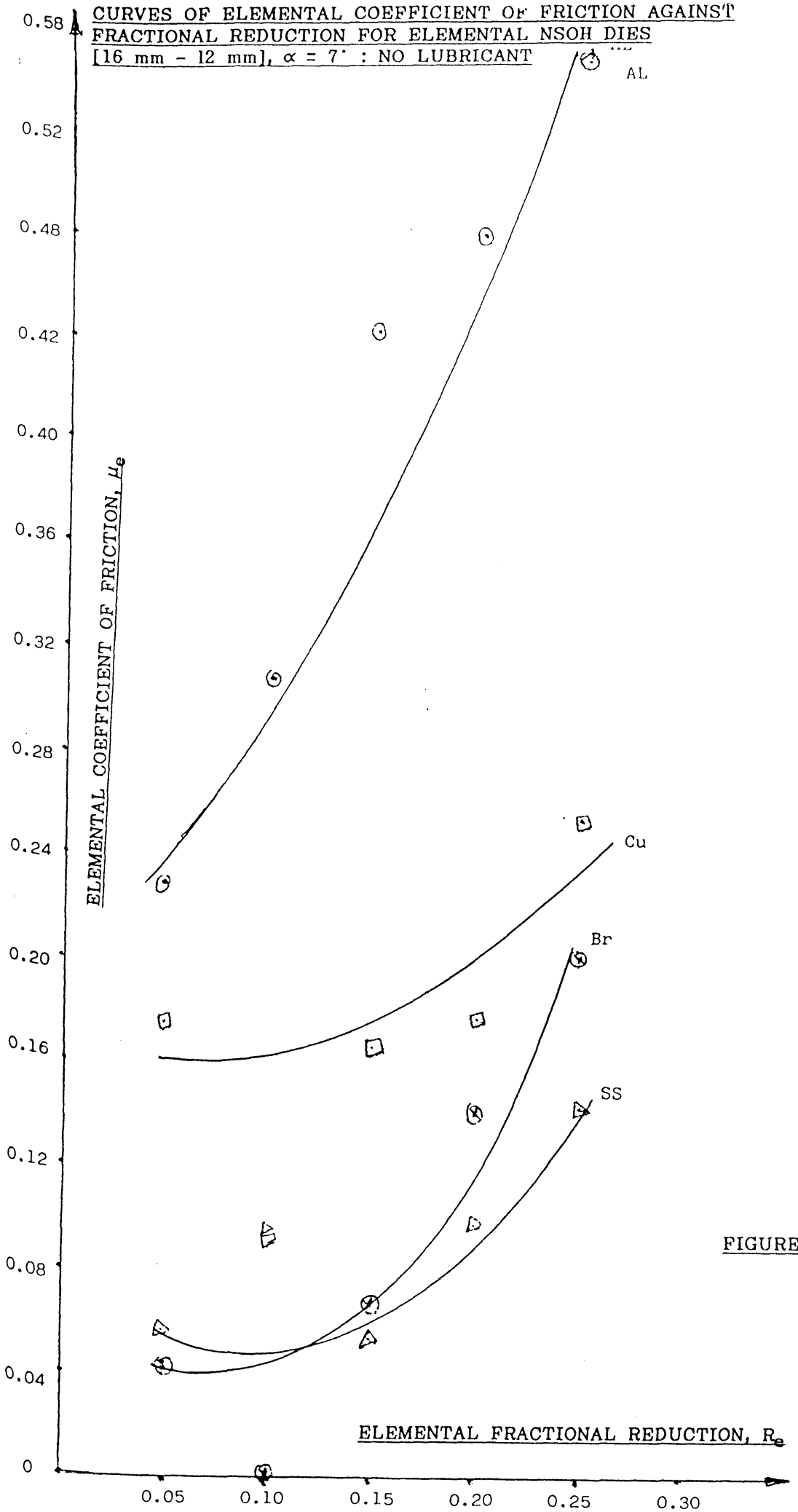
CURVES OF ELEMENTAL COEFFICIENT OF FRICTION AGAINST FRACTIONAL REDUCTION FOR ELEMENTAL NSOH DIES [16 mm - 12 mm], α = 7° : NO LUBRICANT
AL
Cu
Br
SS
ELEMENTAL COEFFICIENT OF FRICTION, μ_e
ELEMENTAL FRACTIONAL REDUCTION, R_e
0.58
0.52
0.48
0.42
0.40
0.36
0.32
0.28
0.24
0.20
0.16
0.12
0.08
0.04
0
0.05
0.10
0.15
0.20
0.25
0.30

FIGURE (6.08)

CURVES OF ELEMENTAL COEFFICIENT OF FRICTION AGAINST FRACTIONAL REDUCTION FOR ELEMENTAL HCHC DIES [16 mm - 12 mm], $\alpha = 7^{\circ}$: NO LUBRICANT

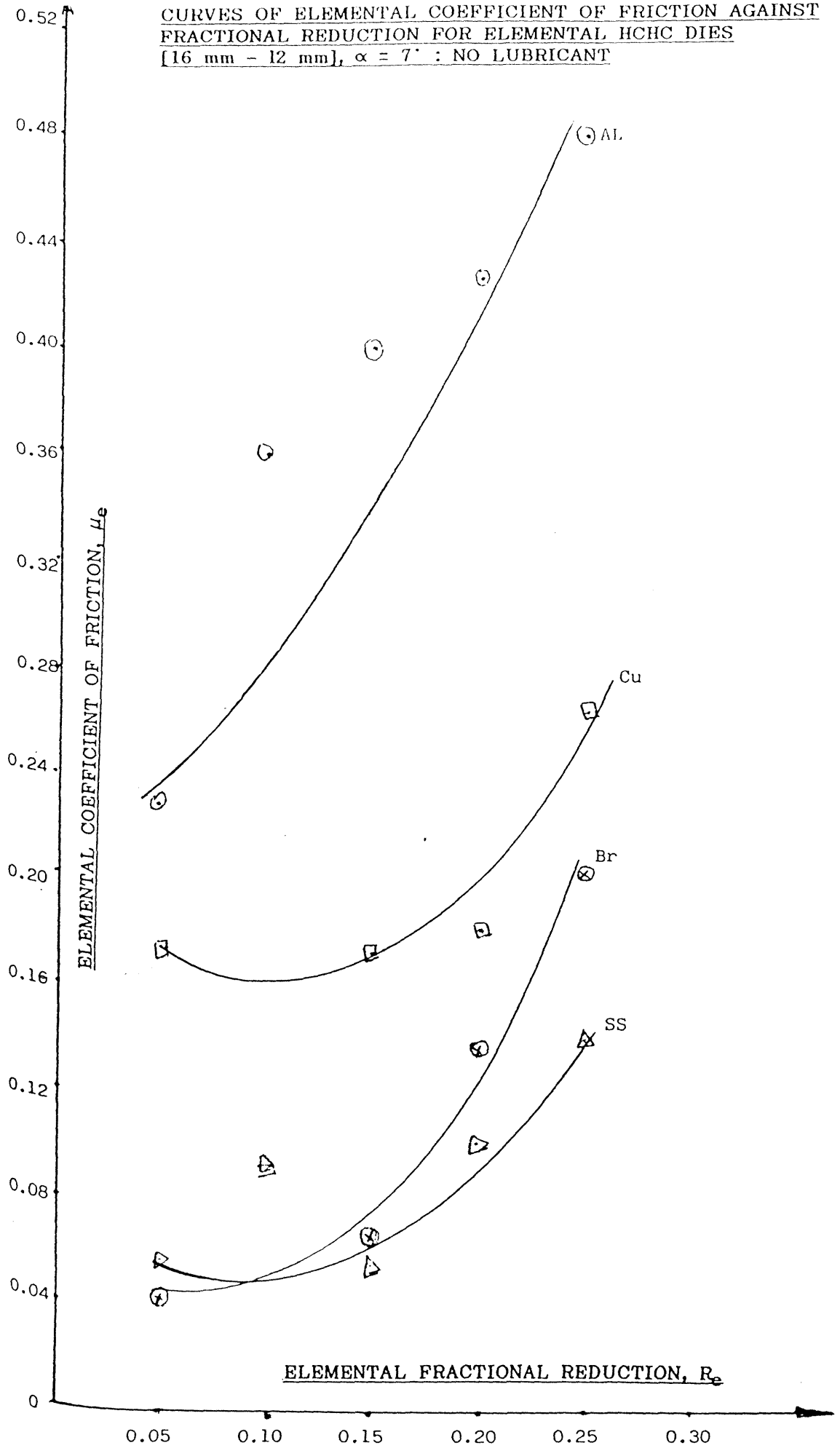

FIGURE (6.09)

CURVES OF ELEMENTAL COEFFICIENT OF FRICTION AGAINST FRACTIONAL REDUCTION FOR ELEMENTAL CAST-IRON DIES [16 mm - 12 mm], $\alpha = 7^{\circ}$: LUBRICATED

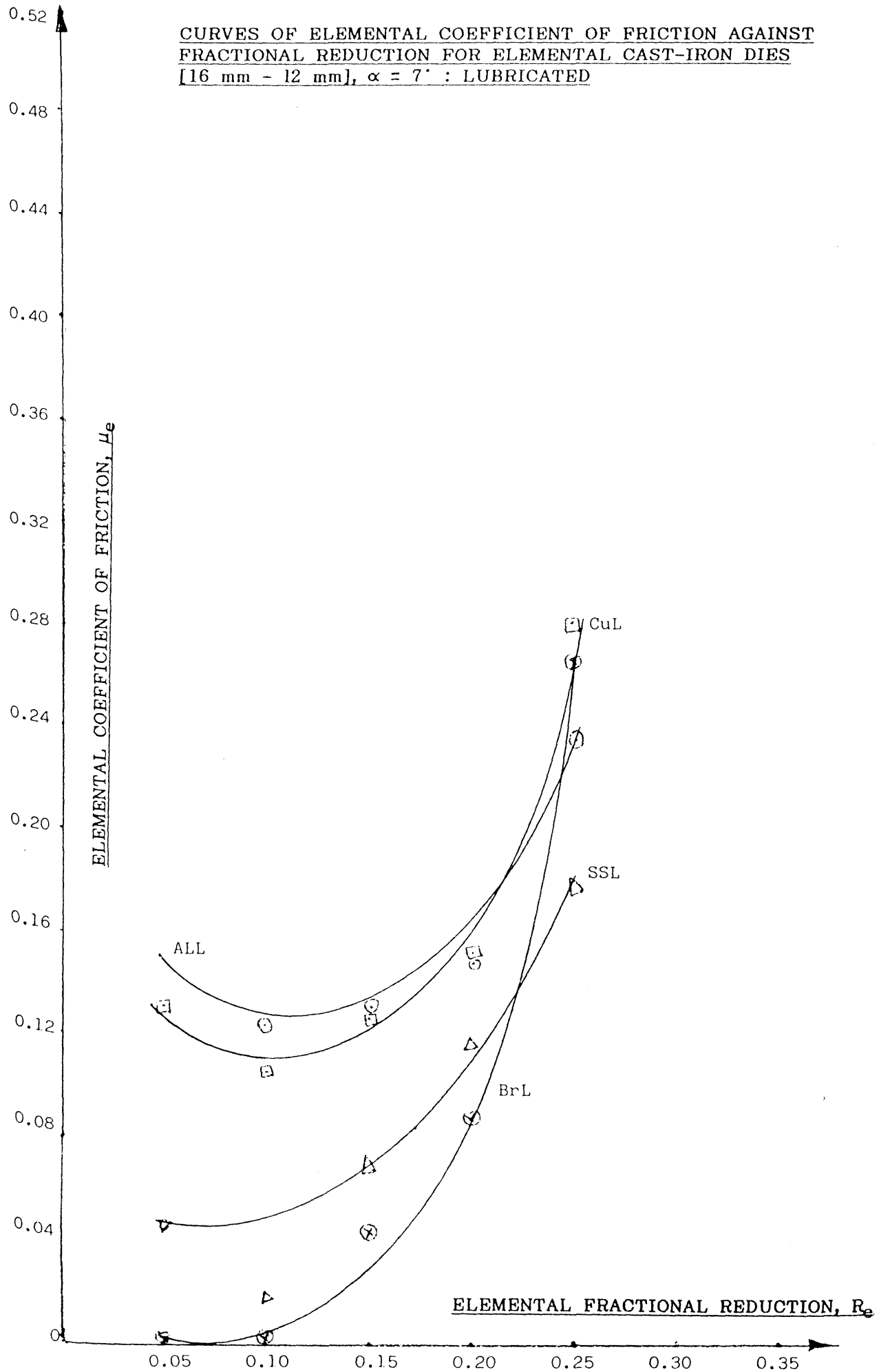

FIGURE (6.10)

CURVES OF ELEMENTAL COEFFICIENT OF FRICTION AGAINST FRACTIONAL REDUCTION FOR ELEMENTAL NSOH DIES [16 mm - 12 mm], $\alpha = 7^{\circ}$: LUBRICATED

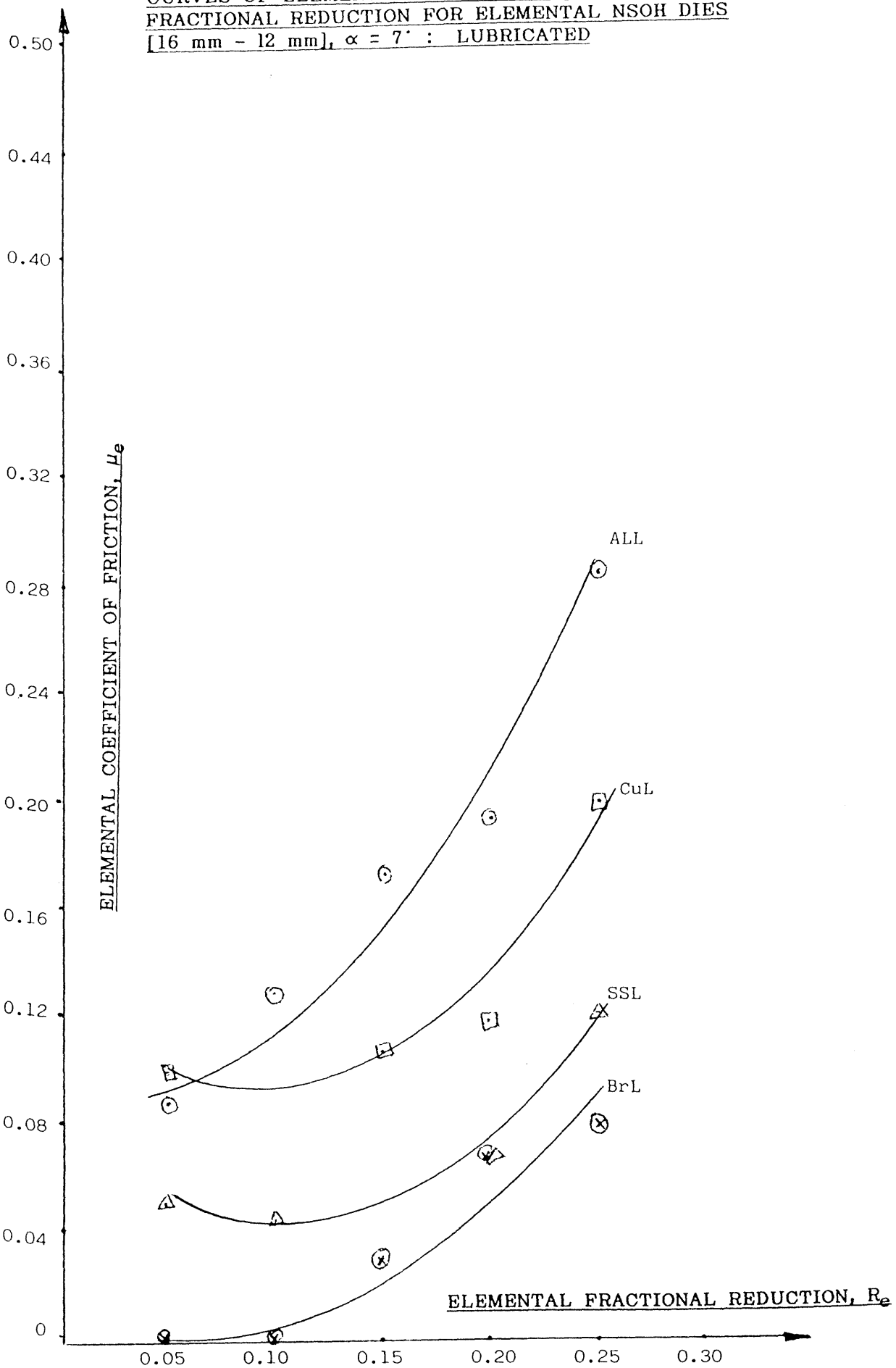

FIGURE (6.12)

CURVES OF ELEMENTAL COEFFICIENT OF FRICTION AGAINST FRACTIONAL REDUCTION FOR ELEMENTAL HCHC DIES [16 mm - 12 mm], $\alpha = 7^{\circ}$: LUBRICATED

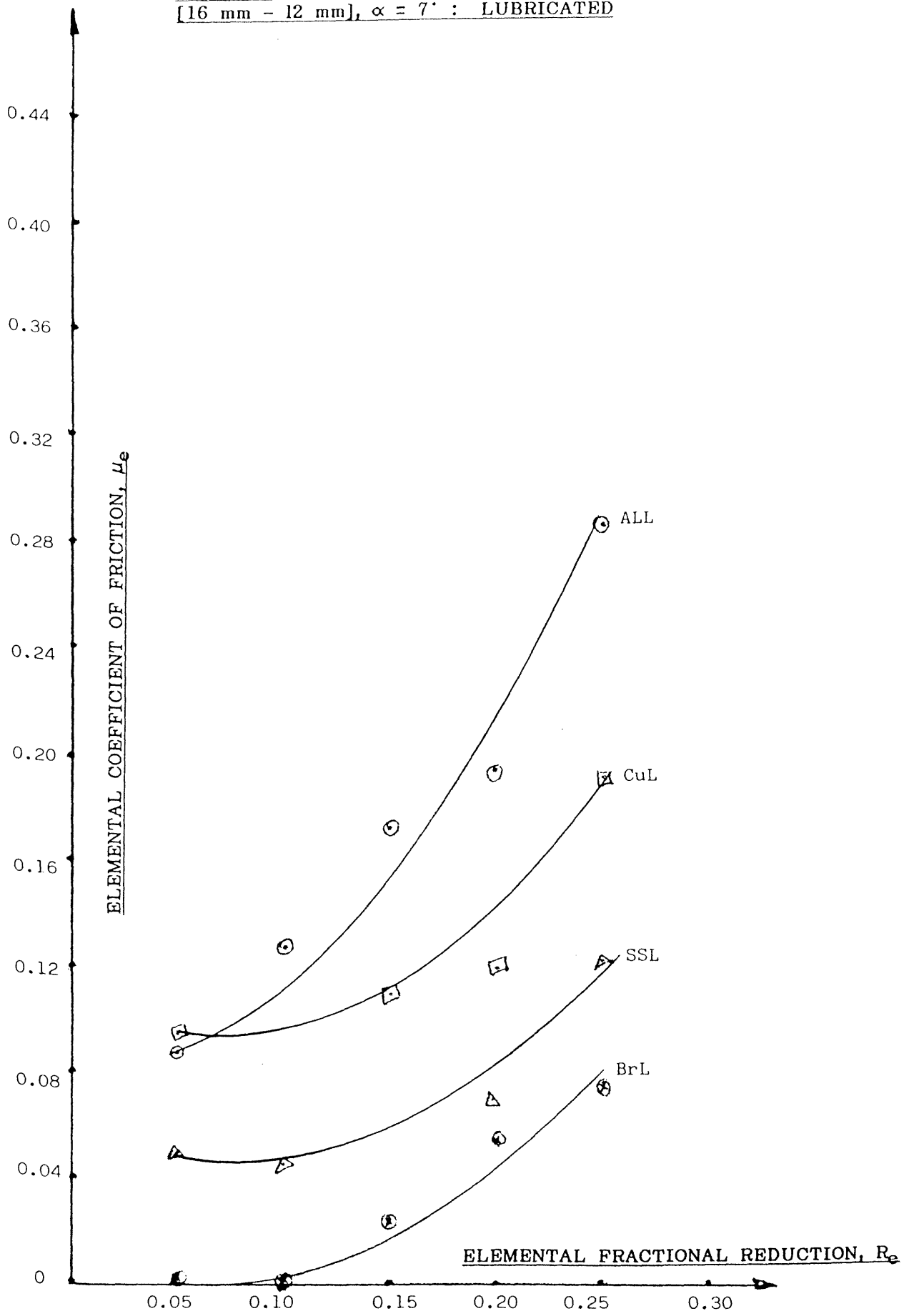

FIGURE (6.13)

CURVES OF ELEMENTAL COEFFICIENT OF FRICTION AGAINST FRACTIONAL REDUCTION FOR ELEMENTAL CAST-IRON DIES [16 mm - 10 mm], α = 15° : NO LUBRICANT

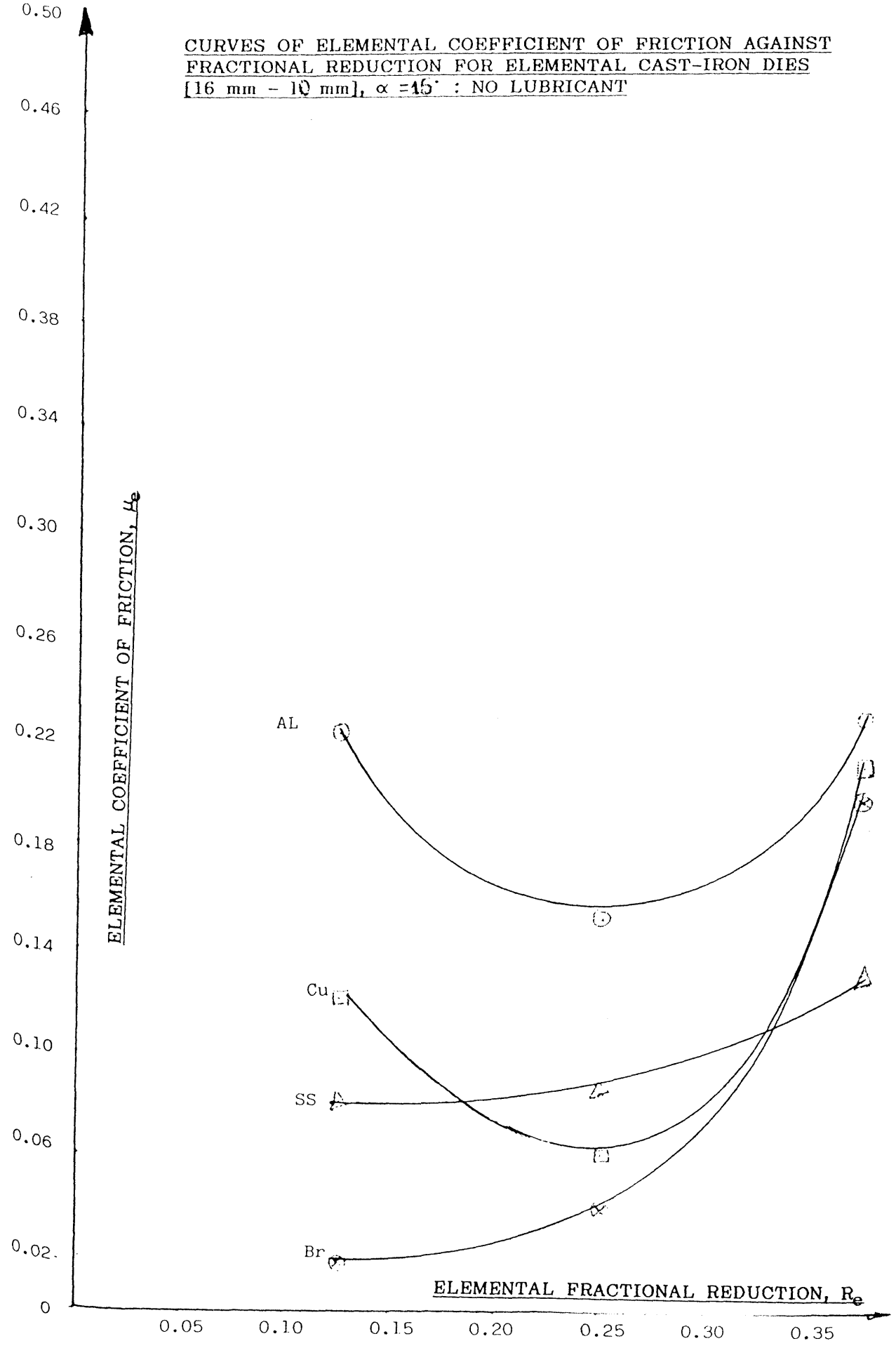

FIGURE (6.14)

CURVES OF ELEMENTAL COEFFICIENT OF FRICTION AGAINST FRACTIONAL REDUCTION FOR ELEMENTAL NSOH DIES [16 mm - 10 mm], α = 15° : NO LUBRICANT

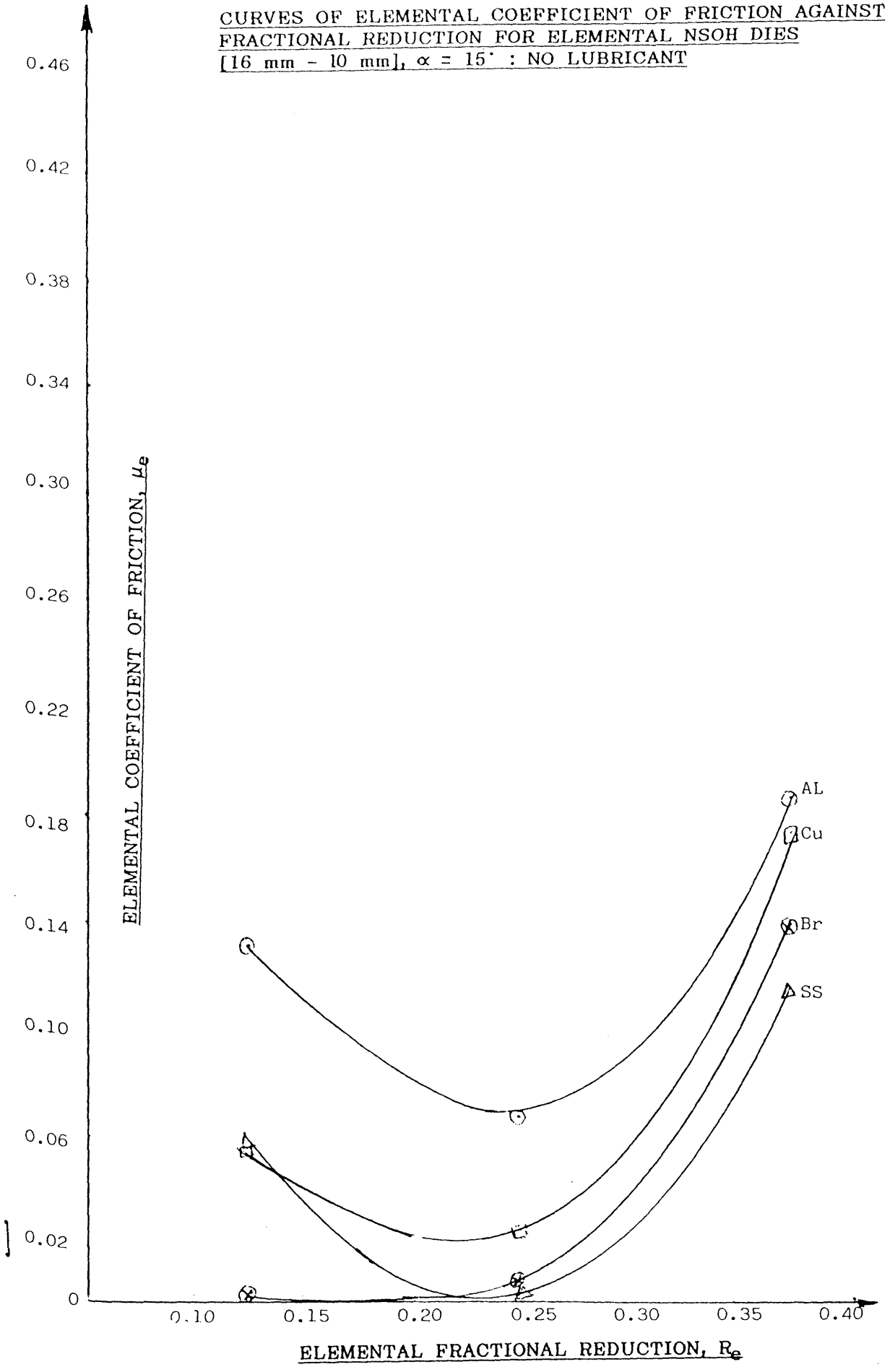

FIGURE (6.15)

CURVES OF ELEMENTAL COEFFICIENT OF FRICTION AGAINST FRACTIONAL REDUCTION FOR ELEMENTAL HCHC DIES [16 mm - 10 mm], $\alpha = 15^{\circ}$: NO LUBRICANT

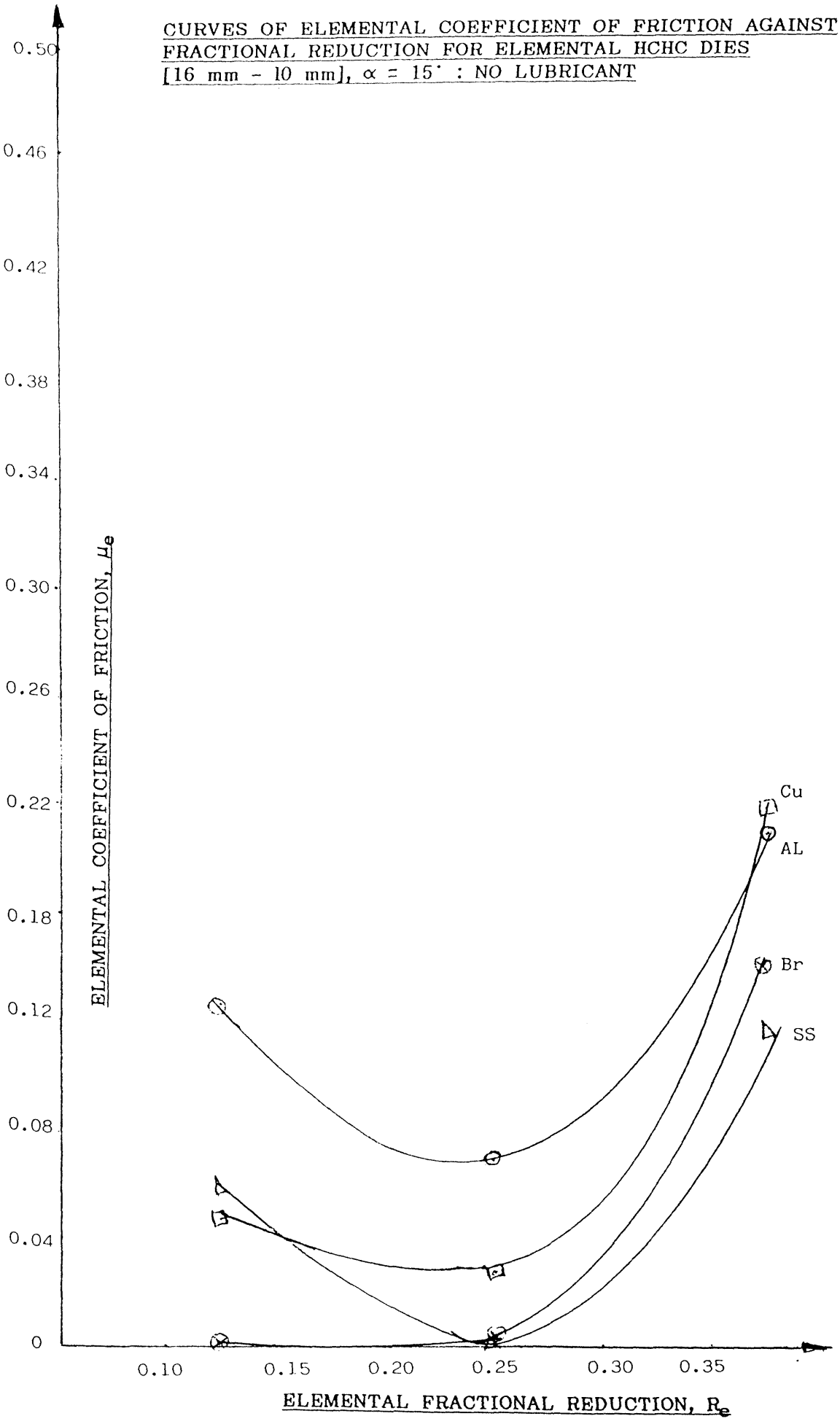

FIGURE (6.16)

CURVES OF ELEMENTAL COEFFICIENT OF FRICTION AGAINST FRACTIONAL REDUCTION FOR ELEMENTAL CAST-IRON DIES [16 mm - 10 mm], α = 15° : LUBRICATED

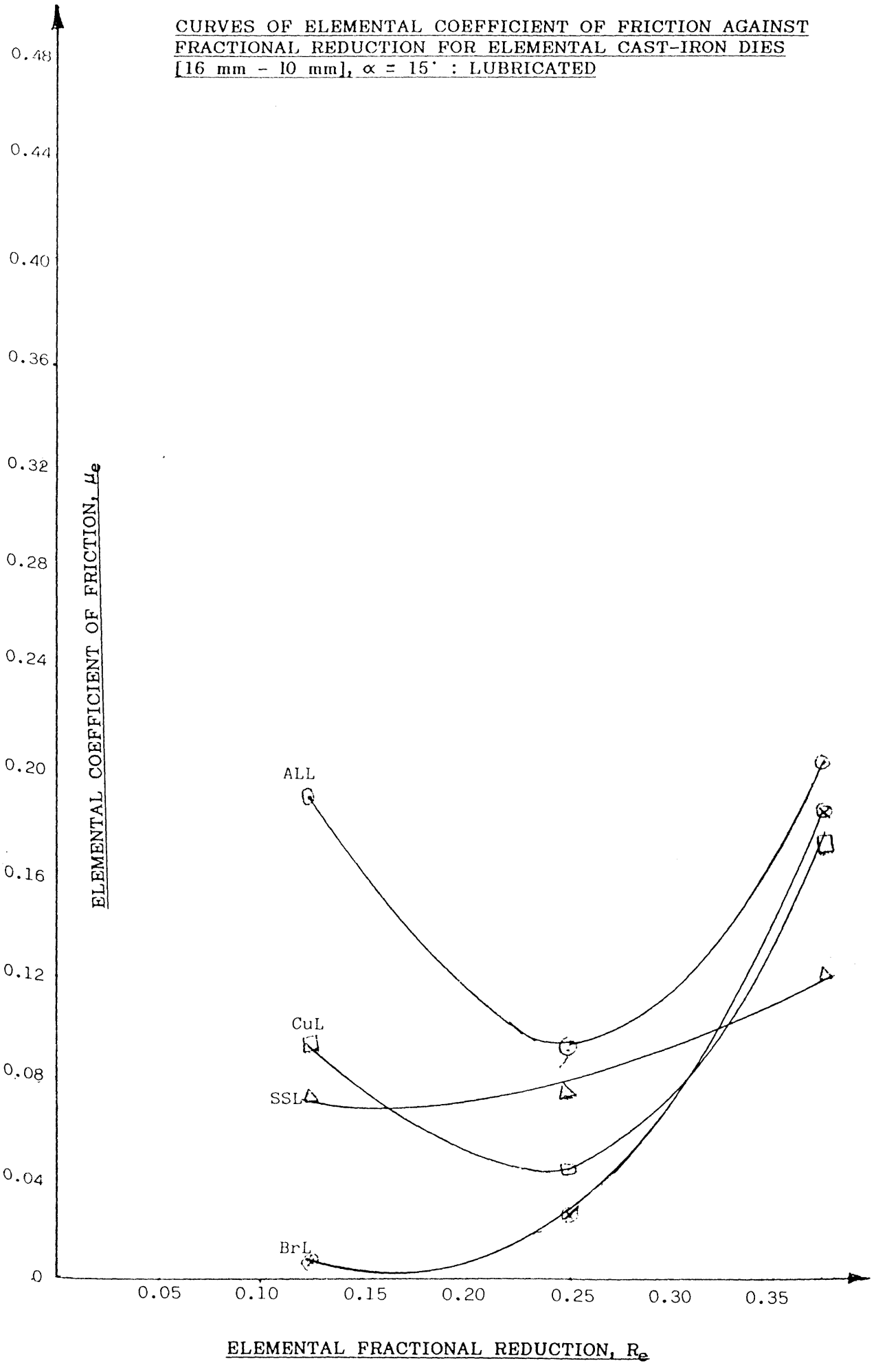

FIGURE 6.16 (b)

CURVES OF ELEMENTAL COEFFICIENT OF FRICTION AGAINST FRACTIONAL REDUCTION FOR ELEMENTAL NSOH DIES [16 mm - 10 mm], α = 15° : LUBRICATED

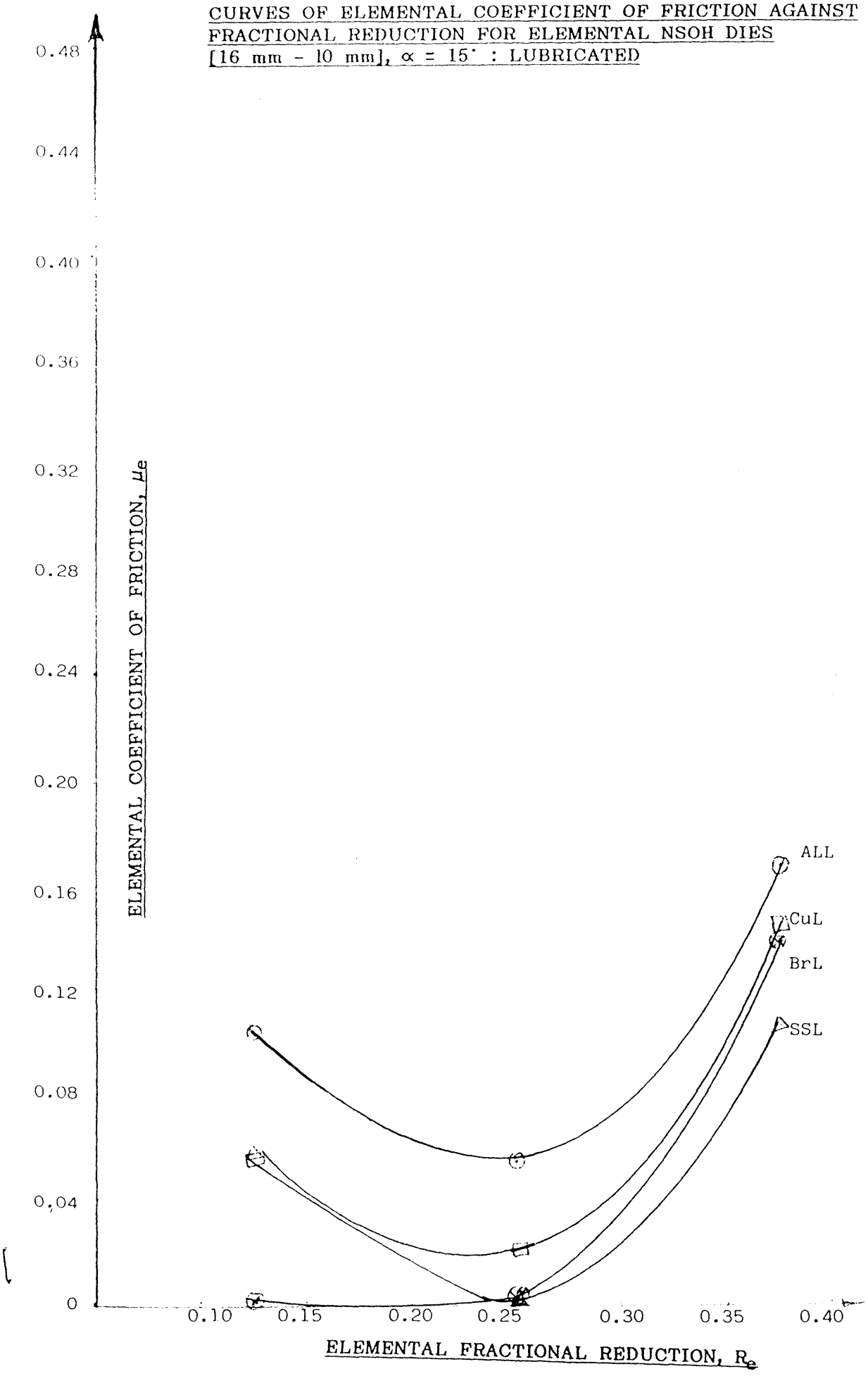

FIGURE (6.17)

CURVES OF ELEMENTAL COEFFICIENT OF FRICTION AGAINST FRACTIONAL REDUCTION FOR ELEMENTAL HCHC DIES [16 mm - 10 mm], $\alpha = 15^{\circ}$: LUBRICATED

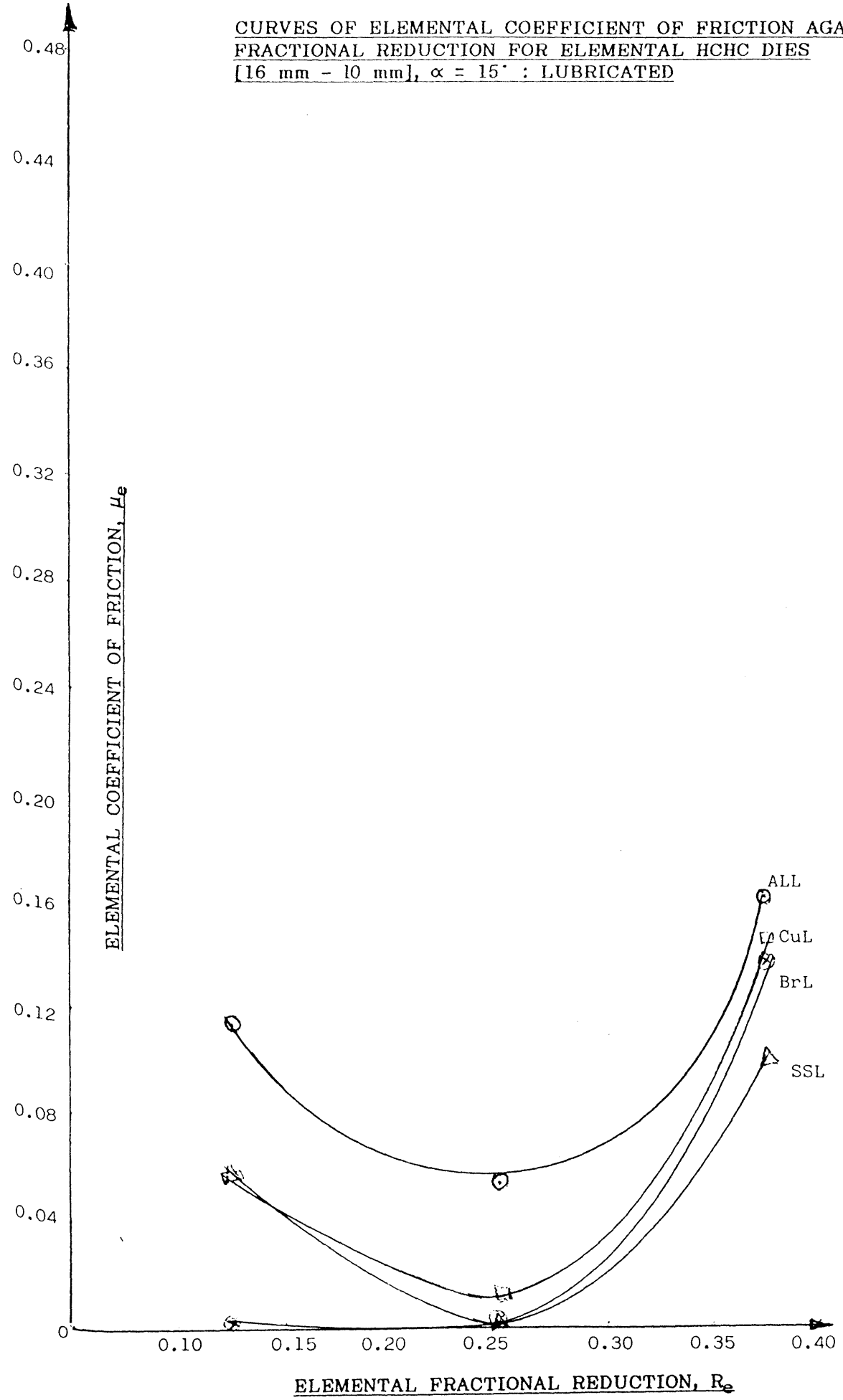

FIGURE (6.18)

CURVES OF ELEMENTAL COEFFICIENT OF FRICTION AGAINST FRACTIONAL REDUCTION FOR ELEMENTAL CAST-IRON DIES [16 mm - 12 mm], α = 15° : NO LUBRICANT

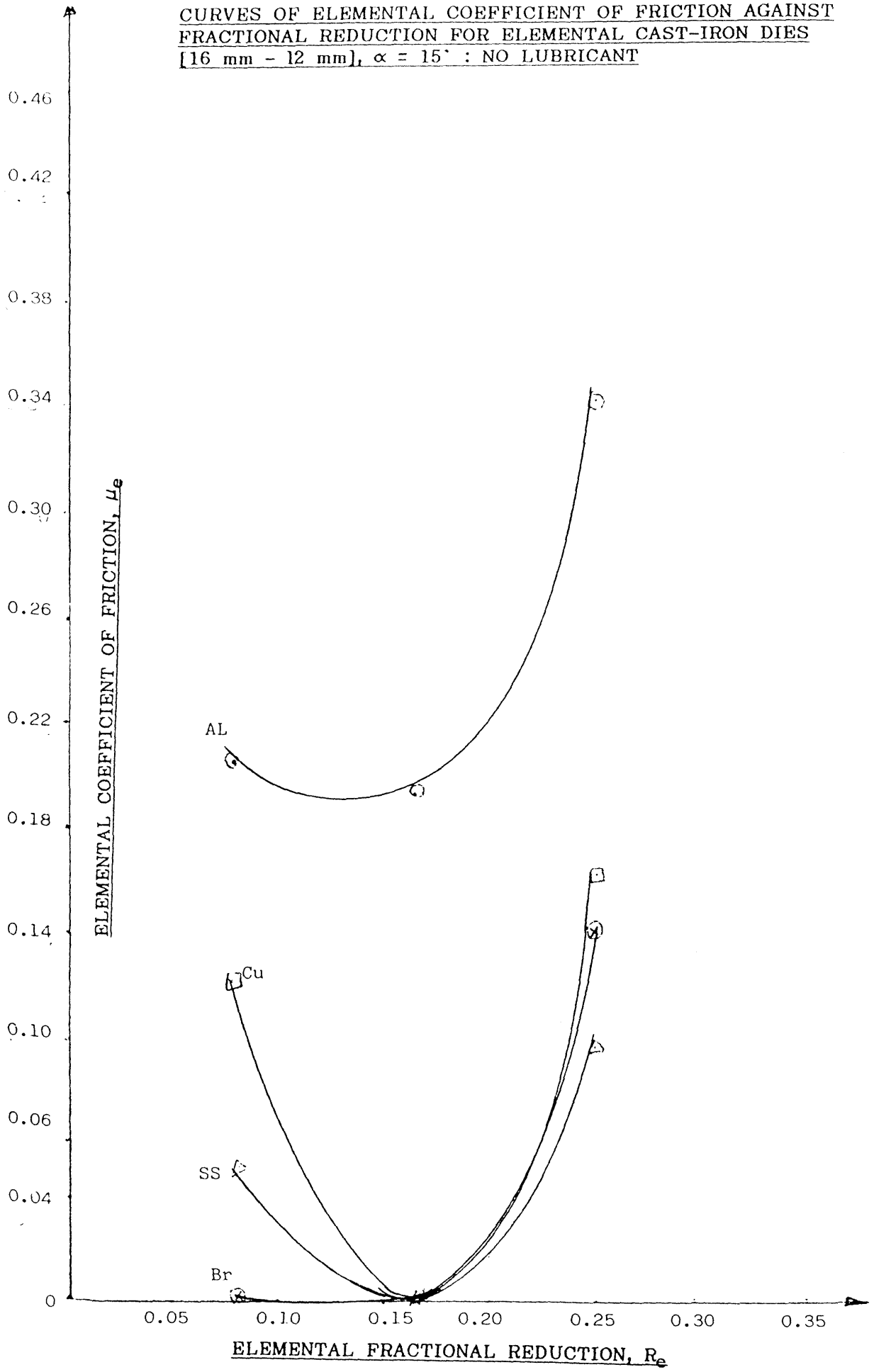

FIGURE (6.19)

CURVES OF ELEMENTAL COEFFICIENT OF FRICTION AGAINST FRACTIONAL REDUCTION FOR ELEMENTAL NSOH DIES [16 mm - 12 mm], α = 15° : NO LUBRICANT

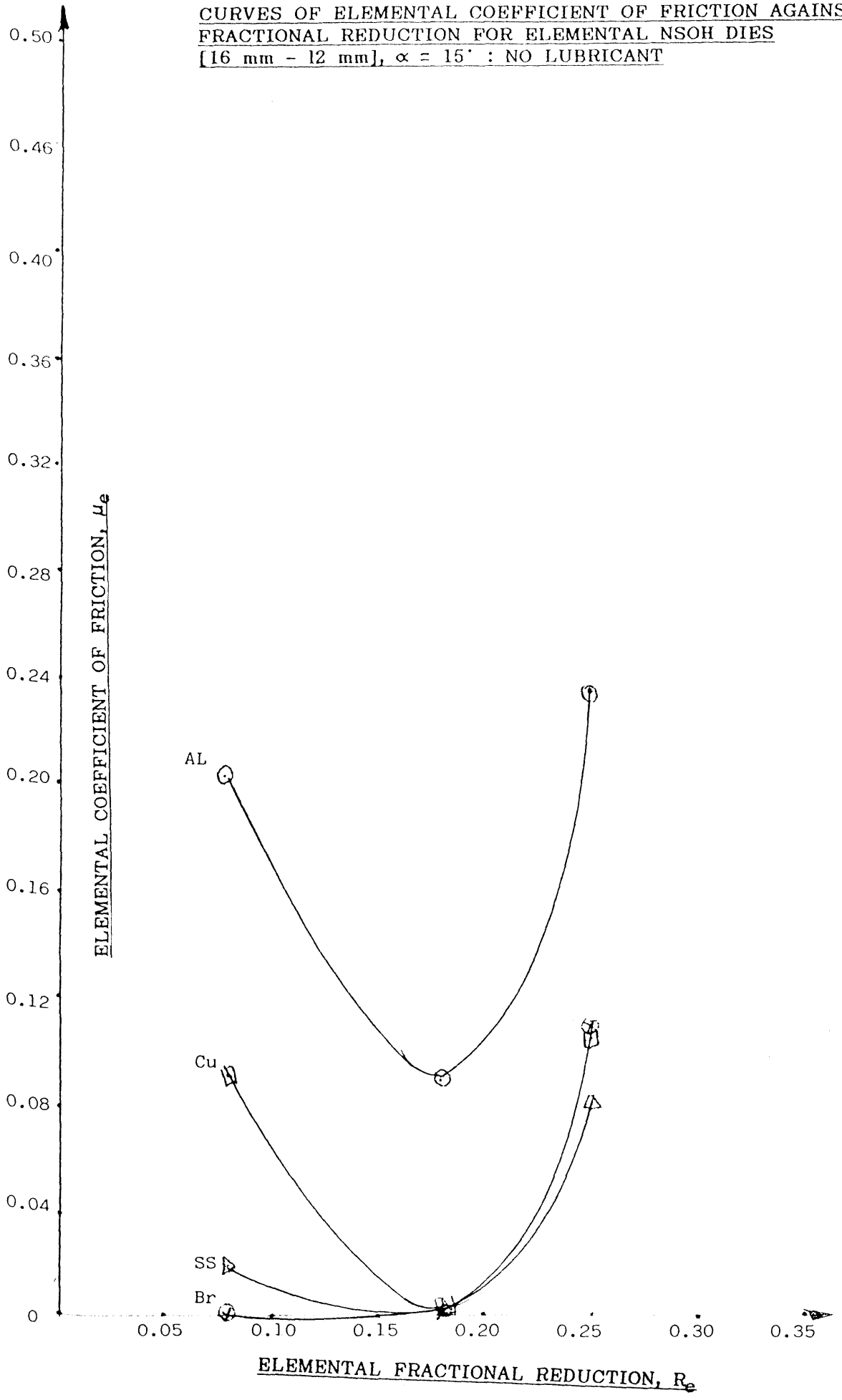

FIGURE (6.20)

CURVES OF ELEMENTAL COEFFICIENT OF FRICTION AGAINST FRACTIONAL REDUCTION FOR ELEMENTAL HCHC DIES [16 mm - 12 mm], α = 15° : NO LUBRICANT

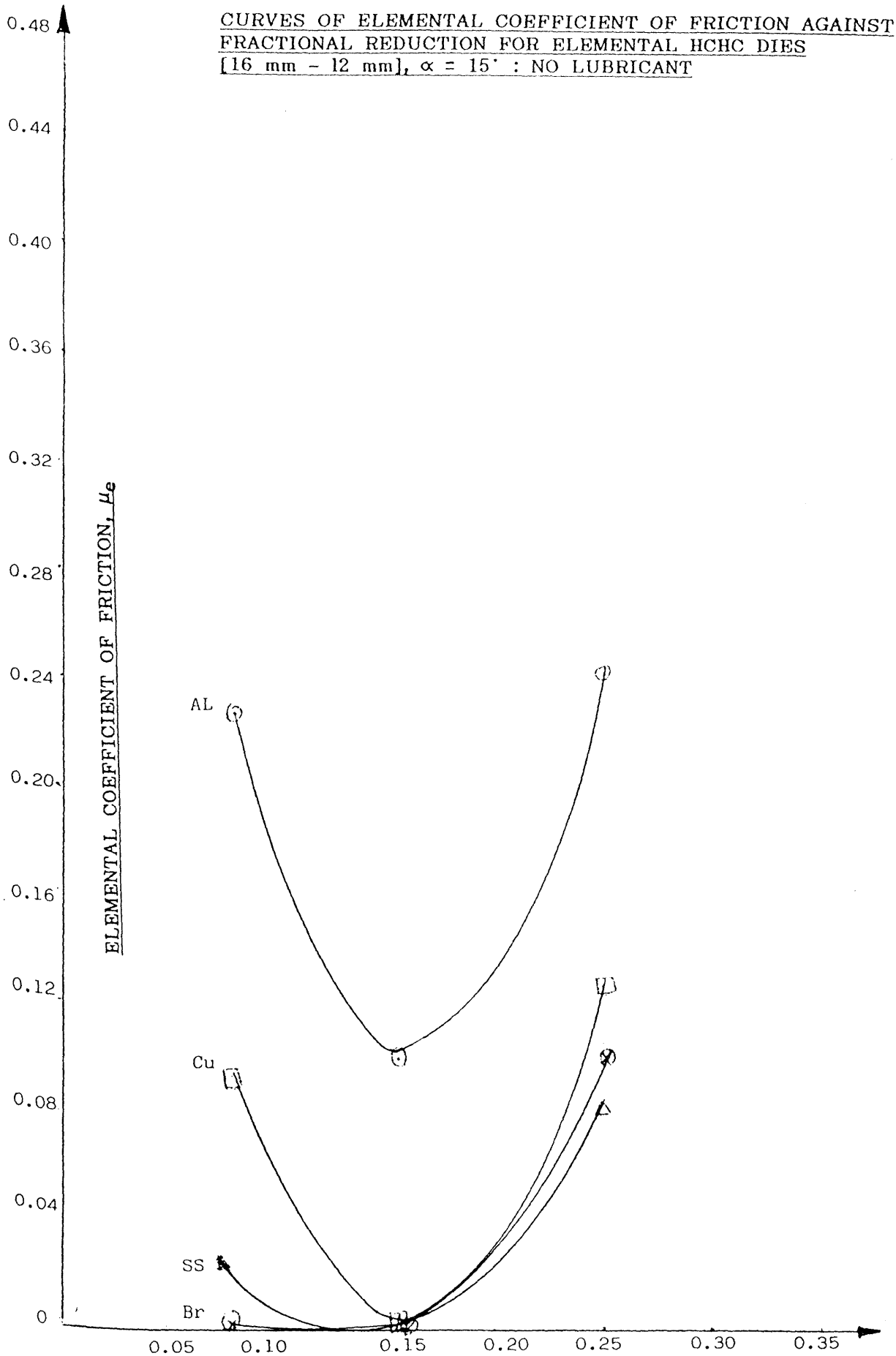

FIGURE (6.21)

CURVES OF ELEMENTAL COEFFICIENT OF FRICTION AGAINST FRACTIONAL REDUCTION FOR ELEMENTAL CAST-IRON DIES [16 mm - 12 mm], $\alpha = 15^{\circ}$: LUBRICATED

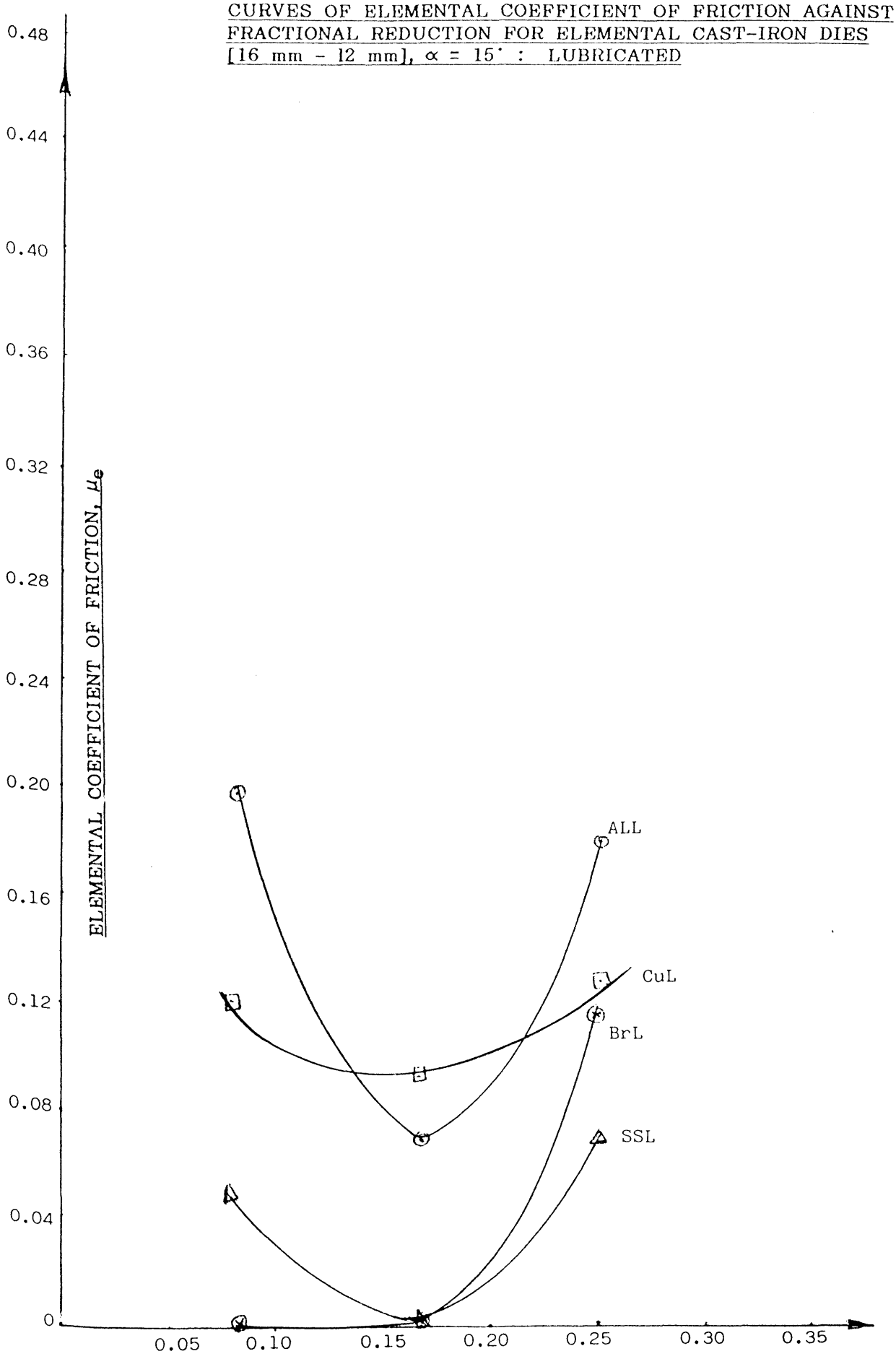

FIGURE (6.22)

CURVES OF ELEMENTAL COEFFICIENT OF FRICTION AGAINST FRACTIONAL REDUCTION FOR ELEMENTAL NSOH DIES [16 mm - 12 mm], $\alpha = 15^{\circ}$: LUBRICATED

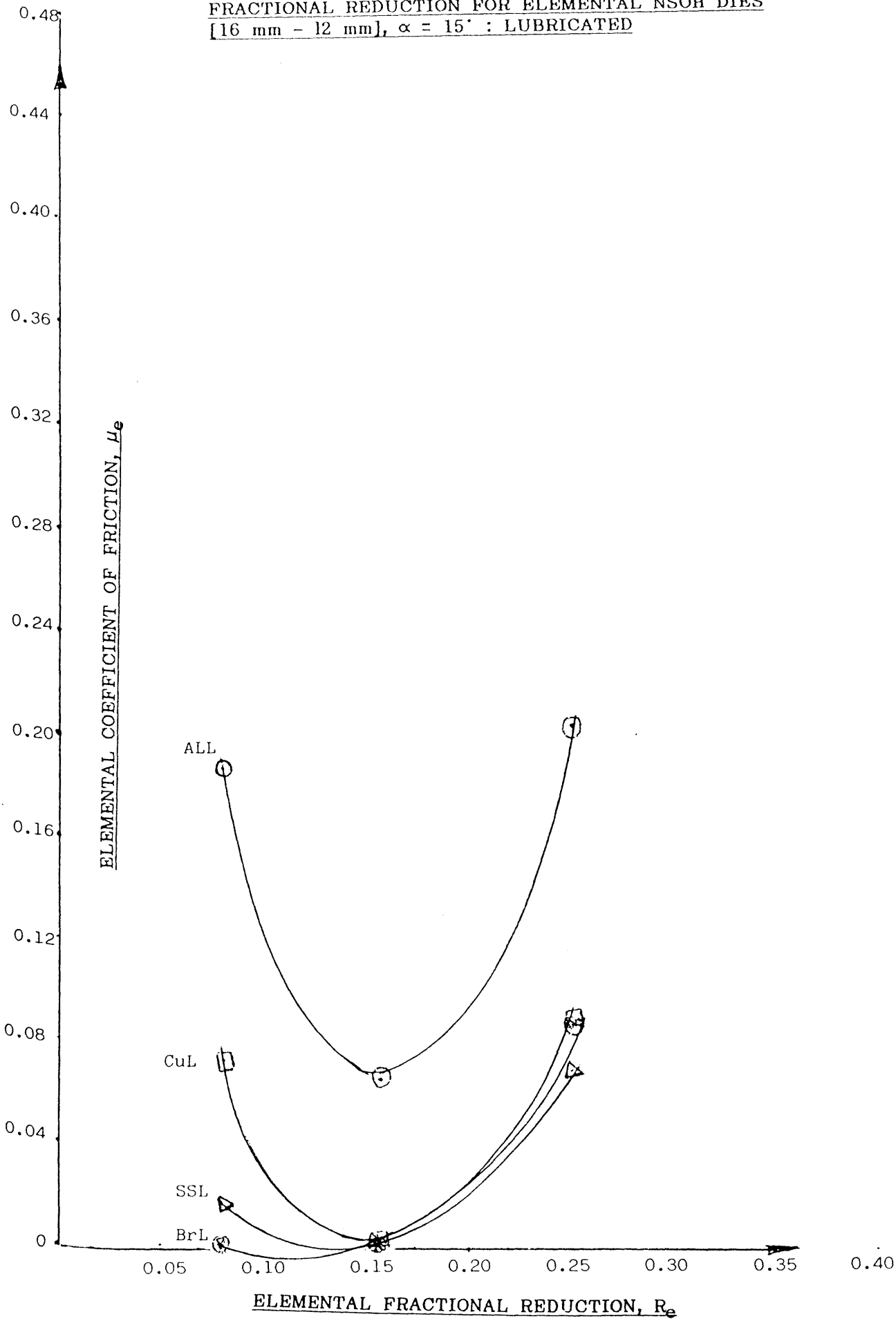

FIGURE (6.23)

CURVES OF ELEMENTAL COEFFICIENT OF FRICTION AGAINST FRACTIONAL REDUCTION FOR ELEMENTAL HCHC DIES [16 mm - 12 mm], α = 15° : LUBRICATED

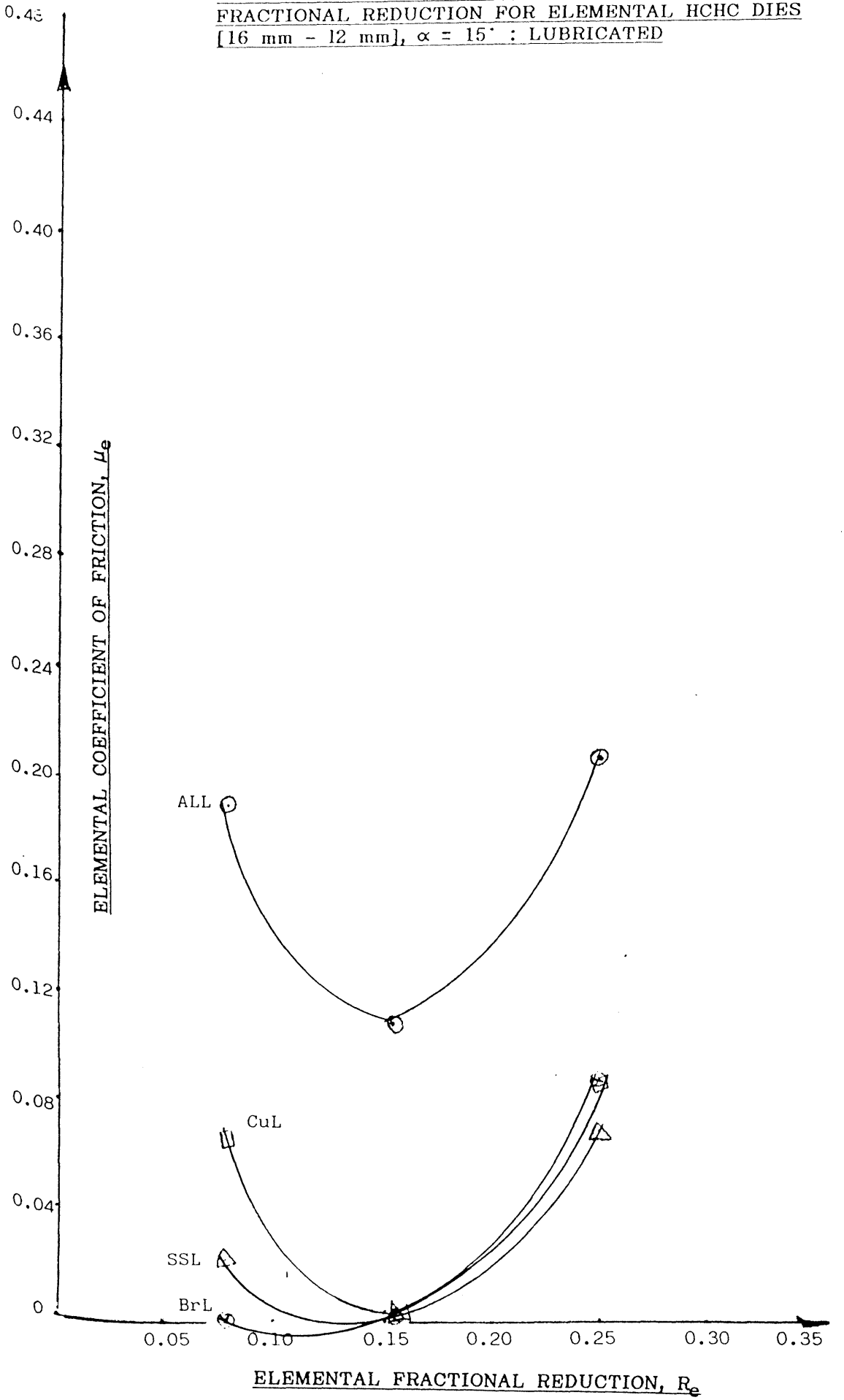

FIGURE (6.24)

GRAPHS OF SIGNIFICANT COEFFICIENT OF FRICTION AGAINST INITIAL HARDNESS OF SPECIMEN MATERIALS [FOR DRAWING WITH 15° SEMI-ANGLE DIES WITH FRACTIONAL REDUCTION OF 0 - 0.375]

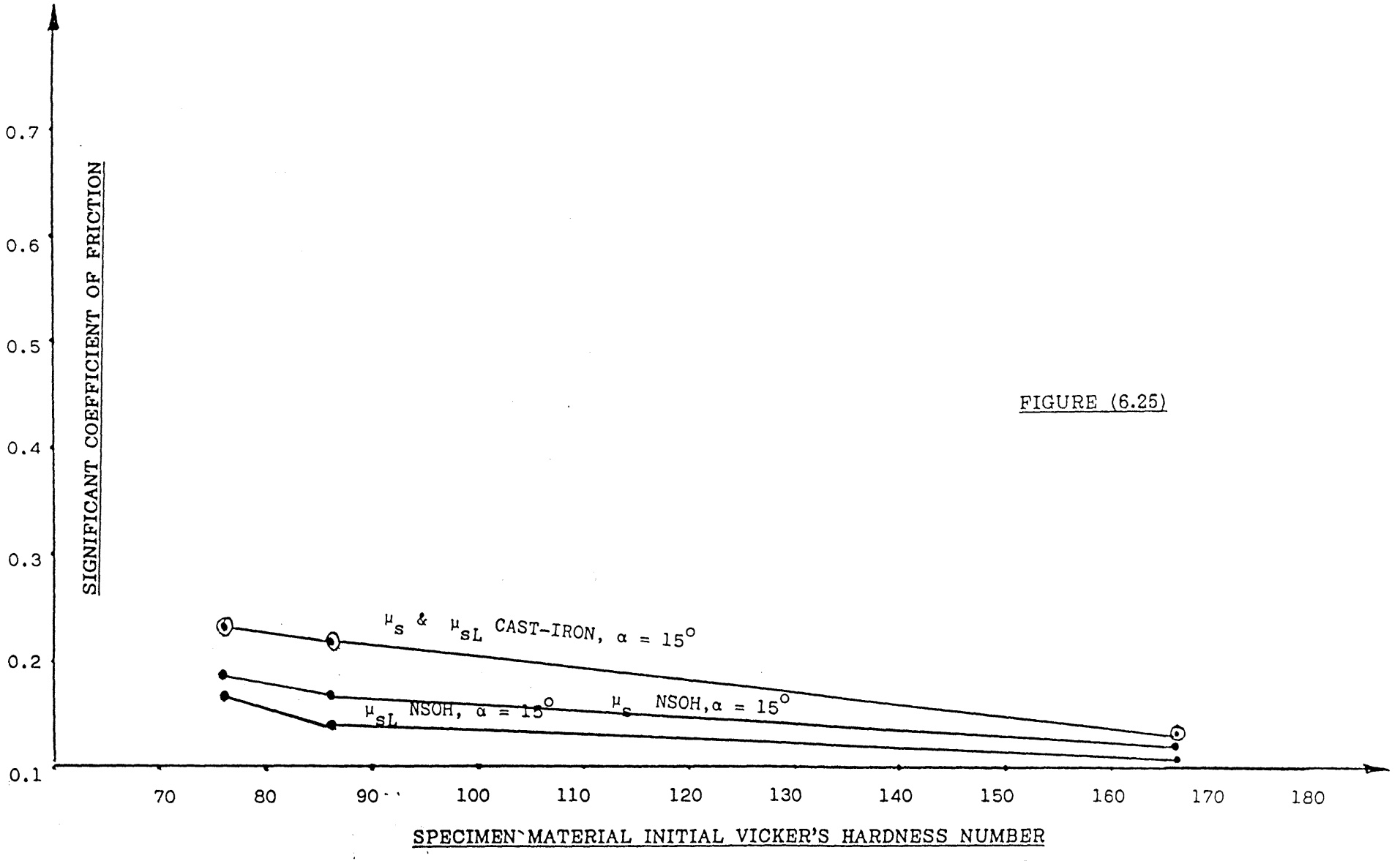

FIGURE (6.25)

GRAPHS OF SIGNIFICANT COEFFICIENT OF FRICTION AGAINST INITIAL HARDNESS OF SPECIMEN MATERIALS
[FOR DRAWING WITH 7° SEMI-ANGLE DIES WITH FRACTIONAL REDUCTION OF 0 - 0.375]

FIGURE (6.26)

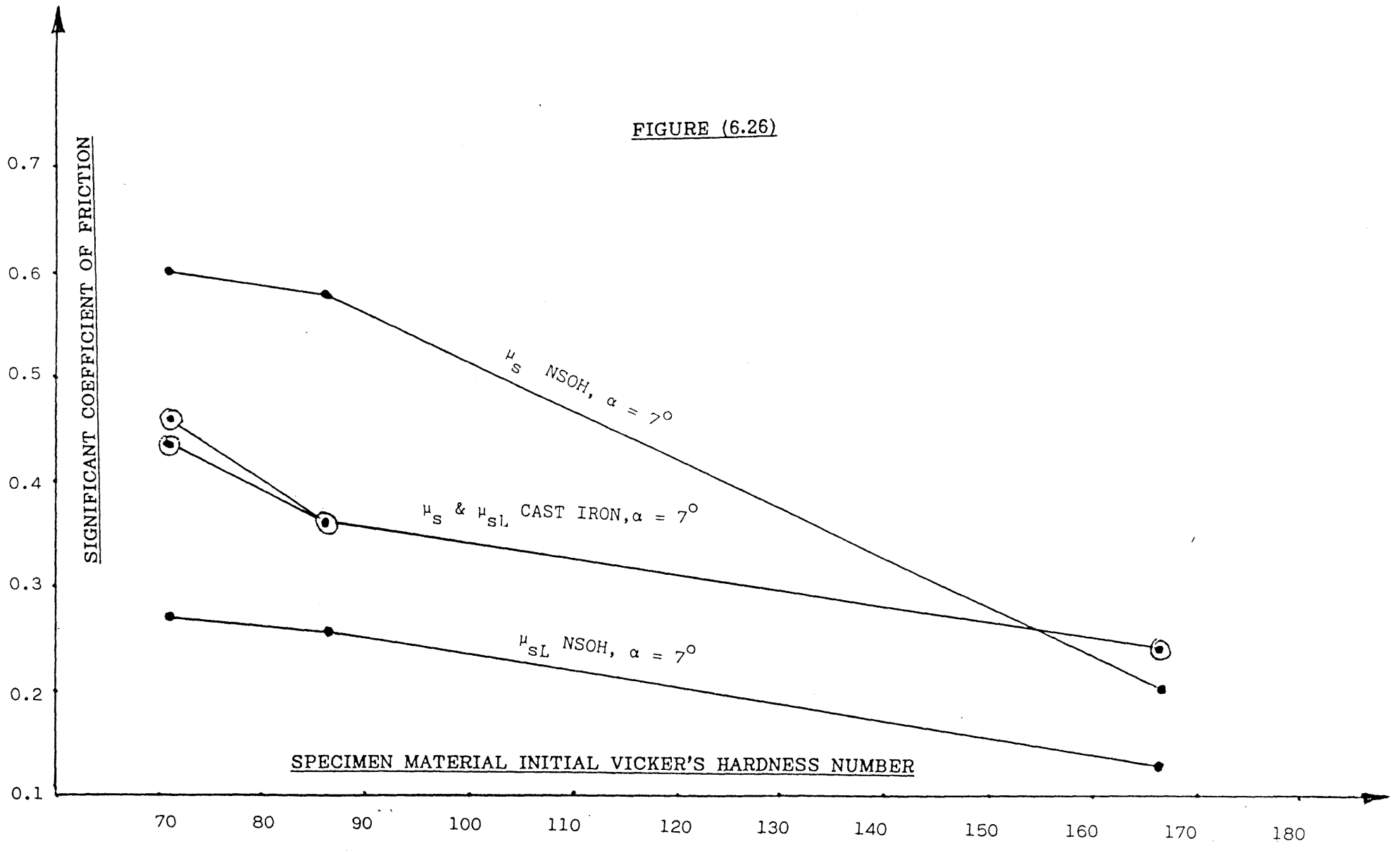

EXPERIMENTAL AND CALCULATED RESULTS FOR R_T = 0.375, NSOH-AL, α = 7°

Re	F_{e1} (mm)	F_{e2} (mm)	F_{e3} (mm)	F_{e4} (mm)	F_{e5} (mm)	F_{Deu} (mm)
0.075	5.1	5.0	5.0	5.0	5.0	5.02
0.150	5.8	5.9	5.9	5.9	5.7	5.84
0.225	6.1	6.0	5.7	5.8	5.7	5.86
0.300	7.0	6.7	6.2	6.2	6.2	6.46
0.375	7.4	7.0	7.4	6.3	6.2	6.66

Table 6.01(a)

Re	F_{Deu} (mm)	F_{Deu} (N)	R_{De} (N)	F_{De} (N)	μ_e
0.075	5.02	2199	323	1876	0.274
0.150	5.84	2558	597	1961	0.2996
0.225	5.86	2567	562	2005	0.305
0.300	6.46	2830	525	2305	0.420
0.375	6.86	3005	243	2762	0.60

Table 6.01(b)

EXPERIMENTAL AND CALCULATED RESULTS FOR R_T = 0.375, HCHC-AL, α = 7°

Re	F_{e1} (mm)	F_{e2} (mm)	F_{e3} (mm)	F_{e4} (mm)	F_{e5} (mm)	F_{Deu} (mm)
0.075	4.9	5.0	5.1	5.0	5.0	5.00
0.150	6.0	6.0	5.9	5.8	5.8	5.90
0.225	6.4	6.0	5.5	5.5	5.5	5.78
0.300	6.8	6.3	6.4	6.3	6.3	6.42
0.375	6.8	6.8	7.0	6.9	7.0	6.90

Table 6.02(a)

Re	F_{Deu} (mm)	F_{Deu} (N)	R_{De} (N)	F_{De} (N)	μ_e
0.075	5.00	2190	323	1867	0.271
0.150	5.90	2590	597	1993	0.308
0.225	5.78	2532	562	1970	0.296
0.300	6.42	2812	525	2287	0.406
0.375	6.90	3022	243	2779	0.640

Table 6.02(b)

EXPERIMENTAL AND CALCULATED RESULTS FOR R_T = 0.375, NSOH-Cu, α = 7°

Re	F_{e1} (mm)	F_{e2} (mm)	F_{e3} (mm)	F_{e4} (mm)	F_{e5} (mm)	F_{Deu} (mm)
0.075	4.8	4.8	4.7	4.8	4.7	4.76
0.150	5.5	5.0	5.1	5.1	5.7	5.22
0.225	6.0	5.8	5.7	5.7	5.7	5.78
0.300	7.0	7.0	6.5	6.0	5.9	6.48
0.375	8.2	8.0	7.3	7.2	7.2	6.48

Table 6.03(a)

Re	F_{Deu} (mm)	F_{Deu} (N)	R_{De} (N)	F_{De} (N)	μ_e
0.075	4.75	2085	372	1713	0.183
0.150	5.22	2286	688	1598	0.163
0.225	5.78	2532	648	1884	0.215
0.300	6.48	2838	605	2233	0.284
0.375	7.58	3320	280	3040	0.581

Table 6.03(b)

EXPERIMENTAL AND CALCULATED RESULTS FOR R_T = 0.375, HCHC, α = 7°

Re	F_{e1} (mm)	F_{e2} (mm)	F_{e3} (mm)	F_{e4} (mm)	F_{e5} (mm)	F_{Deu} (mm)
0.075	4.7	4.7	4.5	4.7	4.6	4.46
0.150	5.4	5.4	5.1	5.0	5.2	5.22
0.225	5.8	5.9	6.0	5.8	5.6	5.82
0.300	6.6	6.1	6.6	6.5	6.4	6.44
0.375	8.2	8.1	8.0	7.2	7.3	7.76

Table 6.04(a)

Re	F_{Deu} (mm)	F_{Deu} (N)	R_{De} (N)	F_{De} (N)	μ_e
0.075	4.46	2032	372	1660	0.172
0.150	5.22	2286	688	1598	0.163
0.225	5.82	2549	648	1901	0.218
0.300	6.44	2821	605	2216	0.28
0.375	7.76	3399	280	3119	0.611

Table 6.04(b)

EXPERIMENTAL AND CALCULATED RESULTS FOR R_T = 0.375, NSOH-SS, α = 7°

Re	F_{e1} (mm)	F_{e2} (mm)	F_{e3} (mm)	F_{e4} (mm)	F_{e5} (mm)	F_{Deu} (mm)
0.075	7.3	7.3	7.4	7.3	7.4	7.34
0.150	10.8	10.7	10.9	10.8	10.8	10.80
0.225	13.7	13.7	13.9	13.8	13.8	13.76
0.300	16.3	16.2	16.2	16.2	16.2	16.22
0.375	17.6	17.5	17.5	17.5	17.5	17.52

Table 6.05(a)

Re	F_{Deu} (mm)	F_{Deu} (N)	R_{De} (N)	F_{De} (N)	μ_e
0.075	7.34	3215	770	2446	0.081
0.150	10.80	4730	1527	3203	0.132
0.225	13.76	6027	2140	3887	0.078
0.300	16.22	7104	2071	5033	0.129
0.375	17.52	7674	1014	6660	0.198

Table 6.05(b)

EXPERIMENTAL AND CALCULATED RESULTS FOR R_T = 0.375, HCHC-SS, α = 7°

Re	F_{e1} (mm)	F_{e2} (mm)	F_{e3} (mm)	F_{e4} (mm)	F_{e5} (mm)	F_{Deu} (mm)
0.075	7.4	7.3	7.4	7.3	7.4	7.36
0.150	10.9	10.8	10.8	10.8	10.8	10.82
0.225	13.8	13.9	13.8	13.8	13.8	13.82
0.300	16.2	16.3	16.2	16.3	16.3	16.26
0.375	17.4	17.5	17.5	17.5	17.5	17.48

Table 6.06(a)

Re	F_{Deu} (mm)	F_{Deu} (N)	R_{De} (N)	F_{De} (N)	μ_e
0.075	7.36	3224	1539	2454	0.082
0.150	10.82	4740	1527	3213	0.133
0.225	13.82	6053	2140	3913	0.079
0.300	16.26	7122	2071	5051	0.130
0.375	17.48	7656	1014	6642	0.197

Table 6.06(b)

EXPERIMENTAL AND CALCULATED RESULTS FOR R_T = 0.375, NSOH-Br, α = 7°

Re	F_{e1} (mm)	F_{e2} (mm)	F_{e3} (mm)	F_{e4} (mm)	F_{e5} (mm)	F_{Deu} (mm)
0.075	6.1	6.1	5.9	6.0	6.0	6.22
0.150	7.3	7.2	7.3	7.3	7.1	7.24
0.225	9.0	8.9	8.7	8.9	8.8	8.84
0.300	9.6	9.5	9.4	9.4	9.5	9.48
0.375	10.0	10.0	9.9	9.9	10.0	9.96

Table 6.07a

Re	F_{Deu} (mm)	F_{Deu} (N)	R_{De} (N)	F_{De} (N)	μ_e
0.075	6.22	2724	635	2089	0.088
0.150	7.24	3171	1179	1993	0.079
0.225	8.84	3872	1110	2762	0.160
0.300	8.84	4152	1037	3115	0.197
0.375	9.96	4363	480	3884	0.228

Table 6.07b

EXPERIMENTAL AND CALCULATED RESULTS FOR R_T = 0.375, HCHC-Br, α = 7°

Re	F_{e1} (mm)	F_{e2} (mm)	F_{e3} (mm)	F_{e4} (mm)	F_{e5} (mm)	F_{Deu} (mm)
0.075	6.0	6.2	6.0	6.1	5.9	6.04
0.150	7.1	7.3	7.2	7.3	7.2	7.22
0.225	9.0	8.9	8.9	8.8	8.7	8.86
0.300	9.7	9.5	9.4	9.4	9.5	9.50
0.375	9.9	9.8	10.0	10.0	10.0	9.94

Table 6.08a

Re	F_{Deu} (mm)	F_{Deu} (N)	R_{De} (N)	F_{De} (N)	μ_e
0.075	6.04	2646	635	2011	0.080
0.150	7.22	3162	1179	1983	0.078
0.225	8.86	3881	1110	2771	0.161
0.300	9.50	4161	1037	3124	0.198
0.375	9.94	4354	480	3874	0.227

Table 6.08b

EXPERIMENTAL AND CALCULATED RESULTS FOR R_T = 0.375, CI-ALm, α = 7°

Re	F_{e1} (mm)	F_{e2} (mm)	F_{e3} (mm)	F_{e4} (mm)	F_{e5} (mm)	F_{Deu} (mm)
0.075	4.0	4.0	4.1	4.0	4.1	4.04
0.150	5.2	5.2	5.1	5.2	5.2	5.18
0.225	5.2	5.2	5.2	5.2	5.2	5.20
0.300	6.2	6.1	6.1	5.4	5.4	5.84
0.375	6.7	6.6	5.5	5.5	5.8	6.02

Table 6.09a

Re	F_{Deu} (mm)	F_{Deu} (N)	R_{De} (N)	F_{De} (N)	μ_e
0.075	4.04	1770	323	1447	0.174
0.150	5.18	2269	597	1672	0.229
0.225	5.20	2278	562	1716	0.234
0.300	5.84	2558	525	2033	0.308
0.375	6.02	2637	243	2394	0.458

Table 6.09b

EXPERIMENTAL AND CALCULATED RESULTS FOR R_T = 0.375, CI-SS, α = 7°

Re	F_{e1} (mm)	F_{e2} (mm)	F_{e3} (mm)	F_{e4} (mm)	F_{e5} (mm)	F_{Deu} (mm)
0.075	7.1	7.0	7.0	7.1	7.1	7.06
0.150	11.0	10.8	10.9	10.8	10.8	10.86
0.225	13.6	13.7	13.7	13.6	13.6	13.64
0.300	15.8	15.9	16.1	16.2	16.2	16.04
0.375	18.6	18.6	18.5	18.6	18.6	18.58

Table 6.10a

Re	F_{Deu} (mm)	F_{Deu} (N)	R_{De} (N)	F_{De} (N)	μ_e
0.075	7.06	3092	1037	2055	0.047
0.150	10.86	4757	1918	2839	0.101
0.225	13.64	5974	1806	4168	0.0933
0.300	16.04	7026	1687	5339	0.146
0.375	18.58	8138	780	7358	0.238

Table 6.10b

EXPERIMENTAL AND CALCULATED RESULTS FOR R_T = 0.375, CI–Br, α = 7°

Re	F_{e1} (mm)	F_{e2} (mm)	F_{e3} (mm)	F_{e4} (mm)	F_{e5} (mm)	F_{Deu} (mm)
0.075	3.9	3.9	3.8	3.9	3.8	3.86
0.150	6.8	6.8	6.7	6.8	6.7	6.76
0.225	8.1	8.0	8.1	8.0	8.0	8.04
0.300	9.5	9.4	9.4	9.5	9.5	9.46
0.375	11.3	11.3	11.2	11.3	11.2	11.26

Table 6.11a

Re	F_{Deu} (mm)	F_{Deu} (N)	R_{De} (N)	F_{De} (N)	μ_e
0.075	3.86	1691	635	1056	7.6×10^{-8}
0.150	6.76	2961	1179	1782	0.056
0.225	8.04	3522	1110	2412	0.121
0.300	9.46	4144	1037	3107	0.196
0.375	11.26	4932	480	4452	0.365

Table 6.11b

EXPERIMENTAL AND CALCULATED RESULTS FOR R_T = 0.375, CI–Cu, α = 7°

Re	F_{e1} (mm)	F_{e2} (mm)	F_{e3} (mm)	F_{e4} (mm)	F_{e5} (mm)	F_{Deu} (mm)
0.075	4.3	4.2	4.3	4.3	4.3	4.28
0.150	5.4	5.5	5.5	5.4	5.6	5.48
0.225	5.8	5.6	5.9	5.8	5.8	5.76
0.300	6.7	6.6	6.4	6.4	6.4	6.50
0.375	6.8	6.7	6.4	6.3	6.5	6.56

Table 6.12a

Re	F_{Deu} (mm)	F_{Deu} (N)	R_{De} (N)	F_{De} (N)	μ_e
0.075	4.28	1875	372	1503	0.142
0.150	5.48	2400	688	1712	0.185
0.225	5.76	2523	648	1875	0.213
0.300	6.50	2847	605	2242	0.286
0.375	6.56	2873	280	2593	0.364

Table 6.12b

EXPERIMENTAL AND CALCULATED RESULTS FOR R_T = 0.375, NSOH-ALL, α = 7°

Re	F_{e1} (mm)	F_{e2} (mm)	F_{e3} (mm)	F_{e4} (mm)	F_{e5} (mm)	F_{Deu} (mm)
0.075	3.3	3.4	3.4	3.4	3.3	3.36
0.150	4.2	4.5	4.1	4.5	4.2	4.30
0.225	4.5	4.5	4.4	4.3	4.5	4.44
0.300	4.7	4.7	4.8	4.6	4.7	4.70
0.375	4.8	4.9	5.0	4.8	4.8	4.86

Table 6.13a

Re	F_{Deu} (mm)	F_{Deu} (N)	R_{De} (N)	F_{De} (N)	μ_e
0.075	3.36	1472	645	1149	0.108
0.150	4.30	1883	597	1286	0.1397
0.225	4.44	1945	562	1383	0.157
0.300	4.70	2059	525	1534	0.187
0.375	4.86	2129	243	1886	0.268

Table 6.13b

EXPERIMENTAL AND CALCULATED RESULTS FOR R_T = 0.375, HCHC-AL, α = 7°

Face oints	F_{e1} (mm)	F_{e2} (mm)	F_{e3} (mm)	F_{e4} (mm)	F_{e5} (mm)	F_{Deu} (mm)
1	3.3	3.3	3.3	3.3	3.3	3.30
2	4.5	4.5	4.1	4.2	4.2	4.30
3	4.3	4.4	4.5	4.4	4.5	4.42
4	4.8	4.7	4.6	4.7	4.6	4.70
5	5.0	4.9	4.8	4.8	4.8	4.86

Table 6.14a

Face Points	F_{Deu} (mm)	F_{Deu} (N)	R_{De} (N)	F_{De} (N)	μ_e
1	3.30	1445	323	1122	0.102
2	4.30	1883	597	1286	0.1397
3	4.42	1936	562	1374	0.155
4	4.70	2059	525	1534	0.187
5	4.86	2129	243	1886	0.268

Table 6.14b

EXPERIMENTAL AND CALCULATED RESULTS FOR R_T = 0.375, NSOH-BrL, α = 7°

Face Points	F_{e1} (mm)	F_{e2} (mm)	F_{e3} (mm)	F_{e4} (mm)	F_{e5} (mm)	F_{Deu} (mm)
1	3.9	4.1	4.0	3.9	3.9	3.96
2	6.0	6.0	6.1	6.0	6.0	6.02
3	8.2	8.1	8.0	8.1	8.1	8.10
4	9.2	9.0	9.2	9.3	9.0	9.14
5	9.2	9.2	9.2	9.0	9.4	9.20

Table 6.15a

Face Points	F_{Deu} (mm)	F_{Deu} (N)	R_{De} (N)	F_{De} (N)	μ_e
1	3.96	1735	635	1100	3.2×10^{-7}
2	6.02	2637	1179	1458	0.022
3	8.10	3548	1110	2438	0.124
4	9.14	4003	1037	2966	0.1795
5	9.20	4030	480	3550	0.189

Table 6.15b

EXPERIMENTAL AND CALCULATED RESULTS FOR R_T = 0.375, HCHC-BrL, α = 7°

Face Points	F_{e1} (mm)	F_{e2} (mm)	F_{e3} (mm)	F_{e4} (mm)	F_{e5} (mm)	F_{Deu} (mm)
1	3.8	3.8	3.8	3.8	3.8	3.80
2	6.3	6.2	6.3	6.3	6.3	6.28
3	7.8	7.7	7.8	7.8	7.8	7.78
4	9.3	9.3	9.3	9.3	9.3	9.30
5	9.4	9.4	9.3	9.4	9.4	9.38

Table 6.16a

Face Points	F_{Deu} (mm)	F_{Deu} (N)	R_{De} (N)	F_{De} (N)	μ_e
1	3.80	1664	635	1029	3×10^{-7}
2	6.28	2751	1179	1572	0.036
3	7.78	3408	1110	2298	0.108
4	9.30	4073	1037	3036	0.189
5	9.38	4108	480	3628	0.198

Table 6.16b

EXPERIMENTAL AND CALCULATED RESULTS FOR R_T = 0.375, NSOH-SSL, α = 7°

Face Points	F_{e1} (mm)	F_{e2} (mm)	F_{e3} (mm)	F_{e4} (mm)	F_{e5} (mm)	F_{Deu} (mm)
1	6.3	6.3	6.3	6.3	6.3	6.30
2	9.4	9.7	9.8	9.7	9.8	9.68
3	11.1	11.2	11.0	11.1	11.2	11.12
4	15.6	15.4	15.5	15.5	15.5	15.15
5	14.7	14.9	14.9	14.9	14.8	14.80

Table 6.17a

Face Points	F_{Deu} (mm)	F_{Deu} (N)	R_{De} (N)	F_{De} (N)	μ_e
1	6.30	2759	770	1989	0.041
2	9.68	4240	1527	2713	0.09
3	11.12	4871	2140	2731	0.015
4	15.50	6789	2071	4718	0.111
5	14.80	6482	1014	5468	0.133

Table 6.17b

EXPERIMENTAL AND CALCULATED RESULTS FOR R_T = 0.375, HCHC-SSL, α = 7°

Face Points	F_{e1} (mm)	F_{e2} (mm)	F_{e3} (mm)	F_{e4} (mm)	F_{e5} (mm)	F_{Deu} (mm)
1	6.3	6.4	6.3	6.4	6.4	6.36
2	9.9	9.2	9.8	9.8	9.8	9.70
3	10.5	11.0	11.5	11.3	11.5	11.16
4	15.5	15.6	15.5	15.7	15.5	15.56
5	14.9	14.8	14.9	15.0	14.9	14.90

Table 6.18a

Face Points	F_{Deu} (mm)	F_{Deu} (N)	R_{De} (N)	F_{De} (N)	μ_e
1	6.36	2786	770	2016	0.043
2	9.70	4249	1527	2722	0.091
3	11.16	4888	2140	2748	0.016
4	15.56	6815	2071	4744	0.113
5	14.90	6526	1014	5512	0.135

Table 6.18a

EXPERIMENTAL AND CALCULATED RESULTS FOR R_T = 0.375, NSOH-CuL, α = 7°

Re	F_{e1} (mm)	F_{e2} (mm)	F_{e3} (mm)	F_{e4} (mm)	F_{e5} (mm)	F_{Deu} (mm)
0.075	3.6	3.6	3.5	3.6	3.6	3.58
0.150	4.0	4.2	4.1	4.1	4.2	4.12
0.225	4.2	4.3	4.3	4.2	4.4	4.28
0.300	5.3	5.3	5.2	5.2	5.2	5.24
0.375	5.8	5.6	5.5	5.5	5.4	5.56

Table 6.19(a)

Re	F_{Deu} (mm)	F_{Deu} (N)	R_{De} (N)	F_{De} (N)	μ_e
0.075	3.58	1568	372	1196	0.084
0.150	4.12	1805	688	1117	0.071
0.225	4.28	1875	648	1227	0.087
0.300	5.24	2295	605	1690	0.171
0.375	5.56	2435	280	2155	0.264

Table 6.19(b)

EXPERIMENTAL AND CALCULATED RESULTS FOR R_T = 0.375, HCHC-CuL, α = 7°

Re	F_{e1} (mm)	F_{e2} (mm)	F_{e3} (mm)	F_{e4} (mm)	F_{e5} (mm)	F_{Deu} (mm)
0.075	3.6	3.5	3.6	3.6	3.5	3.56
0.150	4.2	4.1	4.2	4.1	4.1	4.14
0.225	4.3	4.3	4.3	4.3	4.3	4.30
0.300	5.3	5.2	5.2	5.2	5.2	5.22
0.375	5.3	5.5	5.4	5.5	6.1	5.56

Table 6.20(a)

Re	F_{Deu} (mm)	F_{Deu} (N)	R_{De} (N)	F_{De} (N)	μ_e
0.075	3.56	1559	372	1187	0.0823
0.150	4.14	1813	688	1125	0.072
0.225	4.30	1883	648	1235	0.0884
0.300	5.22	2286	605	1681	0.170
0.375	5.56	2435	560	2155	0.264

Table 6.20(b)

EXPERIMENTAL AND CALCULATED RESULTS FOR R_T = 0.375, CI-AL, α = 7°

Re	F_{e1} (mm)	F_{e2} (mm)	F_{e3} (mm)	F_{e4} (mm)	F_{e5} (mm)	F_{Deu} (mm)
0.075	4.1	4.1	4.0	4.0	4.0	4.04
0.150	5.2	5.1	5.1	5.2	5.1	5.14
0.225	5.2	5.2	5.0	5.2	5.0	5.12
0.300	6.1	5.8	5.7	5.8	5.8	5.84
0.375	6.0	6.0	6.0	6.0	5.8	5.96

Table 6.21(a)

Re	F_{Deu} (mm)	F_{Deu} (N)	R_{De} (N)	F_{De} (N)	μ_e
0.075	4.04	1770	323	1447	0.174
0.150	5.14	2251	597	1654	0.225
0.225	5.12	2243	562	1681	0.226
0.300	5.84	2558	525	2033	0.308
0.375	5.96	2611	243	2368	0.440

Table 6.21(b)

EXPERIMENTAL AND CALCULATED RESULTS FOR R_T = 0.375, CI-SSL, α = 7°

Re	F_{e1} (mm)	F_{e2} (mm)	F_{e3} (mm)	F_{e4} (mm)	F_{e5} (mm)	F_{Deu} (mm)
0.075	7.0	7.0	7.1	7.0	7.0	7.02
0.150	11.0	10.7	10.7	10.7	10.8	10.78
0.225	13.5	13.6	13.6	13.6	13.7	13.60
0.300	16.0	16.3	16.0	16.0	16.1	16.06
0.375	18.6	18.7	18.5	18.5	18.5	18.56

Table 6.22(a)

Re	F_{Deu} (mm)	F_{Deu} (N)	R_{De} (N)	F_{De} (N)	μ_e
0.075	7.02	3075	1037	2038	0.045
0.150	10.78	4722	1918	2804	0.0978
0.225	13.60	5957	1806	4151	0.0923
0.300	16.60	7034	1687	5347	0.146
0.375	18.56	8129	780	7349	0.237

Table 6.22(b)

EXPERIMENTAL AND CALCULATED RESULTS FOR R_T = 0.375, CI-BrL, α = 7°

Re	F_{e1} (mm)	F_{e2} (mm)	F_{e3} (mm)	F_{e4} (mm)	F_{e5} (mm)	F_{Deu} (mm)
0.075	3.8	3.7	3.8	3.8	3.8	3.78
0.150	6.7	6.7	6.6	6.6.	6.7	6.66
0.225	8.0	8.0	7.9	8.0	8.0	7.98
0.300	9.5	9.5	9.4	9.4	9.4	9.44
0.375	10.2	10.2	10.1	10.2	10.2	10.18

Table 6.23(a)

Re	F_{Deu} (mm)	F_{Deu} (N)	R_{De} (N)	F_{De} (N)	μ_e
0.075	3.78	1656	635	1021	6.7×10^{-8}
0.150	6.66	2917	1179	1738	0.052
0.225	7.98	3495	1110	2385	0.118
0.300	9.44	4135	1037	3098	0.195
0.375	10.18	4459	480	3979	0.301

Table 6.23(b)

EXPERIMENTAL AND CALCULATED RESULTS FOR R_T = 0.375, CI-CuL, α = 7°

Re	F_{e1} (mm)	F_{e2} (mm)	F_{e3} (mm)	F_{e4} (mm)	F_{e5} (mm)	F_{Deu} (mm)
0.075	3.8	3.7	4.0	4.0	4.0	3.90
0.150	5.2	5.3	5.3	5.2	5.3	5.26
0.225	5.7	5.7	5.6	5.6	5.7	5.66
0.300	6.6	6.4	6.4	6.5	6.5	6.48
0.375	6.6	6.6	6.6	6.5	6.5	6.56

Table 6.24(a)

Re	F_{Deu} (mm)	F_{Deu} (N)	R_{De} (N)	F_{De} (N)	μ_e
0.075	3.90	1708	372	1336	0.110
0.150	5.26	2304	688	1616	0.166
0.225	6.66	2479	648	1831	0.204
0.300	6.48	2838	605	2233	0.284
0.375	6.56	2873	280	2593	0.364

Table 6.24(b)

EXPERIMENTAL AND CALCULATED RESULTS FOR R_T = 0.25, NSOH-Br, α = 7°

Re	F_{e1} (mm)	F_{e2} (mm)	F_{e3} (mm)	F_{e4} (mm)	F_{e5} (mm)	F_{Deu} (mm)
0.05	4.0	4.0	4.1	4.0	4.0	4.02
0.10	4.2	4.0	4.0	4.0	4.2	4.08
0.15	5.8	5.8	5.7	5.7	5.4	5.68
0.20	6.8	6.8	6.8	6.8	6.7	6.78
0.25	7.7	7.6	7.7	7.7	7.6	7.66

Table 6.25(a)

Re	F_{Deu} (mm)	F_{Deu} (N)	R_{De} (N)	F_{De} (N)	μ_e
0.05	4.02	1761	635	1126	0.042
0.10	4.08	1787	1210	577	1.1×10^{-7}
0.15	5.68	2488	1175	1313	0.067
0.20	6.78	2970	1137	1833	0.141
0.25	7.66	3355	548	2807	0.201

Table 6.25(b)

EXPERIMENTAL AND CALCULATED RESULTS FOR R_T = 0.25, HCHC-Br, α = 7°

Re	F_{e1} (mm)	F_{e2} (mm)	F_{e3} (mm)	F_{e4} (mm)	F_{e5} (mm)	F_{Deu} (mm)
0.05	4.1	4.1	4.0	4.0	4.0	4.04
0.10	4.2	4.1	4.2	4.0	4.0	4.10
0.15	5.8	5.8	5.7	5.6	5.6	5.68
0.20	6.5	6.8	6.7	6.8	6.8	6.70
0.25	7.7	7.7	7.7	7.7	7.7	7.70

Table 6.26(a)

Re	F_{Deu} (mm)	F_{Deu} (N)	R_{De} (N)	F_{De} (N)	μ_e
0.05	4.04	1770	635	1135	0.0437
0.10	4.10	1796	1210	586	1.6×10^{-7}
0.15	5.68	2488	1175	1313	0.067
0.20	6.70	2935	1137	1798	0.136
0.25	7.70	3364	548	2816	0.203

Table 6.26(b)

EXPERIMENTAL AND CALCULATED RESULTS FOR R_T = 0.25, NSOH-AL, α = 7°

Re	F_{e1} (mm)	F_{e2} (mm)	F_{e3} (mm)	F_{e4} (mm)	F_{e5} (mm)	F_{Deu} (mm)
0.05	3.6	3.5	3.4	3.2	3.3	3.40
0.10	4.5	4.5	4.7	4.6	4.7	4.60
0.15	5.5	5.5	4.8	4.7	4.7	5.04
0.20	5.6	5.7	5.6	4.6	4.6	5.22
0.25	5.8	5.4	5.7	5.6	5.2	5.54

Table 6.27(a)

Re	F_{Deu} (mm)	F_{Deu} (N)	R_{De} (N)	F_{De} (N)	μ_e
0.05	3.40	1489	323	1166	0.228
0.10	4.60	2015	613	1402	0.308
0.15	5.04	2208	595	1613	0.444
0.10	5.22	2286	576	1710	0.481
0.25	5.54	2427	278	2150	0.548

Table 6.27(b)

EXPERIMENTAL AND CALCULATED RESULTS FOR R_T = 0.25, HCHC-AL, α = 7°

Re	F_{e1} (mm)	F_{e2} (mm)	F_{e3} (mm)	F_{e4} (mm)	F_{e5} (mm)	F_{Deu} (mm)
0.05	3.8	3.4	3.3	3.3	3.2	3.40
0.10	4.8	4.7	4.7	4.8	4.7	4.74
0.15	5.5	4.8	4.8	4.8	4.7	4.92
0.20	5.8	5.0	4.8	4.9	4.5	5.00
0.25	5.8	5.1	5.2	5.0	5.1	5.24

Table 6.28(a)

Re	F_{Deu} (mm)	F_{Deu} (N)	R_{De} (N)	F_{De} (N)	μ_e
0.05	3.40	1489	323	1166	0.228
0.10	4.74	2076	613	1463	0.361
0.15	4.92	2154	595	1559	0.410
0.20	5.00	2190	576	1614	0.426
0.25	5.24	2295	278	2017	0.480

Table 6.28(b)

EXPERIMENTAL AND CALCULATED RESULTS FOR R_T = 0.25, NSOH-SS, α = 7°

Re	F_{e1} (mm)	F_{e2} (mm)	F_{e3} (mm)	F_{e4} (mm)	F_{e5} (mm)	F_{Deu} (mm)
0.05	5.1	5.2	5.2	5.1	5.2	5.16
0.10	7.7	7.9	7.9	7.7	7.8	7.80
0.15	8.8	8.8	8.8	7.9	8.8	8.78
0.20	10.3	10.4	10.5	10.6	10.5	10.46
0.25	11.0	11.1	11.1	11.0	11.0	11.04

Table 6.29(a)

Re	F_{Deu} (mm)	F_{Deu} (N)	R_{De} (N)	F_{De} (N)	μ_e
0.05	5.16	2260	770	1490	0.057
0.10	7.80	3416	1568	1848	0.094
0.15	8.78	3846	2266	1580	0.053
0.20	10.46	4582	2271	2311	0.096
0.25	11.04	4836	1159	3677	0.14

Table 6.29(b)

EXPERIMENTAL AND CALCULATED RESULTS FOR R_T = 0.25, HCHC-SS, α = 7°

Re	F_{e1} (mm)	F_{e2} (mm)	F_{e3} (mm)	F_{e4} (mm)	F_{e5} (mm)	F_{Deu} (mm)
0.05	5.1	5.2	5.1	5.2	5.1	5.14
0.10	7.8	7.8	7.8	7.8	7.8	7.80
0.15	8.8	8.7	8.7	8.8	8.8	8.76
0.20	10.5	10.5	10.6	10.4	10.7	10.54
0.25	11.0	11.0	11.0	11.0	11.0	11.00

Table 6.30(a)

Re	F_{Deu} (mm)	F_{Deu} (N)	R_{De} (N)	F_{De} (N)	μ_e
0.05	5.14	2251	770	1480	0.056
0.10	7.80	3416	1568	1848	0.094
0.15	8.76	3837	2266	1571	0.052
0.20	10.54	4617	2271	2346	0.099
0.25	11.00	4818	1159	3659	0.139

Table 6.30(b)

EXPERIMENTAL AND CALCULATED RESULTS FOR R_T = 0.25, NSOH-Cu, α = 7°

Re	F_{e1} (mm)	F_{e2} (mm)	F_{e3} (mm)	F_{e4} (mm)	F_{e5} (mm)	F_{Deu} (mm)
0.05	3.5	3.5	3.4	3.5	3.5	3.48
0.10	3.6	3.4	3.5	3.6	3.6	3.54
0.15	4.6	4.4	4.0	4.0	3.8	4.14
0.20	4.3	3.9	4.4	4.3	4.4	4.26
0.25	4.7	4.2	4.1	3.9	4.0	4.18

Table 6.31(a)

Re	F_{Deu} (mm)	F_{Deu} (N)	R_{De} (N)	F_{De} (N)	μ_e
0.05	3.48	1524	372	1152	0.175
0.10	3.54	1551	706	845	0.092
0.15	4.14	1813	686	1127	0.162
0.20	4.26	1866	664	1202	0.176
0.25	4.18	1831	320	1512	0.254

Table 6.31(b)

EXPERIMENTAL AND CALCULATED RESULTS FOR R_T = 0.25, HCHC-Cu, α = 7°

Re	F_{e1} (mm)	F_{e2} (mm)	F_{e3} (mm)	F_{e4} (mm)	F_{e5} (mm)	F_{Deu} (mm)
0.05	3.5	3.5	3.5	3.4	3.4	3.46
0.10	3.5	3.5	3.6	3.4	3.6	3.52
0.15	4.5	4.0	4.2	4.4	4.0	4.22
0.20	4.4	4.4	3.9	4.3	4.4	4.28
0.25	4.5	4.5	4.0	4.2	4.1	4.26

Table 6.32(a)

Re	F_{Deu} (mm)	F_{Deu} (N)	R_{De} (N)	F_{De} (N)	μ_e
0.05	3.46	1516	372	1144	0.173
0.10	3.52	1542	706	836	0.090
0.15	4.22	1848	686	1162	0.172
0.20	4.28	1875	664	1211	0.179
0.25	4.26	1866	320	1546	0.263

Table 6.32(b)

EXPERIMENTAL AND CALCULATED RESULTS FOR R_T = 0.25, CI-Br, α = 7°

Re	F_{e1} (mm)	F_{e2} (mm)	F_{e3} (mm)	F_{e4} (mm)	F_{e5} (mm)	F_{Deu} (mm)
0.05	3.2	3.2	3.1	3.2	3.2	3.18
0.10	4.4	4.5	4.4	4.4	4.4	4.42
0.15	5.4	5.3	5.4	5.4	5.4	5.38
0.20	6.1	6.2	6.5	6.6	6.6	6.40
0.25	7.2	7.2	7.1	7.1	7.2	7.16

Table 6.33(a)

Re	F_{Deu} (mm)	F_{Deu} (N)	R_{De} (N)	F_{De} (N)	μ_e
0.05	3.18	1393	635	758	$1x10^{-7}$
0.10	4.42	1936	1210	726	$1x10^{-7}$
0.15	5.38	2356	1157	1199	0.0497
0.20	6.40	2803	1137	1666	0.116
0.25	7.16	3136	548	2588	0.254

Table 6.33(b)

EXPERIMENTAL AND CALCULATED RESULTS FOR R_T = 0.25, CI-Cu, α = 7°

Re	F_{e1} (mm)	F_{e2} (mm)	F_{e3} (mm)	F_{e4} (mm)	F_{e5} (mm)	F_{Deu} (mm)
0.05	3.0	3.0	3.3	3.3	3.3	3.18
0.10	3.8	3.8	3.7	3.7	3.7	3.74
0.15	4.3	4.3	4.4	4.4.	4.3	4.34
0.20	4.3	4.3	4.4	4.4	4.4	4.36
0.25	4.8	4.7	4.5	4.5	4.5	4.60

Table 6.34(a)

Re	F_{Deu} (mm)	F_{Deu} (N)	R_{De} (N)	F_{De} (N)	μ_e
0.05	3.18	1393	372	1021	0.139
0.10	3.74	1638	706	932	0.116
0.15	4.34	1901	686	1215	0.186
0.20	4.36	1910	664	1246	0.188
0.25	4.60	2015	320	1695	0.305

Table 6.34(b)

EXPERIMENTAL AND CALCULATED RESULTS FOR R_T = 0.25, CI-AL, α = 7°

Re	F_{e1} (mm)	F_{e2} (mm)	F_{e3} (mm)	F_{e4} (mm)	F_{e5} (mm)	F_{Deu} (mm)
0.05	3.3	3.3	3.3	3.4	3.4	3.26
0.10	3.5	3.5	3.6	3.6	3.5	3.46
0.15	3.6	3.6	3.6	3.6	3.6	3.60
0.20	3.6	3.6	3.6	3.6	3.6	3.60
0.25	3.7	3.7	3.6	3.7	3.7	3.68

Table 6.35(a)

Re	F_{Deu} (mm)	F_{Deu} (N)	R_{De} (N)	F_{De} (N)	μ_e
0.05	3.26	1428	323	1105	0.077
0.10	3.46	1516	613	903	0.145
0.15	3.60	1577	595	985	0.165
0.20	3.60	1577	576	1001	0.163
0.25	3.68	1612	278	1334	0.261

Table 6.35(b)

EXPERIMENTAL AND CALCULATED RESULTS FOR R_T = 0.25, CI-SS, α = 7°

Re	F_{e1} (mm)	F_{e2} (mm)	F_{e3} (mm)	F_{e4} (mm)	F_{e5} (mm)	F_{Deu} (mm)
0.05	5.8	5.8	5.8	5.8	5.8	5.80
0.10	7.5	7.6	7.6	7.5	7.6	7.56
0.15	8.8	8.8	8.9	8.8	8.8	8.82
0.20	10.1	10.2	10.1	10.0	10.2	10.12
0.25	11.7	11.6	11.5	11.5	11.6	11.58

Table 6.36(a)

Re	F_{Deu} (mm)	F_{Deu} (N)	R_{De} (N)	F_{De} (N)	μ_e
0.05	5.80	2540	1037	1503	0.058
0.10	7.56	3311	1970	1341	0.032
0.15	8.82	3863	1913	1950	0.096
0.20	10.12	4433	1850	2583	0.123
0.25	11.58	5072	892	4180	0.179

Table 6.36(b)

EXPERIMENTAL AND CALCULATED RESULTS FOR R_T = 0.25, NSOH-AL, α = 7°

Re	F_{e1} (mm)	F_{e2} (mm)	F_{e3} (mm)	F_{e4} (mm)	F_{e5} (mm)	F_{Deu} (mm)
0.05	2.5	2.3	2.4	2.4	2.3	2.38
0.10	3.5	3.3	3.3	3.3	3.3	3.34
0.15	3.4	3.7	3.8	3.7	3.7	3.66
0.20	3.8	3.9	3.8	3.9	3.7	3.82
0.25	3.9	3.9	3.9	3.7	3.9	3.86

Table 6.37(a)

Re	F_{Deu} (mm)	F_{Deu} (N)	R_{De} (N)	F_{De} (N)	μ_e
0.05	2.38	1042	323	719	0.087
0.10	3.34	1462	613	849	0.128
0.15	3.66	1603	595	1008	0.172
0.20	3.82	1673	576	1097	0.193
0.25	3.86	1691	278	1413	0.286

Table 6.37(b)

EXPERIMENTAL AND CALCULATED RESULTS FOR R_T = 0.25, HCHC-AL, α = 7°

Re	F_{e1} (mm)	F_{e2} (mm)	F_{e3} (mm)	F_{e4} (mm)	F_{e5} (mm)	F_{Deu} (mm)
0.05	2.5	2.5	2.3	2.4	2.4	2.42
0.10	3.2	3.1	3.1	3.1	3.0	3.10
0.15	3.7	3.6	3.5	3.8	3.7	3.66
0.20	3.9	3.8	3.8	3.9	3.8	3.84
0.25	3.8	3.8	3.9	3.8	3.7	3.80

Table 6.38(a)

Re	F_{Deu} (mm)	F_{Deu} (N)	R_{De} (N)	F_{De} (N)	μ_e
0.05	2.42	1060	323	737	0.093
0.10	3.10	1358	613	745	0.096
0.15	3.66	1603	595	1008	0.172
0.20	3.84	1682	576	1106	0.196
0.25	3.80	1664	278	1386	0.191

Table 6.38(b)

EXPERIMENTAL AND CALCULATED RESULTS FOR R_T = 0.25, NSOH-SSL, α = 7°

Re	F_{e1} (mm)	F_{e2} (mm)	F_{e3} (mm)	F_{e4} (mm)	F_{e5} (mm)	F_{Deu} (mm)
0.05	5.2	5.0	5.0	5.0	5.0	5.04
0.10	6.1	7.1	7.1	7.0	7.0	6.86
0.15	8.0	8.0	8.0	8.0	8.0	8.00
0.20	9.6	9.6	9.9	10.0	9.9	9.80
0.25	10.4	10.5	10.5	10.5	10.5	10.48

Table 6.39(a)

Re	F_{Deu} (mm)	F_{Deu} (N)	R_{De} (N)	F_{De} (N)	μ_e
0.05	5.04	2208	770	1438	0.0502
0.10	6.86	3005	1568	1437	0.044
0.15	8.00	3504	2266	1238	0.014
0.20	9.80	4292	2271	2021	0.067
0.25	10.48	4590	1159	3431	0.121

Table 6.39(b)

EXPERIMENTAL AND CALCULATED RESULTS FOR R_T = 0.25, HCHC-SSL, α = 7°

Re	F_{e1} (mm)	F_{e2} (mm)	F_{e3} (mm)	F_{e4} (mm)	F_{e5} (mm)	F_{Deu} (mm)
0.05	5.0	5.0	5.0	5.0	5.0	5.00
0.10	6.3	7.0	7.0	7.0	7.0	6.86
0.15	8.0	8.0	8.0	8.3	8.0	8.06
0.20	9.5	9.7	9.8	10.0	10.0	9.80
0.25	10.5	10.5	10.5	10.5	10.5	10.50

Table 6.40(a)

Re	F_{Deu} (mm)	F_{Deu} (N)	R_{De} (N)	F_{De} (N)	μ_e
0.05	5.00	2190	770	1420	0.048
0.10	6.86	3005	1568	1437	0.044
0.15	8.06	3530	2266	1264	0.170
0.20	9.80	4292	2271	2021	0.067
0.25	10.50	4599	1159	3440	0.122

Table 6.40(b)

EXPERIMENTAL AND CALCULATED RESULTS FOR R_T = 0.25, NSOH-CuL, α = 7°

Re	F_{e1} (mm)	F_{e2} (mm)	F_{e3} (mm)	F_{e4} (mm)	F_{e5} (mm)	F_{Deu} (mm)
0.05	2.8	2.9	2.9	2.8	2.8	2.84
0.10	3.0	3.2	3.1	3.1	3.0	3.08
0.15	3.7	3.7	3.6	3.7	3.6	3.66
0.20	3.7	3.8	3.8	3.9	3.7	3.76
0.25	3.7	3.8	3.8	3.7	3.6	3.76

Table 6.41(a)

Re	F_{Deu} (mm)	F_{Deu} (N)	R_{De} (N)	F_{De} (N)	μ_e
0.05	2.84	1244	372	872	0.099
0.10	3.08	1349	706	643	0.039
0.15	3.66	1603	686	917	0.106
0.20	3.76	1647	664	983	0.118
0.25	3.72	1629	320	1309	0.199

Table 6.41(b)

EXPERIMENTAL AND CALCULATED RESULTS FOR R_T = 0.25, HCHC-CuL, α = 7°

Re	F_{e1} (mm)	F_{e2} (mm)	F_{e3} (mm)	F_{e4} (mm)	F_{e5} (mm)	F_{Deu} (mm)
0.05	2.8	2.8	2.8	2.8	2.8	2.80
0.10	3.1	3.0	3.1	3.0	3.0	3.04
0.15	3.7	3.6	3.7	3.7	3.7	3.68
0.20	3.8	3.8	3.7	3.7	3.8	3.76
0.25	3.5	3.8	3.6	3.8	3.6	3.66

Table 6.42(a)

Re	F_{Deu} (mm)	F_{Deu} (N)	R_{De} (N)	F_{De} (N)	μ_e
0.05	2.80	1226	372	854	0.094
0.10	3.04	1332	706	626	0.035
0.15	3.68	1612	686	926	0.109
0.20	3.76	1647	664	983	0.118
0.25	3.66	1603	320	1283	0.192

Table 6.42(b)

EXPERIMENTAL AND CALCULATED RESULTS FOR R_T = 0.25, NSOH-BrL, α = 7°

Re	F_{e1} (mm)	F_{e2} (mm)	F_{e3} (mm)	F_{e4} (mm)	F_{e5} (mm)	F_{Deu} (mm)
0.05	2.8	3.0	3.0	2.9	2.9	2.92
0.10	3.7	3.4	4.3	4.3	4.3	4.04
0.15	5.4	5.0	5.0	5.0	5.1	5.10
0.20	5.5	5.7	5.7	5.7	5.7	5.66
0.25	5.8	5.8	5.8	5.9	5.8	5.82

Table 6.43(a)

Re	F_{Deu} (mm)	F_{Deu} (N)	R_{De} (N)	F_{De} (N)	μ_e
0.05	2.92	1279	635	644	1.37×10^{-7}
0.10	4.04	1768	1210	558	1×10^{-7}
0.15	5.10	2234	1175	1059	0.029
0.20	5.66	2479	1137	1342	0.067
0.25	5.82	2549	548	2001	0.079

Table 6.43(b)

EXPERIMENTAL AND CALCULATED RESULTS FOR R_T = 0.25, HCHC-BrL, α = 7°

Re	F_{e1} (mm)	F_{e2} (mm)	F_{e3} (mm)	F_{e4} (mm)	F_{e5} (mm)	F_{Deu} (mm)
0.05	2.6	2.6	2.6	2.5	2.6	2.58
0.10	4.3	4.3	4.2	4.3	4.3	4.28
0.15	5.5	4.9	4.9	4.9	4.9	5.02
0.20	5.5	5.4	5.5	5.6	5.4	5.48
0.25	5.5	5.8	5.7	5.8	5.8	5.72

Table 6.44(a)

Re	F_{Deu} (mm)	F_{Deu} (N)	R_{De} (N)	F_{De} (N)	μ_e
0.05	2.58	1130	635	495*	1×10^{-7}
0.10	4.28	1875	1210	665	1.4×10^{-7}
0.15	5.02	2199	1175	1024	0.024
0.20	5.48	2400	1137	1263	0.055
0.25	5.72	2505	548	1957	0.073

Table 6.44(b)

EXPERIMENTAL AND CALCULATED RESULTS FOR R_T = 0.25, CI-BrL, α = 7°

Re	F_{e1} (mm)	F_{e2} (mm)	F_{e3} (mm)	F_{e4} (mm)	F_{e5} (mm)	F_{Deu} (mm)
0.05	3.1	3.0	3.0	3.1	3.1	3.06
0.10	4.2	4.3	4.2	4.2	4.3	4.24
0.15	5.2	5.2	5.3	5.2	5.2	5.22
0.20	5.9	6.0	6.0	6.0	6.0	5.98
0.25	7.1	7.1	7.1	7.0	7.0	7.06

Table 6.45(a)

Re	F_{Deu} (mm)	F_{Deu} (N)	R_{De} (N)	F_{De} (N)	μ_e
0.05	3.06	1340	635	705	$1x10^{-7}$
0.10	4.24	1857	1210	647	$1x10^{-7}$
0.15	5.22	2286	1157	1129	0.044
0.20	5.98	2619	1137	1482	0.088
0.25	7.06	3092	548	2544	0.247

Table 6.45(b)

EXPERIMENTAL AND CALCULATED RESULTS FOR R_T = 0.25, CI-CuL, α = 7°

Re	F_{e1} (mm)	F_{e2} (mm)	F_{e3} (mm)	F_{e4} (mm)	F_{e5} (mm)	F_{Deu} (mm)
0.05	3.3	3.0	3.2	3.0	3.1	3.12
0.10	3.7	3.7	3.6	3.7	3.6	3.66
0.15	3.9	3.9	3.8	3.8	3.8	3.84
0.20	4.1	4.0	4.1	4.0	4.0	4.04
0.25	4.4	4.3	4.4	4.4	4.5	4.40

Table 6.46(a)

Re	F_{Deu} (mm)	F_{Deu} (N)	R_{De} (N)	F_{De} (N)	μ_e
0.05	3.12	1367	372	995	0.132
0.10	3.66	1603	706	897	0.106
0.15	3.84	1682	686	996	0.127
0.20	4.04	1770	664	1106	0.151
0.25	4.40	1927	320	1607	0.280

Table 6.46(b)

EXPERIMENTAL AND CALCULATED RESULTS FOR R_T = 0.25, CI-ALL, α = 7°

Re	F_{e1} (mm)	F_{e2} (mm)	F_{e3} (mm)	F_{e4} (mm)	F_{e5} (mm)	F_{Deu} (mm)
0.05	3.3	3.2	3.2	3.1	3.2	3.20
0.10	3.3	3.3	3.3	3.3	3.3	3.30
0.15	3.3	3.4	3.4	3.4	3.3	3.36
0.20	3.4	3.4	3.3	3.4	3.4	3.38
0.25	3.5	3.5	3.5	3.5	3.5	3.50

Table 6.47(a)

Re	F_{Deu} (mm)	F_{Deu} (N)	R_{De} (N)	F_{De} (N)	μ_e
0.05	3.20	1402	323	1079	0.2
0.10	3.30	1445	613	832	0.123
0.15	3.36	1472	595	877	0.131
0.20	3.38	1480	576	904	0.148
0.25	3.50	1533	278	1255	0.236

Table 6.47(b)

EXPERIMENTAL AND CALCULATED RESULTS FOR R_T = 0.25, CI-SSL, α = 7°

Re	F_{e1} (mm)	F_{e2} (mm)	F_{e3} (mm)	F_{e4} (mm)	F_{e5} (mm)	F_{Deu} (mm)
0.05	5.6	5.6	5.5	5.6	5.6	5.58
0.10	7.2	7.3	7.2	7.2	7.2	7.22
0.15	8.7	8.8	8.7	8.7	8.7	8.72
0.20	10.0	0.90	10.0	10.0	9.9	9.96
0.25	11.5	11.5	11.5	11.5	11.5	11.48

Table 6.48(a)

Re	F_{Deu} (mm)	F_{Deu} (N)	R_{De} (N)	F_{De} (N)	μ_e
0.05	5.58	2444	1037	1407	0.0463
0.10	7.22	3162	1970	1192	0.0146
0.15	8.72	3819	1913	1906	0.091
0.20	9.96	4362	1850	2512	0.116
0.25	11.48	5028	892	4136	0.176

Table 6.48(b)

EXPERIMENTAL AND CALCULATED RESULTS FOR R_T = 0.375, , α = 15°

Re	F_{e1} (mm)	F_{e2} (mm)	F_{e3} (mm)	F_{e4} (mm)	F_{e5} (mm)	F_{Deu} (mm)
0.125	6.5	6.5	6.9	6.6	6.6	6.58
0.250	10.0	10.0	10.8	10.8	10.7	10.46
0.375	11.8	11.9	12.0	11.8	11.8	11.86

Table 6.49(a)

Re	F_{Deu} (mm)	F_{Deu} (N)	R_{De} (N)	F_{De} (N)	μ_e
0.125	6.58	2882	1365	1517	6.7×10^{-8}
0.250	10.46	4582	2449	2133	0.0052
0.375	11.86	5195	1075	4120	0.140

Table 6.49(b)

EXPERIMENTAL AND CALCULATED RESULTS FOR R_T = 0.375, HCHC-Br , α = 15°

Re	F_{e1} (mm)	F_{e2} (mm)	F_{e3} (mm)	F_{e4} (mm)	F_{e5} (mm)	F_{Deu} (mm)
0.125	7.0	6.9	6.8	6.9	6.7	6.86
0.250	10.4	10.4	10.0	10.4	10.2	10.28
0.375	11.7	11.8	11.8	11.9	12.0	11.84

Table 6.50(a)

Re	F_{Deu} (mm)	F_{Deu} (N)	R_{De} (N)	F_{De} (N)	μ_e
0.125	6.86	3005	1365	1640	5.5×10^{-7}
0.250	10.28	4502	2449	2053	0.0022
0.375	11.84	5186	1075	3992	0.139

Table 6.50(b)

EXPERIMENTAL AND CALCULATED RESULTS FOR R_T = 0.375, NSOH-AL, α = 15°

Re	F_{e1} (mm)	F_{e2} (mm)	F_{e3} (mm)	F_{e4} (mm)	F_{e5} (mm)	F_{Deu} (mm)
0.125	6.3	6.2	5.9	5.8	5.9	6.02
0.250	6.0	7.0	5.9	5.8	5.8	6.10
0.375	7.0	6.3	6.4	6.4	6.4	6.52

Table 6.51(a)

Re	F_{Deu} (mm)	F_{Deu} (N)	R_{De} (N)	F_{De} (N)	μ_e
0.125	6.02	2672	691	1981	0.132
0.250	6.10	2777	1240	1537	0.066
0.375	6.52	2856	545	2312	0.187

Table 6.51(b)

EXPERIMENTAL AND CALCULATED RESULTS FOR R_T = 0.375, HCHC-AL, α = 15°

Re	F_{e1} (mm)	F_{e2} (mm)	F_{e3} (mm)	F_{e4} (mm)	F_{e5} (mm)	F_{Deu} (mm)
0.125	5.8	6.2	6.2	5.9	5.9	6.00
0.250	6.0	7.1	7.1	5.8	5.8	6.36
0.375	6.4	6.4	6.4	6.4	6.4	6.40

Table 6.52(a)

Re	F_{Deu} (mm)	F_{Deu} (N)	R_{De} (N)	F_{De} (N)	μ_e
0.125	6.00	2628	691	1937	0.125
0.250	6.36	2786	1240	1546	0.068
0.375	6.40	2856	545	2312	0.187

Table 6.52(b)

EXPERIMENTAL AND CALCULATED RESULTS FOR R_T = 0.375, NSOH-Cu, α = 15°

Re	F_{e1} (mm)	F_{e2} (mm)	F_{e3} (mm)	F_{e4} (mm)	F_{e5} (mm)	F_{Deu} (mm)
0.125	5.7	5.6	5.6	5.7	5.6	5.64
0.250	6.8	6.6	6.6	6.2	6.2	6.48
0.375	7.8	7.7	7.0	7.0	7.0	7.30

Table 6.53(a)

Re	F_{Deu} (mm)	F_{Deu} (N)	R_{De} (N)	F_{De} (N)	μ_e
0.125	5.64	2470	797	1674	0.057
0.250	6.48	2838	1429	1409	0.024
0.375	7.30	3197	628	2570	0.173

Table 6.53(b)

EXPERIMENTAL AND CALCULATED RESULTS FOR R_T = 0.375, HCHC-Cu, α = 15°

Re	F_{e1} (mm)	F_{e2} (mm)	F_{e3} (mm)	F_{e4} (mm)	F_{e5} (mm)	F_{Deu} (mm)
0.125	5.6	5.6	5.7	5.7	5.7	5.66
0.250	6.6	6.8	6.7	6.3	6.2	6.52
0.375	7.8	7.7	7.7	7.7	7.5	7.68

Table 6.54(a)

Re	F_{Deu} (mm)	F_{Deu} (N)	R_{De} (N)	F_{De} (N)	μ_e
0.125	5.66	2479	797	1593	0.047
0.250	6.52	2856	1429	1427	0.026
0.375	7.68	3362	628	2734	0.197

Table 6.54(b)

EXPERIMENTAL AND CALCULATED RESULTS FOR R_T = 0.375, NSOH-SS, α = 15°

Re	F_{e1} (mm)	F_{e2} (mm)	F_{e3} (mm)	F_{e4} (mm)	F_{e5} (mm)	F_{Deu} (mm)
0.125	12.6	12.6	12.7	12.7	12.6	12.64
0.250	17.9	17.9	18.1	18.0	18.0	17.98
0.375	23.0	23.0	23.1	23.0	23.0	23.02

Table 6.55(a)

Re	F_{Deu} (mm)	F_{Deu} (N)	R_{De} (N)	F_{De} (N)	μ_e
0.125	12.64	5536	2222	3314	0.058
0.250	17.94	7875	3985	3890	5.9×10^{-8}
0.375	23.02	10083	1750	8333	0.115

Table 6.55(b)

EXPERIMENTAL AND CALCULATED RESULTS FOR R_T = 0.375, HCHC-SS, α = 15°

Re	F_{e1} (mm)	F_{e2} (mm)	F_{e3} (mm)	F_{e4} (mm)	F_{e5} (mm)	F_{Deu} (mm)
0.125	12.7	12.6	12.7	12.7	12.7	12.68
0.250	18.0	18.0	17.9	18.0	17.9	17.96
0.375	23.0	23.1	23.0	23.0	23.0	23.02

Table 6.56(a)

Re	F_{Deu} (mm)	F_{Deu} (N)	R_{De} (N)	F_{De} (N)	μ_e
0.125	12.68	5554	2222	3332	0.060
0.250	17.96	7867	3985	3882	5.7×10^{-8}
0.375	23.02	10083	1750	8333	0.115

Table 6.56(b)

EXPERIMENTAL AND CALCULATED RESULTS FOR R_T = 0.375, CI-AL, α = 15°

Re	F_{e1} (mm)	F_{e2} (mm)	F_{e3} (mm)	F_{e4} (mm)	F_{e5} (mm)	F_{Deu} (mm)
0.125	7.5	7.4	7.4	7.5	7.4	7.44
0.250	7.7	7.6	7.6	7.7	7.6	7.64
0.375	9.2	6.5	6.6	6.5	6.5	7.06

Table 6.57(a)

Re	F_{Deu} (mm)	F_{Deu} (N)	R_{De} (N)	F_{De} (N)	μ_e
0.125	7.44	3259	692	2567	0.223
0.250	7.64	3346	1240	2106	0.150
0.375	7.06	3092	545	2547	0.228

Table 6.57(b)

EXPERIMENTAL AND CALCULATED RESULTS FOR R_T = 0.375, CI-Br, α = 15°

Re	F_{e1} (mm)	F_{e2} (mm)	F_{e3} (mm)	F_{e4} (mm)	F_{e5} (mm)	F_{Deu} (mm)
0.125	8.8	8.4	7.8	7.8	7.8	8.12
0.250	12.4	12.0	11.3	11.3	11.3	11.66
0.375	13.5	13.3	13.0	13.0	13.0	13.16

Table 6.58(a)

Re	F_{Deu} (mm)	F_{Deu} (N)	R_{De} (N)	F_{De} (N)	μ_e
0.125	8.12	3557	1365	2192	0.011
0.250	11.66	5107	2449	2658	0.04
0.375	13.16	5764	1079	4689	0.198

Table 6.58(b)

EXPERIMENTAL AND CALCULATED RESULTS FOR R_T = 0.375, CI-Cu, α = 15°

Re	F_{e1} (mm)	F_{e2} (mm)	F_{e3} (mm)	F_{e4} (mm)	F_{e5} (mm)	F_{Deu} (mm)
0.125	7.0	6.8	6.8	6.8	6.8	6.84
0.250	8.0	7.0	7.0	7.0	7.0	6.20
0.375	9.2	7.7	7.6	7.6	7.6	7.94

Table 6.59(a)

Re	F_{Deu} (mm)	F_{Deu} (N)	R_{De} (N)	F_{De} (N)	μ_e
0.125	6.84	2996	797	2199	0.121
0.250	7.20	3154	1429	1725	0.06
0.375	7.94	3478	628	2850	0.215

Table 6.59(b)

EXPERIMENTAL AND CALCULATED RESULTS FOR R_T = 0.375, CI-SS, α = 15°

Re	F_{e1} (mm)	F_{e2} (mm)	F_{e3} (mm)	F_{e4} (mm)	F_{e5} (mm)	F_{Deu} (mm)
0.125	13.5	13.5	13.4	13.4	13.5	13.46
0.250	19.0	19.0	19.1	19.1	19.0	19.04
0.375	23.8	23.8	23.9	23.8	23.7	23.80

Table 6.60(a)

Re	F_{Deu} (mm)	F_{Deu} (N)	R_{De} (N)	F_{De} (N)	μ_e
0.125	13.46	3896	1748	4148	0.082
0.250	19.04	8340	1834	6506	0.085
0.375	23.80	10424	2275	8149	0.128

Table 6.60(b)

EXPERIMENTAL AND CALCULATED RESULTS FOR R_T = 0.375, NSOH-CuL, α = 15°

Re	F_{e1} (mm)	F_{e2} (mm)	F_{e3} (mm)	F_{e4} (mm)	F_{e5} (mm)	F_{Deu} (mm)
0.125	6.3	5.5	5.4	5.5	5.5	5.64
0.250	6.8	6.3	6.4	6.3	6.3	6.38
0.375	7.3	6.7	6.7	6.8	6.7	6.84

Table 6.61(a)

Re	F_{Deu} (mm)	F_{Deu} (N)	R_{De} (N)	F_{De} (N)	μ_e
0.125	5.64	2470	797	1674	0.057
0.250	6.38	2794	1429	1365	0.019
0.375	6.84	2996	628	2368	0.144

Table 6.61(b)

EXPERIMENTAL AND CALCULATED RESULTS FOR R_T = 0.375, HCHC-CuL, α = 15°

Re	F_{e1} (mm)	F_{e2} (mm)	F_{e3} (mm)	F_{e4} (mm)	F_{e5} (mm)	F_{Deu} (mm)
0.125	6.4	5.6	5.4	5.5	5.4	5.66
0.250	6.6	6.4	6.4	6.4	6.3	6.42
0.375	7.3	6.7	6.8	6.8	6.7	6.86

Table 6.62(a)

Re	F_{Deu} (mm)	F_{Deu} (N)	R_{De} (N)	F_{De} (N)	μ_e
0.125	5.66	2479	797	1682	0.058
0.250	6.42	2812	1429	1383	0.021
0.375	6.86	3005	628	2377	0.144

Table 6.62(b)

EXPERIMENTAL AND CALCULATED RESULTS FOR R_T = 0.375, NSOH-BrL, α = 15°

Re	F_{e1} (mm)	F_{e2} (mm)	F_{e3} (mm)	F_{e4} (mm)	F_{e5} (mm)	F_{Deu} (mm)
0.125	6.4	6.4	6.5	6.5	6.4	6.44
0.250	10.0	9.9	9.9	9.9	10.0	9.94
0.375	11.8	11.7	11.7	11.7	11.6	11.70

Table 6.63(a)

Re	F_{Deu} (mm)	F_{Deu} (N)	R_{De} (N)	F_{De} (N)	μ_e
0.125	6.44	2821	1365	1456	4.8×10^{-8}
0.250	9.94	4354	2449	1905	6.8×10^{-6}
0.375	11.70	5125	1075	3931	0.134

Table 6.63(b)

EXPERIMENTAL AND CALCULATED RESULTS FOR R_T = 0.375, HCHC-BrL, α = 15°

Re	F_{e1} (mm)	F_{e2} (mm)	F_{e3} (mm)	F_{e4} (mm)	F_{e5} (mm)	F_{Deu} (mm)
0.125	6.5	6.4	6.5	6.5	6.5	6.48
0.250	10.8	10.0	10.1	10.0	10.0	10.18
0.375	11.8	11.8	11.7	11.6	11.7	11.74

Table 6.64(a)

Re	F_{Deu} (mm)	F_{Deu} (N)	R_{De} (N)	F_{De} (N)	μ_e
0.125	6.48	2838	1365	1473	4.8×10^{-8}
0.250	10.18	4459	2449	2010	7.1×10^{-4}
0.375	11.74	5142	1075	3948	0.135

Table 6.64(b)

EXPERIMENTAL AND CALCULATED RESULTS FOR R_T = 0.375, NSOH-SSL, α = 15°

Re	F_{e1} (mm)	F_{e2} (mm)	F_{e3} (mm)	F_{e4} (mm)	F_{e5} (mm)	F_{Deu} (mm)
0.125	12.5	12.4	12.4	12.5	12.4	12.44
0.250	17.2	17.3	17.4	17.4	17.4	17.34
0.375	22.4	22.3	22.4	22.5	22.6	22.44

Table 6.65(a)

Re	F_{Deu} (mm)	F_{Deu} (N)	R_{De} (N)	F_{De} (N)	μ_e
0.125	12.44	5449	2222	3228	0.058
0.250	17.34	7595	3985	3611	1×10^{-8}
0.375	22.44	9829	1750	8080	0.106

Table 6.65(b)

EXPERIMENTAL AND CALCULATED RESULTS FOR R_T = 0.375, HCHC-SSL, α = 15°

Re	F_{e1} (mm)	F_{e2} (mm)	F_{e3} (mm)	F_{e4} (mm)	F_{e5} (mm)	F_{Deu} (mm)
0.125	12.4	12.4	12.5	12.4	12.5	12.44
0.250	17.3	17.4	17.4	17.4	17.3	17.36
0.375	22.3	22.5	22.5	22.6	22.5	22.4

Table 6.66(a)

Re	F_{Deu} (mm)	F_{Deu} (N)	R_{De} (N)	F_{De} (N)	μ_e
0.125	12.44	5448	2222	3226	0.058
0.250	17.36	7604	3985	3619	1×10^{-8}
0.375	22.48	9846	1750	8096	0.099

Table 6.66(b)

EXPERIMENTAL AND CALCULATED RESULTS FOR R_T = 0.375, NSOH-ALL, α = 15°

Re	F_{e1} (mm)	F_{e2} (mm)	F_{e3} (mm)	F_{e4} (mm)	F_{e5} (mm)	F_{Deu} (mm)
0.125	5.9	5.8	5.8	5.9	5.8	5.84
0.250	6.7	5.8	5.9	5.9	6.0	6.06
0.375	6.8	6.7	5.9	5.9	5.9	6.24

Table 6.67(a)

Re	F_{Deu} (mm)	F_{Deu} (N)	R_{De} (N)	F_{De} (N)	μ_e
0.125	5.84	2558	691	1859	0.114
0.250	6.06	2654	1240	1441	0.053
0.375	6.24	2733	545	2188	0.166

Table 6.67(b)

EXPERIMENTAL AND CALCULATED RESULTS FOR R_T = 0.375, HCHC-ALL, α = 15°

Re	F_{e1} (mm)	F_{e2} (mm)	F_{e3} (mm)	F_{e4} (mm)	F_{e5} (mm)	F_{Deu} (mm)
0.125	5.8	5.8	5.8	5.9	5.8	5.82
0.250	6.0	6.0	6.3	6.0	6.3	6.12
0.375	6.4	6.4	6.0	5.9	6.0	6.14

Table 6.68(a)

Re	F_{Deu} (mm)	F_{Deu} (N)	R_{De} (N)	F_{De} (N)	μ_e
0.125	5.82	2550	691	1859	0.114
0.250	6.12	2681	1240	1441	0.053
0.375	6.14	2689	545	2144	0.159

Table 6.68(b)

EXPERIMENTAL AND CALCULATED RESULTS FOR R_T = 0.375, CI-ALL, α = 15°

Re	F_{e1} (mm)	F_{e2} (mm)	F_{e3} (mm)	F_{e4} (mm)	F_{e5} (mm)	F_{Deu} (mm)
0.125	7.0	7.0	6.9	6.9	7.0	6.96
0.250	7.0	7.0	6.7	6.7	6.7	6.82
0.375	7.3	7.1	6.5	6.4	6.4	6.74

Table 6.69(a)

Re	F_{Deu} (mm)	F_{Deu} (N)	R_{De} (N)	F_{De} (N)	μ_e
0.125	6.92	3049	692	2357	0.189
0.250	6.82	2987	1240	1747	0.0961
0.375	6.74	2952	545	2407	0.203

Table 6.69(b)

EXPERIMENTAL AND CALCULATED RESULTS FOR R_T = 0.375, CI-BrL, α = 15°

Re	F_{e1} (mm)	F_{e2} (mm)	F_{e3} (mm)	F_{e4} (mm)	F_{e5} (mm)	F_{Deu} (mm)
0.125	8.0	8.0	8.0	8.0	8.0	8.00
0.250	11.2	11.2	11.1	11.1	11.2	11.16
0.375	12.8	12.7	12.8	12.8	12.7	12.76

Table 6.70(a)

Re	F_{Deu} (mm)	F_{Deu} (N)	R_{De} (N)	F_{De} (N)	μ_e
0.125	8.00	3504	1365	2139	0.075
0.250	11.16	4888	2449	2439	0.025
0.375	12.96	5589	1079	4514	0.182

Table 6.70(b)

EXPERIMENTAL AND CALCULATED RESULTS FOR R_T = 0.375, CI–CuL, α = 15°

Re	F_{e1} (mm)	F_{e2} (mm)	F_{e3} (mm)	F_{e4} (mm)	F_{e5} (mm)	F_{Deu} (mm)
0.125	6.3	6.3	6.4	6.4	6.3	6.34
0.250	7.0	6.9	6.9	6.9	6.9	6.92
0.375	7.2	7.0	7.3	7.3	7.4	7.24

Table 6.71(a)

Re	F_{Deu} (mm)	F_{Deu} (N)	R_{De} (N)	F_{De} (N)	μ_e
0.125	6.34	2777	797	1980	0.094
0.250	6.92	3031	1429	1602	0.042
0.375	7.94	3171	628	2543	0.169

Table 6.71(b)

EXPERIMENTAL AND CALCULATED RESULTS FOR R_T = 0.375, CI–SSL, α = 15°

Re	F_{e1} (mm)	F_{e2} (mm)	F_{e3} (mm)	F_{e4} (mm)	F_{e5} (mm)	F_{Deu} (mm)
0.125	13.0	13.1	13.0	13.1	13.0	13.04
0.250	18.3	18.2	18.2	18.3	18.3	18.26
0.375	23.3	23.2	23.2	23.3	23.3	23.26

Table 6.72(a)

Re	F_{Deu} (mm)	F_{Deu} (N)	R_{De} (N)	F_{De} (N)	μ_e
0.125	13.04	5712	1748	3964	0.072
0.250	18.26	7998	1834	6164	0.0725
0.375	23.26	10188	2275	7913	0.119

Table 6.72(b)

EXPERIMENTAL AND CALCULATED RESULTS FOR R_T = 0.25, NSOH-AL, α = 15°

Re	F_{e1} (mm)	F_{e2} (mm)	F_{e3} (mm)	F_{e4} (mm)	F_{e5} (mm)	F_{Deu} (mm)
0.083	6.0	6.1	5.4	5.5	5.5	5.70
0.166	6.5	6.2	5.5	5.0	5.3	5.70
0.250	6.7	6.5	5.2	5.4	5.0	5.76

Table 6.73(a)

Re	F_{Deu} (mm)	F_{Deu} (N)	R_{De} (N)	F_{De} (N)	μ_e
0.083	5.70	2497	691	1806	0.22
0.166	5.70	2497	1299	1198	0.089
0.250	5.76	2523	605	1918	0.235

Table 6.73(b)

EXPERIMENTAL AND CALCULATED RESULTS FOR R_T = 0.25, HCHC-AL, α = 15°

Re	F_{e1} (mm)	F_{e2} (mm)	F_{e3} (mm)	F_{e4} (mm)	F_{e5} (mm)	F_{Deu} (mm)
0.083	5.8	5.9	5.7	5.7	5.8	5.78
0.166	5.7	5.9	5.8	5.8	5.8	5.80
0.250	5.7	5.9	5.8	5.9	5.8	5.82

Table 6.74(a)

Re	F_{Deu} (mm)	F_{Deu} (N)	R_{De} (N)	F_{De} (N)	μ_e
0.083	5.78	2532	691	1841	0.228
0.166	5.80	2540	1299	1241	0.098
0.250	5.82	2549	605	1944	0.241

Table 6.74(b)

EXPERIMENTAL AND CALCULATED RESULTS FOR R_T = 0.25, NSOH-SS, α = 15°

Re	F_{e1} (mm)	F_{e2} (mm)	F_{e3} (mm)	F_{e4} (mm)	F_{e5} (mm)	F_{Deu} (mm)
0.083	8.6	8.7	8.5	8.7	8.7	8.64
0.166	12.6	12.7	12.5	12.7	12.7	12.64
0.250	15.7	15.8	15.7	15.8	15.8	15.76

Table 6.75(a)

Re	F_{Deu} (mm)	F_{Deu} (N)	R_{De} (N)	F_{De} (N)	μ_e
0.083	8.64	3784	2222	1562	0.019
0.166	12.64	5536	4175	1361	$1x10^{-6}$
0.250	15.76	6903	1943	5153	0.0812

Table 6.75 (b)

EXPERIMENTAL AND CALCULATED RESULTS FOR R_T = 0.25, HCHC-SS, α = 15°

Re	F_{e1} (mm)	F_{e2} (mm)	F_{e3} (mm)	F_{e4} (mm)	F_{e5} (mm)	F_{Deu} (mm)
0.083	8.8	8.8	8.8	8.9	8.8	8.78
0.166	12.5	12.6	12.6	12.7	12.7	12.62
0.250	15.8	15.8	15.7	15.7	15.8	15.76

Table 6.76(a)

Re	F_{Deu} (mm)	F_{Deu} (N)	R_{De} (N)	F_{De} (N)	μ_e
0.083	8.78	3846	2222	1624	0.023
0.166	12.62	5528	4175	1353	$1x10^{-6}$
0.250	15.76	6903	1943	4960	0.081

Table 6.76(b)

EXPERIMENTAL AND CALCULATED RESULTS FOR R_T = 0.25, NSOH-Br, α = 15°

Re	F_{e1} (mm)	F_{e2} (mm)	F_{e3} (mm)	F_{e4} (mm)	F_{e5} (mm)	F_{Deu} (mm)
0.083	5.8	5.7	5.8	5.7	5.7	5.74
0.166	8.1	8.0	7.8	7.9	7.9	7.98
0.250	9.0	9.0	8.3	8.2	8.3	8.56

Table 6.77(a)

Re	F_{Deu} (mm)	F_{Deu} (N)	R_{De} (N)	F_{De} (N)	μ_e
0.083	5.74	2514	1365	1149	$1x10^{-7}$
0.166	7.98	3495	2566	929	$5.7x10^{-8}$
0.250	8.56	3749	1194	2555	0.106

Table 6.77(b)

EXPERIMENTAL AND CALCULATED RESULTS FOR R_T = 0.25, HCHC-Br, α = 15°

Re	F_{e1} (mm)	F_{e2} (mm)	F_{e3} (mm)	F_{e4} (mm)	F_{e5} (mm)	F_{Deu} (mm)
0.083	5.6	5.7	5.8	5.7	5.8	5.72
0.166	7.5	7.7	7.8	7.9	7.8	7.74
0.250	8.9	8.4	8.4	9.0	8.7	8.68

Table 6.78(a)

Re	F_{Deu} (mm)	F_{Deu} (N)	R_{De} (N)	F_{De} (N)	μ_e
0.083	5.72	2505	1365	1140	$1.05x10^{-7}$
0.166	7.74	3390	2566	824	$5.6x10^{-8}$
0.250	8.68	3802	1194	2608	0.111

Table 6.78(b)

EXPERIMENTAL AND CALCULATED RESULTS FOR R_T = 0.25, NSOH-Cu, α = 15°

Re	F_{e1} (mm)	F_{e2} (mm)	F_{e3} (mm)	F_{e4} (mm)	F_{e5} (mm)	F_{Deu} (mm)
0.083	5.0	4.9	4.9	4.8	4.9	4.92
0.166	5.0	5.0	4.8	4.9	4.9	4.92
0.250	5.2	5.0	4.9	4.9	4.9	4.96

Table 6.79(a)

Re	F_{Deu} (mm)	F_{Deu} (N)	R_{De} (N)	F_{De} (N)	μ_e
0.083	4.92	2155	797	1358	0.091
0.166	4.92	2155	1497	658	$1x10^{-7}$
0.250	4.96	2173	697	1476	0.103

Table 6.79(b)

EXPERIMENTAL AND CALCULATED RESULTS FOR R_T = 0.25, HCHC-Cu, α = 15°

Re	F_{e1} (mm)	F_{e2} (mm)	F_{e3} (mm)	F_{e4} (mm)	F_{e5} (mm)	F_{Deu} (mm)
0.083	5.0	5.0	5.0	4.9	4.9	4.96
0.166	5.2	5.2	5.1	5.3	5.2	5.20
0.250	5.3	5.3	5.4	5.0	5.3	5.26

Table 6.80(a)

Re	F_{Deu} (mm)	F_{Deu} (N)	R_{De} (N)	F_{De} (N)	μ_e
0.083	4.96	2173	797	1376	0.0940
0.166	5.20	2278	1497	781	$8.7x10^{-6}$
0.250	5.26	2304	697	1607	0.126

Table 6.80(b)

EXPERIMENTAL AND CALCULATED RESULTS FOR R_T = 0.25, CI-AL, α = 15°

Re	F_{e1} (mm)	F_{e2} (mm)	F_{e3} (mm)	F_{e4} (mm)	F_{e5} (mm)	F_{Deu} (mm)
0.083	5.8	5.5	5.5	5.4	5.5	5.54
0.166	7.0	5.5	5.6	5.5	5.5	6.88
0.250	6.7	5.4	5.5	5.5	5.5.	6.82

Table 6.81(a)

Re	F_{Deu} (mm)	F_{Deu} (N)	R_{De} (N)	F_{De} (N)	μ_e
0.083	5.54	2427	692	1735	0.205
0.166	6.88	3013	1299	1714	0.193
0.250	6.82	2987	605	2382	0.341

Table 6.81(b)

EXPERIMENTAL AND CALCULATED RESULTS FOR R_T = 0.25, CI-Br, α = 15°

Re	F_{e1} (mm)	F_{e2} (mm)	F_{e3} (mm)	F_{e4} (mm)	F_{e5} (mm)	F_{Deu} (mm)
0.083	6.3	6.2	6.3	6.2	6.3	6.26
0.166	8.5	8.5	8.4	8.4	8.5	8.46
0.250	9.4	9.3	9.3	9.4	9.3	9.34

Table 6.82(a)

Re	F_{Deu} (mm)	F_{Deu} (N)	R_{De} (N)	F_{De} (N)	μ_e
0.083	6.26	2742	1365	1377	0.03
0.166	8.46	3706	2566	1140	$1x10^{-7}$
0.250	9.34	4091	1194	2897	0.140

Table 6.82(b)

EXPERIMENTAL AND CALCULATED RESULTS FOR R_T = 0.25, CI-Cu, α = 15°

Re	F_{e1} (mm)	F_{e2} (mm)	F_{e3} (mm)	F_{e4} (mm)	F_{e5} (mm)	F_{Deu} (mm)
0.083	5.7	5.1	5.3	5.3	5.2	5.32
0.166	6.0	5.3	5.3	5.2	5.3	5.42
0.250	7.5	5.3	5.3	5.3	5.2	5.72

Table 6.83(a)

Re	F_{Deu} (mm)	F_{Deu} (N)	R_{De} (N)	F_{De} (N)	μ_e
0.083	5.32	2330	797	1533	0.121
0.166	5.42	2374	1497	877	0.08
0.250	5.72	2505	697	1808	0.161

Table 6.83(b)

EXPERIMENTAL AND CALCULATED RESULTS FOR R_T = 0.25, CI-SS, α = 15°

Re	F_{e1} (mm)	F_{e2} (mm)	F_{e3} (mm)	F_{e4} (mm)	F_{e5} (mm)	F_{Deu} (mm)
0.083	9.7	9.6	9.8	9.7	9.7	9.70
0.166	13.3	13.3	13.4	13.2	13.4	13.32
0.250	16.5	16.4	16.5	16.5	16.4	16.46

Table 6.84(a)

Re	F_{Deu} (mm)	F_{Deu} (N)	R_{De} (N)	F_{De} (N)	μ_e
0.083	9.70	4249	1755	2494	0.053
0.166	13.32	5834	4584	1250	8×10^{-8}
0.250	16.46	7210	2358	4852	0.096

Table 6.84(b)

EXPERIMENTAL AND CALCULATED RESULTS FOR R_T = 0.25, NSOH-CuL, α = 15°

Re	F_{e1} (mm)	F_{e2} (mm)	F_{e3} (mm)	F_{e4} (mm)	F_{e5} (mm)	F_{Deu} (mm)
0.083	4.7	4.6	4.7	4.7	4.7	4.68
0.166	4.8	4.5	4.3	4.3	4.3	4.44
0.250	5.4	4.5	4.5	4.5	4.6	4.70

Table 6.85(a)

Re	F_{Deu} (mm)	F_{Deu} (N)	R_{De} (N)	F_{De} (N)	μ_e
0.083	4.68	2050	797	1253	0.0734
0.166	4.44	1945	1497	448	3.5×10^{-6}
0.250	4.70	2059	697	1364	0.0898

Table 6.85(b)

EXPERIMENTAL AND CALCULATED RESULTS FOR R_T = 0.25, HCHC-CuL, α = 15°

Re	F_{e1} (mm)	F_{e2} (mm)	F_{e3} (mm)	F_{e4} (mm)	F_{e5} (mm)	F_{Deu} (mm)
0.083	4.6	4.6	4.5	4.5	4.5	4.56
0.166	4.6	4.6	4.7	4.6	4.7	4.64
0.250	5.3	4.6	4.6	4.5	4.6	4.72

Table 6.86(a)

Re	F_{Deu} (mm)	F_{Deu} (N)	R_{De} (N)	F_{De} (N)	μ_e
0.083	4.56	1997	797	1200	0.065
0.166	4.64	2032	1497	535	3×10^{-6}
0.250	4.72	2067	697	1370	0.0856

Table 6.86(b)

EXPERIMENTAL AND CALCULATED RESULTS FOR R_T = 0.25, NSOH-BrL, α = 15°

Re	F_{e1} (mm)	F_{e2} (mm)	F_{e3} (mm)	F_{e4} (mm)	F_{e5} (mm)	F_{Deu} (mm)
0.083	5.7	5.8	5.7	5.7	5.7	5.72
0.166	7.3	7.3	7.4	7.2	7.3	7.30
0.250	8.2	8.1	8.1	8.2	8.1	8.14

Table 6.87(a)

Re	F_{Deu} (mm)	F_{Deu} (N)	R_{De} (N)	F_{De} (N)	μ_e
0.083	5.72	2505	1365	1140	1.05×10^{-7}
0.166	7.30	3197	2566	631	5.6×10^{-8}
0.250	8.14	3565	1194	2371	0.088

Table 6.87(b)

EXPERIMENTAL AND CALCULATED RESULTS FOR R_T = 0.25, HCHCBrL, α = 15°

Re	F_{e1} (mm)	F_{e2} (mm)	F_{e3} (mm)	F_{e4} (mm)	F_{e5} (mm)	F_{Deu} (mm)
0.083	5.6	5.7	5.6	5.7	5.7	5.66
0.166	7.3	7.2	7.3	7.3	7.2	7.26
0.250	8.1	8.2	8.2	8.1	8.1	8.14

Table 6.88(a)

Re	F_{Deu} (mm)	F_{Deu} (N)	R_{De} (N)	F_{De} (N)	μ_e
0.083	5.66	2479	1365	1114	1×10^{-7}
0.166	7.26	3180	2566	614	5×10^{-8}
0.250	8.14	3565	1194	2371	0.088

Table 6.88(b)

EXPERIMENTAL AND CALCULATED RESULTS FOR R_T = 0.25, NSOH-ALL, α = 15°

Re	F_{e1} (mm)	F_{e2} (mm)	F_{e3} (mm)	F_{e4} (mm)	F_{e5} (mm)	F_{Deu} (mm)
0.083	5.2	5.3	5.3	5.5	5.4	5.34
0.166	5.5	5.4	5.3	5.4	5.4	5.40
0.250	5.3	5.5	5.4	5.4	5.5	5.42

Table 6.89(a)

Re	F_{Deu} (mm)	F_{Deu} (N)	R_{De} (N)	F_{De} (N)	μ_e
0.083	5.34	2339	691	1648	0.186
0.166	5.40	2365	1299	1066	0.064
0.250	5.42	2374	605	1769	0.203

Table 6.89 (b)

EXPERIMENTAL AND CALCULATED RESULTS FOR R_T = 0.25, HCHC-ALL, α = 15°

Re	F_{e1} (mm)	F_{e2} (mm)	F_{e3} (mm)	F_{e4} (mm)	F_{e5} (mm)	F_{Deu} (mm)
0.083	5.5	5.3	5.4	5.4	5.3	5.38
0.166	5.4	5.4	5.5	5.4	5.4	5.42
0.250	5.4	5.5	5.5	5.4	5.5	5.46

Table 6.90(a)

Re	F_{Deu} (mm)	F_{Deu} (N)	R_{De} (N)	F_{De} (N)	μ_e
0.083	5.38	2356	691	1665	0.19
0.166	5.42	2374	1299	1299	0.109
0.250	5.46	2392	605	1787	0.207

Table 6.90(b)

EXPERIMENTAL AND CALCULATED RESULTS FOR R_T = 0.25, NSOH-SSL, α = 15°

Re	F_{e1} (mm)	F_{e2} (mm)	F_{e3} (mm)	F_{e4} (mm)	F_{e5} (mm)	F_{Deu} (mm)
0.083	8.7	8.6	8.6	8.6	8.6	8.62
0.166	12.2	12.2	12.3	12.3	12.3	12.26
0.250	15.2	15.2	15.2	15.2	15.2	15.20

Table 6.91(a)

Re	F_{Deu} (mm)	(N)	R_{De} (N)	F_{De} (N)	μ_e
0.083	8.62	3776	2222	1554	0.018
0.166	12.26	5370	4175	1195	$1x10^{-8}$
0.250	15.20	6658	1943	4715	0.069

Table 6.91(b)

EXPERIMENTAL AND CALCULATED RESULTS FOR R_T = 0.25, HCHC-SSL, α = 15°

Re	F_{e1} (mm)	F_{e2} (mm)	F_{e3} (mm)	F_{e4} (mm)	F_{e5} (mm)	F_{Deu} (mm)
0.083	8.7	8.7	8.7	8.7	8.7	8.70
0.166	12.3	12.2	12.2	12.2	12.2	12.22
0.250	15.3	15.2	15.3	15.2	15.2	15.24

Table 6.92(a)

Re	F_{Deu} (mm)	(N)	R_{De} (N)	F_{De} (N)	μ_e
0.083	8.70	3811	2222	1589	0.021
0.166	12.22	5352	4175	1177	10^{-8}
0.250	15.24	6675	1943	4732	0.070

Table 6.92(b)

EXPERIMENTAL AND CALCULATED RESULTS FOR R_T = 0.25, NSOH-ALL, α = 15°

Re	F_{e1} (mm)	F_{e2} (mm)	F_{e3} (mm)	F_{e4} (mm)	F_{e5} (mm)	F_{Deu} (mm)
0.083	5.5	5.5	5.4	5.5	5.5	5.48
0.166	5.9	5.2	5.4	5.2	5.4	5.52
0.250	5.7	5.1	5.0	5.0	5.0	5.16

Table 6.93(a)

Re	F_{Deu} (mm)	F_{Deu} (N)	R_{De} (N)	F_{De} (N)	μ_e
0.083	5.48	2400	692	1708	0.199
0.166	5.52	2418	1299	1119	0.074
0.250	5.16	2260	605	1655	0.179

Table 6.93(b)

EXPERIMENTAL AND CALCULATED RESULTS FOR R_T = 0.25, CI-BrL, α = 15°

Re	F_{e1} (mm)	F_{e2} (mm)	F_{e3} (mm)	F_{e4} (mm)	F_{e5} (mm)	F_{Deu} (mm)
0.083	6.0	5.9	6.0	6.1	5.9	5.98
0.166	8.2	8.2	8.3	8.2	8.3	8.54
0.250	8.8	8.7	8.8	8.8	8.7	8.76

Table 6.94(a)

Re	F_{Deu} (mm)	F_{Deu} (N)	R_{De} (N)	F_{De} (N)	μ_e
0.083	5.98	2619	1365	1254	2.5×10^{-7}
0.166	8.54	3741	2566	1175	1×10^{-7}
0.250	8.76	3837	1194	2643	0.115

Table 6.94(b)

EXPERIMENTAL AND CALCULATED RESULTS FOR R_T = 0.25, CI-CuL, α = 15°

Re	F_{e1} (mm)	F_{e2} (mm)	F_{e3} (mm)	F_{e4} (mm)	F_{e5} (mm)	F_{Deu} (mm)
0.083	5.8	5.2	5.1	5.2	5.2	5.30
0.166	5.8	5.4	5.4	5.3	5.3	5.44
0.250	5.3	5.2	5.3	5.3	5.3	5.28

Table 6.95(a)

Re	F_{Deu} (mm)	F_{Deu} (N)	R_{De} (N)	F_{De} (N)	μ_e
0.083	5.30	2321	797	1524	0.12
0.166	5.44	2383	1497	886	0.010
0.250	5.28	2313	697	1616	0.127

Table 6.95(b)

EXPERIMENTAL AND CALCULATED RESULTS FOR R_T = 0.25, CI-SSL, α = 15°

Re	F_{e1} (mm)	F_{e2} (mm)	F_{e3} (mm)	F_{e4} (mm)	F_{e5} (mm)	F_{Deu} (mm)
0.083	9.6	9.7	9.6	9.6	9.7	9.64
0.166	13.0	13.0	13.1	13.1	13.0	13.04
0.250	15.2	15.2	15.1	15.3	15.2	15.20

Table 6.96(a)

Re	F_{Deu} (mm)	F_{Deu} (N)	R_{De} (N)	F_{De} (N)	μ_e
0.083	9.64	4222	1755	2467	0.0512
0.166	13.04	5712	4584	1128	2.1×10^{-6}
0.250	15.20	6658	2358	4300	0.069

Table 6.96(b)

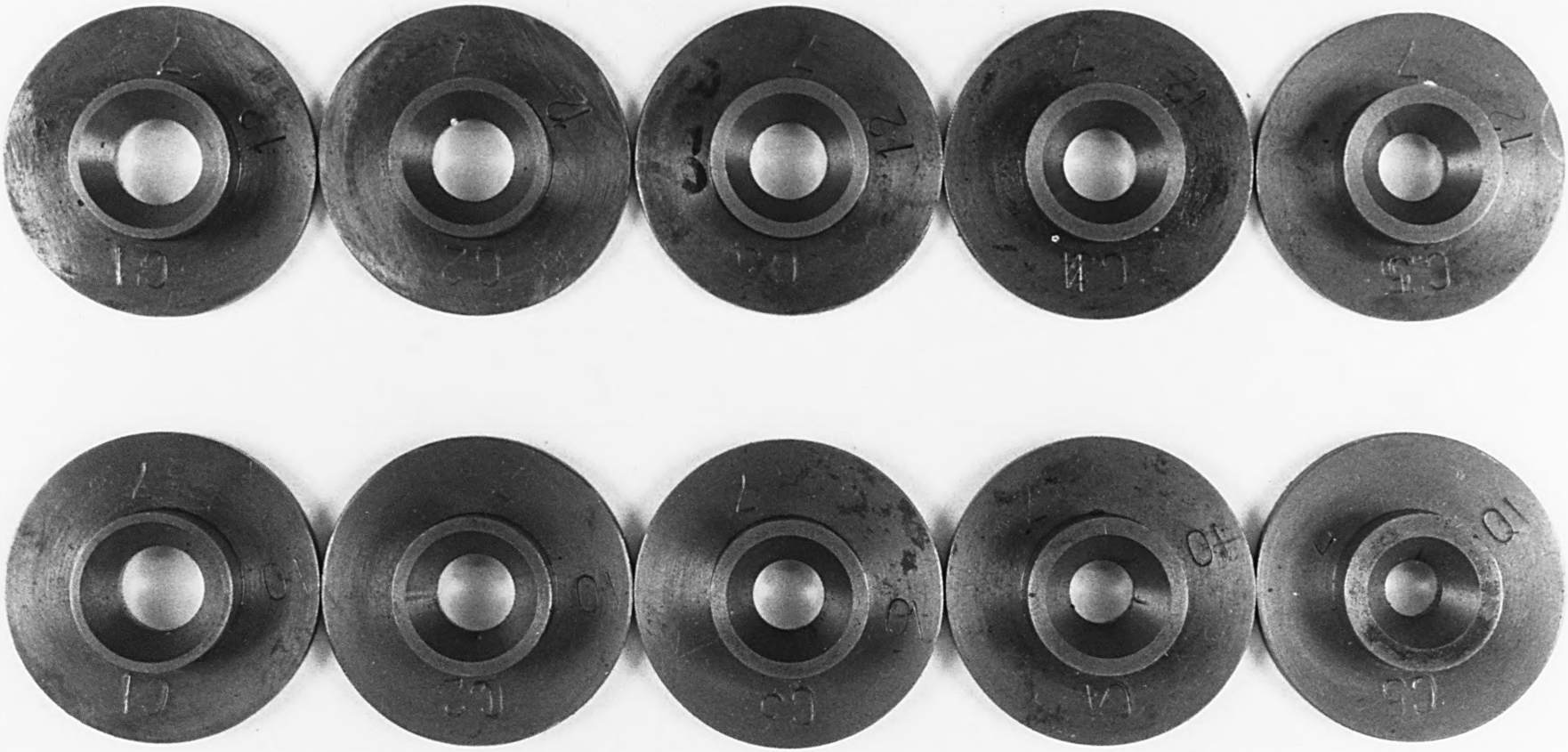

Fig.(6.27)

SETS OF 7° SEMI-ANGLE CAST IRON ELEMENTAL DIES
FOR 0.250 & 0.375 TOTAL FRACTIONAL REDUCTIONS





Fig.(6.29)

SETS OF 7° SEMI-ANGLE HCHC ELEMENTAL DIES
FOR 0.250 & 0.375 TOTAL FRACTIONAL REDUCTIONS

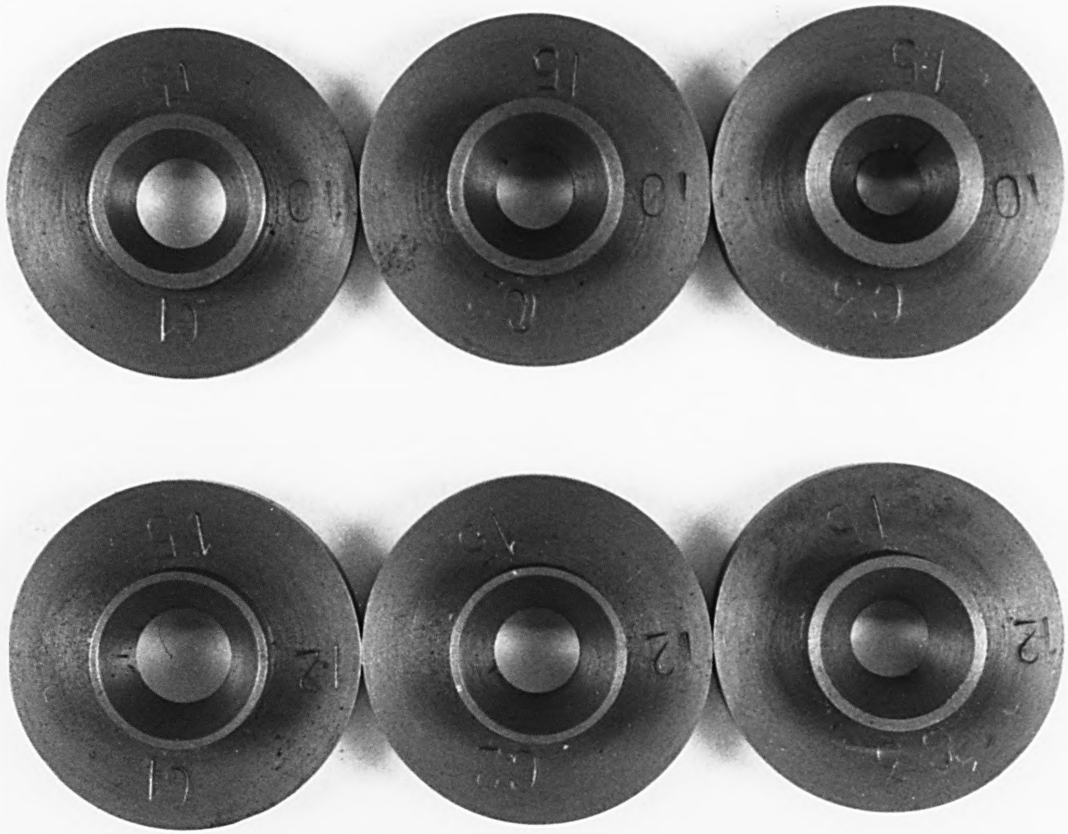

Fig.(6.30)

SETS OF 15° SEMI-ANGLE CAST IRON ELEMENTAL DIES
FOR 0.250 & 0.375 TOTAL FRACTIONAL REDUCTIONS



Fig.(6.31)

SETS OF 15° SEMI-ANGLE NSOH ELEMENTAL DIES
FOR 0.250 & 0.375 TOTAL FRACTIONAL REDUCTIONS

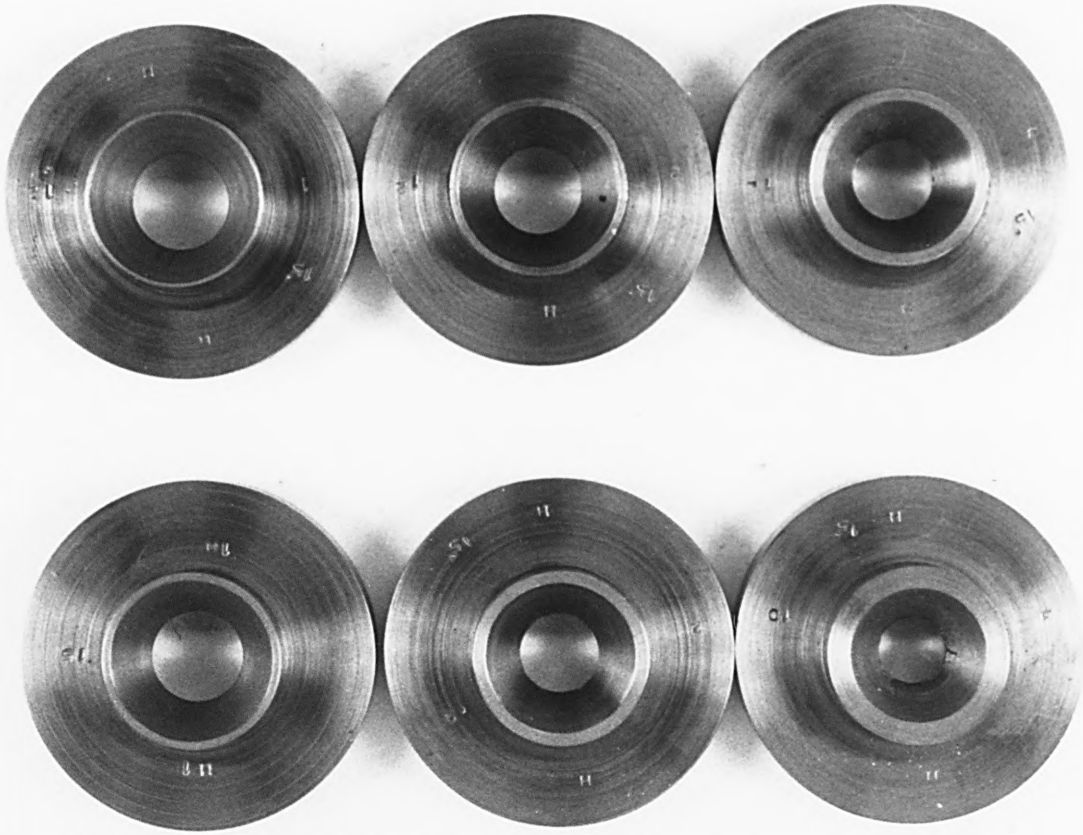

Fig.(6.32)

SETS OF 15° SEMI-ANGLE HCHC ELEMENTAL DIES
FOR 0.250 & 0.375 TOTAL FRACTIONAL REDUCTIONS

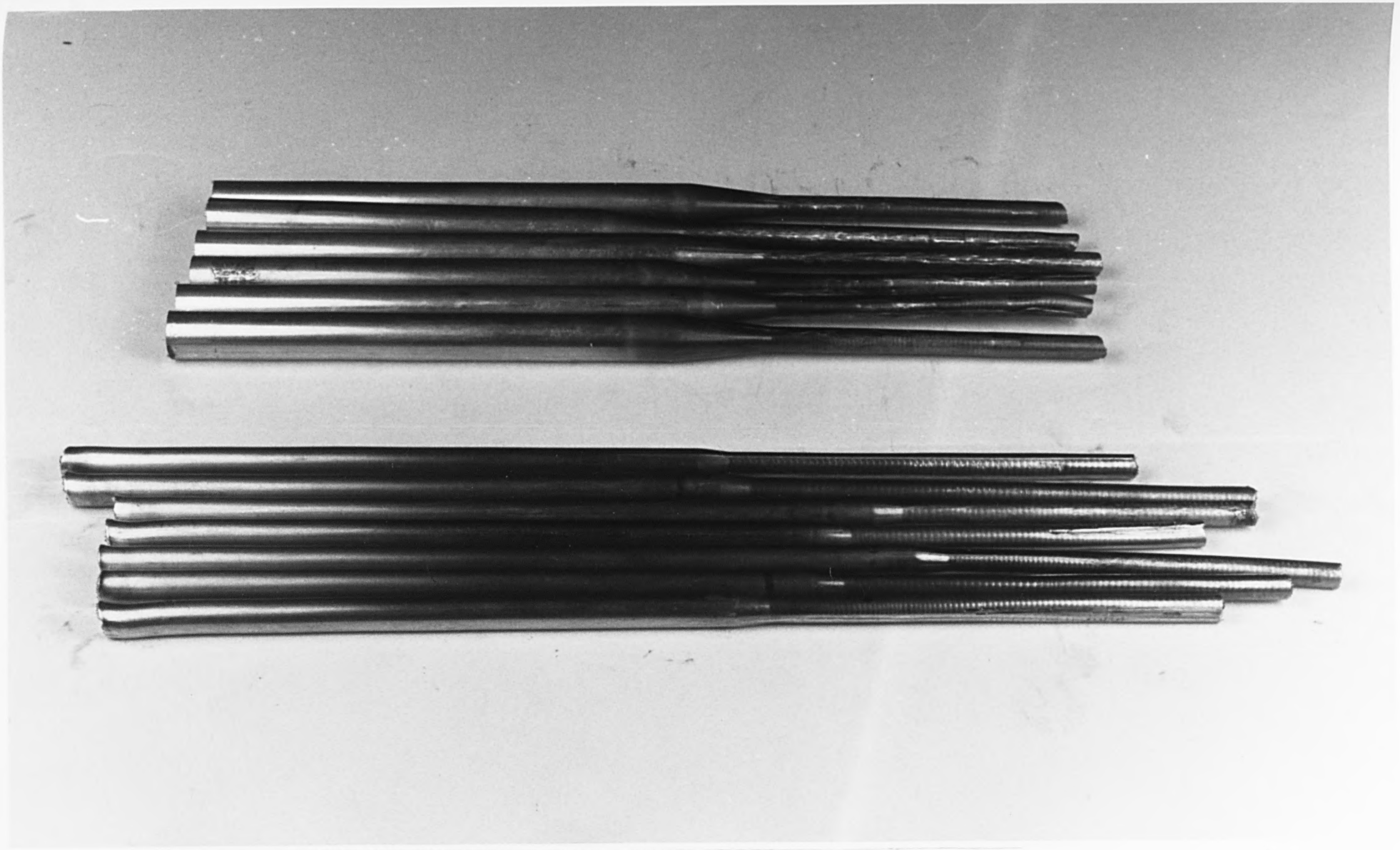

Fig.(6.33)

TYPICAL SETS OF NEW AND USED SPECIMENS

Curves of Elemental Radial Strain Against Elemental Fractional Reduction along Working Face of a Cast Iron Die (α = 7° and R_T = 0.375) Under Different Tribological Treatment
Aluminium Specimen Drawn at 3 cm/min

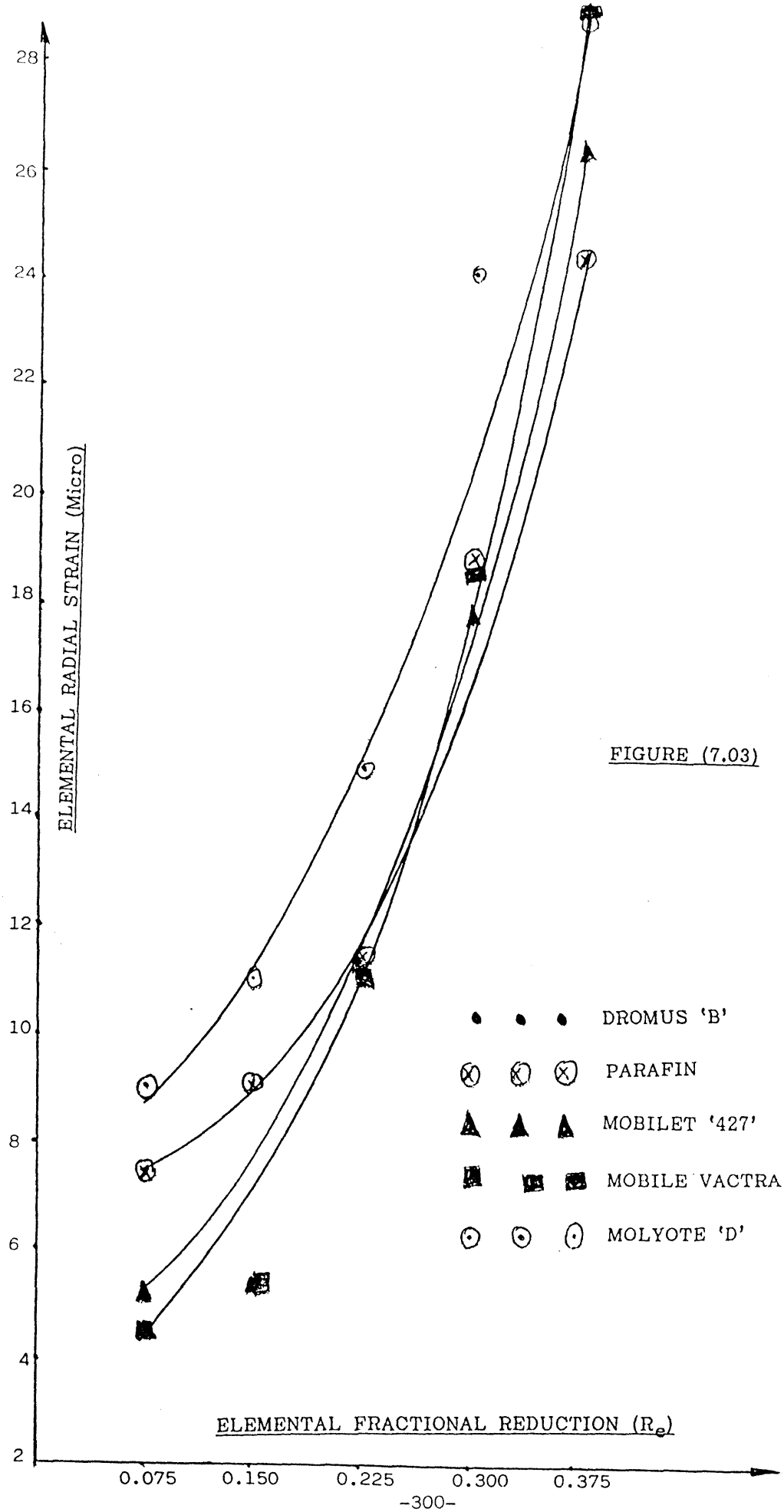

FIGURE (7.03)

Curves of Elemental Radial Strain Against Elemental Fractional Reduction along Working Face of a Cast Iron Die with $\alpha = 7^{\circ}$ Total Fractional Reduction of 0.375 for Different Tribological Treatment Aluminium Specimen Drawn at 2 cm/min

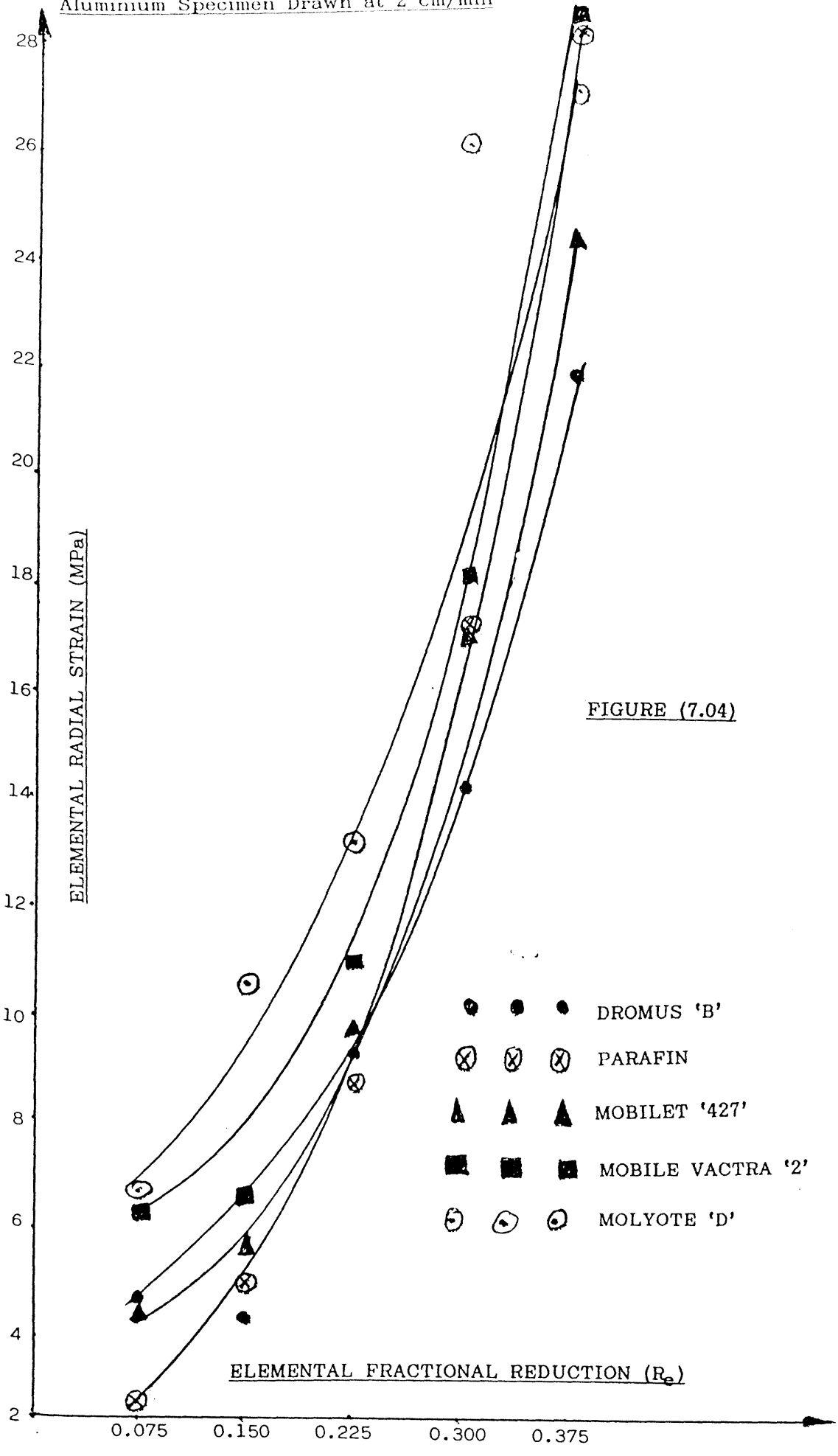

FIGURE (7.04)

Curves of Elemental Radial Pressure Against Elemental Fractional Reduction along Working Face of a Cast Iron Die with 7° Semi-Angle and Total Fractional Reduction of 0.375 for Different Tribological Treatment
Aluminium Specimen Drawn at 2 cm/min

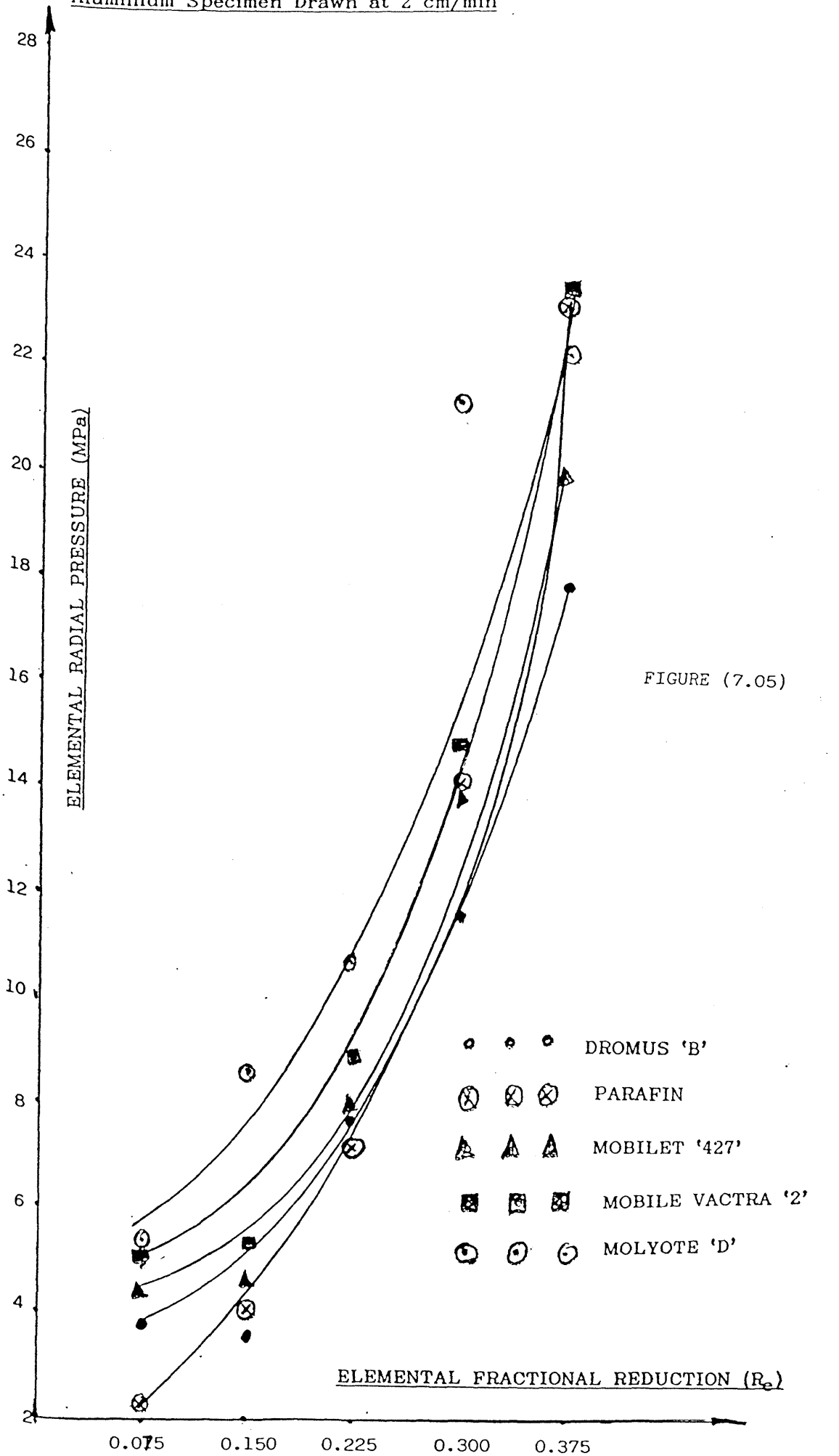

FIGURE (7.05)

Curves of Elemental Radial Pressure Against Elemental Fractional Reduction along Working Face of a Cast Iron Die with $\alpha = 7^{\circ}$ Total Fractional Reduction of 0.375 for Different Tribological Treatment
Aluminium Specimen Drawn at 3 cm/min

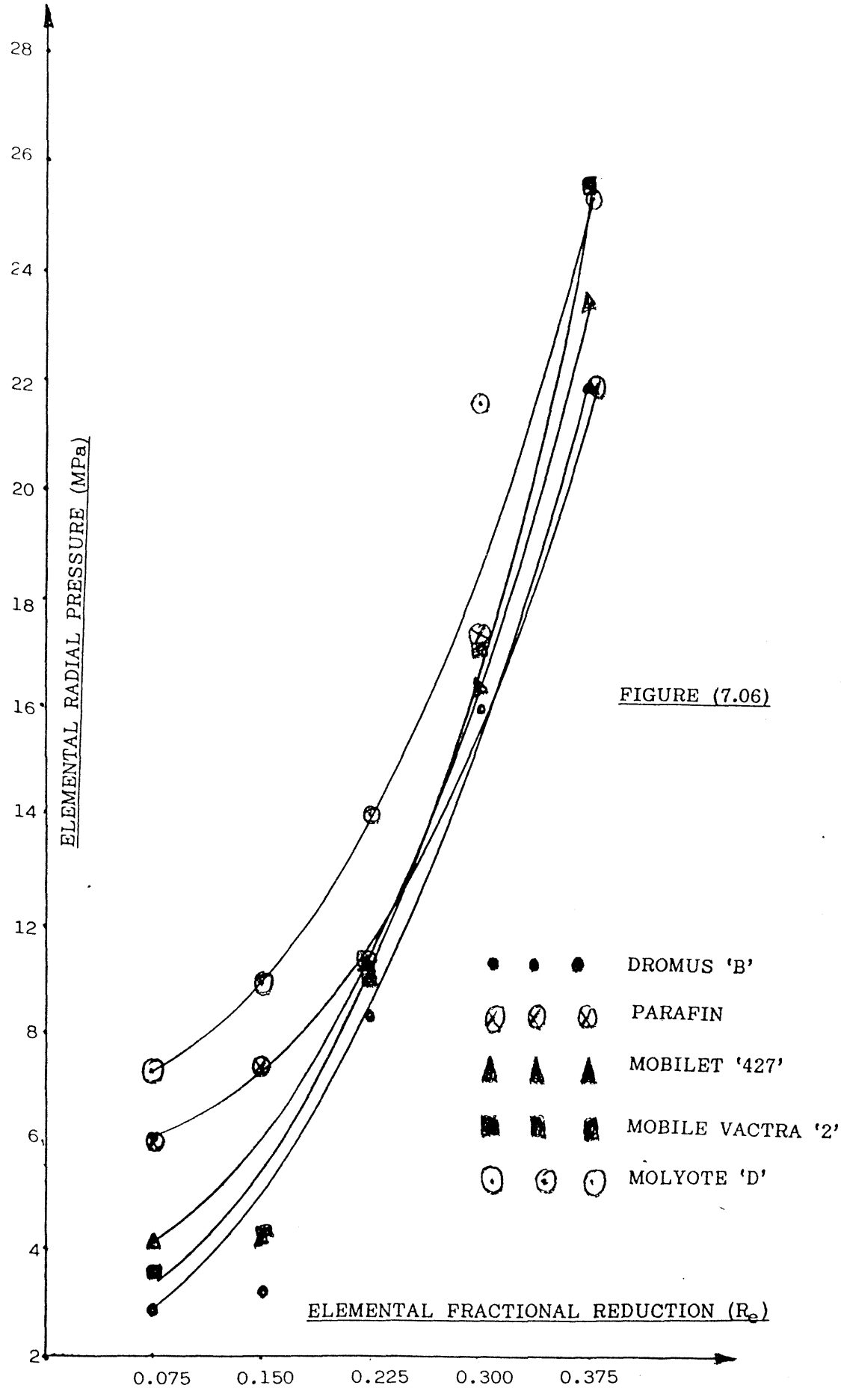

FIGURE (7.06)

Curves of Elemental Frictional Force Against Elemental Fractional Reduction along Working Faces of Proto-Dies with 7° Semi-Angle
(Aluminium Specimen with Dromus As Lubricant)

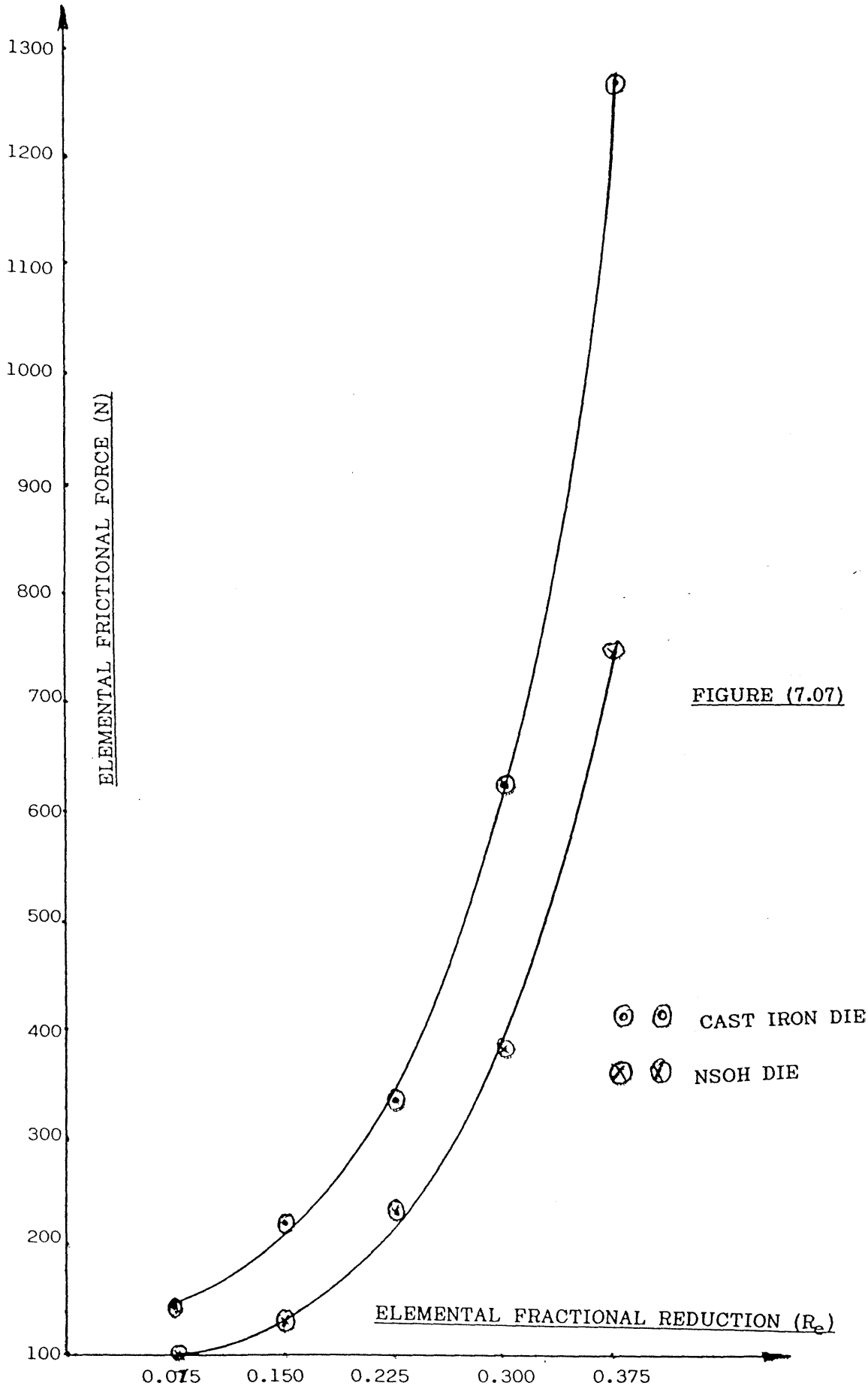

FIGURE (7.07)

CALIBRATION RESULTS AT Re = 0.075

PRESSURE	STRAIN GAUGE READINGS (Micro)				
lb/in^2	ϵ_{r1}	ϵ_{r2}	ϵ_{r3}	ϵ_{r4}	ϵ_{rav}
200	1.40	1.50	1.00	1.30	1.65
400	3.00	3.00	2.60	2.80	3.54
600	4.50	4.50	4.20	4.40	4.40
800	6.10	6.20	5.80	6.00	6.03
1000	7.80	7.80	7.30	7.60	7.63
1200	9.30	9.40	9.00	9.30	9.25
1400	11.00	11.00	10.50	10.90	10.85
1600	12.60	12.70	12.10	12.30	12.43
1800	14.20	14.20	13.8	14.10	14.08
2000	15.70	15.90	15.40	15.70	15.68
2200	17.50	17.40	17.10	17.20	17.24
2400	19.00	19.00	18.70	18.80	18.88
2600	20.60	20.70	20.30	20.40	20.50
2800	22.30	22.20	21.9	22.00	22.10
3000	23.90	24.00	23.4	23.70	23.75

Table (7.01)

CALIBRATION RESULTS AT Re = 0.150

PRESSURE	STRAIN GAUGE READINGS (Micro)				
lb/in^2	ϵ_{r1}	ϵ_{r2}	ϵ_{r3}	ϵ_{r4}	ϵ_{rav}
200	1.50	0.60	1.30	1.40	1.2
400	3.10	2.30	2.80	2.90	2.78
600	4.50	3.90	4.30	4.50	4.30
800	6.20	5.40	5.90	6.10	5.90
1000	7.70	7.10	7.50	7.70	7.50
1200	9.50	8.70	9.20	9.30	9.18
1400	11.00	10.30	10.80	10.80	10.73
1600	12.70	11.90	12.40	12.50	12.38
1800	14.40	13.60	14.10	14.30	14.10
2000	16.00	15.30	15.50	15.70	15.63
2200	17.80	16.90	17.30	17.40	17.35
2400	19.20	18.60	18.90	19.00	18.93
2600	20.80	20.30	20.40	20.60	20.53
2800	22.50	21.90	22.20	22.20	22.20
3000	24.30	23.70	23.90	23.90	23.95

Table (7.02)

CALIBRATION RESULTS AT Re = 0.225

PRESSURE	STRAIN GAUGE READINGS (Micro)				
lb/in^2	ϵ_{r1}	ϵ_{r2}	ϵ_{r3}	ϵ_{r4}	ϵ_{rav}
200	1.30	1.50	1.30	1.10	1.28
400	2.90	3.20	2.80	3.10	3.00
600	4.60	4.80	4.50	4.70	4.65
800	6.20	6.50	6.00	6.10	6.20
1000	7.90	8.10	7.60	7.80	7.85
1200	9.40	9.70	9.20	9.40	9.43
1400	11.00	11.30	10.80	10.90	11.00
1600	12.60	13.10	12.50	12.60	12.70
1800	14.20	14.40	14.20	14.30	14.28
2000	15.90	16.40	15.90	16.00	16.05
2200	17.50	18.00	17.50	17.60	17.25
2400	19.10	19.60	19.20	19.20	19.28
2600	20.40	21.20	20.70	20.80	20.78
2800	22.40	22.90	22.50	22.60	22.60
3000	24.10	24.60	24.10	24.30	24.28

Table (7.03)

CALIBRATION RESULTS AT Re = 0.300

PRESSURE	STRAIN GAUGE READINGS (Micro)				
lb/in^2	ϵ_{r1}	ϵ_{r2}	ϵ_{r3}	ϵ_{r4}	ϵ_{rav}
200	1.40	1.20	1.30	1.50	1.35
400	3.10	2.90	2.80	3.00	2.95
600	4.50	4.50	4.30	4.50	4.45
800	6.20	6.10	5.90	6.10	6.08
1000	7.80	7.60	7.40	7.70	7.63
1200	9.30	9.10	9.00	9.30	9.20
1400	10.90	10.80	10.50	10.80	10.75
1600	12.40	12.50	12.10	12.50	12.38
1800	14.10	14.00	13.80	14.20	14.03
2000	15.70	15.60	15.40	15.70	15.60
2200	17.40	17.20	17.10	17.30	17.25
2400	19.00	18.80	18.60	18.90	18.83
2600	20.50	20.30	20.20	20.50	20.38
2800	22.10	21.90	21.80	22.10	21.98
3000	23.70	23.40	23.40	23.70	23.55

Table (7.04)

CALIBRATION RESULTS AT Re = 0.375

PRESSURE	STRAIN GAUGE READINGS (Micro)				
lb/in^2	ϵ_{r1}	ϵ_{r2}	ϵ_{r3}	ϵ_{r4}	ϵ_{rav}
200	2.90	1.40	1.30	1.10	1.68
400	4.30	2.90	2.70	2.50	3.10
600	5.90	4.50	4.30	4.10	4.70
800	7.50	5.90	5.70	5.50	6.15
1000	9.10	9.00	7.20	6.90	9.77
1200	10.70	10.50	8.70	8.50	9.60
1400	12.20	12.00	10.30	10.20	11.18
1600	13.80	13.60	11.80	11.60	12.70
1800	15.40	15.00	13.30	13.10	14.20
2000	16.70	16.50	14.90	14.60	15.68
2200	18.40	18.10	16.50	16.20	17.30
2400	20.00	19.50	18.00	17.70	18.80
2600	21.50	21.00	19.40	19.20	20.28
2800	23.00	22.60	20.90	20.70	21.80
3000	24.50	24.00	22.60	22.30	23.35

Table (7.05)

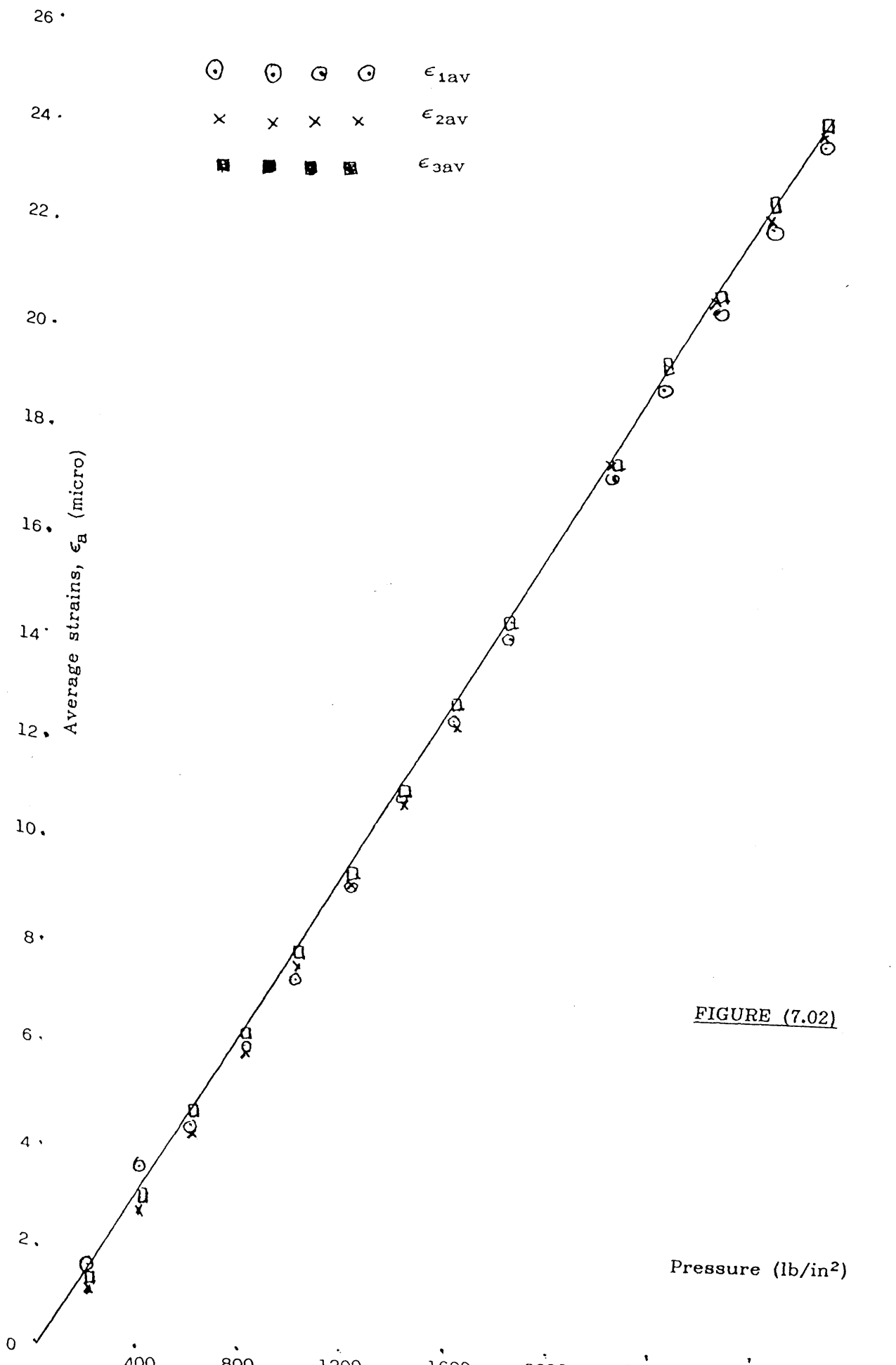
ϵ_{1av}
ϵ_{2av}
ϵ_{3av}
Average strains, ϵ_a (micro)
26
24
22
20
18
16
14
12
10
8
6
4
2
0
400
800
1200
1600
2000
2400
2800
3200
Pressure (lb/in²)

FIGURE (7.02)

Gradient $= \frac{24}{3000} = 8 \times 10^{-3}$ (FIGURE (7.02))

$$y = mx + c$$

From the graph $c = 0$

We want $P = m\epsilon_a + c$

m in this case $= \frac{1}{8 \times 10^{-3}}$

$\therefore \quad P = 125\ \epsilon_a\ (lb/in^2)$

But $1\ lb/in^2 = 6498.76\ N/m^2$

$\therefore \quad P = 125 \times 6498.76\ \epsilon\ (N/m^2)$

$\therefore \quad P = \frac{125 \times 6498.76}{1 \times 10^{-6}}\ \epsilon$

$$= \underline{0.81235\ \epsilon\ MPa} \qquad (7.6)$$

EXPERIMENTAL RESULTS FOR R_T = 0.375

α = 7° SPECIMEN ALUMINIUM ALLOY, DRAWING SPEED: 2 cm/min
TRIBOLOGICAL TREATMENT : LUBRICATED WITH MOLYKOTED

Re	ϵ_{r1}	ϵ_{r2}	ϵ_{r3} (micros)	ϵ_{r4}	ϵ_{rav}	P_e (MPa)
0.075	12.3	4.0	5.1	5.4	6.7	5.44
0.150	14.5	9.1	9.4	9.4	10.6	8.61
0.225	14.9	12.0	12.8	13.0	13.18	10.71
0.300	24.0	26.4	25.4	25.2	26.25	21.32
0.375	27.3	27.2	27.1	27.1	27.18	22.10

Table (7.06)

EXPERIMENTAL RESULTS FOR R_T = 0.375

α = 7° SPECIMEN ALUMINIUM ALLOY, DRAWING SPEED: 3 cm/min
TRIBOLOGICAL TREATMENT : LUBRICATED WITH MOLYKOTED

Re	ϵ_{r1}	ϵ_{r2}	ϵ_{r3} (micros)	ϵ_{r4}	ϵ_{rav}	P_e (MPa)
0.075	8	10	10	8	9.0	7.31
0.150	10	12	11	11	11.0	8.94
0.225	11	16	15	17	14.75	11.98
0.300	24	25	24	23	24.0	19.50
0.375	26	29	30	30	28.75	23.36

Table (7.07)

EXPERIMENTAL RESULTS FOR R_T = 0.375

α = 7° SPECIMEN ALUMINIUM ALLOY, DRAWING SPEED: 4 cm/min
TRIBOLOGICAL TREATMENT : LUBRICATED WITH MOLYKOTED

Re	ϵ_{r1}	ϵ_{r2}	ϵ_{r3} (micros)	ϵ_{rav}	P_e (MPa)
0.075	2.5	2.3	2.4	2.40	1.95
0.150	5.8	5.7	5.7	5.73	4.66
0.225	10.0	11.4	10.7	10.70	8.69
0.300	26	27.7	27.5	27.07	21.99
0.375	30	30	30.2	30.10	24.43

Table (7.08)

EXPERIMENTAL RESULTS FOR R_T = 0.375

α = 7° SPECIMEN ALUMINIUM ALLOY, DRAWING SPEED: 2 cm/min
TRIBOLOGICAL TREATMENT : LUBRICATED WITH PARAFFIN

Re	ϵ_{r1}	ϵ_{r2}	ϵ_{r3} (micros)	ϵ_{rav}	P_e (MPa)
0.075	2.7	2.9	2.8	2.8	2.28
0.150	5.0	5.2	5.0	5.1	4.12
0.225	8.7	9.3	8.5	8.83	7.17
0.300	17.8	17.0	17.5	17.4	14.16
0.375	29.5	27.5	28.2	28.4	23.1

Table (7.09)

EXPERIMENTAL RESULTS FOR R_T = 0.375

α = 7° SPECIMEN ALUMINIUM ALLOY, DRAWING SPEED: 3 cm/min
TRIBOLOGICAL TREATMENT : LUBRICATED WITH PARAFFIN

Re	ϵ_{r1}	ϵ_{r2}	ϵ_{r3} (micros)	ϵ_{rav}	P_e (MPa)
0.075	7.4	7.5	7.3	7.4	6.01
0.150	9.0	9.0	9.2	9.1	7.37
0.225	11.3	11.5	11.5	11.4	8.29
0.300	18.8	18.7	18.8	18.77	15.25
0.375	25.0	23.7	24.2	24.3	19.74

Table (7.10)

EXPERIMENTAL RESULTS FOR R_T = 0.375

α = 7° SPECIMEN ALUMINIUM ALLOY, DRAWING SPEED: 2 cm/min
TRIBOLOGICAL TREATMENT : LUBRICATED WITH MOBILET "427"

Re	ϵ_{r1}	ϵ_{r2}	ϵ_{r3} (micros)	ϵ_{rav}	P_e (MPa)
0.075	5.4	5.7	5.4	5.5	4.47
0.150	5.5	5.9	5.8	5.73	4.66
0.225	9.4	10.3	9.8	9.83	7.99
0.300	16.6	17.4	17.2	17.10	13.87
0.350	24.5	24.5	24.6	24.53	19.93

Table (7.11)

EXPERIMENTAL RESULTS FOR R_T = 0.375

α = 7° SPECIMEN ALUMINIUM ALLOY, DRAWING SPEED: 3 cm/min
TRIBOLOGICAL TREATMENT : LUBRICATED WITH MOBILET "427"

Re	ϵ_{r1}	ϵ_{r2}	ϵ_{r3} (micros)	ϵ_{rav}	P_e (MPa)
0.075	5.2	5.2	5.1	5.17	4.20
0.150	5.0	5.4	5.4	5.27	4.28
0.225	10.2	11.6	12.2	11.33	9.20
0.300	17.6	18.0	17.6	17.73	14.40
0.375	25.4	27.6	26.0	26.33	21.39

Table (7.12)

EXPERIMENTAL RESULTS FOR R_T = 0.375

α = 7° SPECIMEN ALUMINIUM ALLOY, DRAWING SPEED: 2 cm/min
TRIBOLOGICAL TREATMENT : LUBRICATED WITH VACTRA "2"

Re	ϵ_{r1}	ϵ_{r2}	ϵ_{r3} (micros)	ϵ_{rav}	P_e (MPa)
0.075	6.6	6.7	5.8	6.37	5.18
0.150	6.0	7.0	6.9	6.63	5.39
0.225	10.9	11.0	11.1	11.00	8.94
0.300	19.2	17.4	18.2	18.26	14.83
0.375	29.5	28.0	28.8	28.77	23.37

Table (7.13)

EXPERIMENTAL RESULTS FOR R_T = 0.375

α = 7° SPECIMEN ALUMINIUM ALLOY, DRAWING SPEED: 3 cm/min
TRIBOLOGICAL TREATMENT : LUBRICATED WITH VACTRA "2"

Re	ϵ_{r1}	ϵ_{r2}	ϵ_{r3} (micros)	ϵ_{rav}	P_e (MPa)
0.075	4.3	4.6	4.5	4.47	3.63
0.150	5.2	5.2	5.3	5.23	4.25
0.225	10.6	11.7	10.9	11.10	8.99
0.300	18.5	18.4	18.5	18.47	15.00
0.375	29.3	28.8	28.7	28.93	23.50

Table (7.14)

EXPERIMENTAL RESULTS FOR R_T = 0.375

α = 7° SPECIMEN ALUMINIUM ALLOY, DRAWING SPEED: 3 cm/min
TRIBOLOGICAL TREATMENT : LUBRICATED WITH DROMUS "B"

Re	ϵ_{r1}	ϵ_{r2}	ϵ_{r3} (micros)	ϵ_{rav}	P_e (MPa)
0.075	5.2	5.2	5.1	5.17	4.20
0.150	5.0	5.4	5.4	5.27	4.28
0.225	10.2	11.6	12.2	11.33	9.20
0.300	17.6	18. 0	17.6	17.73	14.40
0.375	25.4	27.6	26.0	26.33	21.39

Table (7.15)

EXPERIMENTAL RESULTS FOR R_T = 0.375

α = 7° SPECIMEN ALUMINIUM ALLOY, DRAWING SPEED: 3 cm/min
TRIBOLOGICAL TREATMENT : LUBRICATED WITH DROMUS "B"

Re	ϵ_{r1}	ϵ_{r2}	ϵ_{r3} (micros)	ϵ_{rav}	P_e (MPa)
0.075	3.70	3.3	3.6	3.53	2.87
0.150	4.6	3.5	3.8	3.97	3.23
0.225	11.0	9.4	10.2	10.2	8.29
0.300	17.0	17.0	17.2	17.1	13.87
0.375	24.0	24.9	24.3	24.4	19.82

Table (7.16)

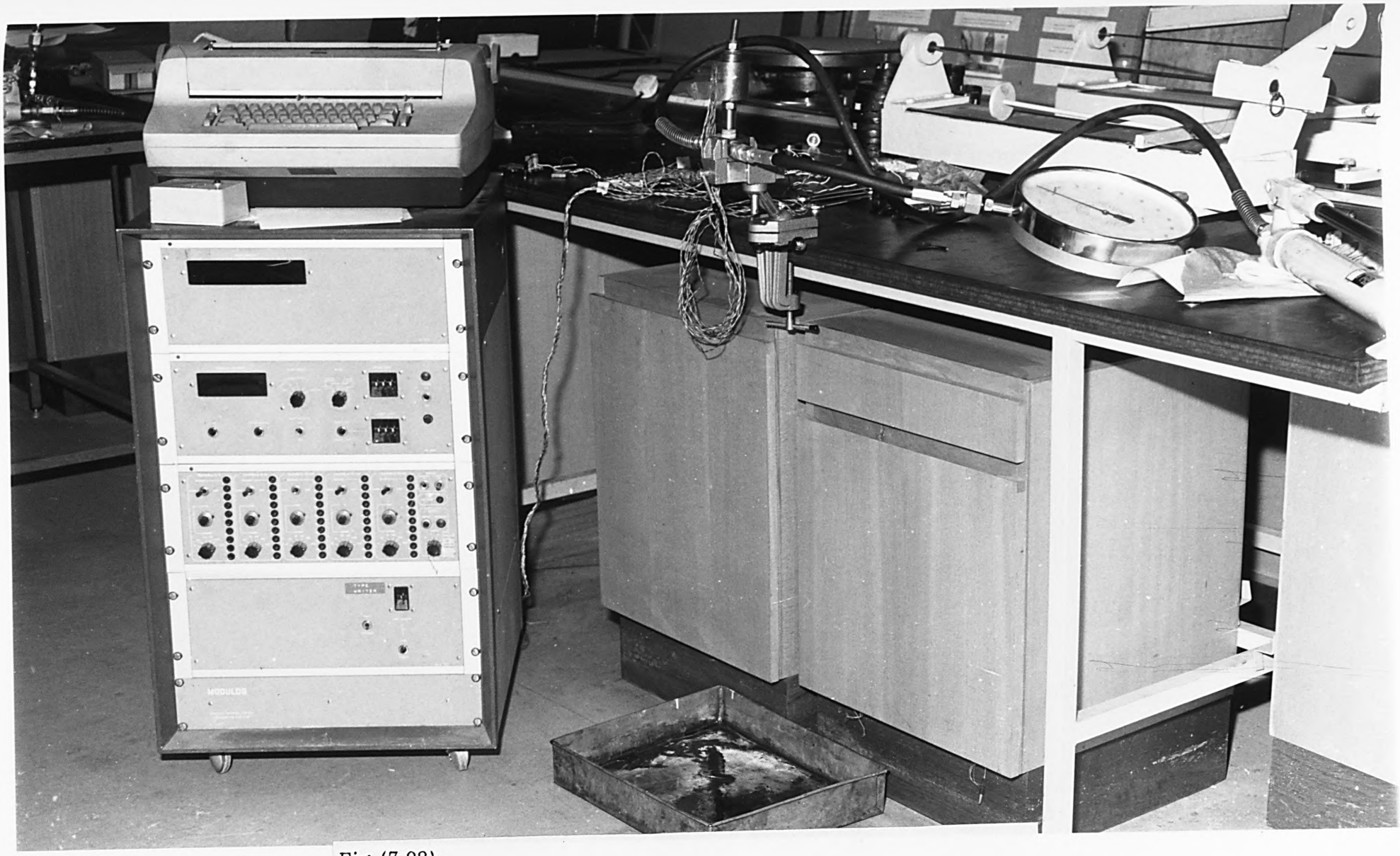

Fig.(7.08)

SET UP OF THE APPARATUS FOR CALIBRATION OF
RADIAL PRESSURE

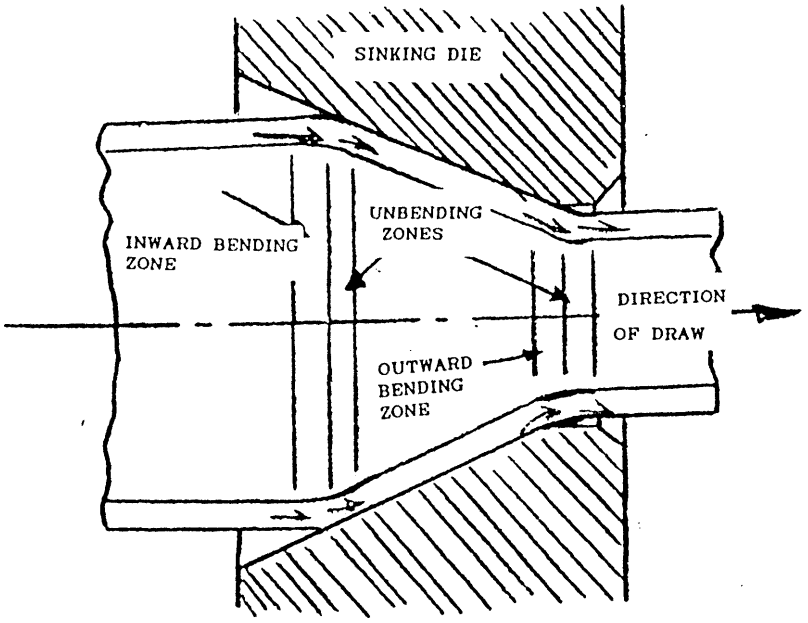

After Swift [10]

Figure (8.1) Showing inward and outward plastic-elastic bending of workpiece

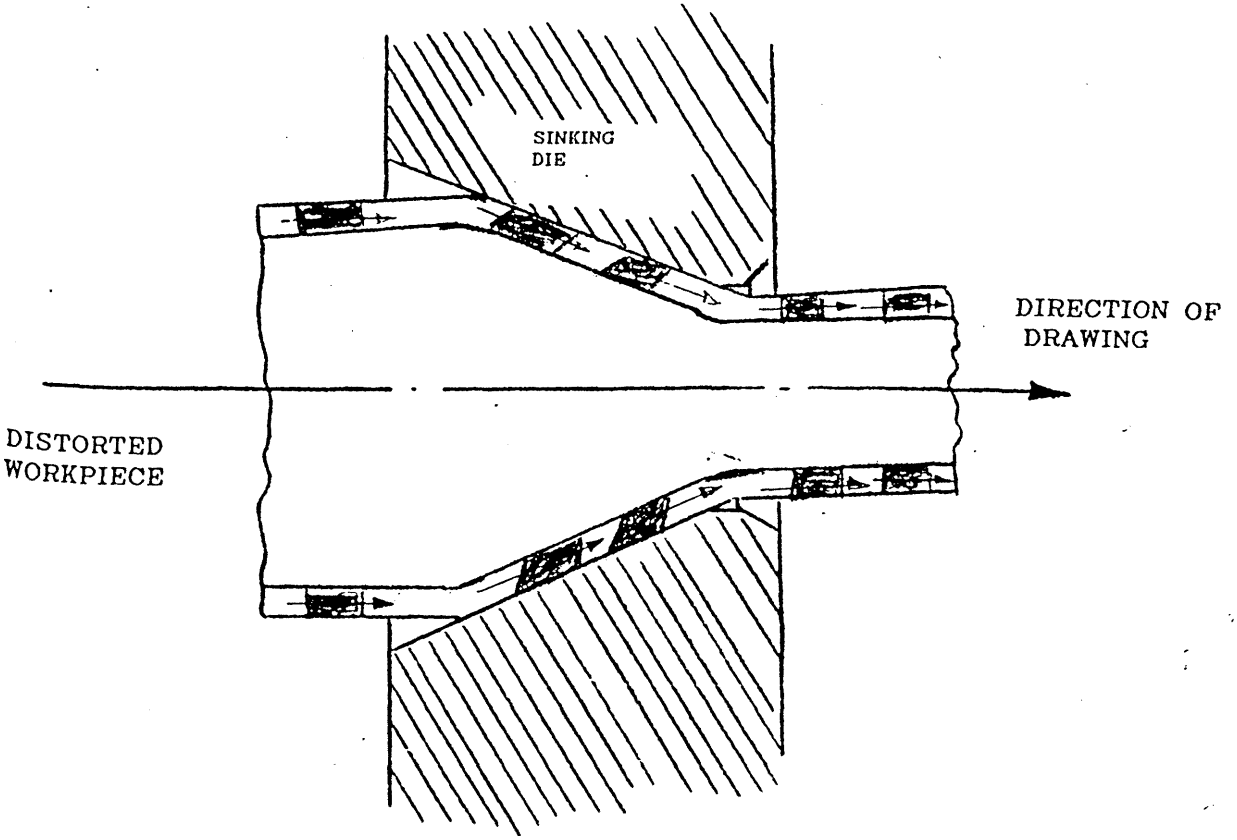

Figure (8.2) Showing the shear distortion of an element as it passes through a Conical die.

TYPICAL THEORETICAL CURVES OF DRAWING STRESS AGAINST FRACTIONAL REDUCTION SHOWING ALLOWANCES FOR FRICTION AND REDUNDANT DEFORMATION
[$\alpha = 7°$; $\mu = 0.2$, and $\bar{y} = 300$ MPa]

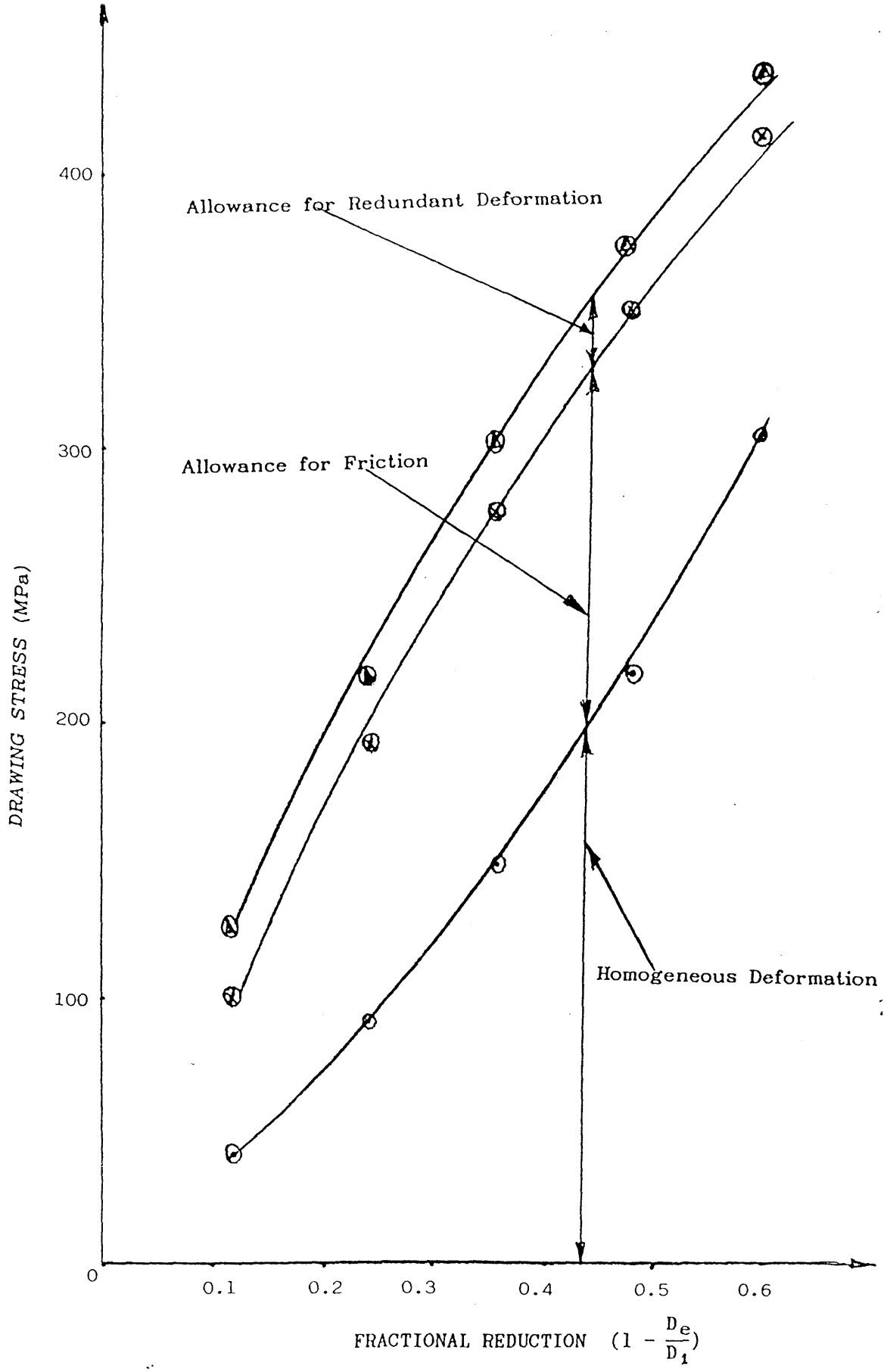

Figure (8.3)

CALIBRATION

Elemental Strains due to Redundant Deformation with the Mean Value, ϵ_{eu1} for Number One Die in Set of Three (α = 15°)

SPECIMEN NO.	STRAIN READINGS PER PASS (Micro) ϵ_{u11}	ϵ_{u12}	ϵ_{u13}	ϵ_{u14}	AVERAGE STRAIN PASS (Micro) ϵ_{u1a}
1	48	46	47	47	47.00
2	46	48	47	47	47.00
3	47	47	49	50	48.25
4	50	48	48	46	48.00
5	47	47	49	48	47.75
6	47	47	48	49	47.75
7	48	48	48	47	47.75

Mean Strain Reading (at Re = 0.125), ϵ_{eu1} = 47.64 (micro)

Table (8.01)

Elemental Strains due to Redundant Deformation with the Mean Value, ϵ_{eu2} for Number Two Die in Set of Three (α = 15°)

SPECIMEN NO.	STRAIN READINGS PER PASS (Micro) ϵ_{u21}	ϵ_{u22}	ϵ_{u23}	ϵ_{u24}	AVERAGE STRAIN PASS (Micro) ϵ_{u2a}
1	58	58	57	58	57.75
2	58	59	58	58	58.25
3	59	60	58	57	58.50
4	59	58	60	58	58.75
5	59	60	58	58	58.75
6	61	58	57	60	59.00
7	58	59	58	58	58.25

Mean Strain Reading (at Re = 0.25), ϵ_{eu2} = 58.46 (micros)

Table (8.02)

Elemental Strains due to Redundant Deformation with the Mean Value, ϵ_{eu3} for Number Three Die in Set of Three (α = 15°)

SPECIMEN NO.	STRAIN READINGS PER PASS (Micro) ϵ_{u31}	ϵ_{u32}	ϵ_{u33}	ϵ_{u34}	AVERAGE STRAIN PASS (Micro) ϵ_{u3a}
1	61	64	60	65	62.50
2	66	64	65	64	64.75
3	63	61	61	61	61.50
4	64	62	63	63	63.00
5	65	66	65	63	64.75
6	64	61	62	62	62.25
7	67	63	64	64	64.50

Mean Strain Reading (at Re = 0.375), ϵ_{eu3} = 63.32

Table (8.03)

SUMMARY OF THE STRAINS DUE TO REDUNDANT DEFORMATION, ϵ_{eu} WITH THEIR CORRESPONDING DRAWING FORCES, F_{Deu} FOR THE ANNEALED BRASS SPECIMEN

ELEMENT No.	F_{Deu} (N)	ϵ_{eu} (micro)
1	2821	47.64
2	4354	58.46
3	5125	63.32

Table (8.04)

Graph of Strains, ϵ_{eu} against Drawing Forces, F_{Deu} Due to Redundant Deformation [for Calibration of 15° Semi-Angle Elemental Dies Assembly Strains ϵ_{De}

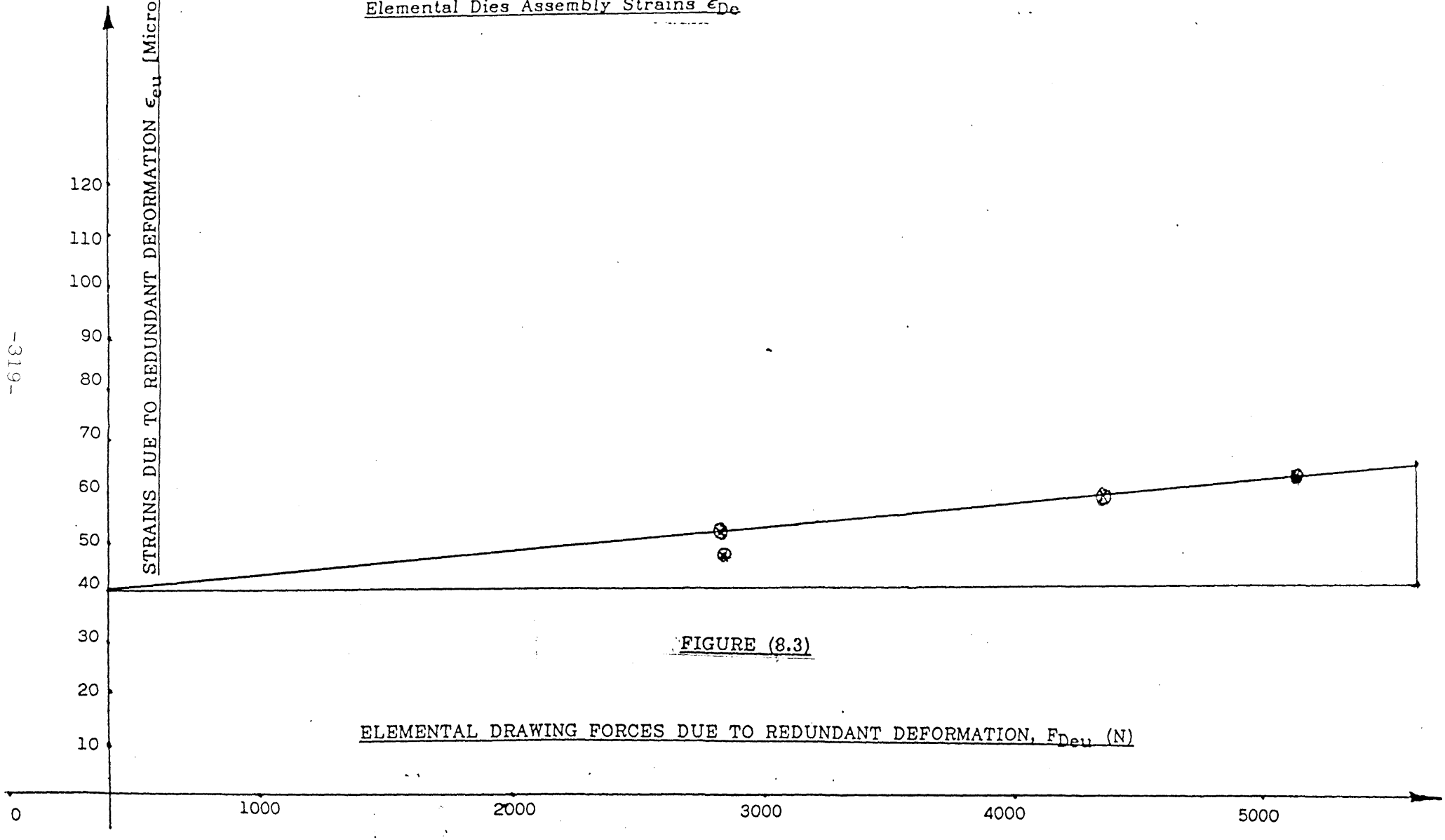

FIGURE (8.3)

$$\epsilon_{eu} = m\ F_{Deu} + c$$

where c = 40 (micro) from the graph.

$$\therefore\ \epsilon_{eu} = m\ F_{Deu} + 40$$

From the graph:

$$m = \frac{25}{5600} = 0.00446$$

$$\therefore\ \epsilon_{eu} = 0.00446\ F_{Deu} + 40 \qquad (8.8)$$

STRAINS DUE TO REDUNDANT DEFORMATION, ϵ_{eu} WITH THEIR EQUIVALENT DRAWING FORCES, F_{Deu} CALCULATED FROM EQUATION (8.8) WITH THEIR CORRESPONDING REDUNDANT STRAINS FOR ALUMINIUM ALLOY SPECIMEN

ELEMENT No.	F_{Deu} (N)	ϵ_{eu} (micro)	R_{De} (N)	ϵ_{Re} (micro)
1	2550	51.373	691	13.92
2	2681	51.96	1240	24.03
3	2681	51.99	545	10.54

Table (8.05)

STRAINS DUE TO REDUNDANT DEFORMATION, ϵ_{eu} WITH THEIR EQUIVALENT DRAWING FORCES, F_{Deu} CALCULATED FROM EQUATION (8.8) WITH THEIR CORRESPONDING REDUNDANT STRAINS FOR COPPER SPECIMEN

ELEMENT No.	F_{Deu} (N)	ϵ_{eu} (micro)	R_{De} (N)	ϵ_{Re} (micro)
1	2479	51.06	650	13.39
2	2812	52.54	1165	21.77
3	3005	53.40	510	9.06

Table (8.06)

Elemental Strains due to Redundant Deformation with the Mean Value, ϵ_{eu1} for Number One Die in Set of Five (α = 7°)

SPECIMEN NO.	STRAIN READINGS PER PASS (Micro) ϵ_{u11}	ϵ_{u12}	ϵ_{u13}	ϵ_{u14}	AVERAGE STRAIN PASS (Micro) ϵ_{u1a}
1	24	23	24	25	24.00
2	23	25	24	24	24.00
3	24	24	24	25	24.25
4	24	24	25	24	24.25
5	23	24	24	25	24.50
6	24	24	24	24	24.00
7	25	24	25	24	24.50

Mean Strain Reading (at Re = 0.075), ϵ_{eu1} = 24.21 (micro)

Table (8.07)

Elemental Strains due to Redundant Deformation with the Mean Value, ϵ_{eu2} for Number Two Die in Set of Five (α = 7°)

SPECIMEN NO.	STRAIN READINGS PER PASS (Micro) ϵ_{u21}	ϵ_{u22}	ϵ_{u23}	ϵ_{u24}	AVERAGE STRAIN PASS (Micro) ϵ_{u2a}
1	26	26	26	26	26.00
2	27	26	27	26	26.50
3	27	28	26	27	27.00
4	27	26	27	28	27.00
5	28	28	27	27	27.50
6	26	27	27	28	27.00
7	28	27	27	28	27.50

Mean Strain Reading (at Re = 0.150), ϵ_{eu2} = 26.93 (micro)

Table (8.08)

Elemental Strains due to Redundant Deformation with the Mean Value, ϵ_{eu3} for Number Three Die in Set of Five ($\alpha = 7^{\circ}$)

SPECIMEN NO.	STRAIN READINGS PER PASS (Micro) ϵ_{u31}	ϵ_{u32}	ϵ_{u33}	ϵ_{u34}	AVERAGE STRAIN PASS (Micro) ϵ_{u3a}
1	31	32	32	32	31.75
2	33	34	33	32	33.00
3	31	31	33	32	31.75
4	32	32	32	33	32.25
5	33	33	31	33	32.50
6	32	31	31	32	31.50
7	32	33	31	32	32.25

Mean Strain Reading (at Re = 0.225), $\epsilon_{eu3} = 32.14$ (micros)

Table (8.09)

Elemental Strains due to Redundant Deformation with the Mean Value, ϵ_{eu4} for Number Four Die in Set of Five ($\alpha = 7^{\circ}$)

SPECIMEN NO.	STRAIN READINGS PER PASS (Micro) ϵ_{u41}	ϵ_{u42}	ϵ_{u43}	ϵ_{u44}	AVERAGE STRAIN PASS (Micro) ϵ_{u4a}
1	35	34	34	35	34.50
2	34	34	35	34	34.25
3	35	35	35	34	34.75
4	34	35	35	34	34.50
5	34	34	34	34	34.00
6	33	35	35	35	35.00
7	34	34	35	35	34.50

Mean Strain Reading (at Re = 0.300), $\epsilon_{eu4} = 34.50$ (micros)

Table (8.10)

Elemental Strains due to Redundant Deformation with the Mean Value, ϵ_{eu5} for Number Five Die in Set of Five ($\alpha = 7^{\circ}$)

SPECIMEN NO.	STRAIN READINGS PER PASS (Micro) ϵ_{u51}	ϵ_{u52}	ϵ_{u53}	ϵ_{u54}	AVERAGE STRAIN PASS (Micro) ϵ_{u5a}
1	37	36	36	36	36.25
2	36	36	37	37	36.50
3	38	38	38	37	37.75
4	38	37	38	38	37.75
5	37	37	36	37	36.50
6	36	36	37	37	36.50
7	37	36	36	37	36.50

Mean Strain Reading (at Re = 0.375), ϵ_{eu5} = 36.82 (micros)

Table (8.11)

SUMMARY OF THE STRAINS DUE TO REDUNDANT DEFORMATION, ϵ_{eus} WITH THEIR CORRESPONDING DRAWING FORCES, F_{Deu} FOR THE ANNEALED BRASS SPECIMEN

ELEMENT No.	F_{Deu} (N)	ϵ_{eu} (micro)
1	2724	24.21
2	3171	26.93
3	3872	32.14
4	4152	34.50
5	4363	36.82

Table (8.12)

Graph of Strains, ϵ_{eu} against Drawing Forces, F_{Deu} Due to Redundant Deformation [for Calibration of 7° Semi-Angle Elemental Dies Assembly Strains ϵ_{De}

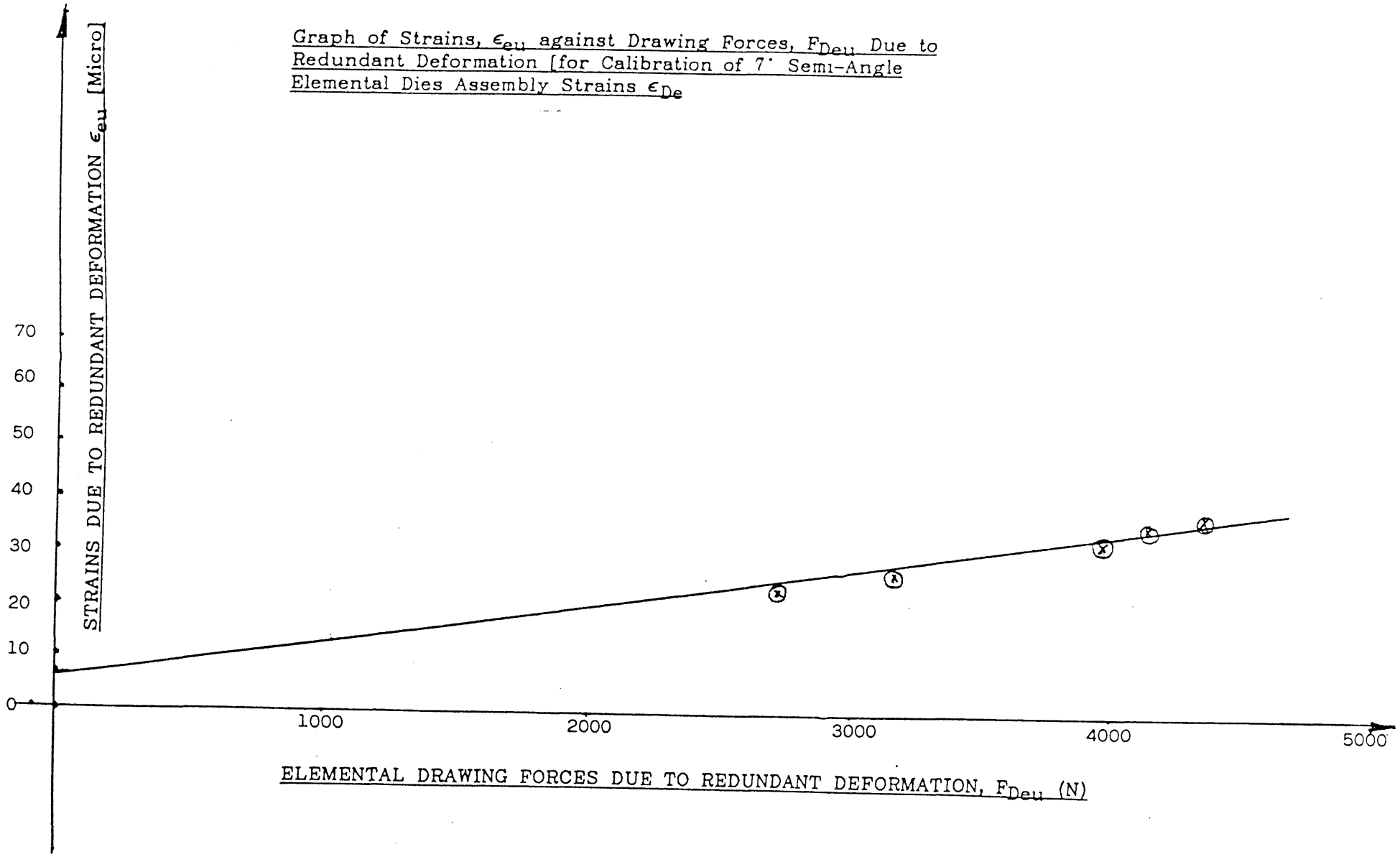

FIGURE (8.4)

$$\epsilon_{eu} = m\ F_{Deu} + c$$

where c = 6 (micro) from the graph.

$$\therefore\ \epsilon_{eu} = m\ F_{Deu} + 6$$

From the graph:

$$m = \frac{37}{5400} = 0.0068$$

$$\therefore\ \epsilon_{eu} = 0.0068\ F_{Deu} + 6 \qquad (8.9)$$

STRAINS DUE TO REDUNDANT DEFORMATION, ϵ_{eu} WITH THEIR EQUIVALENT DRAWING FORCES, F_{Deu} CALCULATED FROM EQUATION (8.9) WITH THEIR CORRESPONDING REDUNDANT STRAINS FOR ALUMINIUM ALLOY SPECIMEN

ELEMENT No.	F_{Deu} (N)	ϵ_{eu} (micro)	R_{De} (N)	ϵ_{Re} (micro)
1	1445	15.826	323	3.952
2	1883	18.800	597	5.962
3	1936	19.170	562	5.563
4	2059	20.00	525	5.100
5	2129	20.480	243	2.338

Table (8.13)

STRAINS DUE TO REDUNDANT DEFORMATION, ϵ_{eu} WITH THEIR EQUIVALENT DRAWING FORCES, F_{Deu} CALCULATED FROM EQUATION (8.9) WITH THEIR CORRESPONDING REDUNDANT STRAINS FOR COPPER SPECIMEN

ELEMENT No.	F_{Deu} (N)	ϵ_{eu} (micro)	R_{De} (N)	ϵ_{Re} (micro)
1	1568	16.99	372	3.95
2	1805	18.27	688	6.964
3	1875	18.75	648	6.48
4	2295	21.61	605	5.70
5	2435	22.56	280	2.594

Table (8.14)

STRAIN READINGS AT VARIOUS POINTS [3] DURING A PASS OF AN ALUMINIUM TUBE SPECIMEN THROUGH 15° SEMI-ANGLE ELEMENTAL DIE ASSEMBLY WITH 10 mm EXIT DIAMETER

READINGS PER PASS	ϵ_{e1}	ϵ_{e2} (micros)	ϵ_{e3}
1	46	60	69
2	55	61	67
3	54	61	66
4	54	61	66
5	53	61	66
6	53	61	66
7	53	61	66
8	53	61	66
9	53	61	66
10	53	61	66
11	53	61	66
12	53	62	66
13	53	62	67
14	54	62	67
15	54	62	67
16	54	62	67
17	54	62	67
18	54	62	67
19	54	62	67
20	53	62	67
21	54	63	68
22	54	63	68
23	51	61	66
ϵ_r	17	19	10
$\lvert\epsilon_{ea}\rvert$	53.46	61.52	66.70

Table (8.15)

STRAIN READINGS AT VARIOUS POINTS [3] DURING A PASS OF AN ALUMINIUM TUBE SPECIMEN THROUGH 15° SEMI-ANGLE ELEMENTAL DIE ASSEMBLY WITH 10 mm EXIT DIAMETER

READINGS PER PASS	ϵ_{e1}	ϵ_{e2} (micros)	ϵ_{e3}
1	47	57	66
2	47	57	66
3	47	57	67
4	47	58	67
5	48	58	68
6	48	58	68
7	48	59	68
8	49	59	69
9	49	59	69
10	49	59	69
11	49	59	69
12	49	59	70
13	49	59	70
14	50	60	70
15	50	60	71
16	50	60	71
17	51	61	71
18	51	61	71
19	51	61	71
20	51	61	71
21	52	62	72
22	51	61	72
23	48	60	72
ϵ_r	13	17	13
$\lvert\epsilon_{ea}\rvert$	49.17	51.35	69.48

Table (8.16)

STRAIN READINGS AT VARIOUS POINTS [3] DURING A PASS OF AN ALUMINIUM TUBE SPECIMEN THROUGH 15° SEMI-ANGLE ELEMENTAL DIE ASSEMBLY WITH 10 mm EXIT DIAMETER

READINGS PER PASS	ϵ_{e1}	ϵ_{e2} (micros)	ϵ_{e3}
1	51	59	75
2	51	60	74
3	49	59	73
4	49	59	72
5	49	59	72
6	48	59	72
7	48	59	72
8	49	59	72
9	49	59	72
10	49	60	72
11	49	60	73
12	49	60	73
13	49	60	73
14	50	61	73
15	50	61	73
16	50	61	73
17	50	61	74
18	50	61	74
19	50	61	74
20	50	61	74
21	50	61	74
22	51	62	74
23	51	62	74
24	51	62	74
ϵ_r	13	18	17
$\lvert\epsilon_{ea}\rvert$	49.61	60.22	73.17

Table (8.17)

STRAIN READINGS AT VARIOUS POINTS [3] DURING A PASS OF AN ALUMINIUM TUBE SPECIMEN THROUGH 15° SEMI-ANGLE ELEMENTAL DIE ASSEMBLY WITH 10 mm EXIT DIAMETER

READINGS PER PASS	ϵ_{e1}	ϵ_{e2} (micros)	ϵ_{e3}
1	52	58	63
2	51	59	63
3	51	59	63
4	52	59	64
5	52	59	64
6	52	59	64
7	52	59	64
8	52	59	64
9	52	59	65
10	52	60	65
11	52	60	65
12	53	60	65
13	53	60	65
14	53	61	66
15	53	61	66
16	54	61	66
17	54	62	67
18	55	62	68
19	56	62	68
20	56	63	68
21	56	63	68
22	56	64	69
ϵ_r	17	18	10
$\lvert\epsilon_{ea}\rvert$	53.22	60.52	65.57

Table (8.18)

TYPICAL STRAIN READINGS ϵ_e's FROM DATA LOGGER AT ONE PASS OF AN ALUMINIUM TUBE SPECIMEN THROUGH 15° SEMI-ANGLE ELEMENTAL DIE ASSEMBLY

STRAIN (Micros)

000 0002 0 001 0002 0 002 0501 0

000 0002 0 001 0002 0 002 0500 0

000 0052 0 001 0058 0 002 0563 0

000 0051 0 001 0059 0 002 0563 0

000 0051 0 001 0059 0 002 0563 0

000 0052 0 001 0059 0 002 0564 0

000 0052 0 001 0059 0 002 0564 0

000 0052 0 001 0059 002 0564 0

000 0052 0 001 0059 0 002 0564 0

000 0052 0 001 0059 0 002 0564 0

000 0052 0 001 0059 0 002 0565 0

000 0052 0 001 0059 0 002 0565 0

000 0052 0 001 0060 0 002 0565 0

000 0053 0 001 0060 0 002 0565 0

000 0053 0 001 0060 0 002 0565 0

000 0053 0 001 0060 0 002 0566 0

000 0053 0 001 0061 0 002 0566 0

000 0054 0 001 0061 0 002 0566 0

000 0054 0 001 0061 0 002 0567 0

000 0055 0 001 0062 0 002 0567 0

000 0055 0 001 0062 0 002 0568 0

000 0056 0 001 0062 0 002 0568 0

000 0056 0 001 0063 0 002 0568 0

000 0056 0 001 0063 0 002 0568 0

000 0056 0 001 0063 0 002 0569 0

000 0017 0 001 0018 0 002 0510 0

000 0017 0 001 0018 0 002 0510 0

TABLE (8.20)

TYPICAL STRAIN READINGS ϵ_e's FROM DATA LOGGER AT ONE PASS OF AN ALUMINIUM TUBE SPECIMEN THROUGH 15° SEMI-ANGLE ELEMENTAL DIE ASSEMBLY

STRAIN (Micros)

000-0001 0 001 0000 0 002 0499 0

000-0001 0 001-0000 0 002 0499 0

000 0000 0 001 0084 0 002 0537 0

000 0051 0 001 0059 0 002 0575 0

000 0051 0 001 0060 0 002 0574 0

000 0049 0 001 0059 0 002 0573 0

000 0049 0 001 0059 0 002 0572 0

000 0049 0 001 0059 0 002 0572 0

000 0048 0 001 0059 0 002 0572 0

000 0048 0 001 0059 0 002 0572 0

000 0048 0 001 0059 0 002 0572 0

000 0049 0 001 0059 0 002 0572 0

000 0049 0 001 0060 0 002 0573 0

000 0049 0 001 0060 0 002 0573 0

000 0049 0 001 0060 0 002 0573 0

000 0049 0 001 0060 0 002 0573 0

000 0050 0 001 0061 0 002 0573 0

000 0050 0 001 0061 0 002 0574 0

000 0050 0 001 0061 0 002 0574 0

000 0050 0 001 00610 002 0574 0

000 0050 0 001 0061 0 002 0574 0

000 0050 0 001 0061 0 002 0574 0

000 0050 0 001 0061 0 002 0574 0

000 0051 0 001 0062 0 002 0574 0

000 0051 0 001 0062 0 002 0574 0

000 0051 0 001 0062 0 002 0575 0

000 0051 0 001 0062 0 002 0575 0

000 0051 0 001 0062 0 002 0575 0

000 0051 0 001 0062 0 002 0575 0

000 0013 0 001 0018 0 002 0517 0

TABLE (8.21)

TYPICAL STRAIN READINGS ϵ_e's FROM DATA LOGGER AT ONE PASS OF AN ALUMINIUM TUBE SPECIMEN THROUGH 15° SEMI-ANGLE ELEMENTAL DIE ASSEMBLY

STRAIN (Micros)

000-0000 0 001 0000 0 002 0500 0

000 0002 0 001 0077 0 002 0580 0

000 0046 0 001 0060 0 002 0569 0

000 0055 0 001 0061 0 002 0567 0

000 0054 0 001 0061 0 002 0566 0

000 0054 0 001 0061 0 002 0566 0

000 0053 0 001 0061 0 002 0566 0

000 0053 0 001 0061 0 002 0566 0

000 0053 0 001 0061 0 002 0566 0

000 0053 0 001 0061 0 002 0566 0

000 0053 0 001 0061 0 002 0566 0

000 0053 0 001 0061 0 002 0566 0

000 0053 0 001 0062 0 002 0566 0

000 0053 0 001 0062 0 002 0567 0

000 0054 0 001 0062 0 002 0567 0

000 0054 0 001 0062 0 002 0567 0

000 0054 0 001 0062 0 002 0567 0

000 0054 0 001 0062 0 002 0567 0

000 0054 0 001 0062 0 002 0567 0

000 0054 0 001 0062 0 002 0567 0

000 0053 0 001 0062 0 002 0567 0

000 0054 0 001 0063 0 002 0568 0

000 0054 0 001 0063 0 002 0568 0

000 0051 0 001 0061 0 002 0568 0

000 0017 0 001 0019 0 002 0510 0

000 0016 0 001 0019 0 002 0510 0

TABLE (8.22)

STRAIN READINGS AT VARIOUS POINTS [3] DURING A PASS OF AN COPPER TUBE SPECIMEN THROUGH 15° SEMI-ANGLE ELEMENTAL DIE ASSEMBLY WITH 10 mm EXIT DIAMETER

READINGS PER PASS	ϵ_{e1}	ϵ_{e2} (micros)	ϵ_{e3}
1	64	64	42
2	62	64	44
3	62	64	46
4	62	64	46
5	6L	65	48
6	62	65	48
7	62	66	49
8	62	67	50
9	59	63	45
10	58	62	44
11	57	61	43
12	57	61	43
13	59	64	46
14	59	65	47
15	61	66	48
16	61	66	49
17	62	66	49
18	60	66	50
19	60	65	52
ϵ_r	24	20	-11
$\lvert\epsilon_{ea}\rvert$	60.53	64.42	49.42

Table (8.23)

STRAIN READINGS AT VARIOUS POINTS [3] DURING A PASS OF AN COPPER TUBE SPECIMEN THROUGH 15° SEMI-ANGLE ELEMENTAL DIE ASSEMBLY WITH 10 mm EXIT DIAMETER

READINGS PER PASS	ϵ_{e1}	ϵ_{e2} (micros)	ϵ_{e3}
1	63	55	68
2	64	55	69
3	64	55	69
4	64	56	70
5	64	56	70
6	65	56	71
7	65	56	71
8	66	57	71
9	66	57	71
10	66	57	72
11	67	58	72
12	67	58	73
13	67	58	73
14	68	58	74
15	68	59	69
16	68	59	74
ϵ_r	30	12	11
$\lvert\epsilon_{ea}\rvert$	65.81	56.94	71.1

Table (8.24)

STRAIN READINGS AT VARIOUS POINTS [3] DURING A PASS OF AN COPPER TUBE SPECIMEN THROUGH 15° SEMI-ANGLE ELEMENTAL DIE ASSEMBLY WITH 10 mm EXIT DIAMETER

READINGS PER PASS	ϵ_{e1}	ϵ_{e2} (micros)	ϵ_{e3}
1	65	61	78
2	64	61	80
3	64	61	79
4	65	62	79
5	60	58	80
6	57	56	75
7	53	57	72
8	58	57	73
9	58	58	73
10	59	59	74
11	60	59	75
12	62	61	76
13	62		77
ϵ_r	24	15	17
$\lvert\epsilon_{ea}\rvert$	60.54	59.17	76.23

Table (8.25)

STRAIN READINGS AT VARIOUS POINTS [3] DURING A PASS OF AN COPPER TUBE SPECIMEN THROUGH 15° SEMI-ANGLE ELEMENTAL DIE ASSEMBLY WITH 10 mm EXIT DIAMETER

READINGS PER PASS	ϵ_{e1}	ϵ_{e2} (micros)	ϵ_{e3}
1	56	51	65
2	55	52	66
3	55	52	66
4	55	53	66
5	55	53	66
6	56	54	67
7	57	55	68
8	57	55	68
9	59	57	70
10	59	57	71
11	60	58	71
12	61	59	72
ϵ_r	21	10	14
$\lvert\epsilon_{ea}\rvert$	57.1	54.67	73.42

Table (8.26)

STRAIN READINGS AT VARIOUS POINTS [3] DURING A PASS OF AN COPPER TUBE SPECIMEN THROUGH 15° SEMI-ANGLE ELEMENTAL DIE ASSEMBLY WITH 10 mm EXIT DIAMETER

READINGS PER PASS	ϵ_{e1}	ϵ_{e2} (micros)	ϵ_{e3}
1	65	61	78
2	64	61	80
3	64	61	79
4	64	61	79
5	65	62	80
6	60	58	75
7	57	56	72
8	53	54	69
9	48	52	66
10	58	57	73
11	58	57	73
12	59	58	74
13	60	59	75
14	62	59	75
15	62	61	76
16	62	59	77
ϵ_r	25	14	16
$\lvert\epsilon_{ea}\rvert$	60.9	58.9	75.7

Table (8.27)

STRAIN READINGS AT VARIOUS POINTS [3] DURING A PASS OF AN COPPER TUBE SPECIMEN THROUGH 15° SEMI-ANGLE ELEMENTAL DIE ASSEMBLY WITH 10 mm EXIT DIAMETER

READINGS PER PASS	ϵ_{e1}	ϵ_{e2} (micros)	ϵ_{e3}
1	56	51	64
2	55	52	65
3	55	52	65
4	55	52	66
5	55	53	66
6	55	53	66
7	56	54	66
8	56	54	67
9	57	55	67
10	57	55	68
11	59	57	68
12	59	57	70
13	60	59	71
14	60	60	71
15	60	60	71
ϵ_r	21	10	8
$\lvert\epsilon_{ea}\rvert$	57.0	54.93	67.4

Table (8.28)

TYPICAL STRAIN READINGS, ϵ_c's FROM DATA LOGGER AT ONE PASS OF A COPPER TUBE SPECIMEN THROUGH 15° SEMI-ANGLE ELEMENTAL DIE ASSEMBLY

STRAIN (Micros)

000-0000 0 001 0000 0

002 0497 0

000-0000 0 001 0000 0 002 0496 0

000-0000 0 001 0000 0 002 0496 0

000-0000 0 001 0000 0 002 0496 0

000-0010 0 001-0005 0 002 0492 0

000-0008 0 001-0005 0 002 0492 0

000-0008 0 001-0005 0 002 0492 0

000-0008 0 001-0005 0 002 0492 0

000 0026 0 001 0049 0 002 0564 0

000 0056 0 001 0051 0 002 0565 0

000 0055 0 001 0052 0 002 0565 0

000 0055 0 001 0052 0 002 0566 0

000 0055 0 001 0052 0 002 0566 0

000 0055 0 001 0053 0 002 0566 0

000 0055 0 001 0053 0 002 0566 0

000 0056 0 001 0054 0 002 0567 0

000 0056 0 001 0054 0 002 0567 0

000 0057 0 001 0055 0 002 0566 0

000 0057 0 001 0055 0 002 0568 0

000 0059 0 001 0057 0 002 0570 0

000 0059 0 001 0057 0 002 0571 0

000 0060 0 001 0058 0 002 0571 0

000 0061 0 001 0059 0 002 0572 0

000 0021 0 001 0010 0 002 0514 0

000 0020 0 001 0010 0 002 0514 0

TABLE (8.29)

TYPICAL STRAIN READINGS, ϵ_e's FROM DATA LOGGER AT ONE PASS OF A COPPER TUBE SPECIMEN THROUGH 15° SEMI-ANGLE ELEMENTAL DIE ASSEMBLY

STRAIN (Micros)

000-0000	0	001	0000	0	002	0500	0
000 0003	0	001	0055	0	002	0568	0
000 0004	0	001	0055	0	002	0569	0
000 0004	0	001	0055	0	002	0569	0
000 0004	0	001	0056	0	002	0569	0
000 0005	0	001	0056	0	002	0570	0
000 0005	0	001	0056	0	002	0570	0
000 0005	0	001	0057	0	002	0571	0
000 0006	0	001	0057	0	002	0571	0
000 0006	0	001	0057	0	002	0571	0
000 0006	0	001	0057	0	002	0571	0
000 0007	0	001	0058	0	002	0572	0
000 0007	0	001	0058	0	002	0572	0
000 0007	0	001	0058	0	002	0573	0
000 0008	0	001	0058	0	002	0573	0
000 0008	0	001	0059	0	002	0574	0
000 0008	0	001	0059	0	002	0574	0
000 0025	0	001	0014	0	002	0516	0
000 0025	0	001	0014	0	002	0515	0

TABLE (8.30)

TYPICAL STRAIN READINGS, ϵ_θ's FROM DATA LOGGER AT ONE PASS OF A COPPER TUBE SPECIMEN THROUGH 15° SEMI-ANGLE ELEMENTAL DIE ASSEMBLY

STRAIN (Micros)		
000 0001 0	001 0000 0	002 0501 0
000 0064 0	001 0064 0	002 0542 0
000 0062 0	001 0064 0	002 0544 0
000 0062 0	001 0064 0	002 0546 0
000 0062 0	001 0064 0	002 0546 0
000 0061 0	001 0065 0	002 0548 0
000 0062 0	001 0065 0	002 0548 0
000 0062 0	001 0066 0	002 0549 0
000 0062 0	001 0067 0	002 0550 0
000 0059 0	001 0063 0	002 0545 0
000 0058 0	001 0062 0	002 0544 0
000 0057 0	001 0061 0	002 0543 0
000 0057 0	001 0061 0	002 0543 0
000 0059 0	001 0064 0	002 0546 0
000 0059 0	001 0065 0	002 0547 0
000 0060 0	001 0066 0	002 0548 0
000 0061 0	001 0066 0	002 0549 0
000 0061 0	001 0066 0	002 0549 0
000 0062 0	001 0066 0	002 0550 0
000 0060 0	001 0065 0	002 0552 0
000 0060 0	001 0065 0	002 0552 0
000 0024 0	001 0020 0	002 0489 0
000 0023 0	001 0020 0	002 0489 0

TABLE (8.31)

STRAIN READINGS AT VARIOUS POINTS [5] DURING A PASS OF AN ALUMINIUM TUBE SPECIMEN THROUGH 7° SEMI-ANGLE ELEMENTAL DIE ASSEMBLY WITH 10 mm EXIT DIAMETER

READINGS PER PASS	ϵ_{e1}	ϵ_{e2}	ϵ_{e3} (micros)	ϵ_{e4}	ϵ_{e5}
1	24	-19	39	-	30
2	24	-19	38	-	30
3	24	-19	38	-	30
4	24	-19	37	-	30
5	24	-19	37	-	29
6	24	-19	37	-	29
7	24	-19	37	-	28
8	23	-19	37	-	28
9	23	-19	37	-	28
10	23	-19	37	-	28
11	23	-18	37	-	27
12	23	-18	37	-	27
13	23	-18	37	-	27
14	23	-18	37	-	27
15	23	-18	37	-	27
16	23	-18	37	-	26
ϵ_r	12	1	20	-	8
$\lvert\epsilon_{ea}\rvert$	23.38	18.63	37.25	-	28.19

Table (8.32)

STRAIN READINGS AT VARIOUS POINTS [5] DURING A PASS OF AN ALUMINIUM TUBE SPECIMEN THROUGH 7° SEMI-ANGLE ELEMENTAL DIE ASSEMBLY WITH 10 mm EXIT DIAMETER

READINGS PER PASS	ϵ_{e1}	ϵ_{e2}	ϵ_{e3} (micros)	ϵ_{e4}	ϵ_{e5}
1	22	-16	31	-19	25
2	22	-16	30	-19	25
3	22	-15	29	-20	26
4	22	-15	29	-20	26
5	22	-15	28	-20	27
6	22	-15	28	-21	28
7	21	-15	28	-21	28
8	21	-15	28	-21	29
9	21	-14	28	-21	29
10	21	-14	28	-21	29
11	21	-14	27	-21	29
12	20	-14	27	-22	30
13	20	-14	27	-22	30
14	20	-14	26	-22	30
15	19	-14	26	-23	30
16	20	-14	26	-22	30
ϵ_r	20	-3	11	-1	8
$\lvert\epsilon_{ea}\rvert$	21.00	14.56	27.88	20.94	28.19

Table (8.33)

STRAIN READINGS AT VARIOUS POINTS [5] DURING A PASS OF AN ALUMINIUM TUBE SPECIMEN THROUGH 7° SEMI-ANGLE ELEMENTAL DIE ASSEMBLY WITH 10 mm EXIT DIAMETER

READINGS PER PASS	ϵ_{e1}	ϵ_{e2}	ϵ_{e3} (micros)	ϵ_{e4}	ϵ_{e5}
1	23	-22	26	-28	42
2	23	-21	26	-28	41
3	23	-20	25	-25	45
4	23	-20	25	-23	44
5	23	-20	25	-23	44
6	23	-20	25	-23	44
7	24	-20	25	-23	44
8	24	-20	25	-23	44
9	23	-20	25	-23	44
10	23	-20	25	-23	44
11	23	-20	25	-23	44
12	24	-20	25	-22	44
13	24	-19	25	-22	44
14	24	-19	25	-22	43
15	24	-19	26	-22	44
16	24	-19	25	-22	43
ϵ_r	11	2	8	1	23
$\lvert\epsilon_{ea}\rvert$	23.44	19.94	25.188	23.44	43.63

Table (8.34)

STRAIN READINGS AT VARIOUS POINTS [5] DURING A PASS OF AN ALUMINIUM TUBE SPECIMEN THROUGH 7° SEMI-ANGLE ELEMENTAL DIE ASSEMBLY WITH 10 mm EXIT DIAMETER

READINGS PER PASS	ϵ_{e1}	ϵ_{e2}	ϵ_{e3} (micros)	ϵ_{e4}	ϵ_{e5}
1	23	-19	36	-30	32
2	23	-19	36	-29	32
3	23	-19	37	-29	32
4	23	-19	37	-29	32
5	23	-19	37	-27	32
6	23	-19	37	-27	32
7	23	-19	37	-27	32
8	24	-19	37	-26	32
9	24	-19	37	-25	32
10	24	-19	37	-23	32
11	24	-19	37	-23	32
ϵ_r	10	1	19	5	11
$\lvert\epsilon_{ea}\rvert$	23.36	19	36.73	26.82	32

Table (8.35)

STRAIN READINGS AT VARIOUS POINTS [5] DURING A PASS OF AN ALUMINIUM TUBE SPECIMEN THROUGH 7° SEMI-ANGLE ELEMENTAL DIE ASSEMBLY WITH 10 mm EXIT DIAMETER

READINGS PER PASS	ϵ_{e1}	ϵ_{e2}	ϵ_{e3} (micros)	ϵ_{e4}	ϵ_{e5}
1	19	-20	29	-10*	37
2	23	-20	21	-16*	44
3	22	-18	30	-5	49
4	22	-18	29	-6*	48
5	22	-17	29	-7*	48
6	22	-17	28	-7*	47
7	22	-17	27	-8*	47
8	21	-17	27	-8*	47
9	21	-16	27	-8*	47
10	21	-16	26	-9*	47
11	20	-15	26	-10*	46
12	19	-15	26	-10*	46
13	18	-14	24	-11*	45
14	18	-13	24	-11*	45
15	18	-13	24	-11*	45
16	19	-13	25	-11*	46
17	19	-13	25	-11*	46
18	18	-13	24	-11*	46
19	18	-13	24	-12*	46
20	18	-13	24	-11*	46
21	18	-13	24	-5*	46
22	18	-15	20	-2*	46
ϵ_r	8	-2	8		25
$\lvert\epsilon_{ea}\rvert$	19.82	15.36	25.6	-	45.91

Table (8.36)

STRAIN READINGS AT VARIOUS POINTS [5] DURING A PASS OF AN ALUMINIUM TUBE SPECIMEN THROUGH 7° SEMI-ANGLE ELEMENTAL DIE ASSEMBLY WITH 10 mm EXIT DIAMETER

READINGS PER PASS	ϵ_{e1}	ϵ_{e2}	ϵ_{e3} (micros)	ϵ_{e4}	ϵ_{e5}
1	23	-20	43	-22	53
2	23	-19	42	-22	52
3	22	-18	41	-22	51
4	21	-18	39	-22	49
5	21	-17	39	-23	48
6	21	-17	38	-22	48
7	21	-17	38	-22	47
8	21	-17	38	-14*	47
9	21	-16	38	-15*	47
10	21	-16	38	-15*	47
11	20	-16	37	-9*	47
12	20	-16	37	-10*	47
13	19	-16	34	-9*	47
14	19	-16	35	-7*	46
15	19	-15	35	-7*	46
16	19	-15	35		46
17	19	-15	35		46
18	19	-15	35		46
ϵ_r	9	-1	20	0	27
$\lvert\epsilon_{ea}\rvert$	20.5	16.61	37.6	22.22	47.78

Table (8.37)

TYPICAL STRAIN READINGS, ϵ_c's FROM DATA LOGGER AT ONE PASS OF A ALUMINIUM TUBE SPECIMEN THROUGH 7° SEMI-ANGLE ELEMENTAL DIE ASSEMBLY STRAIN (Micros)

000-0000	0	001-0097	0	002	0001	0	003-0699	0	004	0000	0
000	0019	0	001-0080	0	002	0029	0	003-0690	0	004	0037	0
000	0023	0	001-0080	0	002	0021	0	003-0684	0	004	0009	0
000	0022	0	001-0082	0	002	0030	0	003-0705	0	004	0049	0
000	0022	0	001-0082	0	002	0029	0	003-0706	0	004	0048	0
000	0022	0	001-0083	0	002	0029	0	003-0707	0	004	0048	0
000	0022	0	001-0083	0	002	0028	0	003-0707	0	004	0047	0
000	0022	0	001-0083	0	002	0027	0	003-0708	0	004	0047	0
000	0021	0	001-0084	0	002	0027	0	003-0708	0	004	0047	0
000	0021	0	001-0084	0	002	0027	0	003-0708	0	004	0047	0
000	0021	0	001-0084	0	002	0026	0	003-0709	0	004	0047	0
000	0020	0	001-0085	0	002	0026	0	003-0710	0	004	0046	0
000	0019	0	001-0085		002	0026	0	003-0710	0	004	0046	0
000	0018	0	001-0086	0	002	0024	0	003-0711	0	004	0045	0
000	0018	0	001-0087	0	002	0024	0	003-0711	0	004	0045	0
000	0018	0	001-0087	0	002	0024	0	003-0711	0	004	0045	0
000	0019	0	001-0087	0	002	0025	0	003-0711	0	004	0046	0
000	0019	0	001-0087	0	002	0025	0	003-0711	0	004	0046	0
000	0018	0	001-0087	0	002	0024	0	003-0711	0	004	0046	0
000	0018	0	001-0087	0	002	0024	0	003-0711	0	004	0046	0
000	0018	0	001-0087	0	002	0024	0	003-0711	0	004	0046	0
000	0018	0	001-0088	0	002	0024	0	003-0712	0	004	0046	0
000	0018	0	001-0087	0	002	0024	0	003-0711	0	004	0046	0
000	0008	0	001-0099	0	002	0008	0	003-0702	0	004	0026	0
000	0007	0	001-0099	0	002	0008	0	003-0702	0	004	0026	0

TABLE (8.38)

TYPICAL STRAIN READINGS, ϵ_c's FROM DATA LOGGER AT ONE PASS OF A ALUMINIUM TUBE SPECIMEN THROUGH 7° SEMI-ANGLE ELEMENTAL DIE ASSEMBLY

STRAIN (Micros)

000 0001 0	000 0001 0	000 0001 0	000 0001 0	000 0001 0
000 0001 0	000 0001 0	000 0001 0	000 0001 0	000 0001 0
001-0099 0	002-0000 0	003-0399 0	004-0000 0	
000 0001 0				
001-0100 0	002-0000 0	003-0399 0	004-0000 0	
000 0001 0	001-0099 0	002-0000 0	003-0399 0	004-0000 0
000 0001 0	001-0099 0	002 0000 0	003-0399 0	004-0000 0
000 0001 0	001-0099 0	002 0000 0	003-0399 0	004-0000 0
000 0001 0	001-0099 0	002 0001 0	003-0405 0	004-0005 0
000 0012 0	001-0094 0	002 0024 0	003-0418 0	004-0016 0
000 0020 0	001-0084 0	002 0031 0	003-0419 0	004-0025 0
000 0022 0	001-0084 0	002 0031 0	003-0419 0	004-0025 0
000 0022 0	001-0084 0	002 0030 0	003-0419 0	004-0025 0
000 0022 0	001-0085 0	002 0029 0	003-0420 0	004-0026 0
000 0022 0	001-0085 0	002 0029 0	003-0420 0	004-0026 0
000 0022 0	001-0085 0	002 0028 0	003-0420 0	004-0027 0
000 0022 0	001-0085 0	002 0028 0	003-0421 0	004-0028 0
000 0021 0	001-0085 0	002 0028 0	003-0421 0	004-0028 0
000 0021 0	001-0085 0	002 0028 0	003-0421 0	004-0029 0
000 0021 0	001-0086 0	002 0028 0	003-0421 0	004-0029 0
000 0021 0	001-0086 0	002 0028 0	003-0421 0	004-0029 0
000 0021 0	001-0086 0	002 0027 0	003-0421 0	004-0029 0
000 0020 0	001-0086 0	002 0027 0	003-0422 0	004-0030 0
000 0020 0	001-0086 0	002 0027 0	003-0422 0	004-0030 0
000 0020 0	001-0086 0	002 0026 0	003-0422 0	004-0030 0
000 0019 0	001-0086 0	002 0026 0	003-0423 0	004-0030 0
000 0020 0	001-0087 0	002 0026 0	003-0422 0	004-0030 0
000 0010 0	001-0097 0	002 0011 0	003-0400 0	004-0008 0
000 0010 0	001 0098 0	002 0011 0	003 0400 0	004-0008 0

TABLE (8.39)

STRAIN READINGS AT VARIOUS POINTS [5] DURING A PASS OF AN COPPER TUBE SPECIMEN THROUGH 7° SEMI-ANGLE ELEMENTAL DIE ASSEMBLY WITH 10 mm EXIT DIAMETER

READINGS PER PASS	ϵ_{e1}	ϵ_{e2}	ϵ_{e3} (micros)	ϵ_{e4}	ϵ_{e5}
1	19	-18	41	-23	15*
2	19	-18	41	-23	18
3	18	-18	41	-23	18
4	19	-18	41	-22	21
5	18	-18	41	-22	22
6	18	-18	41	-22	22
7	18	-18	41	-22	23
8	21	-17	41	-22	23
9	20	-17	40	-22	23
10	22	-17	42	-22	23
11	22	-17	42	-22	23
12	22	-17	42	-22	23
13	22	-17	42	-22	23
14	21	-18	42	-22	23
15	21	-18	42	-22	23
16	19	-18	42	-22	23
17	21	-18	42	-22	24
18	21	-18	42	-21	24
19	21	-18	40	-21	23
20	20	-19	40	-21	24
21	20	-19	40	-21	23
22	20	-19	40	-21	23
23	20	-18	40	-21	23
24	20	-18	40	-21	20
25	21	-17	40	-20	15*
26	20	-17	40	-20	15*
27	20	-17	40	-20	8*
28	20	-17	40	-20	8*
ϵ_r	7	1	24	-2	0
$\lvert\epsilon_{ea}\rvert$	20.11	17.75	40.93	21.57	22.39

Table (8.40)

STRAIN READINGS AT VARIOUS POINTS [5] DURING A PASS OF AN COPPER TUBE SPECIMEN THROUGH 7° SEMI-ANGLE ELEMENTAL DIE ASSEMBLY WITH 10 mm EXIT DIAMETER

READINGS PER PASS	ϵ_{e1}	ϵ_{e2}	ϵ_{e3} (micros)	ϵ_{e4}	ϵ_{e5}
1	23	-17	43	-23	51
2	24	-18	42	-23	49
3	24	-18	42	-22	49
4	24	-17	42	-22	49
5	24	-17	42	-22	48
6	23	-17	41	-22	48
7	23	-17	41	-21	48
8	23	-17	41	-21	48
9	23	-17	41	-21	48
10	23	-17	41	-21	48
11	23	-17	41	-21	47
12	23	-17	41	-21	47
13	23	-17	40	-21	47
14	23	-16	41	-21	47
15	22	-16	41	-21	47
16	22	-16	41	-20	47
17	22	-16	41	-20	46
18	22	-16	41	-20	46
19	22	-16	41	-20	46
20	22	-16	41	-20	46
21	22	-16	40	-20	46
22	22	-16	40	-20	46
23	22	-16	40	-20	46
24	22	-16	40	-20	46
25	21	-15	40	-20	46
ϵ_r	10	0	24	-3	24
$\lvert\epsilon_{ea}\rvert$	22.69	16.56	41.00	20.92	47.28

Table (8.41)

STRAIN READINGS AT VARIOUS POINTS [5] DURING A PASS OF AN COPPER TUBE SPECIMEN THROUGH 7° SEMI-ANGLE ELEMENTAL DIE ASSEMBLY WITH 10 mm EXIT DIAMETER

READINGS PER PASS	ϵ_{e1}	ϵ_{e2}	ϵ_{e3} (micros)	ϵ_{e4}	ϵ_{e5}
1	23	-19	38	-	19
2	27	-20	37	-	19
3	26	-20	35	-	19
4	26	-20	35	-	18
5	26	-20	34	-	18
6	26	-20	34	-	18
7	26	-19	34	-	18
8	26	-19	34	-	18
9	26	-19	34	-	18
10	26	-19	34	-	18
11	26	-19	34	-	18
12	25	-19	33	-	18
13	25	-19	33	-	18
14	25	-19	33	-	18
15	25	-19	33	-	18
16	25	-19	33	-	18
17	25	-19	33	-	18
18	25	-19	33	-	18
19	25	-19	33	-	18
20	25	-18	33	-	18
21	25	-18	33	-	18
22	25	-18	33	-	18
23	25	-18	33	-	18
ϵ_r	12	2	16	-	-4
$\lvert\epsilon_{ea}\rvert$	25.39	19.04	33.87		18.17

Table (8.42)

STRAIN READINGS AT VARIOUS POINTS [5] DURING A PASS OF AN COPPER TUBE SPECIMEN THROUGH 7° SEMI-ANGLE ELEMENTAL DIE ASSEMBLY WITH 10 mm EXIT DIAMETER

READINGS PER PASS	ϵ_{e1}	ϵ_{e2}	ϵ_{e3} (micros)	ϵ_{e4}	ϵ_{e5}
1	26	-33	33	-34	24
2	22	-26	62*	-46	24
3	21	-22	51*	-35	25
4	21	-21	44*	-31	23
5	20	-21	40*	-28	23
6	20	-21	35	-23	23
7	20	-21	30	-21	23
8	20	-21	29	-21	23
9	20	-21	29	-21	22
10	20	-21	29	-21	-
11	20	-21	29	-21	-
12	20	-21	29	-21	-
13	20	-21	29	-21	-
14	20	-20	29	-20	-
15	19	-20	28	-19	-
16	19	-20	28	-19	-
17	19	-20	28	-19	-
18	19	-20	28	-19	-
19	19	-20	28	-19	-
20	19	-20	28	-19	-
ϵ_r	7	4	13	1	1
$\lvert\epsilon_{ea}\rvert$	20.2	21.6	29.31	23.90	23.33

Table (8.43)

STRAIN READINGS AT VARIOUS POINTS [5] DURING A PASS OF AN COPPER TUBE SPECIMEN THROUGH 7° SEMI-ANGLE ELEMENTAL DIE ASSEMBLY WITH 10 mm EXIT DIAMETER

READINGS PER PASS	ϵ_{e1}	ϵ_{e2}	ϵ_{e3} (micros)	ϵ_{e4}	ϵ_{e5}
1	22	-20	49	-12	31
2	21	-20	48	-19	17*
3	21	-19	48	-18	59
4	21	-19	47	-17	59
5	21	-19	48	-17	58
6	21	-19	47	-16	56
7	20	-19	45	-16	56
8	19	-16	44	-14	55
9	20	-19	47	-15	55
10	21	-19	47	-16	52
11	21	-20	48	-16	53
12	22	-20	48	-17	54
13	22	-20	49	-17	54
14	22	-20	48	-16	55
15	22	-20	49	-16	55
16	21	-20	48	-16	55
17	20	-19	47	-15	54
18	19	-18	46	-14	54
19	19	-18	47	-14	54
20	19	-18	46	-16	53
21	19	-18	46	-15	52
22	19	-18	46	-14	52
23	19	-18	46	-14	52
24	19	-18	46	-14	52
25	19	-18	46	-14	52
26	19	-18	46	-14	52
ϵ_r	7	2	31	-8	29
$\lvert\epsilon_{ea}\rvert$	20.31	18.77	47.27	15.46	51.96

Table (8.44)

STRAIN READINGS AT VARIOUS POINTS [5] DURING A PASS OF AN COPPER TUBE SPECIMEN THROUGH 7° SEMI-ANGLE ELEMENTAL DIE ASSEMBLY WITH 10 mm EXIT DIAMETER

READINGS PER PASS	ϵ_{e1}	ϵ_{e2}	ϵ_{e3} (micros)	ϵ_{e4}	ϵ_{e5}
1	20	-22	38	-20	33
2	21	-20	29	-20	15
3	22	-18	28	-21	15
4	21	-20	44	-18	46
5	20	-19	43	-15	44
6	19	-19	42	-13*	43
7	19	-18	42	-12*	43
8	19	-18	42	-11*	43
9	19	-18	42	-9*	43
10	18	-18	41	-8*	42
11	18	-18	41	=8*	42
12	18	-18	42	-8*	42
13	17	-18	41	-8*	44
14	17	-17	41	-7*	44
15	18	-18	42	-7*	44
16	18	-18	42	-6*	44
17	18	-18	42	-5*	44
18	18	-18	42	-4*	45
19	19	-18	42	-1*	44
20	17	-19	42	0*	43
21	17	-18	41		42
22	16	-17	41	5*	42
ϵ_r	7	2	24	-6	18
$\lvert\epsilon_{ea}\rvert$	19.476	18.41	40.453	17.714	40.318

Table (8.45)

STRAIN READINGS AT VARIOUS POINTS [5] DURING A PASS OF AN COPPER TUBE SPECIMEN THROUGH 7° SEMI-ANGLE ELEMENTAL DIE ASSEMBLY WITH 10 mm EXIT DIAMETER

READINGS PER PASS	ϵ_{e1}	ϵ_{e2}	ϵ_{e3} (micros)	ϵ_{e4}	ϵ_{e5}
1	20	-22	38	-20	42
2	21	-20	29	-20	42
3	22	-18	28	-20	42
4	21	-20	44	-20	42
5	20	-19	43	-20	44
6	19	-19	42	-21	43
7	19	-18	42	-21	44
8	19	-18	42	-20	42
9	19	-18	42	-20	42
10	18	-18	41	-18*	42
11	18	-18	41	-15*	42
12	18	-18	42	-12*	42
13	17	-17	41	-12*	42
14	17	-18	41	-7*	42
15	18	-18	42	-7*	41
16	18	-18	42	-5*	42
17	18	-18	42	-5*	42
18	18	-18	42	-5*	42
19	18	-19	42	-2*	42
20	19	-18	41	-1*	42
21	17	-17	40	-1*	42
22	17	-17	40	2	42
ϵ_r	6	2	24	-3	20
$\lvert\epsilon_{ea}\rvert$	18.68	18.364	40.318	20.33	42.182

Table (8.46)

TYPICAL STRAIN READINGS, ϵ_e's FROM DATA LOGGER AT ONE PASS OF A COPPER TUBE SPECIMEN THROUGH 7° SEMI-ANGLE ELEMENTAL DIE ASSEMBLY

STRAIN (Micros)

000-0000 0 001-0100 0 002-0000 0 003-0700 0

004-0000 0

000-0000 0 001-0100 0 002-0000 0 003-0700 0 004-0000 0

000 0000 0 001-0099 0 002 0001 0 003-0699 0 004 0000 0

000 0001 0 001-0101 0 002 0033 0 003-0666 0 004 0052 0

000 0026 0 001-0067 0 002 0062 0 003-0654 0 004 0063 0

000 0022 0 001-0074 0 002 0051 0 003-0665 0 004 0042 0

000 0021 0 001-0078 0 002 0044 0 003-0669 0 004 0037 0

000 0021 0 001-0078 0 002 0040 0 003-0672 0 004 0031 0

000 0020 0 001-0079 0 002 0035 0 003-0677 0 004 0023 0

000 0020 0 001-0079 0 002 0030 0 003-0679 0 004 0016 0

000 0020 0 001-0079 0 002 0029 0 003-0679 0 004 0014 0

000 0020 0 001-0079 0 002 0029 0 003-0679 0 004 0014 0

000 0020 0 001-0079 0 002 0029 0 003-0679 0 004 0014 0

000 0020 0 001-0079 0 002 0029 0 003-0679 0 004 0014 0

000 0020 0 001-0079 0 002 0029 0 003-0679 0 004 0014 0

000 0020 0 001-0079 0 002 0029 0 003-0679 0 004 0014 0

000 0020 0 001-0079 0 002 0029 0 003-0680 0 004 0013 0

000 0019 0 001-0080 0 002 0028 0 003-0681 0 004 0013 0

000 0019 0 001-0080 0 002 0028 0 003-0681 0 004 0013 0

000 0019 0 001-0080 0 002 0028 0 003-0681 0 004 0013 0

000 0019 0 001-0080 0 002 0028 0 003-0681 0 004 0012 0

000 0019 0 001-0080 0 002 0028 0 003-0681 0 004 0012 0

000 0007 0 001-0096 0 002 0013 0 003-0699 0 004 0001 0

000 0007 0 001-0097 0 002 0013 0 003-0699 0 004 0001 0

TABLE (8.47)

TYPICAL STRAIN READINGS, ϵ_θ's FROM DATA LOGGER AT ONE PASS OF A COPPER TUBE SPECIMEN THROUGH 7° SEMI-ANGLE ELEMENTAL DIE ASSEMBLY

STRAIN (Micros)

000-0000 0	001-0099 0	002 0000 0	003-0700 0	004-0000 0
000 0001 0	001-0096 0	002 0003 0	003-0697 0	004 0001
000 0020 0	001-0078 0	002 0038 0	003-0680 0	004 0033 0
000 0021 0	001-0080 0	002 0029 0	003-0680 0	004 0015 0
000 0022 0	001-0082 0	002 0028 0	003-0679 0	004 0015 0
000 0021 0	001-0080 0	002 0044 0	003-0682 0	004 0046 0
000 0020 0	001-0081 0	002 0043 0	003-0685 0	004 0044 0
000 0019 0	001-0081 0	002 0042 0	003-0686 0	004 0044 0
000 0019 0	001-0082 0	002 0042 0	003-0686 0	004 0043 0
000 0019 0	001-0082 0	002 0042 0	003-0687 0	004 0043 0
000 0019 0	001-0082 0	002 0042 0	003-0687 0	004 0043 0
000 0018 0	001-0082 0	002 0041 0	003-0688 0	004 0043 0
000 0018 0	001-0082 0	002 0041 0	003-0688 0	004 0042 0
000 0018 0	001-0082 0	002 0042 0	003-0688 0	004 0042 0
000 0017 0	001-0083 0	002 0041 0	003-0689 0	004 0042 0
000 0017 0	001-0082 0	002 0041 0	003-0691 0	004 0044 0
000 0018 0	001-0082 0	002 0042 0	003-0691 0	004 0044 0
000 0018 0	001-0082 0	002 0042 0	003-0692 0	004 0044 0
000 0018 0	001-0082 0	002 0042 0	003-0692 0	004 0044 0
000 0018 0	001-0082 0	002 0042 0	003-0692 0	004 0044 0
000 0018 0	001-0081 0	002 0042 0	003-0692 0	004 0045 0
000 0019 0	001-0082 0	002 0042 0	003-0693 0	004 0044 0
000 0017 0	001-0083 0	002 0041 0	003-0694 0	004 0043 0
000 0017 0	001-0083 0	002 0041 0	003-0694 0	004 0042 0
000 0016 0	001-0084 0	002 0040 0	003-0695 0	004 0042 0
000 0007 0	001-0098 0	002 0024 0	003-0706 0	004 0018 0
000 0007 0	001-0098 0	002 0024 0	003-0707 0	004 0018 0

TABLE (8.48)

TYPICAL STRAIN READINGS, ϵ_e's FROM DATA LOGGER AT ONE PASS OF A COPPER TUBE SPECIMEN THROUGH 7° SEMI-ANGLE ELEMENTAL DIE ASSEMBLY

STRAIN (Micros)

000	0001	0	001-0099	0	002	0001	0	003-0499	0	004	0009	0
000	0003	0	001-0097	0	002	0004	0	003-0496	0	004	0002	0
000	0001	0	001-0099	0	002	0002	0	003-0499	0	004	0001	0
000	0023	0	001-0083	0	002	0043	0	003-0477	0	004	0051	0
000	0024	0	001-0082	0	002	0042	0	003-0477	0	004	0049	0
000	0024	0	001-0082	0	002	0042	0	003-0478	0	004	0049	0
000	0024	0	001-0083	0	002	0042	0	003-0478	0	004	0049	0
000	0024	0	001-0083	0	002	0042	0	003-0478	0	004	0048	0
000	0023	0	001-0083	0	002	0041	0	003-0478	0	004	0048	0
000	0023	0	001-0083	0	002	0041	0	003-0479	0	004	0048	0
000	0023	0	001-0083	0	002	0041	0	003-0479	0	004	0048	0
000	0023	0	001-0083	0	002	0041	0	003-0479	0	004	0048	0
000	0023	0	001-0083	0	002	0041	0	003-0479	0	004	0048	0
000	0023	0	001-0083	0	002	0041	0	003-0479	0	004	0047	0
000	0023	0	001-0083	0	002	0041	0	003-0479	0	004	0047	0
000	0023	0	001-0083	0	002	0041	0	003-0479	0	004	0047	0
000	0023	0	001-0084	0	002	0041	0	003-0479	0	004	0047	0
000	0022	0	001-0084	0	002	0040	0	003-0479	0	004	0047	0
000	0022	0	001-0084	0	002	0041	0	003-0479	0	004	0047	0
000	0022	0	001-0084	0	002	0041	0	003-0479	0	004	0046	0
000	0022	0	001-0084	0	002	0041	0	003-0480	0	004	0046	0
000	0022	0	001-0084	0	002	0041	0	003-0480	0	004	0046	0
000	0022	0	001-0084	0	002	0041	0	003-04800	004	0046	0
000	0022	0	001-0084	0	002	0040	0	003-0480	0	004	0046	0
000	0022	0	001-0084	0	002	0040	0	003-0480	0	004	0046	0
000	0022	0	001-0084	0	002	0040	0	003-0480	0	004	0046	0
000	0022	0	001-0084	0	002	0040	0	003-0480	0	004	0046	0
000	0021	0	001-0085	0	002	0040	0	003-0479	0	004	0046	0
000	0010	0	001-0099	0	002	0024	0	003-0502	0	004	0024	0
000	0010	0	001-0099	0	002	0024	0	003-0502	0	004	0024	0

TABLE (8.49

Tables of the Relevant Experimental Results for the Analysis of the Experimental Redundant Deformation Strains ϵ_{res*} of Aluminium Specimens Drawn Through 15° Semi-angled Elemental Dies Assembly [Assembly of 3 Elements]

FIRST (ENTRY) ELEMENT OF THE ASSEMBLY

No.of Passes or Specimen	ϵ_{ea1} (micro)	ϵ_{r1} (micro)	ϵ_{c1} (micro)	ϵ_{eu1} (micro)	ϵ_{re1*} (micro) $[\epsilon_{eu}-(\epsilon_{ea}-\epsilon_r-\epsilon_c)]$
1	53.46	17	0	51.373	14.913
2	49.17	13	0	51.373	15.203
3	49.61	13	0	51.373	14.773
4	53.22	17	0	51.373	15.153

Table (8.50)

SECOND ELEMENT OF THE ASSEMBLY

No.of Passes or Specimen	ϵ_{ea2} (micro)	ϵ_{r2} (micro)	ϵ_{c2} (micro)	ϵ_{eu2} (micro)	ϵ_{re2*} (micro) $[\epsilon_{eu}-(\epsilon_{ea}-\epsilon_r-\epsilon_c)]$
1	61.52	19	17	51.96	26.44
2	59.35	17	17	51.96	26.61
3	60.22	18	17	51.96	26.74
4	60.52	18	17	51.96	26.44

Table (8.51)

FINAL (EXIT) ELEMENT OF THE ASSEMBLY

No.of Passes or Specimen	ϵ_{ea3} (micro)	ϵ_{r3} (micro)	ϵ_{c3} (micro)	ϵ_{eu3} (micro)	ϵ_{re3*} (micro) $[\epsilon_{eu}-(\epsilon_{ea}-\epsilon_r-\epsilon_c)]$
1	66.70	10	17	51.99	12.29
2	69.48	13	17	51.99	12.51
3	73.17	17	17	51.99	12.82
4	65.57	10	17	51.99	13.42

Table (8.52)

Tables of the Relevant Experimental Results for the Analysis of the Experimental Redundant Deformation Strains ϵ_{res*} of Copper Specimens Drawn Through 15° Semi-angled Elemental Dies Assembly [Assembly of 3 Elements]

FIRST (ENTRY) ELEMENT OF THE ASSEMBLY

No.of Passes or Specimen	ϵ_{ea1} (micro)	ϵ_{r1} (micro)	ϵ_{c1} (micro)	ϵ_{eu1} (micro)	ϵ_{re1*} (micro) $[\epsilon_{eu}-(\epsilon_{ea}-\epsilon_r-\epsilon_c)]$
1	60.53	24	0	51.06	14.53
2	65.81	30	0	51.06	15.25
3	60.54	24	0	51.06	14.52
4	57.10	21	0	51.06	14.96
5	60.90	25	0	51.06	15.16
6	57.00	21	0	51.06	15.06

Table (8.53)

SECOND ELEMENT OF THE ASSEMBLY

No.of Passes or Specimen	ϵ_{ea2} (micro)	ϵ_{r2} (micro)	ϵ_{c2} (micro)	ϵ_{eu2} (micro)	ϵ_{re2*} (micro) $[\epsilon_{eu}-(\epsilon_{ea}-\epsilon_r-\epsilon_c)]$
1	64.42	20	16	52.54	24.12
2	56.94	12	16	52.54	23.6
3	59.17	15	16	52.54	24.37
4	54.67	10	16	52.54	23.87
5	58.90	14	16	52.54	23.64
6	54.93	10	16	52.54	23.61

Table (8.54)

FINAL (EXIT) ELEMENT OF THE ASSEMBLY

No.of Passes or Specimen	ϵ_{ea3} (micro)	ϵ_{r3} (micro)	ϵ_{c3} (micro)	ϵ_{eu3} (micro)	ϵ_{re3*} (micro) $[\epsilon_{eu}-(\epsilon_{ea}-\epsilon_r-\epsilon_c)]$
1	49.42	-11	17	53.40	9.98
2	71.10	11	17	53.40	10.30
3	76.23	17	17	53.40	11.17
4	73.42	14	17	53.40	10.98
5	75.7	16	17	53.40	10.70
6	67.4	8	17	53.40	11.00

Table (8.55)

Tables of the Relevant Experimental Results for the Analysis of the Experimental Redundant Deformation Strains ϵ_{res*} of Aluminium Specimens Drawn Through 7° Semi-angled Elemental Dies Assembly [Assembly of 5 Elements]

FIRST (ENTRY) ELEMENT OF THE ASSEMBLY

No.of Passes or Specimen	ϵ_{ea1} (micro)	ϵ_{r1} (micro)	ϵ_{c1} (micro)	ϵ_{eu1} (micro)	ϵ_{re1*} (micro) $[\epsilon_{eu}-(\epsilon_{ea}-\epsilon_r-\epsilon_c)]$
1	23.38	12	0	15.826	4.446
2	21.00	10	0	15.826	4.826
3	23.44	11	0	15.826	3.386
4	23.36	11	0	15.826	3.466
5	19.82	8	0	15.826	4.006
6	20.50	9	0	15.826	4.326

Table (8.56)

SECOND ELEMENT OF THE ASSEMBLY

No.of Passes or Specimen	ϵ_{ea2} (micro)	ϵ_{r2} (micro)	ϵ_{c2} (micro)	ϵ_{eu2} (micro)	ϵ_{re2*} (micro) $[\epsilon_{eu}-(\epsilon_{ea}-\epsilon_r-\epsilon_c)]$
1	18.63	1	6	18.8	7.17
2	14.56	-3	6	18.8	7.24
3	19.94	2	6	18.8	6.86
4	19.00	1	6	18.8	6.80
5	15.36	-2	6	18.8	7.44
6	16.61	-1	6	18.8	7.19

Table (8.57)

THIRD ELEMENT OF THE ASSEMBLY

No.of Passes or Specimen	ϵ_{ea3} (micro)	ϵ_{r3} (micro)	ϵ_{c3} (micro)	ϵ_{eu3} (micro)	ϵ_{re3*} (micro) $[\epsilon_{eu}-(\epsilon_{ea}-\epsilon_r-\epsilon_c)]$
1	37.25	20	5	19.17	6.92
2	27.88	11	5	19.17	7.29
3	25.188	8	5	19.17	6.982
4	36.73	19	5	19.17	6.44
5	25.6	8	5	19.17	6.57
6	37.6	20	5	19.17	6.57

Table (8.58)

FOURTH ELEMENT OF THE ASSEMBLY

No.of Passes or Specimen	ϵ_{ea4} (micro)	ϵ_{r4} (micro)	ϵ_{c4} (micro)	ϵ_{eu4} (micro)	ϵ_{re4*} (micro) $[\epsilon_{eu}-(\epsilon_{ea}-\epsilon_r-\epsilon_c)]$
1	–	–	8	20.0	–
2	20.94	-1	8	20.0	6.06
3	23.44	1	8	20.0	5.56
4	26.82	5	8	20.0	6.18
5	–	–	8	20.0	–
6	22.22	0	8	20.0	5.78

Table (8.59)

FINAL (EXIT) ELEMENT OF THE ASSEMBLY

No.of Passes or Specimen	ϵ_{ea5} (micro)	ϵ_{r5} (micro)	ϵ_{c5} (micro)	ϵ_{eu5} (micro)	ϵ_{re5*} (micro) $[\epsilon_{eu}-(\epsilon_{ea}-\epsilon_r-\epsilon_c)]$
1	28.19	8	3	20.48	3.29
2	28.19	8	3	20.48	3.29
3	43.625	23	3	20.48	2.855
4	32.00	11	3	20.48	2.48
5	45.11	25	3	20.48	2.57
6	47.78	27	3	20.48	2.70

Table (8.60)

Tables of the Relevant Experimental Results for the Analysis of the Experimental Redundant Deformation Strains ϵ_{res*} of Copper Specimens Drawn Through 7° Semi-angled Elemental Dies Assembly [Assembly of 5 Elements]

FIRST (ENTRY) ELEMENT OF THE ASSEMBLY

No.of Passes or Specimen	ϵ_{ea1} (micro)	ϵ_{r1} (micro)	ϵ_{c1} (micro)	ϵ_{eu1} (micro)	ϵ_{re1*} (micro) $[\epsilon_{eu}-(\epsilon_{ea}-\epsilon_r-\epsilon_c)]$
1	20.11	7	0	16.99	3.88
2	22.69	10	0	16.99	4.30
3	25.39	12	0	16.99	3.60
4	20.20	7	0	16.99	3.79
5	20.31	7	0	16.99	3.68
6	19.476	7	0	16.99	4.516
7	18.68	6	0	16.99	4.31

Table (8.61)

SECOND ELEMENT OF THE ASSEMBLY

No.of Passes or Specimen	ϵ_{ea2} (micro)	ϵ_{r2} (micro)	ϵ_{c2} (micro)	ϵ_{eu2} (micro)	ϵ_{re2*} (micro) $[\epsilon_{eu}-(\epsilon_{ea}-\epsilon_r-\epsilon_c)]$
1	17.75	1	6	18.27	7.52
2	16.56	0	6	18.27	7.71
3	19.04	2	6	18.27	7.23
4	21.60	4	6	18.27	6.67
5	18.77	2	6	18.27	7.50
6	18.41	2	6	18.27	7.83
7	18.364	2	6	18.27	7.906

Table (8.62)

FINAL (EXIT) ELEMENT OF THE ASSEMBLY

No.of Passes or Specimen	ϵ_{ea3} (micro)	ϵ_{r3} (micro)	ϵ_{c3} (micro)	ϵ_{eu3} (micro)	ϵ_{re3*} (micro) $[\epsilon_{eu}-(\epsilon_{ea}-\epsilon_r-\epsilon_c)]$
1	40.93	24	5	18.75	6.82
2	41.00	24	5	18.75	6.75
3	33.87	16	5	18.75	5.88
4	29.31	13	5	18.75	7.44
5	47.27	31	5	18.75	7.48
6	40.453	24	5	18.75	7.297
7	40.318	24	5	18.75	7.432

Table (8.63)

FOURTH ELEMENT OF THE ASSEMBLY

No.of Passes or Specimen	ϵ_{ea4} (micro)	ϵ_{r4} (micro)	ϵ_{c4} (micro)	ϵ_{eu4} (micro)	ϵ_{re4*} (micro) $[\epsilon_{eu}-(\epsilon_{ea}-\epsilon_r-\epsilon_c)]$
1	21.57	-2	8	21.61	6.04
2	20.92	-3	8	21.61	5.69
3	-	-	8	21.61	-
4	23.90	1	8	21.61	6.71
5	15.46	-8	8	21.61	6.15
6	17.714	-6	8	21.61	5.90
7	20.33	-3	8	21.61	6.28

Table (8.64)

FINAL (EXIT) ELEMENT OF THE ASSEMBLY

No.of Passes or Specimen	ϵ_{ea5} (micro)	ϵ_{r5} (micro)	ϵ_{c5} (micro)	ϵ_{eu5} (micro)	ϵ_{re5*} (micro) $[\epsilon_{eu}-(\epsilon_{ea}-\epsilon_r-\epsilon_c)]$
1	22.39	0	3	22.56	3.17
2	47.28	24	3	22.56	2.28
3	18.17	-4	3	22.56	3.39
4	23.33	1	3	22.56	3.23
5	51.96	29	3	22.56	2.60
6	40.318	18	3	22.56	3.242
7	42.183	20	3	22.56	3.377

Table (8.65)

Resulting Table from Further Analysis of the Results (Strains and Forces) Related to Elemental Die Number One of the Assembly of the 3 Elemental Dies [α = 15° - Aluminium Specimens]

PASSES OR SPECIMEN	ϵ_{re1}	ϵ_{re1*}	$\Delta\epsilon_r$ $[\epsilon_{re*}-\epsilon_{re}]_1$	R_{De1}	$R_{De1}\left[\frac{R_{De}}{\epsilon_{re}} x\epsilon_{re*}\right]$	ΔR_D $[R_{De}-R_{De}]_1$	$\left\{\frac{\Delta\epsilon_r}{\epsilon_{re}}\right\}_1=\left\{\frac{\Delta R_D}{R_{De}}\right\}_1$	$\%\Delta_1$
		(micros)		(N)	(N)	(N)		%
1	13.92	14.913	0.993	691	740	49	0.071	7.1
2	13.92	15.203	1.283	691	755	64	0.092	9.2
3	13.92	14.773	0.853	691	733	42	0.061	6.1
4	13.92	15.153	1.233	69	752	61	0.089	8.9

Table (8.66)

Resulting Table from Further Analysis of the Results (Strains and Forces) Related to Elemental Die Number Two of the Proto-Die Assembly the 3 Elemental Dies [α = 15° - Aluminium Specimens]

PASSES OR SPECIMEN	ϵ_{re2}	ϵ_{re2*}	$\Delta\epsilon_r$ $[\epsilon_{re*}-\epsilon_{re}]$	R_{De2}	$R_{De2}\left[\frac{R_{De}}{\epsilon_{re}} x\epsilon_{re*}\right]$	ΔR_D $[R_{De}-R_{De}]$	$\left\{\frac{\Delta\epsilon_r}{\epsilon_{re}}\right\}_2=\left\{\frac{\Delta R_D}{R_{De}}\right\}_2$	$\%\Delta_2$
		(micros)		(N)	(N)	(N)		%
1	24.03	26.44	2.41	1240	1364	124	0.10	10.0
2	24.03	26.61	2.5	1240	1373	133	0.107	10.7
3	24.03	26.74	2.71	1240	1380	140	0.113	11.3
4	24.03	26.44	2.41	1250	1364	124	0.10	10.0

Table (8.67)

Resulting Table from Further Analysis of the Results (Strains and Forces) Related to Elemental Die Number Three (Exit) of the Assembly o the 3 Elemental Dies [α = 15° - Aluminium Specimens]

PASSES OR SPECIMEN	ϵ_{re3}	ϵ_{re3*}	$\Delta\epsilon_r$ $[\epsilon_{re*}-\epsilon_{re}]$	R_{De3}	$R_{De3}\left[\frac{R_{De}}{\epsilon_{re}} x\epsilon_{re*}\right]$	ΔR_D $[R_{De}-R_{De}]_3$	$\left\{\frac{\Delta\epsilon_r}{\epsilon_{re}}\right\}_3=\left\{\frac{\Delta R_D}{R_{De}}\right\}_3$	$\%\Delta_3$
		(micros)		(N)	(N)	(N)		%
1	10.54	12.29	1.75	545	636	91	0.166	16.6
2	10.54	12.51	1.97	545	647	102	0.187	18.7
3	10.54	12.82	2.28	545	663	118	0.216	21.6
4	10.54	13.42	2.88	545	694	149	0.273	27.3

Table (8.68)

Resulting Table from Further Analysis of the Results Related to Elemental Die Number One (Entry) of the Proto-Die Assembly of the 3 Elemental Dies
[α = 15° - Copper Specimens]

PASSES OR SPECIMEN	ϵ_{re1}	ϵ_{re1*}	$\Delta\epsilon_r$ $[\epsilon_{re*}-\epsilon_{re}]$	R_{De1}	R_{De1} $\left[\frac{R_{De}}{\epsilon_{re}} \times \epsilon_{re*}\right]$	ΔR_D $[R_{De}-R_{De}]$	$\frac{\Delta\epsilon_r}{\epsilon_{re}} = \frac{\Delta R_D}{R_{De}}$	$\%\Delta_1$
		(micros)		(N)	(N)	(N)		%
1	13.39	14.53	1.14	650	705	55	0.085	8.5
2	13.39	15.25	1.86	650	740	90	0.139	13.9
3	13.39	14.52	1.13	650	705	55	0.084	8.4
4	13.39	14.96	1.57	650	726	76	0.117	11.7
5	13.39	15.16	1.77	650	736	86	0.132	13.2
6	13.39	15.06	1.67	650	731	81	0.125	12.5

Table (8.69)

Resulting Table from Further Analysis of the Results Related to Elemental Die Number Two of the Proto-Die Assembly of the 3 Elemental Dies
[α = 15° - Copper Specimens]

PASSES OR SPECIMEN	ϵ_{re2}	ϵ_{re2*}	$\Delta\epsilon_r$ $[\epsilon_{re*}-\epsilon_{re}]$	R_{De2}	R_{De2} $\left[\frac{R_{De}}{\epsilon_{re}} \times \epsilon_{re*}\right]$	ΔR_D $[R_{De}-R_{De}]$	$\frac{\Delta\epsilon_r}{\epsilon_{re}} = \frac{\Delta R_D}{R_{De}}$	$\%\Delta$
		(micros)		(N)	(N)	(N)		%
1	21.77	24.12	2.35	1165	1291	126	0.108	10.8
2	21.77	23.6	1.83	1165	1263	98	0.084	8.4
3	21.77	24.37	2.60	1165	1304	139	0.119	11.9
4	21.77	23.87	2.10	1165	1277	112	0.097	9.7
5	21.77	23.64	1.87	1165	1265	100	0.086	8.6
6	21.77	23.61	1.84	1165	1264	99	0.085	8.5

Table (8.70)

Resulting Table from Further Analysis of the Results Related to Elemental Die Number Three (Exit) of the Proto-Die Assembly of the 3 Elemental Dies
[α = 15° - Copper Specimens]

PASSES OR SPECIMEN	ϵ_{re2}	ϵ_{re2*}	$\Delta\epsilon_r$ $[\epsilon_{re*}-\epsilon_{re}]$	R_{De2}	R_{De2} $\left[\frac{R_{De}}{\epsilon_{re}} \times \epsilon_{re*}\right]$	ΔR_D $[R_{De}-R_{De}]$	$\frac{\Delta\epsilon_r}{\epsilon_{re}} = \frac{\Delta R_D}{R_{De}}$	$\%\Delta$
		(micros)		(N)	(N)	(N)		%
1	9.06	9.98	0.92	510	562	52	0.102	10.2
2	9.06	10.30	1.24	510	580	70	0.137	13.7
3	9.06	11.17	2.11	510	629	119	0.233	23.3
4	9.06	10.98	1.92	510	618	108	0.212	21.2
5	9.06	10.70	1.64	510	602	92	0.181	18.1
6	9.06	11.00	1.94	510	619	109	0.214	21.4

Table (8.71)

Resulting Table from Further Analysis of the Results Related to Elemental Die Number One (Entry) of the Proto-Die Assembly of the 5 Elemental Dies
[$\alpha = 7^{\circ}$ - Aluminium Specimens]

PASSES OR SPECIMEN	ϵ_{re1}	ϵ_{re1*}	$\Delta\epsilon_r$ $[\epsilon_{re*}-\epsilon_{re}]$	R_{De1}	R_{De1} $\left[\frac{R_{De}}{\epsilon_{re}} \times \epsilon_{re*}\right]$	ΔR_D $[R_{De}-R_{De}]$	$\frac{\Delta R_D}{R_{De}} = \frac{\Delta\epsilon_r}{\epsilon_{re}}$	%Δ
		(micros)		(N)	(N)	(N)		%
1	3.952	4.446	0.494	323	363	40	0.125	12.5
2	3.952	4.826	0.874	323	394	71	0.221	22.1
3	3.952	3.386	-0.566	323	277	-46	-0.143	14.3
4	3.952	3.466	-0.486	323	283	-40	-0.123	12.3
5	3.952	4.006	0.054	323	327	4*	0.014	1.4*
6	3.952	4.326	0.374	323	354	31	0.095	9.5

Table (8.72)

Resulting Table from Further Analysis of the Results Related to Elemental Die Number Two of the Proto-Die Assembly of the 5 Elemental Dies
[$\alpha = 7^{\circ}$ - Aluminium Specimens]

PASSES OR SPECIMEN	ϵ_{re2}	ϵ_{re2*}	$\Delta\epsilon_r$ $[\epsilon_{re*}-\epsilon_{re}]$	R_{De2}	R_{De2*} $\left[\frac{R_{De}}{\epsilon_{re}} \times \epsilon_{re*}\right]$	ΔR_D $[R_{De}-R_{De}]$	$\frac{\Delta\epsilon_r}{\epsilon_{re}} = \frac{\Delta R_D}{R_{De}}$	%Δ
		(micros)		(N)	(N)	(N)		%
1	5.962	7.17	1.208	597	718	121	0.203	20.3
2	5.962	7.24	1.278	597	725	128	0.214	21.4
3	5.962	6.86	0.898	597	687	90	0.151	15.1
4	5.962	6.80	0.838	597	681	84	0.141	14.1
5	5.962	7.44	1.478	597	745	148	0.248	24.8
6	5.962	7.19	1.228	597	720	123	0.206	20.6

Table (8.73)

Resulting Table from Further Analysis of the Results Related to Elemental Die Number Three of the Proto-Die Assembly of the 5 Elemental Dies
[$\alpha = 7^{\circ}$ - Aluminium Specimens]

PASSES OR SPECIMEN	ϵ_{re3}	ϵ_{re3*}	$\Delta\epsilon_r$ $[\epsilon_{re*}-\epsilon_{re}]$	R_{De3}	R_{De} $\left[\frac{R_{De}}{\epsilon_{re}} \times \epsilon_{re*}\right]$	ΔR_D $[R_{De}-R_{De}]$	$\frac{\Delta\epsilon_r}{\epsilon_{re}} = \frac{\Delta R_D}{R_{De}}$	%Δ
		(micros)		(N)	(N)	(N)		%
1	5.563	6.92	1.357	562	699	137	0.244	24.4
2	5.563	7.29	1.727	562	737	175	0.310	31.0
3	5.563	6.982	1.419	562	705	143	0.255	25.5
4	5.563	6.44	0.877	562	651	89	0.158	15.8
5	5.563	6.57	1.007	562	664	102	0.181	18.1
6	5.563	6.57	1.007	562	664	102	0.181	18.1

Table (8.74)

Resulting Table from Further Analysis of the Results Related to Elemental Die Number Four of the Proto-Die Assembly of the 5 Elemental Dies
[$\alpha = 7^{\circ}$ - Aluminium Specimens]

PASSES OR SPECIMEN	ϵ_{re4}	ϵ_{re4*}	$\Delta\epsilon_r$ $[\epsilon_{re*}-\epsilon_{re}]$	R_{De4}	R_{De4} $\left[\frac{R_{De}}{\epsilon_{re}} \times \epsilon_{re*}\right]$	ΔR_D $[R_{De}-R_{De}]$	$\frac{\Delta\epsilon_r}{\epsilon_{re}} = \frac{\Delta R_D}{R_{De}}$	%Δ
		(micros)		(N)	(N)	(N)		%
1	5.10	-	-	525	-	-	-	-
2	5.10	6.06	0.96	525	624	99	0.188	18.8
3	5.10	5.56	0.46	525	573	48	0.09	9.0
4	5.10	6.18	1.08	525	636	111	0.212	21.2
5	5.10	-	-	525	-	-	-	-
6	5.10	5.78	0.68	525	595	70	0.133	13.3

Table (8.75)

Resulting Table from Further Analysis of the Results Related to Elemental Die Number Five (Exit) of the Proto-Die Assembly of the 5 Elemental Dies
[$\alpha = 7^{\circ}$ - Aluminium Specimens]

PASSES OR SPECIMEN	ϵ_{re5}	ϵ_{re5*}	$\Delta\epsilon_r$ $[\epsilon_{re*}-\epsilon_{re}]$	R_{De5}	R_{De5} $\left[\frac{R_{De}}{\epsilon_{re}} \times \epsilon_{re*}\right]$	ΔR_D $[R_{De}-R_{De}]$	$\frac{\Delta\epsilon_r}{\epsilon_{re}} = \frac{\Delta R_D}{R_{De}}$	%Δ
		(micros)		(N)	(N)	(N)		%
1	2.338	3.29	0.952	243	342	99	0.407	40.7
2	2.338	3.29	0.952	243	342	99	0.407	40.7
3	2.338	2.855	0.517	243	297	54	0.221	22.1
4	2.338	2.48	0.142	243	258	15	0.061	6.1
5	2.338	2.57	0.232	243	267	24	0.099	9.9
6	2.338	2.70	0.362	243	281	38	0.155	15.5

Table (8.76)

Resulting Table from Further Analysis of the Results Related to Elemental Die Number One (Entry) of the Proto-Die Assembly of the 5 Elemental Dies
[$\alpha = 7^{\circ}$ - Copper Specimens]

PASSES OR SPECIMEN	ϵ_{re1}	ϵ_{re1*}	$\Delta\epsilon_r$ $[\epsilon_{re*}-\epsilon_{re}]$	R_{De1}	R_{De1*} $\left[\frac{R_{De}}{\epsilon_{re}} \times \epsilon_{re*}\right]$	ΔR_D $[R_{De}-R_{De}]$	$\frac{\Delta R_D}{R_{De}} = \frac{\Delta\epsilon_r}{\epsilon_{re}}$	%Δ
		(micros)		(N)	(N)	(N)		%
1	3.95	3.88	-0.07	372	365	-7	-0.018	-1.8
2	3.95	4.30	0.35	372	404	32	0.089	8.9
3	3.95	3.60	-0.35	372	339	-33	-0.089	-8.9
4	3.95	3.79	-0.16	372	357	-15	-0.041	-4.1
5	3.95	3.68	-0.27	372	347	-25	-0.068	-6.8
6	3.95	4.514	0.564	372	425	53	0.143	14.3
7	3.95	4.31	0.36	372	406	34	0.091	9.1

Table (8.77)

Resulting Table from Further Analysis of the Results Related to Elemental Die Number Two of the Proto-Die Assembly of the 5 Elemental Dies
[$\alpha = 7^{\circ}$ - Copper Specimens]

PASSES OR SPECIMEN	ϵ_{re2}	ϵ_{re2*}	$\Delta\epsilon_r$ $[\epsilon_{re*}-\epsilon_{re}]$	R_{De2}	R_{De2*} $\left[\frac{R_{De}}{\epsilon_{re}} \times \epsilon_{re*}\right]$	ΔR_D $[R_{De}-R_{De}]$	$\frac{\Delta\epsilon_r}{\epsilon_{re}} = \frac{\Delta R_D}{R_{De}}$	%Δ
		(micros)		(N)	(N)	(N)		%
1	6.964	7.52	0.556	688	743	55	0.08	8.0
2	6.964	7.71	0.746	688	762	74	0.107	10.7
3	6.964	7.23	0.266	688	714	26	0.038	3.8
4	6.964	6.67	-0.294	688	659	-29	-0.042	-4.2
5	6.964	7.50	0.536	688	741	53	0.077	7.7
6	6.964	7.83	0.866	688	774	86	0.124	12.4
7	6.964	7.906	0.942	688	781	93	0.135	13.5

Table (8.78)

Resulting Table from Further Analysis of the Results Related to Elemental Die Number Three of the Proto-Die Assembly of the 5 Elemental Dies [$\alpha = 7^{\circ}$ - Copper Specimens]

PASSES OR SPECIMEN	ϵ_{re3}	ϵ_{re3*} (micros)	$\Delta\epsilon_r$ $[\epsilon_{re*}-\epsilon_{re}]$	R_{De3} (N)	R_{De} $\left[\frac{R_{De}}{\epsilon_{re}} \times \epsilon_{re*}\right]$ (N)	ΔR_D $[R_{De}-R_{De}]$ (N)	$\frac{\Delta\epsilon_r}{\epsilon_{re}} = \frac{\Delta R_D}{R_{De}}$	%Δ %
1	6.48	6.82	0.34	648	682	34	0.053	5.3
2	6.48	6.75	0.27	648	675	27	0.042	4.2
3	6.48	5.88	-0.60	648	588	-60	-0.093	-9.3
4	6.48	7.44	0.96	648	744	96	0.148	14.8
5	6.48	7.48	1.00	648	748	100	0.154	15.4
6	6.48	7.297	0.817	648	730	82	0.126	12.6
7	6.48	7.432	0.952	648	743	95	0.147	14.7

Table (8.79)

Resulting Table from Further Analysis of the Results Related to Elemental Die Number Four of the Proto-Die Assembly of the 5 Elemental Dies [$\alpha = 7^{\circ}$ - Copper Specimens]

PASSES OR SPECIMEN	ϵ_{re4}	ϵ_{re4*} (micros)	$\Delta\epsilon_r$ $[\epsilon_{re*}-\epsilon_{re}]$	R_{De4} (N)	R_{De4} $\left[\frac{R_{De}}{\epsilon_{re}} \times \epsilon_{re*}\right]$ (N)	ΔR_D $[R_{De}-R_{De}]$ (N)	$\frac{\Delta\epsilon_r}{\epsilon_{re}} = \frac{\Delta R_D}{R_{De}}$	%Δ %
1	5.70	6.04	0.34	605	641	36	0.06	6.0
2	5.70	5.69	-0.01	605	604	-1.0*	0.06	0.2
3	5.70	-	-	605	-	-	-	-
4	5.70	6.71	1.01	605	712	107	0.177	17.7
5	5.70	6.15	0.45	605	653	48	0.08	8.0
6	5.70	5.90	0.20	605	626	21	0.035	3.5
7	5.70	6.28	0.58	605	667	62	0.102	10.2

Table (8.80)

Resulting Table from Further Analysis of the Results Related to Elemental Die Number Five (Exit) of the Proto-Die Assembly of the 5 Elemental Dies
[α = 7° - Copper Specimens]

PASSES OR SPECIMEN	ϵ_{re5}	ϵ_{re5*}	$\Delta\epsilon_r$ $[\epsilon_{re*}-\epsilon_{re}]$	R_{De5}	R_{De5} $\left[\frac{R_{De}}{\epsilon_{re}} \times \epsilon_{re*}\right]$	ΔR_D $[R_{De}-R_{De}]$	$\frac{\Delta\epsilon_r}{\epsilon_{re}} = \frac{\Delta R_D}{R_{De}}$	%Δ
		(micros)		(N)	(N)	(N)		%
1	2.594	3.17	0.576	280	342	62	0.222	22.2
2	2.594	2.28	-0.314	280	246	-34	-0.121	-12.1
3	2.594	3.39	0.796	280	366	86	0.307	30.7
4	2.594	3.23	0.636	280	349	69	0.245	24.5
5	2.594	2.60	0.006	280	281	1.0	0.0023	0.23
6	2.594	3.24	0.646	280	350	70	0.249	24.9
7	2.594	3.377	0.783	280	365	85	0.302	30.2

Table (8.81)

Example of Unreliable Contact Strains Recorded for Individual Elements when subjected to a Total Drawing Force, F_{dT}

ϵ_{c1}	ϵ_{c2}	ϵ_{c3}	ϵ_{c4}	ϵ_{c5}
		(micro)		
13	0	54	8	20
22	12	90	15	33
31	28	127	24	42
41	46	165	36	53
47	65	195	55	63
55	86	225	77	69
62	107	250	100	75
71	129	273	124	79
79	150	290	145	84
82	170	304	165	88
84	187	317	191	91
84	200	328	218	94
84	216	339	246	99

TABLE (8.92)

TYPICAL SPECIMEN CONTACT STRAINS PRINT-OUT WHEN ASSEMBLY OF THREE ELEMENTAL DIES WAS SUBJECTED TO A TOTAL DRAWING FORCE F_{dT}

STRAIN (Micros)

000 0001 0 001 0001 0 002 05000

000-0001 0 001-0004 0 002 0495 0

000-0001 0 001-0005 0 002 0492 0

000-0002 0 001-0007 0 002 0489 0

000-0003 0 001-0008 0 002 0488 0

000-0004 0 001-0010 0 002 0486 0

000-0004 0 001-0011 0 002 0485 0

000-0005 0 001-0013 0 002 0484 0

000-0005 0 001-0015 0 002 0483 0

000-0006 0 001-0016 0 002 0483 0

000-0006 0 001-0018 0 002 0482 0

000-0006 0 001-0017 0 002 0482 0

000-0005 0 001-0017 0 002 0483 0

000-0006 0 001-0017 0 002 0482 0

000-0006 0 001-0018 0 002 0481 0

000 0000 0 001 0000 0 002 0499 0

000 0000 0 001 0000 0 002 0499 0

TABLE (8.93)

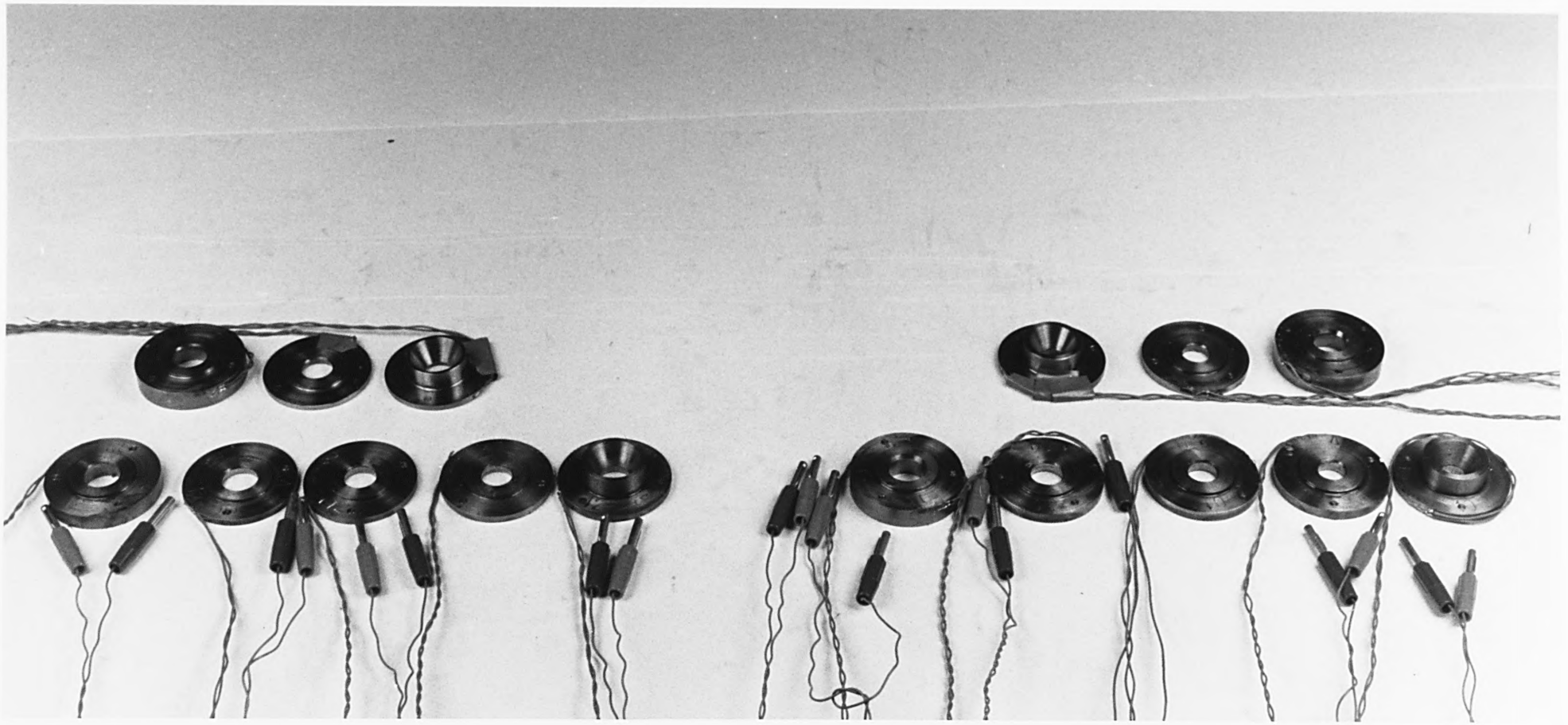

Fig.(8.4)

SET OF NSOH ELEMENTAL DIES FOR MEASUREMENT OF STRAINS AND ANALOGUE OF ELEMENTAL DRAWING FORCE, ϵ_{Deu}, & F_{Deu}

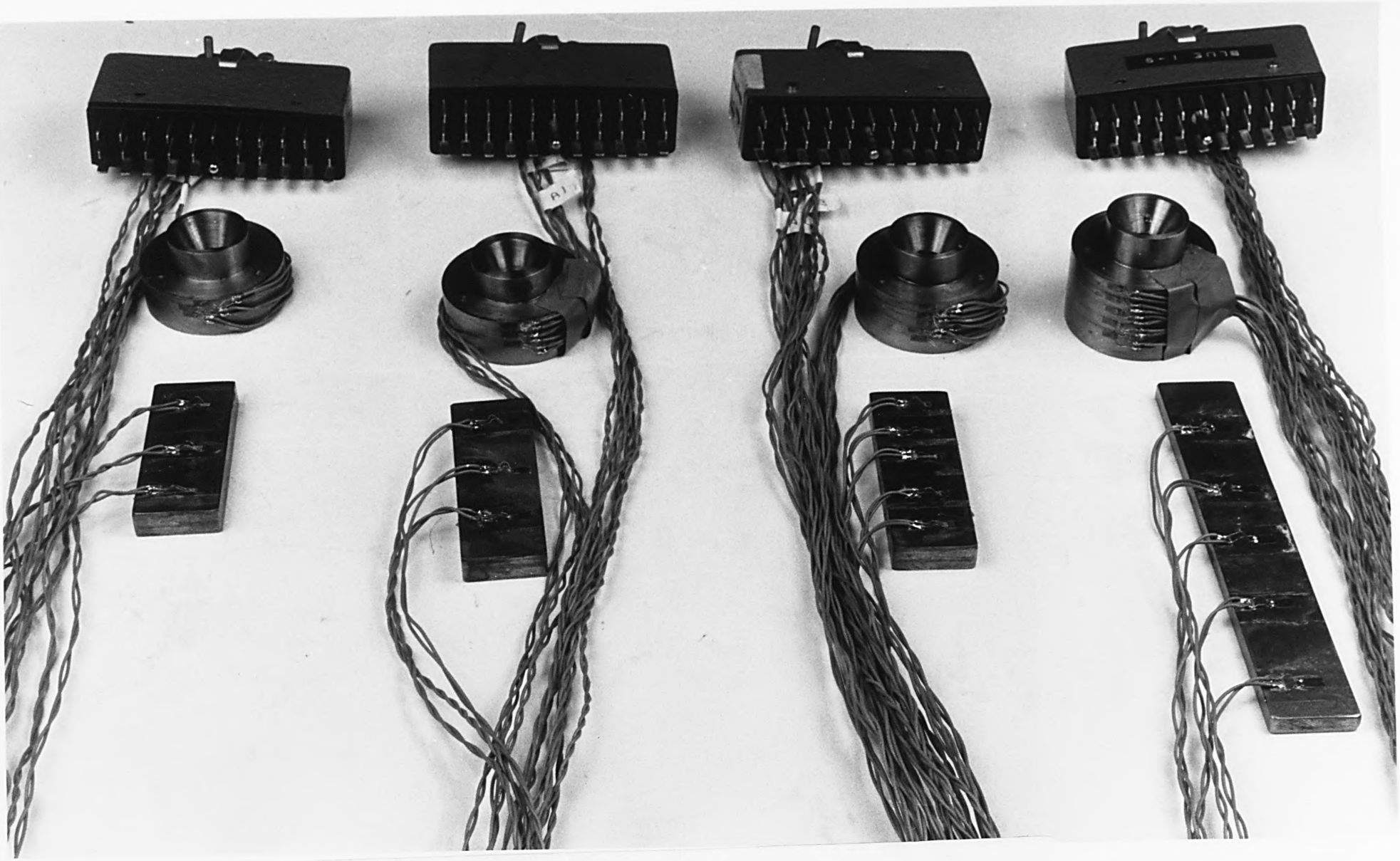

Fig.(8.5)

ASSEMBLIES OF ELEMENTAL DIES WITH 7° AND 15° SEMI-ANGLES FOR 0.250 & 0.375 TOTAL FRACTIONAL REDUCTIONS

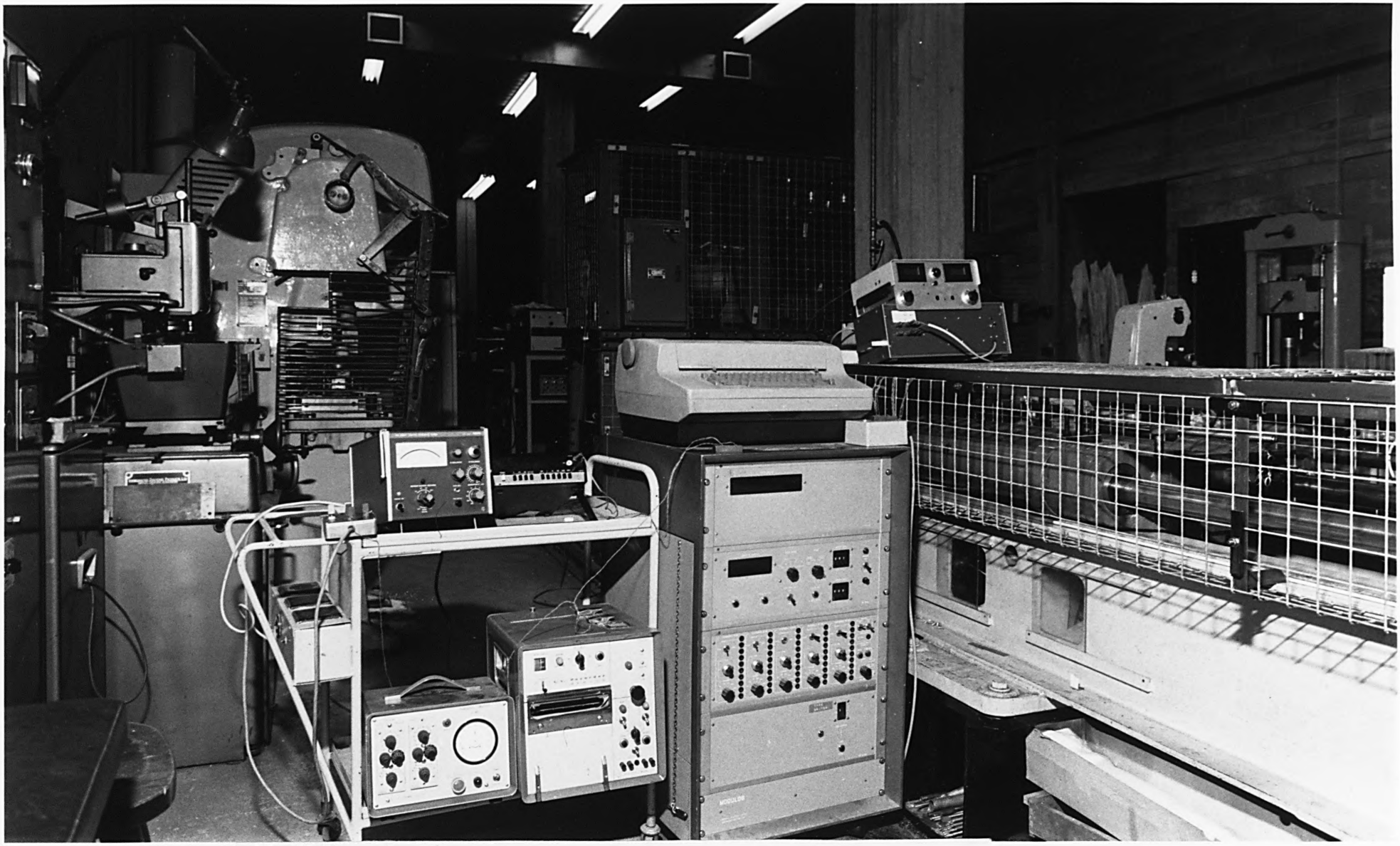

Fig.(8.6)

SET UP OF THE EQUIPMENT EMPLOYED FOR REDUNDANT DEFORMATION AND COEFFICIENT OF FRICTION EXPERIMENTS